U.PORTO

FACULDADE DE CIÊNCIAS
UNIVERSIDADE DO PORTO

TU Graz

# Engineering the cyanobacterial chassis for improved electron supply

Jelena Spasic

Thesis to obtain the academic degree
*Doutor em Biologia* / Doktorin der Naturwissenschaften/doctor rerum naturalium
at the Faculty of Sciences of the University of Porto / at the Graz University of Technology
2022

**Supervisor**
Paula Tamagnini, Professora Associada
Faculdade de Ciências,
i3S - Instituto de Investigação e Inovação em Saúde,
IBMC - Instituto de Biologia Molecular e Celular,
Universidade do Porto

**Supervisor**
Robert Kourist, Univ.-Prof. Dr.rer.nat.
Head of Institute of Molecular Biotechnology,
Graz University of Technology

**Co-supervisor**
Paulo Oliveira
IBMC - Instituto de Biologia Molecular e Celular,
i3S - Instituto de Investigação e Inovação em Saúde,
Prof. Auxiliar Convidado, Faculdade de Ciências,
Universidade do Porto

TU
Graz

U.PORTO
FACULDADE DE CIÊNCIAS
UNIVERSIDADE DO PORTO

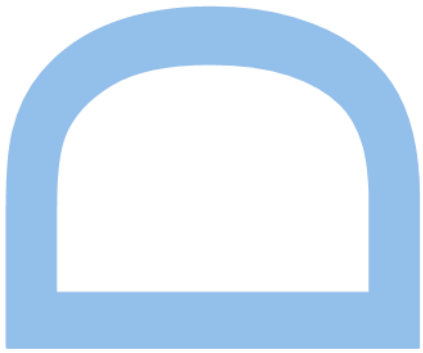

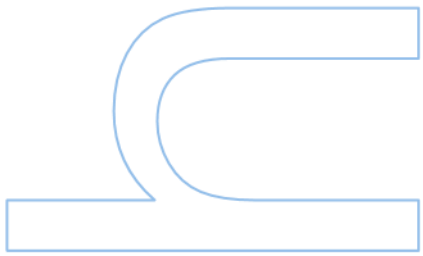

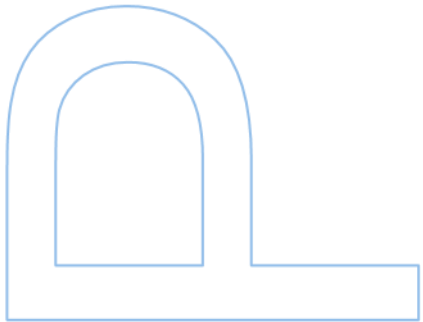

All the corrections determined by the jury, and only those, were made.

The Supervisor,

Assinado por: **PAULA MARIA SEQUEIRA TAMAGNINI BARBOSA OXELFELT**
Num. de Identificação: 08513660
Data: 2022.07.04 11:08:36+01'00'

Porto, _____ / _____ / _____

CARTÃO DE CIDADÃO

## AFFIDAVIT

I declare that I have authored this thesis independently, that I have not used other than the declared sources/resources, and that I have explicitly indicated all material which has been quoted either literally or by content from the sources used. The text document uploaded to TUGRAZonline is identical to the present doctoral thesis.

25.05.2022.

Date, Signature

‘*Vreme koje sami stvorimo svojim smislenim I stvaralačkim životom trajno je i neiscrpno.* ‘

‘*The time we create with our meaningful and creative life is permanent and inexhaustible.* ‘

Ranko Radović

## Acknowledgments

The last years have been a rollercoaster, and on this rollercoaster, I was not alone. Therefore, I would like to take this opportunity to express gratitude to everyone who traveled with me during this period to see the light.

First, I would like to thank my supervisors Prof. Paula Tamagnini and Prof. Robert Kourist for giving me the opportunity to join their research groups and work on this exciting project. Their tremendous availability and the amount of work brought us together to do this interdisciplinary research. I would like to especially thank Dr. Paulo Oliveira and Dr. Catarina Pacheco for being the first front of all the questions I had. Thank you for your patience.

The two research groups I had the opportunity to join were my homes for the last few years. The Bioengineering & Synthetic Microbiology Group in Porto was a great scientific environment where I stepped into the cyanobacterial world. I thank Eunice, Joao, Sara, Filipe x 2, Jessica, Steeve, Jose, Angela, Rita, Marta, Marina and the rest who stumbled upon me in this period. Hope I was able to bring a smile or so to your faces and hope we get the chance to interact again on our research ways. The Cell and Protein Engineering Group in Graz was the second home, where I get to know more about biocatalysis and that wouldn't go so smoothly without Lenny, Hanna, Anna, Kamela, Daniel, Elia, Sunny, Ina, Mirna. You cheered me up in hard days in Graz and let's hope that stays a story for grandchildren.

In addition, I want to thank Dan Enke and Cyano Biotech GmbH for giving me the opportunity to peak into industrial settlements and work with cyano in different ways. Thank you, Stefan, for showing me all the hands-on work in there.

Furthermore, I want to thank all the (ex)students of the PhotoBioCat project where the rollercoaster was especially the fun part to be in, with many project meetings we attended in different cities of Europe. Especially, I want to thank Valentina, Francesco, Markus, Elif, Feyza, Robert, Luca, Hitesh, Alice, Alex, Piera, Hanna and Leen who were great drivers to bring the science we have today. See you around and hope we have a chance to work or drink together soon!

Lastly, I must express my very profound gratitude to the village behind me, Slavica, Nenad, Irena, Srđan, Dragan and all my friends for their immerse support and encouragement on this

road. Unfortunately, this won't be seen by my two biggest cheerleaders, Slavica and Irena, but it goes for them.

## Financial support

This project has received funding from the European Union's Horizon 2020 research and innovation programme under the Marie Skłodowska-Curie grant agreement No 764920.

## Abstract

With energy consumption growing rapidly over the last decades, our responsibilities will be maintaining balance of society's activities and harmonizing them with the existing natural processes. Therefore, the development of innovative technologies based on renewable energy resources, such as solar irradiance, needs to be a strategy for the sustainable production of chemicals. Cyanobacteria are gaining attention as chassis for light-driven biotechnology due to their photosynthetic nature, robust physiology, ability to grow under varying conditions, coupled with amenability to genetic manipulations. Particularly, light-driven biocatalysis hosted in cyanobacteria is recently gaining interest, as this approach allows for the substitution of sacrificial organic co-substrates using water as the electron donor. Coupling whole-cell redox reactions to photosynthetic electron flow lead the way towards sustainable production of chemicals, especially interesting for stereoselective catalysis. Previous studies demonstrated that engineered cyanobacteria are beneficial for several reductive biotransformations and oxyfunctionalizations.

In this work, we tackle different aspects of improvement in the field of photobiocatalysis ranging from chassis engineering, development of regulatory elements for controllable gene expression to scaling up photobiotransformations. We showed that the development of customized chassis for the expression of a heterologous ene-reductase leads up to 39% improvement in the specific activity, namely in a mutant lacking an active bidirectional hydrogenase. Further on, we explored different cultivation conditions with a particular focus on light as energy input and the composition of the cultivation medium. We have observed that adaptation of the chassis prior to light-driven reactions can affect the reaction rates. Harnessing the power of synthetic biology, we showed that the design and development of customized regulatory tools namely RNA thermometers offer an approach to expand the customized molecular toolbox for cyanobacteria, in particular for *Synechocystis*. We successfully characterized a library of 12 RNA thermometers, showing up to a 3-fold change in translational levels upon temperature shifts. Finally, we established an efficient scale-up system for the stereoselective light-driven biocatalysis demonstrated on ene-reduction of 2-methylmaleimide catalyzed by ene-reductase. We proved that internal illumination provided by floating wireless light emitters can overcome cell density limitations, leading to a more than a two-fold rate increase compared to the external illumination. Product formation rates up to 3.7 mM $h^{-1}$ and specific activities of up to 65.5 U $g_{DCW}^{-1}$ were achieved applying the cell density of 2.4 g $L^{-1}$.

Overall, this work demonstrates that synthetic biology approaches focused on rational engineering of the chassis and the development of customized regulatory tools can facilitate optimization towards further applications of cyanobacteria as hosts for light-driven biocatalysis. Additionally, establishing close collaboration with process engineers light-driven biocatalysis performed in cyanobacteria can be efficiently scaled up utilizing a bubble column reactor with internal illumination.

**Keywords**: cyanobacteria, chassis development, RNA thermometers, scale-up systems, light-driven biocatalysis, ene-reductase, *Synechocystis*

## Sumário

Com uma exigência energética que tem crescido muito rapidamente nas últimas décadas para sustentar actividades humanas, as nossas responsabilidades actuais e futuras irão recair essencialmente no estabelecimento de equilíbrios entre o bem-estar da sociedade e os recursos e processos naturais existentes. Deste modo, o desenvolvimento de tecnologias inovadoras baseadas em fontes de energia renovável, como a luz solar, será uma das estratégias para a produção sustentável de produtos químicos de interesse. As cianobactérias têm atraído bastante atenção como *chassis* para o desenvolvimento de tecnologias energizadas e dependentes da luz solar, baseada na capacidade destas bactérias de realizarem a fotossíntese, de possuírem uma fisiologia robusta, de crescerem em variadas condições, ao mesmo tempo que são passíveis de serem modificadas geneticamente. Em particular, a biocatálise conduzida pela luz solar operada em cianobactérias tem ganho especial interesse, uma vez que esta abordagem biotecnológica permite a substituição de co-substratos orgânicos sacrificiais dadores de electrões simplesmente por água para o mesmo efeito. O acoplamento de reacções de redução-oxidação (redox) ao fluxo de electrões derivados do processo da fotossíntese em células inteiras (fotobiocatálise) abre o caminho para a produção sustentável de produtos químicos, especialmente interessantes para a catálise estereosseletiva. Estudos recentes demonstraram que as cianobactérias geneticamente modificadas são viáveis como solução para diversos tipos de biotransformações dependentes de reações de redução e oxifuncionalizações.

Neste trabalho, diferentes aspectos de melhoria no campo da fotobiocatálise são abordados, incluindo a modificação racional do *chassi* cianobacteriano, o desenvolvimento de elementos

reguladores para controlo de expressão génica e o desenvolvimento de processos para aumento de escala de fotobiotransformações. Deste modo, aqui mostra-se que o desenvolvimento personalizado do *chassi* cianobacteriano para a expressão de uma eno-redutase heteróloga leva a um aumento em 39% na atividade específica da enzima, nomeadamente num mutante sem a hidrogenase bidirecional. Mais ainda, o efeito de diferentes condições de cultivo na actividade enzimática foi avaliado, com especial atenção para a disponibilidade de energia luminosa e para a composição do meio de cultivo. Como resultado, foi observado que a adaptação prévia do *chassi* cianobacteriano à realização das reacções accionadas pela luz pode afetar as taxas de reacção. Aproveitando o conhecimento e a plasticidade da biologia sintética, demonstra-se neste trabalho que o desenho e desenvolvimento de ferramentas regulatórias personalizadas, como termómetros de RNA, oferecem uma alternativa para expandir a caixa de ferramentas moleculares para cianobactérias, em particular para *Synechocystis*. Uma biblioteca de 12 termómetros de RNA foi caracterizada, mostrando uma mudança de até 3 vezes nos níveis de tradução após mudanças de temperatura. Finalmente, foi estabelecido um sistema eficiente de aumento de escala para a biocatálise estereosseletiva conduzida pela luz, demonstrada na redução de 2-metilmaleimida catalisada pela enzima eno-redutase. Com este trabalho, foi possível demonstrar que a iluminação interna fornecida por emissores de luz sem fio flutuantes pode superar as limitações de densidade celular, levando a um aumento de taxa de produção em mais de duas vezes em comparação com um sistema baseado em iluminação externa. Taxas de formação de produto de até 3.7 mM $h^{-1}$ e atividades específicas de até 65.5 U $g_{DCW}^{-1}$ foram alcançadas aplicando-se uma densidade celular de 2.4 g $L^{-1}$.

No geral, este trabalho demonstra que as abordagens de biologia sintética focadas na engenharia racional do *chassi* cianobacteriano e no desenvolvimento de ferramentas regulatórias personalizadas podem facilitar a optimização para outras aplicações destes microrganismos fotossintéticos como mini-fábricas para biocatálise accionada pela luz solar. Além disso, o diálogo e estabelecimento de estreitas colaborações com engenheiros de processo, levou a que a biocatálise accionada pela luz realizada em cianobactérias tenha sido ampliada de forma eficiente, utilizando um reactor de coluna de bolhas com iluminação interna.

**Palavras-chave:** Cianobactérias, desenvolvimento de *chassi*, termómetros de RNA, sistemas de aumento de escala, biocatálise accionada pela luz, ene-redutase, *Synechocystis*

## Zusammenfassung

Da der Energieverbrauch in den letzten Jahrzehnten rapide angestiegen ist, wird es unsere Aufgabe sein, das Gleichgewicht der gesellschaftlichen Aktivitäten aufrechtzuerhalten und sie mit den bestehenden natürlichen Prozessen in Einklang zu bringen. Daher muss die Entwicklung innovativer Technologien, die auf erneuerbaren Energieressourcen wie der Sonneneinstrahlung basieren, eine Strategie für die nachhaltige Produktion von Chemikalien sein. Cyanobakterien gewinnen aufgrund ihrer photosynthetischen Natur, ihrer robusten Physiologie, ihrer Fähigkeit, unter verschiedenen Bedingungen zu wachsen, und ihrer leichten genetischen Manipulierbarkeit zunehmend an Aufmerksamkeit als Grundlage für die lichtgetriebene Biotechnologie. Dieser Ansatz ermöglicht die Substitution von organischen Opfersubstraten durch Wasser als Elektronendonator. Die Kopplung von Redoxreaktionen in der Zelle mit dem photosynthetischen Elektronenfluss weist den Weg zu einer nachhaltigen Produktion von Chemikalien, die insbesondere für die stereoselektive Katalyse interessant ist. Frühere Studien haben gezeigt, dass technisch veränderte Cyanobakterien für verschiedene reduktive Biotransformationen und Oxyfunktionalisierungen von Nutzen sind.

In dieser Arbeit befassen wir uns mit verschiedenen Aspekten der Verbesserung im Bereich der Photobiokatalyse, von der Entwicklung von Chassis, über die Entwicklung von regulatorischen Elementen für die kontrollierbare Genexpression bis hin zur Maßstabsvergrößerung von Photobiotransformationen. Wir haben gezeigt, dass die Entwicklung eines maßgeschneiderten Chassis für die heterologe Expression einer Enreduktase zu einer Verbesserung der spezifischen Aktivität um bis zu 39% führt, und zwar bei einer Mutante, der eine aktive bidirektionale Hydrogenase fehlt. Darüber hinaus haben wir verschiedene Kultivierungsbedingungen untersucht, wobei wir uns besonders auf Licht als Energiequelle und die Zusammensetzung des Kultivierungsmediums konzentriert haben. Wir haben festgestellt, dass die Anpassung des Chassis vor den lichtgesteuerten Reaktionen die Reaktionsgeschwindigkeiten beeinflussen kann. Unter Nutzung der Möglichkeiten der synthetischen Biologie haben wir gezeigt, dass das Design und die Entwicklung von maßgeschneiderten regulatorischen Werkzeugen, nämlich RNA-Thermometern, einen Ansatz zur Erweiterung des maßgeschneiderten molekularen Werkzeugkastens für Cyanobakterien, insbesondere für *Synechocystis*, darstellt. Wir haben eine Bibliothek von 12

RNA-Thermometern erfolgreich charakterisiert und konnten eine bis zu 3-fache Änderung der Translationsraten bei Temperaturveränderungen feststellen. Schließlich etablierten wir ein effizientes Scale-up-System für die stereoselektive, lichtgetriebene Biokatalyse, die an der Reduktion von 2-Methylmaleimid durch eine Enreduktase demonstriert wurde. Wir haben bewiesen, dass die interne Beleuchtung durch schwimmende, drahtlose Lichtstrahler die Beschränkungen der Zelldichte überwinden kann, was zu einer mehr als zweifachen Ratensteigerung im Vergleich zur externen Beleuchtung führt. Bei einer Zelldichte von 2.4 g $L^{-1}$ wurden Produktbildungsraten von bis zu 3.7 mM $h^{-1}$ und spezifische Aktivitäten von bis zu 65.5 U $g_{DCW}^{-1}$ erreicht.

Insgesamt zeigt diese Arbeit, dass synthetische Biologieansätze, die sich auf rationales Engineering des Chassis und die Entwicklung maßgeschneiderter regulatorischer Werkzeuge konzentrieren, die Optimierung für weitere Anwendungen von Cyanobakterien als Wirte für lichtgetriebene Biokatalyse erleichtern können. Darüber hinaus kann die lichtgetriebene Biokatalyse, die in Cyanobakterien durchgeführt wird, durch eine enge Zusammenarbeit mit Prozessingenieuren unter Verwendung eines Blasensäulenreaktors mit interner Beleuchtung effizient hochskaliert werden.

**Stichwörter:** Cyanobakterien, Chassis-Entwicklung, RNA-Thermometer, Maßstabsvergrößerung, lichtgetriebene Biokatalyse, Ene-Reduktase, *Synechocystis*

# Table of Contents

Acknowledgments ..... IX
Financial support ..... X
Abstract ..... XI
Sumário ..... XII
Zusammenfassung ..... XIV
List of tables ..... XXI
List of figures ..... XXIII

Chapter I General introduction ..... 1

1. Solar energy to power the future ..... 3
2. Cyanobacteria as potential hosts for light-driven biotechnology ..... 5
2.1. Synthetic biology to enhance solar-powered sustainable biotechnologies ..... 6
2.2. Cyanobacterial chassis for the light-driven biotechnology ..... 6
2.3. Engineering chassis as improved bioproduction platforms ..... 9
2.3.1. Expanding the range of light absorption ..... 10
2.3.2. Antenna reduction for optimal energy conversion ..... 11
2.3.3. Redirecting photosynthetic electron flux ..... 11
2.3.4. Enhancing carbon fixation activity and utilizing carbon sinks ..... 12
2.4. Model cyanobacterial strains and emerging strains ..... 13
3. The role of biocatalysis toward sustainability ..... 15
3.1. The bottlenecks of the application of redox enzymes ..... 18
3.2. Cofactor recycling in autotrophic microorganisms ..... 21
3.3. Cyanobacteria as chassis for light-driven biotechnology ..... 23
3.4. Light-driven whole-cell biotransformations in wild-type cyanobacteria ..... 23
3.5. Light-driven whole-cell biotransformations in engineered cyanobacteria ..... 24
3.6. Challenges and opportunities for scaling up light-driven biotransformations ..... 25
4. Aims of this work ..... 29
5. References ..... 30

Chapter II Engineering cyanobacterial chassis for improved electron supply toward a heterologous ene-reductase ..... 43

1. Introduction ..... 47
2. Materials and methods ..... 50
2.1. Chemicals and reagents ..... 50
2.2. Organisms and standard growth conditions ..... 51
2.3. DNA extraction and recovery ..... 51
2.4. Plasmid construction ..... 51
2.5. Generation of Synechocystis deletion mutants ..... 52
2.6. Introduction of the yqjM into Synechocystis chassis ..... 53
2.7. Growth experiments ..... 53
2.8. Light-driven biotransformations ..... 54
2.9. Nitrogen limiting and mixotrophic cultivation conditions ..... 54
2.10. 12h light / 12 h dark or continuous blue/red light cultivation conditions ..... 55
2.11. Quantitative GC-FID Analysis ..... 55
2.12. SDS PAGE and Western blot ..... 55
2.13. in vitro NADPH assay ..... 56
2.14. $O_2$ evolution measurements ..... 57
2.15. Cell dry weight ..... 57
2.16. Statistical analysis ..... 57
3. Results and Discussion ..... 57
3.1. Generation of Synechocystis chassis and introduction of the ene-reductase YqjM 57
3.2. Growth performance of the Synechocystis engineered strains ..... 58
3.3. Redirecting electron flow increases in vivo YqjM activity ..... 59
3.4. Evaluation of YqjM activity in the ΔhoxYH chassis ..... 63
4. Conclusions ..... 67
References ..... 69
Supplementary material ..... 73

Chapter III Characterization of a library of RNA thermometers as potential regulatory elements ..... 89

1. Introduction ..... 91
2. Materials and Methods ..... 93
   2.1. Chemicals and reagents ..... 93
   2.2. Organisms and culture conditions ..... 93
   2.3. Design of synthetic RNA thermometers ..... 94
   2.4. Plasmid construction ..... 95
   2.5. Synechocystis transformation and transformants confirmation ..... 97
   2.6. GFP fluorescence analysis ..... 98
3. Results and Discussion ..... 99
3.1. Design of a library of RNA thermometers ..... 99
3.2. Plasmids construction and transformation of Synechocystis ..... 102
3.3. Temperature responsiveness of synthetic RNATs ..... 103
3.4. Assessment of computational analysis and experimental data ..... 110
4. Conclusions ..... 111
5. References ..... 112

Chapter IV Internal illumination to overcome the cell density limitation in the scale-up of whole-cell photobiocatalysis ..... 115

Conclusions and future perspectives ..... 139

# List of tables

## Chapter I

**Table 1.** Key steps required toward chassis development and progress associated with cyanobacteria……7

**Table 2.** Selected model cyanobacterial strains……..……14

**Table 3.** The 12 principles of green chemistry for the design of new chemical products and processes and solutions offered by biocatalysis…….…...……16

**Table 4.** Metrics used to evaluate the efficacy of the biocatalytic processes……..…...…17

## Chapter II

### Supporting tables

**Table S1**. Oligonucleotide primers used in this study……..……74

**Table S2.** Plasmids used to transform *Synechocystis*……..…75

**Table S3.** S*ynechocystis* strains used in this work……..……76

**Table S4.** Parameters for the GC-FID method used to detect the substrate and product……78

## Chapter III

**Table 1.** The selected RNAT sequences……94

**Table 2.** Oligonucleotide primers used in this study……..……95

**Table 3.** The list of S*ynechocystis* strains used in this work……97

## Chapter IV

### Supporting tables

**Table S1.** Strains utilized in this work……128

**Table S2.** Gas Chromatography Flame Ionization Detector Method……128

**Table S3.** Average light intensity in BCR.....131

# List of figures

## Chapter I

**Figure 1.** Schematics of photosynthetic light reactions in the thylakoid membranes of cyanobacteria.....5

**Figure 2.** Different strategies employed for engineering cyanobacterial chassis toward improved productivities.....10

**Figure 3.** Asymmetric bioreduction of activated alkenes using ene-reductases.....19

**Figure 4.** Schematic representation of the most common *in vitro* systems for cofactor recycling.....20

**Figure 5.** Schematic representation of harnessing photosynthetic reductants for biocatalytic reactions performed by heterologous oxidoreductases.....22

**Figure 6.** Schematic representation of the different photobioreactors. A) stirred tank, B) vertical flat panel, C) fence tubular, D) bubble column.....27

## Chapter II

**Figure 1**. Growth rates of *Synechocystis* sp. PCC 6803 (wt), Δ*hoxYH*, Δ*flv3*, Δ*ndhD2* and Δ*hoxYH*Δ*flv3* mutants, and of these chassis expressing YqjM. Cells were cultivated in 96-well microplates in BG-11 at 28 ºC with orbital shaking (150 rpm) under 12 h white light (20 µmol $m^{-2}$ $s^{-1}$) / 12 h dark regimen. Error bars correspond to standard deviations from at least three biological replicates with technical triplicates and statistical analysis is presented based on an unpaired *t*-test (n.s., not significant).....58

**Figure 2.** Light-driven biotransformation of 2-methylmaleimide into 2-methylsuccinimide catalyzed by YqjM expressed in *Synechocystis* sp. PCC 6803 (wt) and Δ*hoxYH*, Δ*flv3*, Δ*ndhD2* and Δ*hoxYH*Δ*flv3* chassis. A) Product formation rate and B) *In vivo* specific activity. Cells were cultivated in BG-11 at 30 ºC with orbital shaking (140 rpm) under continuous white light (50 µmol $m^{-2}$ $s^{-1}$), grown until $OD_{750}$ 1-1.5, harvested and applied for the biotransformation of 10 mM 2-MM (1 ml, 2.4 $g_{DCW}$ $L^{-1}$, BG-11, white light of 150 µmol $m^{-2}$ $s^{-1}$, 130 rpm, 30 ºC); C) *in vitro* YqjM activity determined in NADPH assay using crude cell-free extracts. Error bars correspond to standard deviations from three biological replicates and statistical analysis is

presented based on unpaired *t*-test (***, $P < 0.001$; **, $P < 0.01$; *, $P < 0.05$; n.s., not significant).……..61

**Figure 3.** Oxygen evolution rates by *Synechocystis* sp. PCC 6803 (wt), Δ*hoxYH*, Δ*flv3*, Δ*ndhD2* and Δ*hoxYH*Δ*flv3* mutants, and of these chassis expressing YqjM. Cells were cultivated in BG-11 at 30 ºC with orbital shaking (140 rpm) under continuous white light (50 µmol $m^{-2}$ $s^{-1}$), grown until $OD_{730}$ 1-1.5 and harvested for the measurements (for details Material and Methods). Error bars correspond to standard deviations from three biological replicates and statistical analysis is presented based on unpaired *t*-test (n.s., not significant).……..62

**Figure 4.** Light-driven biotransformation of 2-methylmaleimide (2-MM) into 2-methylsuccinimide (2-MS) catalyzed by YqjM expressed in *Synechocystis* wt and Δ*hoxYH* chassis and oxygen evolution rates. A) *In vivo* specific activity of YqjM at different cell densities or carrying out the reaction in the dark; B) Product formation rates at different cell densities or carrying out the reaction in the dark; C) 2-MM conversion over time. Cells were cultivated in BG-11 at 30 ºC with orbital shaking (140 rpm) under continuous white light (50 µmol $m^{-2}$ $s^{-1}$), grown until $OD_{750}$ 1-1.5, harvested and applied for the biotransformation of 10 mM 2-MM (1 mL, BG-11, white light of 150 µmol $m^{-2}$ $s^{-1}$ or dark, 130 rpm, 30 ºC). D) Oxygen evolution rates of wt and Δ*hoxYH*, and of these chassis expressing YqjM in the absence (-) or presence (+) of 10 mM 2-MM. Cells were cultivated in BG-11 at 30 ºC with orbital shaking (140 rpm) under continuous white light (50 µmol $m^{-2}$ $s^{-1}$), grown until $OD_{730}$ 1-1.5, harvested and the oxygen evolution rate measured (under two different light intensities 150 and 800 µmol $m^{-2}$ $s^{-1}$). Error bars correspond to standard deviations from three biological replicates and statistical analysis is presented based on unpaired *t*-test (***, $P < 0.001$; **, $P < 0.01$; *, $P < 0.05$; n.s., not significant).……65

**Supporting figures**

**Figure S1.** Example of a graph plotted using raw data from the quantification of NADPH absorbance in crude cell free extract of *Synechocystis* sp. PCC 6803 expressing YqjM under the control of $P_{cpcB}$ promoter (wt $P_{cpcB}$::*yqjM*) without (dotted line) and with the presence of the substrate (full line): 1 mM 2-methylmaleimide (2-MM).……..79

**Figure S2.** Generation of *Synechocystis* sp. PCC 6803 customized chassis by deletion of selected genes coding for Flv3 or NdhD2. Schematic representation of the position of the

primers (A and C) and PCR analysis confirming the segregation of *Synechocystis* Δ*flv3*, Δ*hoxYH*Δ*flv3* (B) and Δ*ndhD2* mutants (D). PCRs were performed using outer and inner primers for *flv3* and *ndhD2*. For details on the primers used see Table S1. The amplicon expected size is indicated below each lane. wt, wild-type, $C^-$, negative control (no template); M, molecular marker GeneRuler DNA Ladder Mix (Thermo Scientific™)..……80

**Figure S3.** PCR analysis confirming the segregation of *Synechocystis* wt ($wt^+$) Δ*hoxYH,* Δ*flv3*, Δ*hoxYH*Δ*flv3* and Δ*ndhD2* mutants containing the gene encoding for the enzyme YqjM under the control of $P_{cpcB}$ promoter ($P_{cpcB}$::*yqjM*). PCR reactions were performed using primer pair Seg_fw / Seg_rv (Table S1). The amplicon expected size is indicated below each lane. wt, wild-type, $C^-$, negative control (no template); M, molecular marker GeneRuler DNA Ladder Mix (Thermo Scientific™).……82

**Figure S4.** Growth curves of *Synechocystis* sp. PCC 6803 (wt), Δ*hoxYH*, Δ*flv3*, Δ*ndhD2* and Δ*hoxYH*Δ*flv3*, and these chassis expressing YqjM. Cells were cultivated in BG-11 at 28ºC with orbital shaking (150 rpm) under 12 h white light (20 µmol $m^{-2}$ $s^{-1}$), 12 h dark regime. Error bars correspond to standard deviations from at least three biological replicates with technical triplicates……..82

**Figure S5.** Light-driven conversion of 2-methylmaleimide to 2-methylsuccinimide catalyzed by YqjM expressed in *Synechocystis wt* and Δ*hoxYH*, Δ*flv3*, Δ*ndhD2* and Δ*hoxYH*Δ*flv3* chassis. A) 2-methylmaleimide conversion over time and B) 2-MS concentration over time. Cells were cultivated in BG-11 at 30ºC with orbital shaking (140 rpm) under continuous white light (50 µmol $m^{-2}$ $s^{-1}$), grown until $OD_{750}$ 1-1.5, harvested and applied for the biotransformation of 10 mM 2-MM (1 ml, BG-11, white light of 150 µmol $m^{-2}$ $s^{-1}$ or dark, 130 rpm, 30ºC). Error bars correspond to standard deviations from three biological replicates……...83

**Figure S6.** Analysis of protein extracts of *Synechocystis* sp. PCC 6803 wild-type (wt), and *Synechocystis* wild-type, Δ*hoxYH*, Δflv3, Δ*hoxYH*Δ*flv3* and Δ*ndhD2* chassis expressing YqjM: wt $P_{cpcB}$::*yqjM*, Δ*hoxYH* $P_{cpcB}$::*yqjM,* Δ*flv3* $P_{cpcB}$::*yqjM,* Δ*hoxYH*Δ*flv3* $P_{cpcB}$::*yqjM* and Δ*ndhD2* $P_{cpcB}$::*yqjM*, respectively. A) SDS-PAGE and stained with PageBlue, 10 µg of protein extract was loaded in each lane, the location of the YqjM band is indicated by a star (expected size of approximately 38.7 kDa). B) Western blot using an anti-His-tag as a primary antibody, 10 µg of protein extract was loaded in each lane. Cells were cultivated in BG-11 at 30ºC with orbital shaking (140 rpm) under continuous white light (50 µmol $m^{-2}$ $s^{-1}$), grown until $OD_{750}$ 1-

1.5, harvested and used for the preparation of crude cell extracts. M- NZYColour protein marker II (NZYTech)..……84

**Figure S7.** Light-driven biotransformations of 2-methylmaleimide into 2-methylsuccinimide catalyzed by YqjM expressed in *Synechocystis* wt and Δ*hoxYH* chassis cultivated under 12 h white light 12 h dark regimen or continuous blue/red light. A) *In vivo* specific activity of YqjM expressed in chassis cultivated under 12 h white light (50 µmol $m^{-2}$ $s^{-1}$)/12 h dark conditions. B) *In vivo* specific activity of YqjM expressed in chassis cultivated under blue red light (150 µmol $m^{-2}$ $s^{-1}$). The cells were cultivated in BG-11 at 30ºC with orbital shaking (140 rpm) grown until $OD_{750}$ 1-2, harvested and applied for the biotransformation of 10 mM 2-MM (1 mL, 2.4 $g_{DCW}$ $L^{-1}$, BG-11, 150 µmol $m^{-2}$ $s^{-1}$ white light, 130 rpm, 30ºC). Error bars correspond to standard deviations from three biological replicates and statistical analysis is presented based on unpaired *t*-test (n.s., not significant).……...85

**Figure S8.** Light-driven biotransformations of 2-methylmaleimide into 2-methylsuccinimide catalyzed by YqjM expressed in *Synechocystis* wt or Δ*hoxYH* cultivated under nitrogen limiting or nitrate-limiting mixotrophic conditions. A) *In vivo* specific activity of cells cultivated in BG-$11_0$ with the addition of 17.6 mM,1.76 $mM_3$ or 0.88 mM $NaNO_3$ with orbital shaking (140 rpm) under continuous white light (50 µmol $m^{-2}$ $s^{-1}$) harvested at $OD_{750}$ 1-1.5 and applied for the biotransformation of 10 mM 2-MM (1 ml, 2.4 $g_{DCW}$ $L^{-1}$, BG-$11_0$ + 17.6 mM,1.76 $mM_3$ or 0.88 mM $NaNO_3$, 150 µmol $m^{-2}$ $s^{-1}$ white light, 130 rpm, 30ºC); B) *In vivo* specific activity of cells cultivated in BG-$11_0$ with the addition of 5 mM arginine and 10 mM glucose. Cells were cultivated in the BG-$11_0$ supplemented with 5 mM arginine and 10 mM glucose with orbital shaking (140 rpm) under continuous white light (50 µmol $m^{-2}$ $s^{-1}$) harvested at $OD_{750}$ 1-1.5 and applied for the biotransformation of 10 mM 2-MM (1 ml, 2.4 $g_{DCW}$ $L^{-1}$, BG-$11_0$ + 5 mM arginine + 10 mM glucose, 150 µmol $m^{-2}$ $s^{-1}$ white light, 130 rpm, 30ºC). Error bars correspond to standard deviations from two biological replicates, and statistical analysis is presented based on unpaired *t* test (n.s., not significant).……...86

**Figure S9.** Standard curves generated for quantification of 2-MM and 2-MS. Data derive from two independent technical replicates and the corresponding line equations and $R^2$ values were generated by simple linear regression and forced through zero.……..87

**Figure S10.** Representative GC-FID chromatograms for quantification of 2-MM and 2-MS. A) Reference chromatogram of 2-MM and 2-MS standards. B) Extracted sample of *in vivo* biotransformation of 2-MM to 2-MS……..…….87

## Chapter III

**Figure 1.** Schematic representation of a simple RNA thermometer. A stem-loop structure locks the RBS and prevents the binding of the ribosome. Upon temperature shift, the stem-loop structure opens, unveiling the RBS and allowing binding of the small ribosomal subunit and initiation of translation…….92

**Figure 2.** Free energies (in ΔG in kcal/mol) of designed RNAT at 30 ºC estimated using the Quikfold program……..100

**Figure 3.** Secondary structures of the entire 5'-UTR as predicted by the Quikfold program (Markham and Zuker, 2005, Markham and Zuker, 2008). The SD sequence is highlighted in violet……...101

**Figure 4.** A) Schematic representation of the GFP expression cassette used to test redesigned RNAT for their possible function as thermometers. The sequences, including the *hsp17* RBS 5'-AGGAGU'-3', were inserted in between the promoter $P_{trc.x.tetO2}$ and the *gfp* coding region. B) PCR reactions were performed using TS1-FP and PS2 primes (Table 2). The expected band size is 945 bp. +, positive control (pSEVA251 $P_{trc.x.tetO2}$::B0032::*gfp*); -, negative control (no template); M, molecular marker GeneRuler DNA Ladder Mix (Thermo Scientific™)……...103

**Figure 5.** Characterization of RNA thermometers response in *Synechocystis* regarding $OD_{730}$ tested using A) cultures of $OD_{730}$ 0.5 and B) cultures of $OD_{730}$ 1.0. The bars represent normalized GFP fluorescence of *Synechocystis* cells harboring the corresponding RNAT sequence. GFP fluorescence was measured before (0h) and after the temperature shift from 30 to 37° (1 h, 2 h, 4 h and 24 h). The fluorescence of the control strain harboring the pSEVA251 was subtracted from each sample. Error bars correspond to standard deviations from a single experiment with technical triplicates (measured in duplicate). $P_{trc.x.tetO2}$::B0032::*gfp* was included for comparison purposes……104

**Figure 6.** Characterization of RNA thermometers response in *Synechocystis*. The bars represent normalized GFP fluorescence of *Synechocystis* cells harboring the corresponding RNAT. GFP fluorescence was measured before (0 h) and after the temperature shift from 30 to 37 °C (4 h and 24 h). The fluorescence of the control strain harboring the empty pSEVA251 was subtracted from each sample. Error bars correspond to standard deviations from a single

experiment with technical triplicates (measured in duplicate). $P_{trc.x.tetO2}$:: B0032::*gfp* was included for comparison purposes……107

**Figure 7.** Characterization of RNA thermometers response in *Synechocystis* maintained in dark. The bars represent normalized GFP fluorescence of *Synechocystis* cells harboring the RNAT. GFP fluorescence was measured before (0 h) and after the temperature shift from 30 to 37 °C (4 h and 24 h) maintaining the cells in dark. The fluorescence of the control strain harboring the empty pSEVA251 was subtracted from each sample. Error bars correspond to standard deviations from a single experiment with technical triplicates (measured in duplicate). $P_{trc.x.tetO2}$:: B0032::*gfp* was included for comparison purposes……108

**Figure 8.** Characterization of RNA thermometers response in *Synechocystis*. The bars represent normalized GFP fluorescence of *Synechocystis* cells harboring the RNAT. GFP fluorescence was measured before (0 h) and after the temperature shift from 25 to 37° (4 h and 24 h). The fluorescence of the control strain harboring the pSEVA251 was subtracted from each sample. Error bars correspond to standard deviations from a single experiment with technical triplicates (measured in duplicate). $P_{trc.x.tetO2}$:: B0032::*gfp* was included for comparison purposes……..109

**Figure 9.** Characterization of RNA thermometers response in *Synechocystis*. The bars represent normalized GFP fluorescence of *Synechocystis* cells harboring the RNAT. GFP fluorescence was measured before (0 h) and after the temperature shift from 25 to 40° (4 h and 24 h). The fluorescence of the control strain harboring the pSEVA251 was subtracted from each sample. Error bars correspond to standard deviations from a single experiment with technical triplicates (measured in duplicate)……110

**Figure 10.** Assessment of the correlation between experimental measurements and computational analysis. The plot represents the fold change of the GFP fluorescence during the temperature shift from 25 to 37 ºC and the difference in the predicted free energy of the elements under these temperatures. TS9 was excluded from the analysis, as it was an outliner. The prediction was done using the Quikfold program (Markham and Zuker, 2005, Markham and Zuker, 2008)……111

## Chapter IV

**Figure 11.** a): Whole cell light-driven biotransformations catalyzed by *Synechocystis* $P_{cpcB}$::*yqjM*. b) Specific activity and initial product formation rates achieved at 1 mL-scale using

various cell densities, independent biological triplicates; c) Conversion of 2-MM during photobiotransformations (1 mL, 10 mM 2-methylmaleimide, 160 rpm, 30ºC, 200 µE $m^{-2}$ $s^{-1}$), independent biological triplicates..……118

**Figure 12.** Above: Photo-biotransformations performed in the BCR with internal illumination provided by 40 floating wireless light emitters at a cell density of 0.48 g $L^{-1}$ (left side) and 2.4 g $L^{-1}$ (right side). Below: determination of the light intensity inside BCR with internal illumination by 40 WLEs at a cell density of 0.48 g $L^{-1}$ or 2.4 g $L^{-1}$, respectively..……119

**Figure 13.** Whole cell biotransformation catalyzed by *Synechocystis* $P_{cpcB}$::*yqjM* in a BCR. a) Specific activity and initial product formation rate of *Synechocystis* $P_{cpcB}$::*yqjM* in a BCR with internal illumination provided by WLEs (200 mL, 10 mM 2--methylmaleimide, 0.6 L $min^{-1}$ airflow), independent biological triplicates; b) Time course of the reactions using different cell densities with 40 WLEs, independent biological triplicates; c) Specific activity and initial product formation rate of *Synechocystis* $P_{cpcB}$::*yqjM* in a BCR externally illuminated with LED strips (300 µE $m^{-2}$ s-1) or in dark (200 mL, 10 mM 2-methylmaleimide, 0.6 L $min^{-1}$ airflow), single measurements; d) Time course of the reactions with external illumination or in dark, single measurements..……120

**Figure 14.** a) Conversion of 10 mM 2-MM into corresponding 2-MS during photobiotransformations catalyzed by *Synechocystis* $P_{cpcB}$::*yqjM* and *Synechocystis* $P_{psbA2}$::*yqjM* both at a cell density of 2.4 g $L^{-1}$; b) Specific activity and initial product formation rate of *Synechocystis* $P_{cpcB}$::*yqjM* and *Synechocystis* $P_{psbA2}$::*yqjM*; c) Time course of the preparative 10 mM 2-MM photobiotransformation catalyzed by *Synechocystis* $P_{cpcB}$::*yqjM,* single measurements; d) 2-MM substrate converted by *Synechocystis* $P_{cpcB}$::*yqjM* cells (2.4 g $L^{-1}$) using a substrate feeding approach, with initial substrate concentration introduced 20mM and a subsequent feeding of 20 mM at 3 h, single measurements..……...121

**Supporting figures**

**Figure S1.** Light Intensity Measurements inside BCR with a) internal illumination at cell density 1.2 g $L^{-1}$; b) internal illumination at cell density 2.4 g $L^{-1}$; c) external illumination provided by LED strips..……..130

**Figure S2.** a) Schematic illustration of the Bubble Column Reactor with a working volume of 200 mL cyanobacterial mixture, the air was delivered using a pump at a flowrate of 0.6 L $min^{-1}$; b) Wireless Light Emitters (WLEs) utilized for internal illumination in the BCR..……131

**Figure S3.** a) Cultivation of *Synechocystis* in gas washing tubes in an aquarium maintained at 30 °C, the air was delivered using a pump and passed through 0.2 µm filters; b) Light intensity measurements for each tube (measured in water).....132

**Figure S4.** $^{1}$H NMR of 2-MS obtained after whole-cell biotransformation.....134

**Figure S5.** $^{13}$C NMR of 2-MS obtained after whole-cell biotransformation.....134

**Figure S6.** Consumption of 2-MM substrate over time by Synechocystis sp. PCC 6803 WT (1.2 g $L^{-1}$, 200 mL, 10 mM 2-methylmaleimide, 0.6 L $min^{-1}$ airflow, 40 WLEs).....135

**Figure S7.** External illumination of BCR provided by LED strips (BOXXX).....135

**Figure S8.** Example GC-Chromatogram with 2-MM substrate (ret. time 5.660 min) and 2-MS product (ret. time 6.262 min). *n*-decanol (ret. time 7.229 min) was used as an internal standard.....136

**Figure S9.** The emission spectrum of a white WLE.....136

# List of abbreviations

| | |
|---|---|
| 2-MM | 2-methylmaleimide |
| 2-MS | 2-methylsuccinimide |
| 3PGA | 3-Phosphoglyceric acid |
| ADP | Adenosine diphosphate |
| ATP | Adenosine triphosphate |
| BCR | Bubble column reactor |
| BDW | Biomass dry weight |
| BG-11 | Blue-green medium |
| CA | Carbonic anhydrase |
| CBB | Calvin–Benson–Bassham cycle |
| CDW | Cell dry weight |
| chl *a* | Chlorophyll *a* |
| Cm | Chloramphenicol |
| CRISPR/CRISPRi | Clustered regularly interspaced short palindromic repeats |
| cyt $b_6f$ | cytochrome $b_6f$ complex |
| cyt $c_6$ | cytochrome $c_6$ |
| *ee* | Enantiomeric excess |
| Fd | Ferredoxin |
| FDH | Formate dehydrogenase |
| Flv | Flavodiiron |
| FMN | Flavin mononucleotide |
| FNR | Ferredoxin-$NADP^+$ oxidoreductase |
| GC-FID | Gas chromatography flame ionization detector |
| GDH | Glucose dehydrogenase |
| GFP | Green fluorescent protein |
| HOX | Hydrogenase |

| | |
|---|---|
| Km | Kanamycin |
| LB | Luria-Bertani medium |
| LED | Light emitting diode |
| $NADP^+$ | Nicotinamide adenine dinucleotide phosphate, oxidized |
| NADPH | Nicotinamide adenine dinucleotide phosphate, reduced |
| NDH-1 | NAD(P)H:quinone oxidoreductase |
| NMR | Nuclear magnetic resonance |
| OD | Optical density |
| PAM | Pulse amplitude modulation |
| PAR | Photosynthetically active radiation |
| PC | Plastocyanin |
| PCR | Polymerase chain reaction |
| PHB | Polyhydroxybutyrate |
| PQ | Plastoquinone |
| $PQH_2$ | Plastoquinol |
| PSI | Photosystem I |
| PSII | Photosystem II |
| RBS | Ribosome binding site |
| RNAT | RNA thermometer |
| RubBP | Ribulose 1,5-bisphosphate |
| RubisCO | Ribulose-1,5-bisphosphate carboxylase/oxygenase |
| SD | Shine-Dalgarno sequence |
| SDS-PAGE | Sodium dodecyl sulfate polyacrylamide gel |
| Sm | Streptomycin |
| RT-qPCR | Quantitative reverse transcription PCR |
| UTR | Untranslated region |
| WLE | Wireless light emitters |
| WT | Wild-type |

| | |
|---|---|
| YqjM | Ene-reductase from *Bacillus subtilis* |

# CHAPTER I

# General introduction

# 1. Solar energy to power the future

Modern civilization thrives on a constant flow of energy, with consumption growing rapidly over the past 25 years. It is projected that our energy usage will increase by 30% until 2040, mainly supplied through fossil fuels (Newell et al., 2019). Fossil fuels are finite energy sources contributing to the cumulative emissions of $CO_2$ into the atmosphere, recognized as one of the great factors of global climate change. Society's future challenges will be maintaining chemical balances of humankind's activities and harmonizing them with the existing natural processes (Dhillon and von Wuehlisch, 2013). Therefore, paradigm shifts are beyond doubt needed to overcome our dependency on fossil fuels toward technologies based on renewable energy resources. The priority of relying on carbon-neutral energy conversion is embedded in the 7$^{th}$ sustainable development goal aimed to ''Ensure access to affordable, reliable, sustainable and modern energy'' set up by the General Assembly of the United Nations (Cf, 2015).

The abundance of solar irradiance makes it a clean and attractive energy source to power the industries of the future. The annual flow of energy from the sun exceeds all other (non)renewable energy flows with several orders of magnitude beyond society's needs (Inganäs and Sundström, 2016). Harnessing the power of solar radiation and converting it into chemical energy via photosynthesis, can simultaneously mitigate excessive $CO_2$ levels while converting $CO_2$ into value-added chemicals. As photosynthesis-based technologies offer the shortest route between harvested energy and chemical synthesis, the light-driven production processes are genuinely sustainable (de María, 2021). Therefore, in recent years photosynthetic microorganisms have received considerable attention as biological platforms for the production of chemical compounds and natural products (Knoot et al., 2018, Angermayr et al., 2015).

The progenitors of photosynthesis, cyanobacteria, are an excellent starting point for exploring the possibility of moving into a green future (Nikkanen et al., 2021). It is generally accepted that oxygenic photosynthesis evolved in cyanobacteria approximately 2.4 billion years ago (Hohmann-Marriott and Blankenship, 2011), generating the planet's oxygen-rich atmosphere (Hamilton et al., 2016). Evolutionary, photosynthetic eukaryotes, including terrestrial plants and algae, could trace the ancestry of their chloroplasts to cyanobacteria (Falcón et al., 2010). Cyanobacteria play a significant role in the global carbon and nitrogen cycles, accounting for about 25% of the planet's primary productivity and about 60% of the primary productivity in

the open ocean (Flombaum et al., 2013, Bullerjahn and Post, 2014), demonstrating their great capacity for productivity. These organisms inhabit a range of environmental niches growing under diverse conditions (Whitton and Potts, 2007). This ecological plasticity originates from their metabolic flexibility in light utilization (pigmentation), carbon utilization (autotrophic and mixotrophic growth) and nitrogen utilization (ammonia, nitrate, dinitrogen).

### 1.1. Cyanobacterial photosynthetic machinery

In most cyanobacteria, excluding a couple of strains such as *Gloeobacter* species, the photosynthetic electron transport occurs in internal thylakoid membranes, which delimitate the thylakoid lumen. Light energy is converted into chemical energy in the form of ATP and reducing power in the form of NADPH by a series of photochemical reactions, at the expense of water and producing $O_2$ as a by-product. The vast majority of NADPH and ATP produced are used for $CO_2$ fixation in the Calvin–Benson–Bassham (CBB) cycle (Lea-Smith et al., 2016, Zhou et al., 2018).

The linear electron transport is initiated in the photosystem II, a large membrane-bound complex associated with the phycobilisomes, the large soluble light-harvesting complex excited by photons. Upon illumination, the phycobilisome transfers the excitation energy to chlorophylls in the PSII P680 reaction center, catalyzing the photolysis of water, leading to the release of the electrons and $O_2$. In the PSII, for each water molecule split, 2 protons and 1/2 $O_2$ are released. The excited electrons are further transferred along the electron transport chain, starting with the reduction of plastoquinone (PQ) into plastoquinol ($PQH_2$). $PQH_2$ is released from PSII, diffuses through the membrane to the cytochrome $b_6f$ complex (cyt $b_6f$) where it is deprotonated and oxidized on the luminal side of the membrane. Electrons are further transferred either to copper ion-containing plastocyanin (PC) or the heme-containing cytochrome $c_6$ (cyt $c_6$). These redox carriers further transfer electrons to the oxidized photosystem I reaction center chlorophyll, P700. PSI is also associated with phycobilisomes, transferring excitation energy to the core of the complex. Further on, the electrons from the PSI are transferred to soluble electron carrier proteins, such as ferredoxin, which functions as a distribution hub for the photosynthetic electrons. In the case of iron depletion, ferredoxin is substituted by flavodoxin. Both reduced ferredoxin and flavodoxin are capable of donating electrons to different biosynthetic pathways. The majority of electrons is transferred to ferredoxin-$NADP^+$ reductase (FNR) leading to the conversion of $NADP^+$ to NADPH with two electrons required for each NADPH to be produced. In total, to produce one NADPH molecule,

one water molecule is split and an electrochemical gradient across the thylakoid membrane equivalent to 6 protons could be formed. The proton gradient is concomitantly used to drive ATP production via ATP synthase (Lea-Smith et al., 2016, Lea-Smith and Hanke, 2021) (Fig. 1).

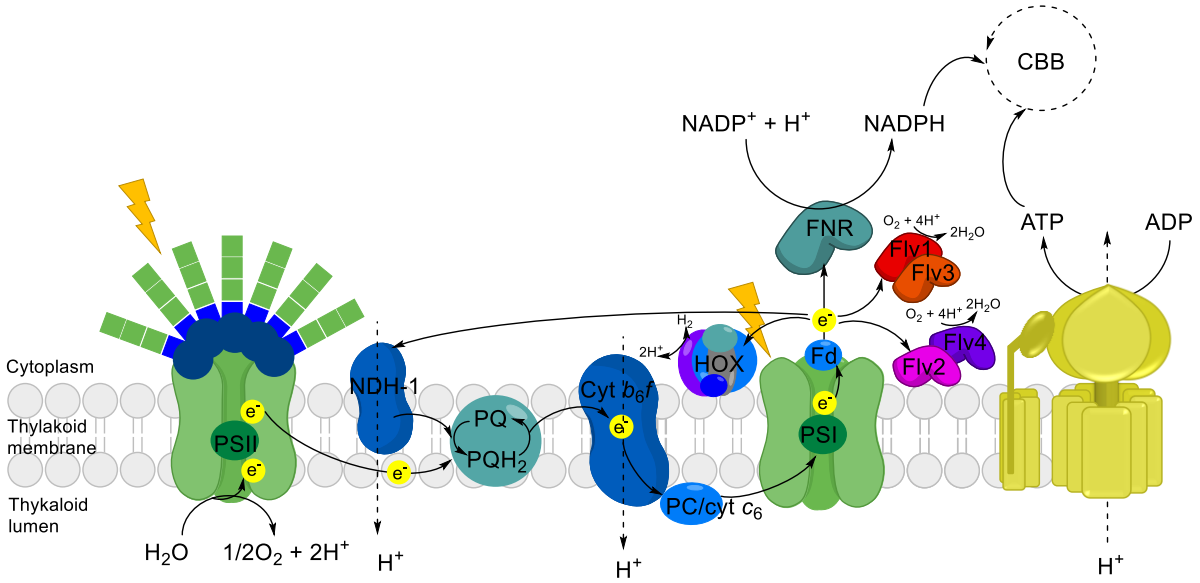


**Figure 1.** Schematics of photosynthetic light reactions in the thylakoid membranes of cyanobacteria. (Adapted from Nikkanen et al., 2021)

The ability to photosynthesize and adapt to variable environments are some of the fundamental reasons for the great potential of cyanobacteria to be used in biotechnological applications (Montgomery, 2014).

## 2. Cyanobacteria as potential hosts for light-driven biotechnology

Cyanobacteria are potential hosts for light-driven biotechnological applications (Calero and Nikel, 2019), with several advantages compared to other photosynthetic organisms, namely plants and algae. In comparison to plants, cyanobacteria are more efficient at capturing solar energy, converting up to 9% of solar energy into biomass compared to only 0.5-3% for higher plants (Dismukes et al., 2008, Branco dos Santos et al., 2014). Cyanobacteria are more amenable to genetic modifications compared to algae, making the engineering of at least a few model strains quite straightforward (Knoot et al., 2018). In addition, the genetic complexity of algae has made their metabolic engineering rather challenging (Gimpel et al., 2015). Furthermore, cyanobacteria display moderately faster growth rates and high $CO_2$ fixation efficiency. Having minimal nutritional requirements allows their growth on arid land, minimizing

the competition with food crops for natural resources (Knoot et al., 2018). Although most of the strains require nitrogen and phosphorus inputs, there has been significant progress growing them in waste and wastewaters usually abundant in these nutrients (Markou and Georgakakis, 2011). In a closed system, nitrogen and phosphorus inputs can be recycled.

Their photosynthetic nature, robust physiology, ability to grow under varying conditions, coupled with their amenability to genetic manipulations, have led to an increased interest in cyanobacteria for renewable and sustainable production of chemicals, especially with the benefit of developments in the field of synthetic biology.

### 2.1. Synthetic biology to enhance solar-powered sustainable biotechnologies

Synthetic biology has emerged as an interdisciplinary field applying engineering approaches to biological systems to generate novel or (re)designed biological networks (Adams, 2016). The applications of synthetic biology could be of key importance to meet some of the large global challenges, in particular accelerating the transition to clean energy resources (Ng et al., 2020). The toolkit of synthetic biology is employed to characterize components unique in different organisms, and incorporate biological parts from different organisms within an engineering framework (Vavitsas et al., 2021). As cyanobacteria have evolved a wide array of useful and unique physiological properties, synthetic biology approaches can be adopted to improve productivity in cyanobacterial hosts/chassis (Luan et al., 2020). Engineering of hosts is mainly assisted by synthetic biology workflow based on building the assembly, testing the output, and generating the knowledge to improve successive design cycles (also called Design–Build–Test–Learn cycle) (Ng et al., 2020). With this approach, we can tap into traits desirable in biotechnological applications, extending the panel of next-generation microbial platforms.

### 2.2. Cyanobacterial chassis for the light-driven biotechnology

One of the core concepts of synthetic biology is the development of the chassis, referring to an organism serving as a foundation housing genetic modules and providing the resources for functioning, such as the transcription and translation machinery. Extensive research efforts have focused on developing tools to rationally design, synthesize, and build genetic networks for tailored biological functions. However, developing the chassis organism attracted far less attention (Adams, 2016). There are several key features to meet the practical necessities of chassis toward biotechnological applications. These include extended basic knowledge of the

microorganism, as a basis for the design of culture media and bioprocesses, particularly focusing on simple nutritional requirements, cheap and available carbon, and if needed nitrogen sources. Important characteristics also focus on resistance to physicochemical stress, fast growth and tolerance to fluctuating conditions. Finally, the availability of tools and the possibility of developing novel ones for genome manipulation is a crucial step toward creating chassis (Calero and Nikel, 2019). There are very few microorganisms that naturally fulfill the traits needed for chassis development. The pioneer chassis were based on the model organisms already established in molecular biology such as *Escherichia coli*, *Bacillus subtilis* and *Saccharomyces cerevisiae* (Adams, 2016). Nevertheless, novel concepts in biotechnology need an expanded repertoire of bacterial chassis. In recent years, cyanobacteria are increasingly becoming attractive chassis to host heterologous pathways to produce a wide variety of fuels, commodity chemicals and value-added products.

Rational design and construction of robust chassis require extensive insight to fully exploit the host's potential, preceding the applications. Recently, several key features essential for chassis development have been summarized (Calero and Nikel, 2019). The enlargement of cyanobacterial resources strengthens the tremendous progress made toward establishing cyanobacterial strains as chassis (Table 1.).

**Table 1.** Key steps required toward chassis development (Calero and Nikel, 2019) and progress associated with cyanobacteria.

| **Feature** | **Resources** | **References** |
|---|---|---|
| Sequenced genomes | CyanoBase | (Fujisawa et al., 2017) |
| *In silico* metabolic models | Several models for *Synechocystis* sp. PCC 6803 | (Fu, 2009, Montagud et al., 2010, Montagud et al., 2011, Knoop et al., 2013) |
| Toolbox of genetic tools | Neutral sites | (Ng et al., 2015, Pinto et al., 2015, Wang et al., 2019a, Nagy et al., 2021) |
| | Plasmids | (Zhou et al., 2016, Ferreira et al., 2018) |
| | Promoters | (Huang et al., 2010, Huang and Lindblad, 2013, Englund |

| | | |
|---|---|---|
| | | et al., 2016, Zhou et al., 2014, Ferreira et al., 2018, Markley et al., 2015) |
| | RBS | Heidorn et al., 2011, Englund et al., 2016, Liu and Pakrasi, 2018, Wang et al., 2018, Thiel et al., 2018) |
| | Riboswitches | (Nakahira et al., 2013, Pérez et al., 2016, Ohbayashi et al., 2016) |
| | Terminators | (Liu and Pakrasi, 2018) |
| | CRISPR/CRISPRi | (Yao et al., 2020, Gordon et al., 2016, Li et al., 2016, Wendt et al., 2016, Xiao et al., 2018) |
| Physiological characterization | CyanoEXpress, CyanoOmicsDB | (Hernandez-Prieto and Futschik, 2012)<br>(Zhou et al., 2021) |
| Mutant collection | Upcoming CyanoSource: A Barcoded Mutant Library for *Synechocystis* sp. PCC 6803 | (Gale et al., 2019) |

Nevertheless, there are still challenges when engineering cyanobacteria as chassis for light-driven biotechnology. One of them being the poor performance in cyanobacteria of the existing parts developed for established hosts such as *E.coli*, *B. subtilis* and *S.cerevisiae* (Huang et al., 2010). Tools cannot always be directly transferred between organisms, due to differences in transcriptional machinery, genetics, and regulation (Stensjö et al., 2018). In recent years, there have been several studies focusing on developing customized tools for different cyanobacterial chassis with a particular focus on achieving tight, dynamic, specific and orthogonal regulation of multiple parts, allowing stable pathway maintenance and predictable performance under conditions relevant to commercial applications (Hitchcock et al., 2020). These tools are especially in the need of achieving long-term strain stability. However, they still generally lag behind those routinely used in heterotrophic microbes. Therefore, the development and availability of synthetic biology toolboxes for the standardized assembly of genetic constructs is important.

Another particular challenge of cyanobacterial genetic manipulation is polyploidy, referring to harboring multiple copies of genome per cell, depending on the strain, growth phase and growth conditions (Watanabe, 2020). This prolongs the period to obtain fully segregated clones. Therefore, a better understanding of polyploidy could lead to the generation of clones with fewer genome copies per cell. This could speed up further genome modification, however, may come with undesirable consequences to cell fitness (Hitchcock et al., 2020). Finally, decreased bioproduction due to genetic instability of heterologous pathways has been observed and may constitute an additional drawback (Jones, 2014).

To economically compete with already established biotechnological platforms it is essential increasing the productivity of engineered strains. Providing tailored microbes by rational manipulation of the microbial physiology, stress response or engineering the core metabolism in the selected chassis will be necessary. Moreover, designing chassis with the end goal in mind is a notably important aspect of the development.

### 2.3. Engineering chassis as improved bioproduction platforms

Cyanobacteria are promising chassis for various biotechnological applications. However, on the road to becoming economically feasible, employing strategies of rational engineering offers significant improvements. The emphasis is to optimize chassis toward improved conversion of light energy into value-added compounds. The theoretical predictions showed that photosynthetic photon-to-biomass conversion efficiency is around 10–13%, whereas in reality efficiency rarely surpasses 1-3% (Melis, 2009). In natural environments, cyanobacteria have been selected to survive, but do not have the ability to produce a desired maximal amount of biomass or target products. Although the photosynthetic reducing power is abundant, intrinsic regulation of light-harvesting and photosynthetic electron transport together with the competition from native electron transfer pathways may form hurdles (Russo et al., 2019). Particularly, the amount of light energy captured during photosynthesis is often larger than needed in metabolic reactions and excess energy is usually dissipated (Foyer and Noctor, 2009). With bioengineering, this can be seen as an opportunity to take the advantage of otherwise wasted reducing energy and to redirect it toward commercially valuable chemicals. Therefore, in recent years, there has been a variety of engineering strategies using synthetic biology and metabolic engineering to improve cyanobacterial chassis. The focus was on different aspects of cyanobacterial metabolism, from expanding the absorbed

photosynthetic spectrum to balancing absorbed light energy and metabolic capacity (Luan et al., 2020) (Fig. 2).

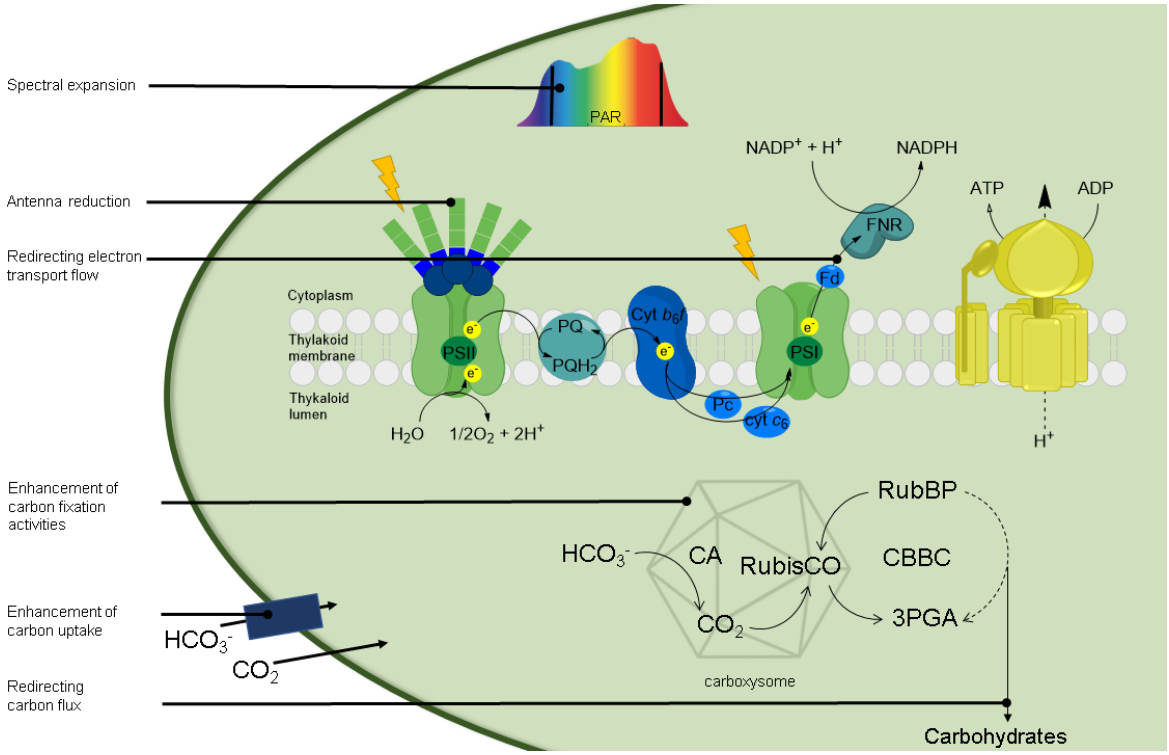


**Figure 2.** Different strategies employed for engineering cyanobacterial chassis toward improved productivities (Adapted from Luan et al., 2020).

### 2.3.1. Expanding the range of light absorption

Light-harvesting efficiency, referring to the efficiency of light energy conversion to chemical energy is one of the factors that could be improved in cyanobacteria (Chen and Blankenship, 2011). Most cyanobacteria can utilize solar energy in the visible light range from 400 to 700 nm (Blankenship, 2021). Particularly, the absorption of visible light is concentrated in a narrow band from 660 to 700 nm, while absorption of the green band (450–550 nm) is relatively weak, a phenomenon known as the 'green gap' (Gundlach et al., 2009). Broadening the cyanobacterial spectral absorption offers revenue for improved light conversion efficiency. One of the approaches focused on broadening the absorption spectra to include 750 nm that could lead to a 19% increase in the available photons (Chen and Blankenship, 2011, Blankenship et al., 2011). The discovery of red-shifted chlorophyll *d* (Miyashita et al., 1996) and *f* (Chen et al., 2010) having absorption peaks above 700 nm offers promising improvement of photosynthetic efficiency by harvesting infrared energy (Chen et al., 2010,

Miyashita et al., 1996). To extend the photosynthetically active radiation, heterologous synthesis of chlorophyll *f* was attempted in *Synechococcus* sp. PCC 7002 (Shen et al., 2019, Tros et al., 2020), resulting in a rather small absorption in far-red light. An additional promising engineering approach was focused on filling the 'green gap' by the proteorhodopsin–retinal system. This was recently tested by expressing a green-absorbing proteorhodopsin in a PSI-deletion strain of *Synechocystis* sp. PCC 6803 leading to an increased growth rate (Chen et al., 2019).

### 2.3.2. Antenna reduction for optimal energy conversion

To thrive in environments with fluctuating light intensities, cyanobacteria have maximized the expression of pigments and antennae complex (Melis, 2009). The light-harvesting antennae have evolved to capture as much solar energy as possible under natural conditions, where cells usually face light-limiting conditions. Under conditions encountered in photobioreactors, excessive photon capture by the cells in the surface layer can reduce the light availability for the cells underneath (Melis, 2009). Therefore, truncating antennae complex has been proposed as an approach to enable deeper light penetration into the cultures leading to increased light absorption and consequently culture productivity (Montgomery, 2014). Minimizing the light-harvesting antenna complex has been the focus of several studies (Lea-Smith et al., 2014, Ajlani and Vernotte, 1998). One study showed that minimizing the antennae size through deletion of *apcE* gene, encoding the anchor protein linking the phycobilisome to the thylakoid membrane, improved biomass production by 60% (Joseph et al., 2014). In another study, the excess absorption of light has been minimized by creating a phycocyanin-deletion mutant which enhanced biomass production by 57% (Kirst et al., 2014).

### 2.3.3. Redirecting photosynthetic electron flux

The imbalance between the energy supply and metabolic requirements can be described as one of the limiting factors affecting photosynthetic efficiency. From the theoretical calculations, the light reaction generates a ratio of 2.57 ATP/2 NADPH, whereas a ratio of 3 ATP/2 NADPH is required for the $CO_2$ fixation (Kramer and Evans, 2011). Therefore, to better balance the ATP/NADPH ratio between light and dark reactions, it was hypothesized that increasing the consumption of NADPH generated from the light reactions might improve the photosynthetic efficiency. This hypothesis was tested by introducing an NADPH-consuming pathway into *Synechocystis* sp. PCC 6803 and indeed resulted in enhanced photosynthetic efficiency and biomass production (Zhou et al., 2016). Similarly, the expression of an artificial electron sink,

NADPH-consuming mammalian cytochrome P450, increased the maximum rate of photosynthetic electron flow by 31.3% (Berepiki et al., 2016). Additionally, the coexpression of two heterologous sinks had additive impacts on the photosynthetic efficiency (Santos-Merino et al., 2021).

Cyanobacteria have evolved several protection mechanisms to mitigate the overcapacity of the light reactions and prevent over-reduction of the photosynthetic electron transport chain that can lead to the generation of reactive oxygen species and subsequent photoinhibition (Lea-Smith et al., 2016). In recent years, rational engineering of alternative electron transfer routes, particularly involved in photoprotection, has been gaining attention. Main protein complexes involved in redirecting electron flux, such as flavodiirons, hydrogenases and dehydrogenase complex (Mullineaux, 2014) have been the focus of several studies to rationally engineer electron flow. One study showed deleting a subunit of the type I NADH dehydrogenase complex, suggested to be involved in cyclic photosynthetic electron flow, resulted in increased activity of heterologous cytochrome P450 (Berepiki et al., 2018). Several studies focused on flavodiiron proteins, crucial players in alleviating excessive reduction of the electron transfer chain (Allahverdiyeva et al., 2013). In a recently published study, it is suggested that deletion of *flv3* could be an approach to optimize the electron flux between photosynthetic light reactions and the downstream biosynthetic pathways funneling cellular resources more effectively towards the generation of target chemicals (Thiel et al., 2019). Indeed, the elimination of *flv1*/*3* in *Synechocystis* increased the specific activity and product formation rate of the heterologous ene-reductase (Assil-Companioni et al., 2020). Also, a similar approach led to an increase in D-lactate production in *Synechococcus* sp. PCC 7002 expressing D-lactate dehydrogenase (Selão et al., 2020). Interestingly, overexpression of *flv3* leads to increased ATP supply and biomass accumulation (Hasunuma et al., 2014).

### 2.3.4. Enhancing carbon fixation activity and utilizing carbon sinks

Most of the metabolic engineering of cyanobacteria has focused on improving or redirecting carbon metabolism. Several approaches have been proven useful for enhancing biomass and increasing the production of compounds of interest. Cyanobacteria have evolved highly effective carbon concentrating mechanisms, absorbing $CO_2$ and $HCO_3^-$ and concentrating them in the carboxysomes, to prevent photorespiration and enhance the activity of enzymes involved in the CBB cycle (Wang et al., 2012). Enhancing carbon uptake by overexpression of the *bicA* gene, encoding bicarbonate transporter led to the improved growth rate of

*Synechocystis* (Kamennaya et al., 2015). Overexpression of selected enzymes of the CBB cycle (ribulose-1,5-bisphosphate carboxylase/oxygenase, sedoheptulose 1,7-biphosphatase and fructose-bisphosphate aldolase) led to an increase in oxygen evolution activity and growth rates (Liang and Lindblad, 2016). Other studies showed enhancing the carbon fixation rate can be an approach to increase ethanol production (Liang et al., 2018, Roussou et al., 2021). Previous studies showed that cyanobacterial strains with engineered extra carbon sinks, either through their incorporation in particular products or through the export of carbon-based compounds, exhibited higher rates of $CO_2$ assimilation and enhanced photosynthetic efficiency (Montgomery, 2014), demonstrated during the rerouting of carbon flux into the production of sucrose (Ducat et al., 2012) and 2,3-butanediol (Oliver et al., 2013). This could be a direction to further enhance photosynthetic efficiency and improve the productivity of selected chassis. Reducing carbon partitioning into storage compounds and subsequent rerouting to the desired product offers another direction of improved productivities. This was shown with the inactivation of PHB biosynthesis that led to increased yields of 3-hydroxybutyrate (Wang et al., 2013), and in the glycogen storage deficient mutant that exhibited improved production of lactic acid (van der Woude et al., 2014).

### 2.4. Model cyanobacterial strains and emerging strains

The different engineering approaches toward chassis optimization mentioned above have been performed using several cyanobacterial model strains, predominantly *Synechocystis* sp. PCC 6803, but also *Synechococcus elongatus* PCC 7942, *Synechococcus* sp. PCC 7002 and *Nostoc* sp. PCC 7120 (Table 2). *Synechocystis* sp. PCC 6803 is a non-nitrogen fixing freshwater strain being the first autotrophic microorganism to have its genome fully sequenced (Kaneko et al., 1996). It has been extensively studied and used in synthetic biology, being recognized as the “green *E.coli*” (Branco dos Santos et al., 2014). *Synechococcus elongatus* PCC 7942 has been extensively used as a model organism for studying the prokaryotic circadian clock (Cohen and Golden, 2015). Filamentous *Nostoc* sp. PCC 7120 has been used as a model organism to study cellular differentiation (Kumar et al., 2010) as it has the capability of fixing nitrogen by forming heterocysts, differentiated cells for fixing dinitrogen (Cai and Wolk, 1997, Herrero et al., 2001). Recently, *Synechococcus* PCC 7002 has been gaining attention as a fast-growing, naturally transformable marine strain (Bernstein et al., 2016).

**Table 2.** Selected model cyanobacterial strains (Adapted from Santos-Merino et al., 2019).

| Strain | Genome size | Doubling time | Lifestyle features |
|---|---|---|---|
| *Synechocystis* sp. PCC 6803 | 3.5 Mb | 6-12 h | Freshwater, unicellular |
| *Synechococcus elongatus* PCC 7942 | 2.7 Mb | 5 h | Freshwater, unicellular |
| *Nostoc* sp. PCC 7120 | 6.4 Mb | 14 h | Freshwater, filamentous |
| *Synechococcus* PCC 7002 | 3.0 Mb | 2.6 h | Euryhaline, unicellular |

In recent years there has been a wide exploration of novel cyanobacterial strains, particularly focusing on fulfilling criteria needed for prospective industrial applications. These characteristics include traits such as fast growth, high biomass accumulation and/or resistance to a variety of abiotic stress, particularly high light and salinity (Santos-Merino et al., 2019). One of the most promising candidate is *Synechococcus elongatus* UTEX 2973 with the shortest doubling time of 1.9 h under optimal growth conditions (Yu et al., 2015). This strain was of particular interest to study genetic changes associated with the fast growth that were further introduced into *Synechococcus elongatus* PCC 7942. This resulted in a reduction of doubling time from 8.5 h to 3.1 h, with increased tolerance to high light and temperature (Ungerer et al., 2018). New promising candidates have been described recently including *Synechococcus elongatus* PCC 11801 having a higher growth rate under atmospheric $CO_2$ (Jaiswal et al., 2018) and *Synechococcus elongatus* PCC 11802 showing faster growth at high $CO_2$ and elevated temperature conditions (Jaiswal et al., 2020). Finally, high biomass production candidate *Synechococcus* sp. PCC 11901 was recently described as reaching 32.6 g $L^{-1}$ of dry weight biomass (Włodarczyk et al., 2020).

These cyanobacterial chassis strains will boost the evolution of synthetic biology beyond the proof-of-concept stage and closer to industry-relevant applications. One of the fields that thrive from the utilization of cyanobacteria and can benefit from rational engineering of the chassis is biocatalysis. A significant amount of fundamental research can pave the way for

the development of commercially viable, engineered cyanobacteria with the desired properties to achieve improved productivity.

## 3. The role of biocatalysis toward sustainability

The growing and numerous applications of biocatalysts in various industrial sectors have been recognized as a key technology for a more rapid transition toward a sustainable bioeconomy (Wohlgemuth, 2021). The phenomenal advances in enzyme discovery combining metagenomics with the power of bioinformatics and directed evolution for enzyme improvement have revolutionized biocatalysis in the last two decades (Sheldon et al., 2020). Advances in protein engineering through rational design, *in silico* modeling and the infiltrated power of machine learning through recently described AlphaFold (Jumper et al., 2021) will enable offering enzymes tailored toward targeted process parameters, such as activity, specificity and stability (Sheldon and Woodley, 2018, Bell et al., 2021).

With the abovementioned innovations, biocatalysis has become a state-of-the-art approach for the synthesis in the pharmaceutical, fine chemical, agriculture, food and polymer industries, with several excellent examples that reached commercial scales demonstrating the versatility of this approach (Prier and Kosjek, 2019, Bell et al., 2021).

Notably, the synthesis and production of the high-price low-volume complex molecules, such as pharmaceuticals, represent the industrial sector where biocatalysis had the greatest contribution, tapping into outstanding selectivity of the enzymes with several hundred processes in operation (Woodley, 2019, Bell et al., 2021). Examples of biocatalytic synthesis of atorvastatin (Ma et al., 2010) and sitagliptin (Savile et al., 2010), have set standards to demonstrate the feasibility of biocatalysis.

The widespread use of biocatalysis is also a consequence of numerous economic and environmental benefits. Biocatalytic reactions offer several advantages over established chemical synthesis, complying with 10 out of 12 green chemistry principles founded for the design of sustainable chemical processes (Table 3). The remaining two (principles 4 and 10) are not being relevant because they relate to the product, rather than the process design (Anastas and Eghbali, 2010, Sheldon and Woodley, 2018).

**Table 3.** The 12 principles of green chemistry for the design of new chemical products and processes and solutions offered by biocatalysis (Adapted from Sheldon and Woodley, 2018).

| Green chemistry principle | Biocatalytic solution |
|---|---|
| Waste prevention | Significantly reduced waste |
| Atom economy | More atom- and step-economical |
| Less hazardous synthesis | Generally low toxicity |
| Design for safer products | *Not relevant* |
| Safer solvents and auxiliaries | Usually performed in water |
| Energy efficiency | Mild conditions/energy-efficient |
| Renewable feedstocks | Enzymes are renewable stocks |
| Reduced derivatization | Avoids protection/deprotection steps |
| Catalysis | Enzymes are catalysts |
| Design for degradation | *Not relevant* |
| Real-time analysis | Applicability to biocatalytic processes |
| Inherently safer processes | Mild and safe conditions |

Biocatalysts are produced from renewable sources such as biomass being biocompatible, biodegradable, non-hazardous and non-toxic. The utilization of enzymes provides an alternative for using scarce metals as catalysts and avoids the costs of removing metal traces from the end products. Enzymatic reactions generally avoid the need for functional-group activation, protection, and deprotection steps, allowing routes with fewer steps producing less waste than conventional organic synthesis. Furthermore, biocatalytic reactions run under mild reaction conditions including ambient temperature, atmospheric pressure, and usually neutral pH. High regio-, chemo- and stereoselectivity of enzymes lead to shorter routes, resulting in substantial savings in terms of costs, energy and waste formation (Sheldon et al., 2020, Sheldon and Woodley, 2018).

Several important parameters have been established to assess biocatalytic reactions and benchmark them against industry standards to understand bottlenecks and required biocatalyst development and process improvements. These parameters include economic and green chemistry metrics (Table 4).

**Table 4.** Metrics used to evaluate the efficacy of the biocatalytic processes (Adapted from Grimm and Kourist, Bell et al., 2021).

| | Parameter | Commonly used unit | Description |
|---|---|---|---|
| **Economic metrics** | Conversion | $mol_{product}\ mol_{substrate}^{-1}$ | Represents how much of the initially provided substrate was transformed into a product |
| | Isolated yield | $mol_{product}\ mol_{substrate}^{-1}$ | Product concentration in correlation to the provided amount of substrate or the total amount of isolated product |
| | Initial reaction rate | $g_{product}\ h^{-1}$<br>$mol_{product}\ h^{-1}\ L^{-1}$ | The velocity of the reaction in the time interval with less than 10% conversion |
| | Specific activity [$A_{spec.}$] | $\mu mol_{product}\ g_{catalyst}^{-1}\ min^{-1}$ | Expresses how much product is converted by the given amount of catalysts in a specific time interval |
| | Productivity | $g_{product}\ g_{catalyst}^{-1}$<br>$mol_{product}\ g_{catalyst}^{-1}$ | The total product formed using a specific amount of catalyst |
| | Space-time yield | $g_{product}\ L^{-1}\ h^{-1}$ | Quantity of product per unit of volume and time |
| | Enantiomeric excess (*ee*) | % | Excess of one enantiomer in a mixture of both enantiomers |
| **Green chemistry metrics** | Atom economy | $g\ mol^{-1}$ per $g\ mol^{-1}$ | The molecular weight of the desired product as a function of the sum of the molecular weight of all products |
| | *E* factor | $g\ g^{-1}$ | Amount of waste made as a function of the amount of product made |

| | | |
|---|---|---|
| *C* factor | g $g^{-1}$ | Amount of $CO_2$ equivalents as a function of the amount of product made |
| Process mass intensity | g $g^{-1}$ | Amount of raw material input as the function of the amount of the desired product made |

### 3.1. The bottlenecks of the application of redox enzymes

NAD(P)H-dependent oxidoreductases are a versatile group of enzymes of great interest from an industrial point of view as they perform the critical steps in the production of many hard-to-synthesize compounds (Vidal et al., 2018). These redox enzymes catalyze the reduction or oxidation of a substrate, and they represent the largest class of enzymes including some of the most widely employed industrial biocatalysts (Prier and Kosjek, 2019). Members of this enzyme class have gained interest in asymmetric synthesis due to their high enantioselectivity. Stereoselective catalysis is of particular interest for the production of stereoisomeric compounds due to distinctly different properties, reactivities and chemical or biological functions of different enantiomers. The importance of asymmetric catalysis is highlighted by the 2021 Nobel prize in chemistry awarded for organic catalysts developed by List and MacMillan. One of the most widely employed synthetic steps is the asymmetric hydrogenation of alkene bonds, with the generation of up to two stereogenic centers. A biocatalytic alternative for this transformation gained attention, through the application of flavin-dependent ene-reductases, which are members of the ‘old yellow enzyme’ family (OYE) (Faber, 2011). Since the discovery of the ene-reductases in the 1930s, over 100 proteins of this family have been identified in microorganisms and plants, having different physiological roles, such as being part of the biosynthesis of secondary metabolites or detoxification of xenobiotics. Due to their remarkably high enantioselectivity with a broad range of substrates, they have been employed in the synthesis of amino acid derivatives, terpenoids, fragrance compounds and chiral building blocks (Winkler et al., 2012, Parmeggiani et al., 2021). The catalytic mechanism of the ene-reductase-catalyzed reduction of alkenes has been studied in great detail (Kohli and Massey, 1998). During the ‘oxidative half reaction’, hydride derived from a reduced flavin cofactor is stereoselectively transferred onto Cβ, while a Tyr-residue adds a proton which is derived from the solvent onto Cα from the opposite side (Fig. 3). As

the result of the stereochemistry of this mechanism, the overall addition of [$H_2$] proceeds in a *trans*-fashion with absolute stereospecificity. The catalytic cycle is completed by the 'reductive half reaction' via reduction of the oxidized flavin cofactor at the expense of NAD(P)H (Faber, 2011). It has been also described that reduced flavin cofactor can oxidase molecular oxygen leading to the formation of hydrogen peroxide. This is commonly known as cofactor decoupling, where reducing equivalents are consumed but the desired product is not formed.

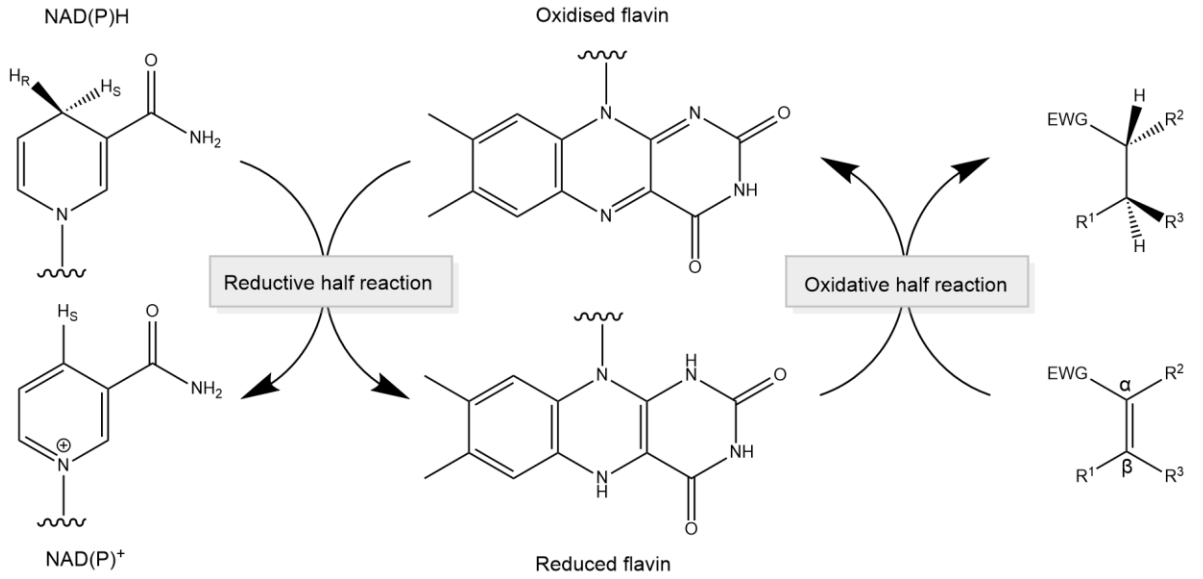


**Figure 3.** Asymmetric bioreduction of activated alkenes using ene-reductases. EWG=electron withdrawing group (Adapted from Kohli and Massey, 1998).

One of the most prominent member of the class is ene-reductase YqjM, originally from *Bacillus subtilis* and suggested to be involved in the oxidative stress response (Fitzpatrick et al., 2003). The crystal structure of a YqjM revealed a new subclass of OYEs with unique structural properties, such as its occurrence as a homotetramer and distinct sequence features (Kitzing et al., 2005). YqjM accepts both NADPH and NADH as cofactors, however, shows a preference for NADPH (Fitzpatrick et al., 2003). YqjM was subjected to iterative saturation mutagenesis studies to generate variants with an improved catalytic ability (Bougioukou et al., 2009) The biocatalytic potential of this enzyme has been investigated extensively, due to remarkably broad substrate spectrum (Hall et al., 2008, Winkler et al., 2012, Toogood and Scrutton, 2018).

The application of oxidoreductases, such as ene-reductases, is dependent on the addition of cofactors such as NADPH or NADH. The high price of nicotinamide cofactors (eg. NADPH costs ~1 500 €/1 g, Merck KGaA, Germany) limits the addition of stoichiometric amounts and

the large-scale application. Their cofactor-dependency has for a long time been regarded as a major hurdle for preparative applications (Hollmann et al., 2011). To be useful on an industrial-scale one of the requirements for the enzyme process is that cofactors and other reagents must be economically supplied or regenerated (Prier and Kosjek, 2019). Therefore, several recycling strategies ranging from chemical, electrochemical, photochemical, microbial to enzymatic reactions have been developed for the *in situ* recycling of cofactors (Liu and Wang, 2007). This is achieved by adding a large excess of a co-substrate e.g. isopropanol or the second enzyme in combination with a co-substrate. The widely used combinations are formate/formate dehydrogenase (FDH) and glucose/glucose dehydrogenase (GDH) (Fig. 4). However, applying oxidoreductases with the established cofactor recycling systems often encounters low atom economy, as only a fraction of the electrons of sacrificial co-substrates is being utilized. Additional issues are cost and effort for the separation of side-products. Therefore, these approaches jeopardize green chemistry principles.

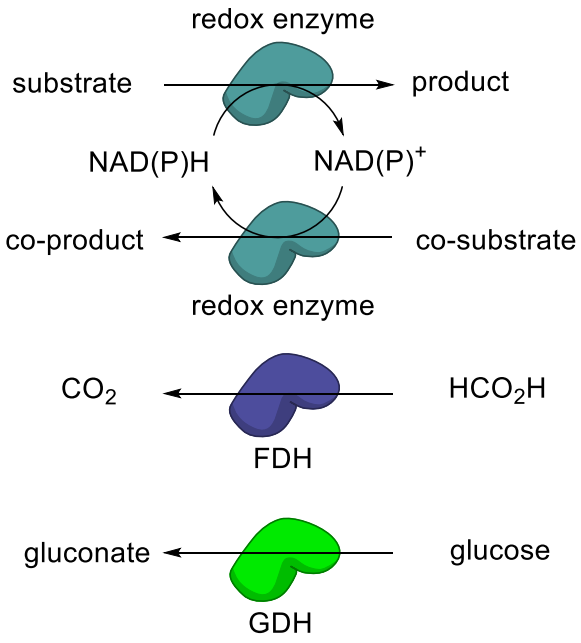


**Figure 4.** Schematic representation of the most common *in vitro* systems for cofactor recycling (Adapted from Sheldon et al., 2020).

Complicated molecular architecture and poor stability of the isolated enzyme, together with cofactor requirements somewhat resulted in the application of oxidoreductases mainly as a whole-cells system (Hollmann et al., 2011, Vidal et al., 2018). Whole-cell biotransformations performed in heterotrophic microorganisms such as *E. coli*, usually rely on enhanced cofactor regeneration systems, mainly via mimicking the methods for *in vitro* cofactor recycling by co-

expressing dehydrogenases, most commonly FDH and GDH, and supplying the sacrificial co-substrates (Kratzer et al., 2015). However, in this case, co-substrates might be used suboptimally, since they might also be used elsewhere in the metabolic processes of host organisms, resulting in a further decrease of atom economy. Additionally, microbial cells can contain various variants of the actual production enzyme exhibiting complementary selectivity, resulting in poor (enantio)selectivities (Hollmann et al., 2011).

### 3.2. Cofactor recycling in autotrophic microorganisms

To overcome the challenge of sustainable cofactor recycling systems and substitution of sacrificial organic co-substrates, coming closer to a better atom economy, several biological platforms gained attention for the renewable production of chemicals based on advantageous cofactor recycling systems. These platforms include chemolithoautotrophic and autotrophic microorganisms, such as *Cupriavidus necator*, *Rhodobacter sphaeroides* and several cyanobacterial strains.

Hydrogen-driven cofactor regeneration hosted in *Cupriavidus necator* has been an interesting approach already shown to sustain the activity of heterologously expressed alcohol dehydrogenase (Oda et al., 2013) and ene-reductase (Assil-Companioni et al., 2019). However, providing a mixture of $H_2$, $O_2$, and $CO_2$ requires special care as this is in the gas explosion range that could be an obstacle for the further development of this approach.

Light-driven cofactor regeneration systems hosted in easy to handle autotrophic microorganisms, offer an attractive approach to circumvent this problem. *Rhodobacter sphaeroides*, a metabolically versatile anoxygenic photosynthetic organism, has been engineered to express alcohol dehydrogenase for the synthesis of a chiral alcohol (Ma et al., 2017). However, this organism uses thiosulphate as an electron donor, where only oxygenic photosynthesis allows utilizing water as a reductant.

Coupling whole-cell redox reactions to photosynthesis in cyanobacteria allow for the substitution of sacrificial organic co-substrates using water splitting as the stoichiometric reductant, tapping into photosynthetic machinery to generate NADPH and concomitantly regenerate used $NADP^+$ (Fig. 5).

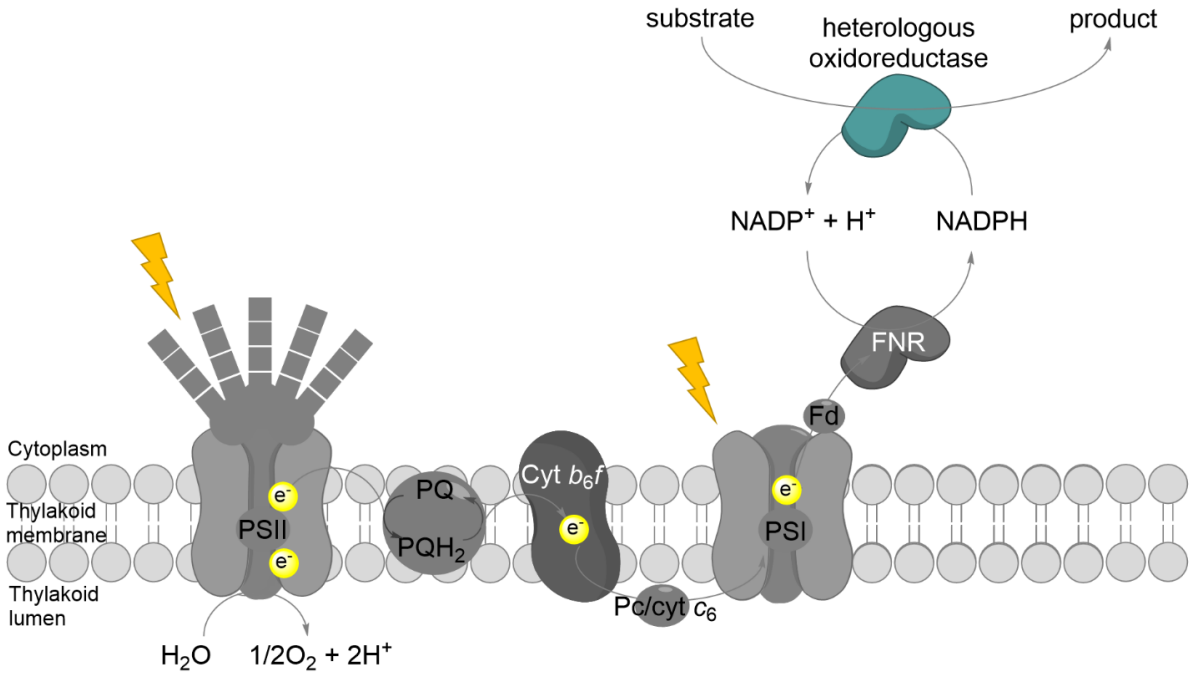


**Figure 5.** Schematic representation of harnessing photosynthetic reductants for biocatalytic reactions performed by heterologous oxidoreductases.

To fully utilize cyanobacteria as hosts for redox enzymes several points should be considered. Cyanobacteria have higher intracellular NADPH levels compared to NADH, reported to be up to 6.5-fold higher (Tamoi et al., 2005). However, heterotrophic hosts usually used in biotransformations, such as *E.coli*, have 4 to 5 times higher levels of NADH compared to NADPH (Meyer et al., 2006). Therefore, to efficiently couple enzymes with the expression hosts for helpful provision and recycling of cofactors, NADPH-dependent enzymes are of preference for the heterologous expression in cyanobacteria. However, even if NADH-dependent enzyme is of interest to be expressed, recent studies offer several alternatives. Increasing intracellular NADH level can be achieved by balancing cofactors through co-expression of a soluble transhydrogenase catalyzing conversion between NADPH and NADH (Angermayr et al., 2012, Varman et al., 2013). Additionally, exchanging cofactor specificity of the enzymes can be an approach to match the cyanobacterial host (Richter et al., 2011, Lerchner et al., 2016). To predict specific mutations which might allow reversal of the cofactor specificity of a given NAD(P)H-dependent oxidoreductase, we can benefit from computational tools such as CSR-SALAD (Cahn et al., 2017).

Cyanobacteria are attractive hosts for biocatalytic oxyfunctionalization supplying reducing equivalents and by-product $O_2$ via photosynthetic water splitting. However, $O_2$ can be

detrimental for an oxygen-sensitive enzyme. In the case of enzymes such as ene-reductases, a certain $O_2$ sensitivity was observed, as they can act as NADPH oxidase in the absence of the substrate. The issue of oxygen-sensitive enzymes can be overcome utilizing spatial segregation based on natural compartmentalization recently demonstrated for a 1,3-propanediol biosynthetic pathway insulated within heterocysts (Liu et al., 2018).

### 3.3. Cyanobacteria as chassis for light-driven biotechnology

Cyanobacteria have been predominantly seen as chassis for the direct conversion of $CO_2$ into a final product. Therefore, over the years wild-type and engineered strains have been extensively studied for product formation directly from $CO_2$, light and water (Angermayr et al., 2015, Knoot et al., 2018). Cyanobacterial, or 'solar', cell factories are a particularly advantageous strategy as an alternative for the heterotrophic production platforms that require plant-derived fermentable sugars and therefore compete with food production (Knoot et al., 2018). Some of the first studies using engineered cyanobacterial strains focused on the production of ethylene (Sakai et al., 1997), ethanol (Deng and Coleman, 1999) and pigments (Lagarde et al., 2000). In the last 20 years, subsequent studies established cyanobacterial cell factories to produce a range of value-added products. Significant progress with the help of metabolic engineering and synthetic biology has resulted in several excellent examples, such as isobutyraldehyde and isobutanol (Atsumi et al., 2009), lipids (Liu and Curtiss, 2009), fatty acids (Liu et al., 2011), D-lactic acid (Varman et al., 2013), and butanediol (Oliver et al., 2013). Extension to the production of low-titer-high-price products, such as terpenoids (Pattanaik and Lindberg, 2015), limonene (Kiyota et al., 2014) and caffeic acid (Xue et al., 2014), underlines that the improvement in synthetic biology tools and a better understanding of the cyanobacterial metabolism helps to develop their bioengineering potential.

Streamlining photosynthetically activated electrons, derived from water-splitting, to power biotransformations has gained less attention, however, constitutes an interesting approach for the development of a circular economy.

### 3.4. Light-driven whole-cell biotransformations in wild-type cyanobacteria

The feasibility to provide and recycle cofactors, such as NADPH, within cyanobacteria posses an outstanding potential. Already in 1986, the first study was published using five cyanobacterial wild-type strains for the biotransformations of aldehydes and ketones (Jüttner and Hans, 1986). In the last 20 years, several studies were published using wild-type

cyanobacterial strains as biocatalysts for the reduction of prochiral ketones, enones, maleimides, terpenes, hydrocortisone, oxophosphonates and chalcones (Nakamura et al., 2000, Nakamura and Yamanaka, 2002, Hamada et al., 2003, Yamanaka et al., 2015, Shimoda et al., 2004, Havel and Weuster-Botz, 2006, Yazdi et al., 2004). Wild-type strains can be an excellent starting point exploring innate enzymes and are still being employed in recently published studies (Tanaka et al., 2020, Fan et al., 2021). However, the low product concentrations with a long reaction time emphasize considerable limitations toward advanced applications.

Further development coming closer to industry requires optimized levels of enzyme expression and/or expression of heterologous enzymes. When we employ heterologous enzymes, the reaction mechanisms, selectivity and preferred reaction conditions are often better understood, which is of great advantage for further development and applications. This is a necessity, particularly when developing an alternative process to already established routes of chemical synthesis. With the advances in genetic engineering tools, the field of photobiocatalysis expanded to heterologously expressed enzymes hosted in cyanobacteria.

### 3.5. Light-driven whole-cell biotransformations in engineered cyanobacteria

In recent years, an increasing number of examples demonstrated the power of photobiocatalysis hosted in cyanobacteria, focusing on reductive biotransformations and oxyfunctionalizations. Up to date, the light-driven biotransformations in engineered cyanobacteria have been hosted in two model organisms, namely *Synechocystis* sp. PCC 6803 and *Synechococcus elongatus* PCC 7942. The proof-of-concept of photosynthetic reductive biotransformation with heterologous oxidoreductases in cyanobacteria was performed by expression of the ene-reductase from *Bacillus* sp. in *Synechocystis* sp. PCC 6803. The cells converted a series of seven substrates with the initial reaction rates above 100 U $g_{CDW}^{-1}$ (Köninger et al., 2016). Further optimization, by promoter exchange and deletion of native electron sinks led to improved reaction rates (Assil-Companioni et al., 2020). Several studies followed, expressing enzymes such as imine reductases for the conversion of prochiral imines into stereoselective amines (Büchsenschütz et al., 2020), alcohol dehydrogenase for asymmetric conversion of acetophenone to chiral 1-phenylethanol (Sengupta et al., 2019) and the most recently published study including hydroxyisocaproate dehydrogenases (Jurkaš et al., 2021). Additionally, oxyfunctionalizations were demonstrated using alkane monooxygenase for hydroxylation of nonanoic acid methyl ester to ω-hydroxynonanoic acid methyl ester (Hoschek et al., 2017), further applied in a continuous

system (Hoschek et al., 2019a). A recent study explored hydroxylation of cyclohexane to cyclohexanol based on the expression of a cytochrome P450 monooxygenase (Hoschek et al., 2019c). Finally, two studies focused on exploring heterologous Baeyer–Villiger monooxygenases for oxidation of cyclic ketones (Böhmer et al., 2017, Erdem et al., 2021).

These studies demonstrate that engineered cyanobacteria are beneficial for reductive biotransformations and oxyfunctionalizations due to the light-driven cofactor regeneration and/or oxygen formation. This paves the way for more sustainable biocatalysis in the future, shifting the paradigm of cyanobacteria as solely $CO_2$ converting factories toward biocatalysts converting compounds that are essential building blocks in pharmaceutical and fine chemical industries. Several biotechnological challenges need to be addressed and overcome before light-powered biotransformations become commercially viable. Up to date, the published studies are primarily proofs-of-concept. However, commercialization of the technology has yet to be realized. Some of the targets to improve biocatalytic reactions could be further utilization of synthetic biology toolbox to optimize the enzyme levels or improve the host organism focusing on photosynthetic efficiency and electron flow. However, further advancement of the photobiocatalytic field is required also in the scale-up systems used for running the reactions.

### 3.6. Challenges and opportunities for scaling up light-driven biotransformations

Recent years have seen enlargement of the library of cyanobacterial light-driven biocatalysts including various bioengineering approaches toward improved productivities. However, bioprocess engineering required for scaling up has received far less attention (Knoot et al., 2018). It is important to highlight factors of commercial success lie mainly in the productivity and stability of the engineered strains in industrial settings. Further on, if a technology is not economically competitive, it will not be sustainable in the long term (Knoot et al., 2018, Sheldon and Woodley, 2018).

To become economically feasible, fine chemical synthesis requires a minimum space-time-yield of 0.1 g $L^{-1}$ $h^{-1}$ and a minimum final product concentration of 1 g $L^{-1}$ (Straathof et al., 2002). For pharmaceuticals, estimated minimum process requirements are space-time-yield of 0.001 g $L^{-1}$ $h^{-1}$ and product concentration of 0.1 g $L^{-1}$ (Straathof et al., 2002, Julsing et al., 2008). Regarding biotransformations, this can be achieved with high specific activities of >100 U $g_{CDW}^{-1}$ and/or high cell densities of >10 $g_{CDW}$ $L^{-1}$ (Hoschek et al., 2018).

During scale-up efficient substrate supply and product removal, appropriate $CO_2$ dispersion and $O_2$ degassing have to be achieved (Bux and Chisti, 2016). However, the main challenges of scaling up light-driven biotransformations are related to the technical limitations of balancing light intensity to maintain productivity and avoid inhibition, while facing light adsorption by cells and self-shading (Chanquia et al., 2021). It is particularly challenging knowing that higher space-time-yields can be achieved by increasing the cell concentrations (Hoschek et al., 2018). However, higher cell densities need increased light intensities and/or additional light sources to be installed within the reactor system. Light-emitting diode (LED) operated photobioreactors offer more tight control of the wavelength that can lead to improved efficiency (Hellingwerf et al., 2021). Some very interesting engineering approaches have been gaining attention, such as utilizing wavelengths shifting dyes, proven to improve biomass production (Burak et al., 2019).

Established cultivation systems for photosynthetic microorganisms can be an initial point for developing systems for scaling up light-driven biocatalysis. The simple ones are based on open pond reactor systems, such as raceway ponds. Recently, there have been some technological advances in the development of open thin-layer cascade photobioreactors (Apel et al., 2017) that have been applied for the production of lipids (Schädler et al., 2019). However, closed photobioreactors would be a preferred system for running light-driven biocatalysis to produce fine chemicals and pharmaceuticals. Closed photobioreactors allow tight control of important reaction parameters such as pH, temperature, supply of $CO_2$ and $O_2$ degassing, reduce the risk of contaminations and limit the escape of heterologous strains usually used (Wijffels et al., 2013). Different designs of photobioreactors have been developed and the most common include stirred tank, flat panel, tubular, soft-frame and bubble column (Doppler and Spadiut, 2021) (Fig. 6).

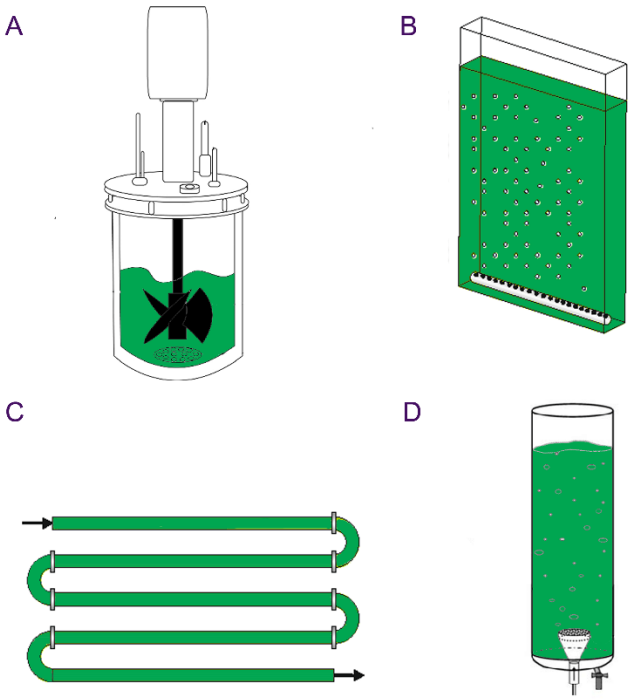


**Figure 6.** Schematic representation of the different photobioreactors. A) stirred tank, B) vertical flat panel, C) fence tubular, D) bubble column.

Stirred tank reactors are well known for the cultivation of heterotrophic microorganisms and have already been further developed as photobioreactors to include light sources (Labfors 5 Lux, Infors AG). They are actively stirred by various forms of different impellers which improve $CO_2$ and $O_2$ mass transfer rates, ensuring homogenous distribution with exact control of process parameters, such as pH and temperature (Doppler and Spadiut, 2021). However, shear forces imposed by impellers can have harmful effects on the cells (Wang and Lan, 2018). Available stirred tank bioreactor has been applied for the scale-up of biotransformation of cyclohexane to cyclohexanol by engineered *Synechocystis* leading to the average productivity of 0.04 g $L^{-1}$ $h^{-1}$ (Hoschek et al., 2019c). This example is far from economically viable productivities but offered insights into required improvements. An additional example is ω-hydroxylation of nonanoic acid methyl ester using engineered *Synechocystis* with a maximum space-time yield of 0.086 $mmol_{total\ product} \cdot L_{aq}^{-1} \cdot h^{-1}$ (Hoschek et al., 2019a). Some of the drawbacks of scaling standard stirred tank bioreactors are related to decreasing surface-to-volume ratio, resulting in impaired light distribution together with high energy input needed to provide efficient mixing (Chanquia et al., 2021).

Flat panel reactors come up with the advantage of a higher surface-to-volume ratio with a consistent light supply leading to high photosynthetic rates and biomass (Doppler and Spadiut, 2021). One of the drawbacks of using flat panels is difficulties for enlarging, controlling temperature and high energy consumption to provide efficient mixing of the cultures (Touloupakis and Carlozzi, 2021). Continuous development offers novel technologies, such as recently described modification of the flat panel reactor focused on immobilization of cells on a grid further applied for the hydrogen production (Wang et al., 2019).

Tubular bioreactors are constructed as transparent tubes being in various configurations (e.g. loop, coil, manifold) and orientations (e.g. horizontal, vertical and inclined) with large illumination surface areas (Touloupakis and Carlozzi, 2021). A major factor influencing the efficiency is the diameter of the tubes, as lower diameter results in better light penetration (Doppler and Spadiut, 2021). One of the largest tubular photobioreactors, with a vertical arrangement of the tubes, is located in Germany, with a capacity of 700 $m^3$ and a total pipe length of 500 km, set-up for the production of up to 150 tonnes of *Chlorella* sp. dry mass per year (Płaczek et al., 2017). Diverse novel tubular designs are being developed to improve the mass transfer and the surface-to-volume ratio. Recently, a new tubular photobioreactor design based on the Fibonacci equation to optimize light absorption was described (Díaz et al., 2019) and a novel tangential double tube photobioreactor composed of two horizontal tubes providing more efficient aeration (Cui et al., 2021).

Soft frames bioreactors are made of soft materials, usually polyethylene foils. They have been already applied for the production of dhurrin (Wlodarczyk et al., 2016); however, often come with several drawbacks, such as cleaning, sterilization and short lifetimes (Doppler and Spadiut, 2021).

Bubble column bioreactors composed of a cylindrical vessel fitted with a gas sparger have been extensively used. Compared to the flat panel and tubular bioreactors limited by gas transport, column photobioreactors are mostly light-limited. The main challenge using column photobioreactors for light-driven biocatalysis is providing equal light intensity to all cells in the culture, as the outer layer is usually facing high illumination, however inner zones have limited light availability (Doppler and Spadiut, 2021). These light intensity gradients, from the surface to the axis of the column, are due to cell-shading and an issue even at low cell density (Richmond et al., 2003). To enable efficient light supply, novel technologies have been

developed, based on optical fibers as inner light sources (Xue et al., 2013) or recently described wireless light emitters (Heining et al., 2015).

Novel approaches have been focused on using high cell density to achieve higher productivities. Some of the new advances recently developed include capillary bioreactors for cultivating high cell density photoautotrophic biofilms reaching 48 $g_{BDW}$ $L^{-1}$ and producing 3.76 g $m^{-2}$ $day^{-1}$ of cyclohexanol (Hoschek et al., 2019b). Additional interesting high cell density approach is based on CellDEG technology being able to reach more than 30 g $L^{-1}$ of cell dry weight (Bähr et al., 2016). This technology was already applied for the production of cyanophycin (Lippi et al., 2018) and sesquiterpenoids (Dienst et al., 2020).

## 4. Aims of this work

The major aim of this study was to expand the knowledge on cyanobacteria as hosts for photobiotransformations toward possible applications. For this purpose, the model unicellular cyanobacterium *Synechocystis* sp. PCC 6803 was used as a chassis to:

i) rationally engineer electron flow toward improved activities of a model redox enzyme (Chapter II)

ii) characterize a library of RNA thermometers as potential regulatory elements (Chapters III)

iii) investigate redox biotransformation in a scale-up system using internal illumination (Chapter IV).

# 5. References

Adams, B. L. (2016) 'The next generation of synthetic biology chassis: moving synthetic biology from the laboratory to the field', *ACS Synthetic Biology*, *5*(12), pp.1328-1330.

Ajlani, G. and Vernotte, C. (1998) 'Construction and characterization of a phycobiliprotein-less mutant of Synechocystis sp. PCC 6803', *Plant Molecular Biology,* 37(3), pp. 577-580.

Allahverdiyeva, Y., Mustila, H., Ermakova, M., Bersanini, L., Richaud, P., Ajlani, G., Battchikova, N., Cournac, L. and Aro, E.-M. (2013) 'Flavodiiron proteins Flv1 and Flv3 enable cyanobacterial growth and photosynthesis under fluctuating light', *Proceedings of the National Academy of Sciences,* 110(10), pp. 4111-4116.

Anastas, P. and Eghbali, N. (2010) 'Green chemistry: principles and practice', *Chemical Society Reviews,* 39(1), pp. 301-312.

Angermayr, S. A., Paszota, M. and Hellingwerf, K. J. (2012) 'Engineering a cyanobacterial cell factory for production of lactic acid', *Applied and Environmental Microbiology,* 78(19), pp. 7098-7106.

Angermayr, S. A., Rovira, A. G. and Hellingwerf, K. J. (2015) 'Metabolic engineering of cyanobacteria for the synthesis of commodity products', *Trends in Biotechnology,* 33(6), pp. 352-361.

Apel, A., Pfaffinger, C., Basedahl, N., Mittwollen, N., Göbel, J., Sauter, J., Brück, T. and Weuster-Botz, D. (2017) 'Open thin-layer cascade reactors for saline microalgae production evaluated in a physically simulated Mediterranean summer climate', *Algal Research,* 25, pp. 381-390.

Assil-Companioni, L., Büchsenschütz, H. C., Solymosi, D., Dyczmons-Nowaczyk, N. G., Bauer, K. K., Wallner, S., Macheroux, P., Allahverdiyeva, Y., Nowaczyk, M. M. and Kourist, R. (2020) 'Engineering of NADPH supply boosts photosynthesis-driven biotransformations', *ACS Catalysis,* 10(20), pp. 11864-11877.

Assil-Companioni, L., Schmidt, S., Heidinger, P., Schwab, H. and Kourist, R. (2019) 'Hydrogen-driven cofactor regeneration for stereoselective whole-cell C= C bond reduction in Cupriavidus necator', *ChemSusChem,* 12(11), pp. 2361-2365.

Atsumi, S., Higashide, W. and Liao, J. C. (2009) 'Direct photosynthetic recycling of carbon dioxide to isobutyraldehyde', *Nature Biotechnology,* 27(12), pp. 1177-1180.

Bähr, L., Wüstenberg, A. and Ehwald, R. (2016) 'Two-tier vessel for photoautotrophic high-density cultures', *Journal of Applied Phycology,* 28(2), pp. 783-793.

Bell, E. L., Finnigan, W., France, S. P., Green, A. P., Hayes, M. A., Hepworth, L. J., Lovelock, S. L., Niikura, H., Osuna, S. and Romero, E. (2021) 'Biocatalysis', *Nature Reviews Methods Primers,* 1(1), pp. 1-21.

Berepiki, A., Gittins, J. R., Moore, C. M. and Bibby, T. S. (2018) 'Rational engineering of photosynthetic electron flux enhances light-powered cytochrome P450 activity', *Synthetic Biology,* 3(1), pp. ysy009.

Berepiki, A., Hitchcock, A., Moore, C. M. and Bibby, T. S. (2016) 'Tapping the unused potential of photosynthesis with a heterologous electron sink', *ACS Synthetic Biology,* 5(12), pp. 1369-1375.

Bernstein, H. C., McClure, R. S., Hill, E. A., Markillie, L. M., Chrisler, W. B., Romine, M. F., McDermott, J. E., Posewitz, M. C., Bryant, D. A. and Konopka, A. E. (2016) 'Unlocking the constraints of cyanobacterial productivity: acclimations enabling ultrafast growth', *MBio,* 7(4), pp. e00949-16.

Blankenship, R. E. (2021) *Molecular mechanisms of photosynthesis.* John Wiley & Sons.

Blankenship, R. E., Tiede, D. M., Barber, J., Brudvig, G. W., Fleming, G., Ghirardi, M., Gunner, M., Junge, W., Kramer, D. M. and Melis, A. (2011) 'Comparing photosynthetic and

photovoltaic efficiencies and recognizing the potential for improvement', *Science,* 332(6031), pp. 805-809.

Böhmer, S., Köninger, K., Gómez-Baraibar, Á., Bojarra, S., Mügge, C., Schmidt, S., Nowaczyk, M. M. and Kourist, R. (2017) 'Enzymatic oxyfunctionalization driven by photosynthetic water-splitting in the cyanobacterium Synechocystis sp. PCC 6803', *Catalysts,* 7(8), pp. 240.

Bougioukou, D. J., Kille, S., Taglieber, A. and Reetz, M. T. (2009) 'Directed evolution of an enantioselective enoate-reductase: testing the utility of iterative saturation mutagenesis', *Advanced Synthesis & Catalysis,* 351(18), pp. 3287-3305.

Branco dos Santos, F., Du, W. and Hellingwerf, K. J. (2014) 'Synechocystis: not just a plug-bug for CO2, but a green E. coli', *Frontiers in Bioengineering and Biotechnology,* 2, pp. 36.

Büchsenschütz, H. C., Vidimce-Risteski, V., Eggbauer, B., Schmidt, S., Winkler, C. K., Schrittwieser, J. H., Kroutil, W. and Kourist, R. (2020) 'Stereoselective biotransformations of cyclic imines in recombinant cells of Synechocystis sp. PCC 6803', *ChemCatChem,* 12(3), pp. 726-730.

Bullerjahn, G. S. and Post, A. F. (2014) 'Physiology and molecular biology of aquatic cyanobacteria', *Frontiers in Microbiology,* 5, pp. 359.

Burak, H., Dunbar, A. and Gilmour, D. J. (2019) 'Enhancement of Dunaliella salina growth by using wavelength shifting dyes', *Journal of Applied Phycology,* 31(5), pp. 2791-2796.

Bux, F. and Chisti, Y. (2016) *Algae Biotechnology: Products and Processes.* Springer.

Cahn, J. K., Werlang, C. A., Baumschlager, A., Brinkmann-Chen, S., Mayo, S. L. and Arnold, F. H. (2017) 'A general tool for engineering the NAD/NADP cofactor preference of oxidoreductases', *ACS Synthetic Biology,* 6(2), pp. 326-333.

Cai, Y. and Wolk, C. P. (1997) 'Anabaena sp. strain PCC 7120 responds to nitrogen deprivation with a cascade-like sequence of transcriptional activations', *Journal of Bacteriology,* 179(1), pp. 267-271.

Calero, P. and Nikel, P. I. (2019) 'Chasing bacterial chassis for metabolic engineering: a perspective review from classical to non-traditional microorganisms', *Microbial Biotechnology,* 12(1), pp. 98-124.

Cf, O. (2015) 'Transforming our world: the 2030 Agenda for Sustainable Development', *United Nations: New York, NY, USA*.

Chanquia, S. N., Vernet, G. and Kara, S. (2021) 'Photobioreactors for cultivation and synthesis: Specifications, challenges, and perspectives', *Engineering in Life Sciences*.

Chen, M. and Blankenship, R. E. (2011) 'Expanding the solar spectrum used by photosynthesis', *Trends in Plant Science,* 16(8), pp. 427-431.

Chen, M., Schliep, M., Willows, R. D., Cai, Z.-L., Neilan, B. A. and Scheer, H. (2010) 'A red-shifted chlorophyll', *Science,* 329(5997), pp. 1318-1319.

Chen, Q., Arents, J., Schuurmans, J. M., Ganapathy, S., Willem, J., Cheregi, O., Funk, C., Dos Santos, F. B. and Hellingwerf, K. J. (2019) 'Combining retinal-based and chlorophyll-based (oxygenic) photosynthesis: Proteorhodopsin expression increases growth rate and fitness of aΔ PSI strain of Synechocystis sp. PCC6803', *Metabolic Engineering,* 52, pp. 68-76.

Cohen, S. E. and Golden, S. S. (2015) 'Circadian rhythms in cyanobacteria', *Microbiology and Molecular Biology Reviews,* 79(4), pp. 373-385.

Cui, X., Yang, J., Cui, M., Zhang, W. and Zhao, J. (2021) 'Comparative experiments of two novel tubular photobioreactors with an inner aerated tube for microalgal cultivation: Enhanced mass transfer and improved biomass yield', *Algal Research,* 58, pp. 102364.

de María, P. D. (2021) 'Biocatalysis, sustainability, and industrial applications: Show me the metrics', *Current Opinion in Green and Sustainable Chemistry*, 31, pp. 100514.

Deng, M.-D. and Coleman, J. R. (1999) 'Ethanol synthesis by genetic engineering in cyanobacteria', *Applied and Environmental Microbiology,* 65(2), pp. 523-528.

Dhillon, R. and von Wuehlisch, G. (2013) 'Mitigation of global warming through renewable biomass', *Biomass and Bioenergy,* 48, pp. 75-89.

Díaz, J. P., Inostroza, C. and Fernández, F. A. (2019) 'Fibonacci-type tubular photobioreactor for the production of microalgae', *Process Biochemistry,* 86, pp. 1-8.

Dienst, D., Wichmann, J., Mantovani, O., Rodrigues, J. S. and Lindberg, P. (2020) 'High density cultivation for efficient sesquiterpenoid biosynthesis in Synechocystis sp. PCC 6803', *Scientific Reports,* 10(1), pp. 1-16.

Dismukes, G. C., Carrieri, D., Bennette, N., Ananyev, G. M. and Posewitz, M. C. (2008) 'Aquatic phototrophs: efficient alternatives to land-based crops for biofuels', *Current Opinion in Biotechnology,* 19(3), pp. 235-240.

Doppler, P. and Spadiut, O. (2021) 'Chapter 5 Introduction to autotrophic cultivation of microalgae in photobioreactors', in Robert, K. & Sandy, S. (eds.) *The Autotrophic Biorefinery: Raw Materials from Biotechnology*: De Gruyter, pp. 113-130.

Ducat, D. C., Avelar-Rivas, J. A., Way, J. C. and Silver, P. A. (2012) 'Rerouting carbon flux to enhance photosynthetic productivity', *Applied and Environmental Microbiology,* 78(8), pp. 2660-2668.

Englund, E., Liang, F. and Lindberg, P. (2016) 'Evaluation of promoters and ribosome binding sites for biotechnological applications in the unicellular cyanobacterium Synechocystis sp. PCC 6803', *Scientific Reports,* 6(1), pp. 1-12.

Erdem, E., Malihan-Yap, L., Assil-Companioni, L., Grimm, H., Barone, G. D., Serveau-Avesque, C., Amouric, A., Duquesne, K., de Berardinis, V. and Allahverdiyeva, Y. (2021) 'Photobiocatalytic Oxyfunctionalization with High Reaction Rate using a Baeyer–Villiger Monooxygenase from Burkholderia xenovorans in Metabolically Engineered Cyanobacteria', *ACS Catalysis,* 12(1), pp. 66-72.

Faber, K. (2011) *Biotransformations in organic chemistry: a textbook.* Springer.

Falcón, L. I., Magallón, S. and Castillo, A. (2010) 'Dating the cyanobacterial ancestor of the chloroplast', *The ISME journal,* 4(6), pp. 777-783.

Fan, J., Zhang, Y., Wu, P., Zhang, X. and Bai, Y. (2021) 'Enhancing Cofactor Regeneration of Cyanobacteria for the Light-Powered Synthesis of Chiral Alcohols', *Bioorganic Chemistry*, 118, pp. 105477.

Ferreira, E. A., Pacheco, C. C., Pinto, F., Pereira, J., Lamosa, P., Oliveira, P., Kirov, B., Jaramillo, A. and Tamagnini, P. (2018) 'Expanding the toolbox for Synechocystis sp. PCC 6803: validation of replicative vectors and characterization of a novel set of promoters', *Synthetic Biology,* 3(1), pp. ysy014.

Fitzpatrick, T. B., Amrhein, N. and Macheroux, P. (2003) 'Characterization of YqjM, an Old Yellow Enzyme homolog from Bacillus subtilis involved in the oxidative stress response', *Journal of Biological Chemistry,* 278(22), pp. 19891-19897.

Flombaum, P., Gallegos, J. L., Gordillo, R. A., Rincón, J., Zabala, L. L., Jiao, N., Karl, D. M., Li, W. K., Lomas, M. W. and Veneziano, D. (2013) 'Present and future global distributions of the marine Cyanobacteria Prochlorococcus and Synechococcus', *Proceedings of the National Academy of Sciences,* 110(24), pp. 9824-9829.

Foyer, C. H. and Noctor, G. (2009) 'Redox regulation in photosynthetic organisms: signaling, acclimation, and practical implications', *Antioxidants & Redox Signaling,* 11(4), pp. 861-905.

Fu, P. (2009) 'Genome-scale modeling of Synechocystis sp. PCC 6803 and prediction of pathway insertion', *Journal of Chemical Technology & Biotechnology: International Research in Process, Environmental & Clean Technology,* 84(4), pp. 473-483.

Fujisawa, T., Narikawa, R., Maeda, S.-i., Watanabe, S., Kanesaki, Y., Kobayashi, K., Nomata, J., Hanaoka, M., Watanabe, M. and Ehira, S. (2017) 'CyanoBase: a large-scale update on its 20th anniversary', *Nucleic Acids Research,* 45(D1), pp. D551-D554.

Gale, G. A., Schiavon Osorio, A. A., Mills, L. A., Wang, B., Lea-Smith, D. J. and McCormick, A. J. (2019) 'Emerging species and genome editing tools: future prospects in cyanobacterial synthetic biology', *Microorganisms,* 7(10), pp. 409.

Gimpel, J. A., Henríquez, V. and Mayfield, S. P. (2015) 'In metabolic engineering of eukaryotic microalgae: potential and challenges come with great diversity', *Frontiers in Microbiology,* 6, pp. 1376.

Gordon, G. C., Korosh, T. C., Cameron, J. C., Markley, A. L., Begemann, M. B. and Pfleger, B. F. (2016) 'CRISPR interference as a titratable, trans-acting regulatory tool for metabolic engineering in the cyanobacterium Synechococcus sp. strain PCC 7002', *Metabolic Engineering,* 38, pp. 170-179.

Grimm, H. C. and Kourist, R. (2021) '3 Cyanobacteria as catalysts for light-driven biotransformations', *Photosynthesis: Biotechnological Applications with Microalgae*, pp. 57.

Gundlach, K., Werwie, M., Wiegand, S. and Paulsen, H. (2009) 'Filling the “green gap” of the major light-harvesting chlorophyll a/b complex by covalent attachment of Rhodamine Red', *Biochimica et Biophysica Acta (BBA)-Bioenergetics,* 1787(12), pp. 1499-1504.

Hall, M., Stueckler, C., Ehammer, H., Pointner, E., Oberdorfer, G., Gruber, K., Hauer, B., Stuermer, R., Kroutil, W. and Macheroux, P. (2008) 'Asymmetric bioreduction of C□ C bonds using enoate reductases OPR1, OPR3 and YqjM: enzyme-based stereocontrol', *Advanced Synthesis & Catalysis,* 350(3), pp. 411-418.

Hamada, H., Kondo, Y., Ishihara, K., Nakajima, N., Hamada, H., Kurihara, R. and Hirata, T. (2003) 'Stereoselective biotransformation of limonene and limonene oxide by cyanobacterium, Synechococcus sp. PCC 7942', *Journal of Bioscience and Bioengineering,* 96(6), pp. 581-584.

Hamilton, T. L., Bryant, D. A. and Macalady, J. L. (2016) 'The role of biology in planetary evolution: cyanobacterial primary production in low-oxygen Proterozoic oceans', *Environmental Microbiology,* 18(2), pp. 325-340.

Hasunuma, T., Matsuda, M., Senga, Y., Aikawa, S., Toyoshima, M., Shimakawa, G., Miyake, C. and Kondo, A. (2014) 'Overexpression of flv3 improves photosynthesis in the cyanobacterium Synechocystis sp. PCC6803 by enhancement of alternative electron flow', *Biotechnology for Biofuels,* 7(1), pp. 1-10.

Havel, J. and Weuster-Botz, D. (2006) 'Comparative study of cyanobacteria as biocatalysts for the asymmetric synthesis of chiral building blocks', *Engineering in Life Sciences,* 6(2), pp. 175-179.

Heining, M., Sutor, A., Stute, S., Lindenberger, C. and Buchholz, R. (2015) 'Internal illumination of photobioreactors via wireless light emitters: a proof of concept', *Journal of Applied Phycology,* 27(1), pp. 59-66.

Hellingwerf, K. J., Chen, Q. and Branco dos Santos, F. (2021) 'Optimizing the Spectral Fit Between Cyanobacteria and Solar Radiation in the Light of Sustainability Applications', *Cyanobacteria Biotechnology*, pp. 65-88.

Hernandez-Prieto, M. A. and Futschik, M. E. (2012) 'CyanoEXpress: a web database for exploration and visualisation of the integrated transcriptome of cyanobacterium Synechocystis sp. PCC6803', *Bioinformation,* 8(13), pp. 634.

Herrero, A., Muro-Pastor, A. M. and Flores, E. (2001) 'Nitrogen control in cyanobacteria', *Journal of Bacteriology,* 183(2), pp. 411-425.

Hitchcock, A., Hunter, C. N. and Canniffe, D. P. (2020) 'Progress and challenges in engineering cyanobacteria as chassis for light-driven biotechnology', *Microbial Biotechnology,* 13(2), pp. 363-367.

Hohmann-Marriott, M. F. and Blankenship, R. E. (2011) 'Evolution of photosynthesis', *Annual Review of Plant Biology,* 62(1), pp. 515-548.

Hollmann, F., Arends, I. W., Buehler, K., Schallmey, A. and Bühler, B. (2011) 'Enzyme-mediated oxidations for the chemist', *Green Chemistry,* 13(2), pp. 226-265.

Hoschek, A., Bühler, B. and Schmid, A. (2017) 'Overcoming the gas–liquid mass transfer of oxygen by coupling photosynthetic water oxidation with biocatalytic oxyfunctionalization', *Angewandte Chemie International Edition,* 56(47), pp. 15146-15149.

Hoschek, A., Bühler, B. and Schmid, A. (2019a) 'Stabilization and scale-up of photosynthesis-driven ω-hydroxylation of nonanoic acid methyl ester by two-liquid phase whole-cell biocatalysis', *Biotechnology and Bioengineering,* 116(8), pp. 1887-1900.

Hoschek, A., Heuschkel, I., Schmid, A., Bühler, B., Karande, R. and Bühler, K. (2019b) 'Mixed-species biofilms for high-cell-density application of Synechocystis sp. PCC 6803 in capillary reactors for continuous cyclohexane oxidation to cyclohexanol', *Bioresource Technology,* 282, pp. 171-178.

Hoschek, A., Schmid, A. and Bühler, B. (2018) 'In situ O2 generation for biocatalytic oxyfunctionalization reactions', *ChemCatChem,* 10(23), pp. 5366-5371.

Hoschek, A., Toepel, J., Hochkeppel, A., Karande, R., Bühler, B. and Schmid, A. (2019c) 'Light-dependent and aeration-independent gram-scale hydroxylation of cyclohexane to cyclohexanol by CYP450 harboring Synechocystis sp. PCC 6803', *Biotechnology Journal,* 14(8), pp. 1800724.

Huang, H.-H., Camsund, D., Lindblad, P. and Heidorn, T. (2010) 'Design and characterization of molecular tools for a synthetic biology approach towards developing cyanobacterial biotechnology', *Nucleic acids research,* 38(8), pp. 2577-2593.

Huang, H.-H. and Lindblad, P. (2013) 'Wide-dynamic-range promoters engineered for cyanobacteria', *Journal of Biological Engineering,* 7(1), pp. 1-11.

Inganäs, O. and Sundström, V. (2016) 'Solar energy for electricity and fuels', *Ambio,* 45(1), pp. 15-23.

Jaiswal, D., Sengupta, A., Sengupta, S., Madhu, S., Pakrasi, H. B. and Wangikar, P. P. (2020) 'A novel cyanobacterium Synechococcus elongatus PCC 11802 has distinct genomic and metabolomic characteristics compared to its neighbor PCC 11801', *Scientific Reports,* 10(1), pp. 1-15.

Jaiswal, D., Sengupta, A., Sohoni, S., Sengupta, S., Phadnavis, A. G., Pakrasi, H. B. and Wangikar, P. P. (2018) 'Genome features and biochemical characteristics of a robust, fast growing and naturally transformable cyanobacterium Synechococcus elongatus PCC 11801 isolated from India', *Scientific Reports,* 8(1), pp. 1-13.

Jones, P. R. (2014) 'Genetic instability in cyanobacteria–an elephant in the room?', *Frontiers in Bioengineering and Biotechnology,* 2, pp. 12.

Joseph, A., Aikawa, S., Sasaki, K., Matsuda, F., Hasunuma, T. and Kondo, A. (2014) 'Increased biomass production and glycogen accumulation in apcE gene deleted Synechocystis sp. PCC 6803', *AMB Express,* 4(1), pp. 1-6.

Julsing, M. K., Cornelissen, S., Bühler, B. and Schmid, A. (2008) 'Heme-iron oxygenases: powerful industrial biocatalysts?', *Current Opinion in Chemical Biology,* 12(2), pp. 177-186.

Jumper, J., Evans, R., Pritzel, A., Green, T., Figurnov, M., Ronneberger, O., Tunyasuvunakool, K., Bates, R., Žídek, A. and Potapenko, A. (2021) 'Highly accurate protein structure prediction with AlphaFold', *Nature,* 596(7873), pp. 583-589.

Jurkaš, V., Winkler, C. K., Poschenrieder, S., Oliveira, P., Pacheco, C. C., Ferreira, E. A., Weissensteiner, F., De Santis, P., Kara, S. and Kourist, R. (2021) 'Expression and activity of heterologous hydroxyisocaproate dehydrogenases in Synechocystis sp. PCC 6803 ΔhoxYH', *Engineering Microbiology*, 2(1), pp. 100008.

Jüttner, F. and Hans, R. (1986) 'The reducing capacities of cyanobacteria for aldehydes and ketones', *Applied Microbiology and Biotechnology,* 25(1), pp. 52-54.

Kamennaya, N. A., Ahn, S., Park, H., Bartal, R., Sasaki, K. A., Holman, H.-Y. and Jansson, C. (2015) 'Installing extra bicarbonate transporters in the cyanobacterium Synechocystis sp. PCC6803 enhances biomass production', *Metabolic Engineering,* 29, pp. 76-85.

Kaneko, T., Sato, S., Kotani, H., Tanaka, A., Asamizu, E., Nakamura, Y., Miyajima, N., Hirosawa, M., Sugiura, M. and Sasamoto, S. (1996) 'Sequence analysis of the genome of the unicellular cyanobacterium Synechocystis sp. strain PCC6803. II. Sequence determination of the entire genome and assignment of potential protein-coding regions', *DNA Research,* 3(3), pp. 109-136.

Kirst, H., Formighieri, C. and Melis, A. (2014) 'Maximizing photosynthetic efficiency and culture productivity in cyanobacteria upon minimizing the phycobilisome light-harvesting antenna size', *Biochimica et Biophysica Acta (BBA)-Bioenergetics,* 1837(10), pp. 1653-1664.

Kitzing, K., Fitzpatrick, T. B., Wilken, C., Sawa, J., Bourenkov, G. P., Macheroux, P. and Clausen, T. (2005) 'The 1.3 Å crystal structure of the flavoprotein YqjM reveals a novel class of old yellow enzymes', *Journal of Biological Chemistry,* 280(30), pp. 27904-27913.

Kiyota, H., Okuda, Y., Ito, M., Hirai, M. Y. and Ikeuchi, M. (2014) 'Engineering of cyanobacteria for the photosynthetic production of limonene from CO2', *Journal of Biotechnology,* 185, pp. 1-7.

Knoop, H., Gründel, M., Zilliges, Y., Lehmann, R., Hoffmann, S., Lockau, W. and Steuer, R. (2013) 'Flux balance analysis of cyanobacterial metabolism: the metabolic network of Synechocystis sp. PCC 6803', *PLoS Computational Biology,* 9(6), pp. e1003081.

Knoot, C. J., Ungerer, J., Wangikar, P. P. and Pakrasi, H. B. (2018) 'Cyanobacteria: promising biocatalysts for sustainable chemical production', *Journal of Biological Chemistry,* 293(14), pp. 5044-5052.

Kohli, R. M. and Massey, V. (1998) 'The oxidative half-reaction of Old Yellow Enzyme: the role of tyrosine 196', *Journal of Biological Chemistry,* 273(49), pp. 32763-32770.

Köninger, K., Gómez Baraibar, Á., Mügge, C., Paul, C. E., Hollmann, F., Nowaczyk, M. M. and Kourist, R. (2016) 'Recombinant cyanobacteria for the asymmetric reduction of C= C bonds fueled by the biocatalytic oxidation of water', *Angewandte Chemie International Edition,* 55(18), pp. 5582-5585.

Kramer, D. M. and Evans, J. R. (2011) 'The importance of energy balance in improving photosynthetic productivity', *Plant physiology,* 155(1), pp. 70-78.

Kratzer, R., Woodley, J. M. and Nidetzky, B. (2015) 'Rules for biocatalyst and reaction engineering to implement effective, NAD (P) H-dependent, whole cell bioreductions', *Biotechnology Advances,* 33(8), pp. 1641-1652.

Kumar, K., Mella-Herrera, R. A. and Golden, J. W. (2010) 'Cyanobacterial heterocysts', *Cold Spring Harbor Perspectives in Biology,* 2(4), pp. a000315.

Lagarde, D., Beuf, L. and Vermaas, W. (2000) 'Increased production of zeaxanthin and other pigments by application of genetic engineering techniques to Synechocystis sp. strain PCC 6803', *Applied and Environmental Microbiology,* 66(1), pp. 64-72.

Lea-Smith, D. J., Bombelli, P., Dennis, J. S., Scott, S. A., Smith, A. G. and Howe, C. J. (2014) 'Phycobilisome-deficient strains of Synechocystis sp. PCC 6803 have reduced size and require carbon-limiting conditions to exhibit enhanced productivity', *Plant Physiology,* 165(2), pp. 705-714.

Lea-Smith, D. J., Bombelli, P., Vasudevan, R. and Howe, C. J. (2016) 'Photosynthetic, respiratory and extracellular electron transport pathways in cyanobacteria', *Biochimica et Biophysica Acta (BBA)-Bioenergetics,* 1857(3), pp. 247-255.

Lea-Smith, D. J. and Hanke, G. T. (2021) 'Electron Transport in Cyanobacteria and Its Potential in Bioproduction', *Cyanobacteria Biotechnology*, pp. 33-63.

Lerchner, A., Jarasch, A. and Skerra, A. (2016) 'Engineering of alanine dehydrogenase from Bacillus subtilis for novel cofactor specificity', *Biotechnology and Applied Biochemistry,* 63(5), pp. 616-624.

Li, H., Shen, C. R., Huang, C.-H., Sung, L.-Y., Wu, M.-Y. and Hu, Y.-C. (2016) 'CRISPR-Cas9 for the genome engineering of cyanobacteria and succinate production', *Metabolic Engineering,* 38, pp. 293-302.

Liang, F., Englund, E., Lindberg, P. and Lindblad, P. (2018) 'Engineered cyanobacteria with enhanced growth show increased ethanol production and higher biofuel to biomass ratio', *Metabolic Engineering,* 46, pp. 51-59.

Liang, F. and Lindblad, P. (2016) 'Effects of overexpressing photosynthetic carbon flux control enzymes in the cyanobacterium Synechocystis PCC 6803', *Metabolic Engineering,* 38, pp. 56-64.

Lippi, L., Bähr, L., Wüstenberg, A., Wilde, A. and Steuer, R. (2018) 'Exploring the potential of high-density cultivation of cyanobacteria for the production of cyanophycin', *Algal Research,* 31, pp. 363-366.

Liu, D. and Pakrasi, H. B. (2018) 'Exploring native genetic elements as plug-in tools for synthetic biology in the cyanobacterium Synechocystis sp. PCC 6803', *Microbial Cell Factories,* 17(1), pp. 1-8.

Liu, H., Ni, J., Xu, P. and Tao, F. (2018) 'Enhancing light-driven 1, 3-propanediol production by using natural compartmentalization of differentiated cells', *ACS Synthetic Biology,* 7(10), pp. 2436-2446.

Liu, W. and Wang, P. (2007) 'Cofactor regeneration for sustainable enzymatic biosynthesis', *Biotechnology Advances,* 25(4), pp. 369-384.

Liu, X. and Curtiss, R. (2009) 'Nickel-inducible lysis system in Synechocystis sp. PCC 6803', *Proceedings of the National Academy of Sciences,* 106(51), pp. 21550-21554.

Liu, X., Fallon, S., Sheng, J. and Curtiss, R. (2011) 'CO2-limitation-inducible Green Recovery of fatty acids from cyanobacterial biomass', *Proceedings of the National Academy of Sciences,* 108(17), pp. 6905-6908.

Luan, G., Zhang, S. and Lu, X. (2020) 'Engineering cyanobacteria chassis cells toward more efficient photosynthesis', *Current Opinion in Biotechnology,* 62, pp. 1-6.

Ma, S. K., Gruber, J., Davis, C., Newman, L., Gray, D., Wang, A., Grate, J., Huisman, G. W. and Sheldon, R. A. (2010) 'A green-by-design biocatalytic process for atorvastatin intermediate', *Green Chemistry,* 12(1), pp. 81-86.

Ma, X., Liang, H., Ning, C., Deng, S. and Su, E. (2017) 'Integrating a light-driven coenzyme regeneration system by expression of an alcohol dehydrogenase in phototrophic bacteria for synthesis of chiral alcohol', *Journal of Biotechnology,* 259, pp. 120-125.

Markley, A. L., Begemann, M. B., Clarke, R. E., Gordon, G. C. and Pfleger, B. F. (2015) 'Synthetic biology toolbox for controlling gene expression in the cyanobacterium Synechococcus sp. strain PCC 7002', *ACS Synthetic Biology,* 4(5), pp. 595-603.

Markou, G. and Georgakakis, D. (2011) 'Cultivation of filamentous cyanobacteria (blue-green algae) in agro-industrial wastes and wastewaters: a review', *Applied Energy,* 88(10), pp. 3389-3401.

Melis, A. (2009) 'Solar energy conversion efficiencies in photosynthesis: minimizing the chlorophyll antennae to maximize efficiency', *Plant Science,* 177(4), pp. 272-280.

Meyer, D., Bu, B. and Schmid, A. (2006) 'Process and catalyst design objectives for specific redox biocatalysis', *Advances in Applied Microbiology,* 59, pp. 53-91.

Miyashita, H., Ikemoto, H., Kurano, N., Adachi, K., Chihara, M. and Miyachi, S. (1996) 'Chlorophyll d as a major pigment', *Nature,* 383(6599), pp. 402-402.

Montagud, A., Navarro, E., de Córdoba, P. F., Urchueguía, J. F. and Patil, K. R. (2010) 'Reconstruction and analysis of genome-scale metabolic model of a photosynthetic bacterium', *BMC Systems Biology,* 4(1), pp. 1-16.

Montagud, A., Zelezniak, A., Navarro, E., de Córdoba, P. F., Urchueguía, J. F. and Patil, K. R. (2011) 'Flux coupling and transcriptional regulation within the metabolic network of the photosynthetic bacterium Synechocystis sp. PCC6803', *Biotechnology Journal,* 6(3), pp. 330-342.

Montgomery, B. L. (2014) 'The regulation of light sensing and light-harvesting impacts the use of cyanobacteria as biotechnology platforms', *Frontiers in Bioengineering and Biotechnology,* 2, pp. 22.

Mullineaux, C. W. (2014) 'Electron transport and light-harvesting switches in cyanobacteria', *Frontiers in Plant Science,* 5, pp. 7.

Nagy, C., Thiel, K., Mulaku, E., Mustila, H., Tamagnini, P., Aro, E.-M., Pacheco, C. C. and Kallio, P. (2021) 'Comparison of alternative integration sites in the chromosome and the native plasmids of the cyanobacterium Synechocystis sp. PCC 6803 in respect to expression efficiency and copy number', *Microbial Cell Factories,* 20(1), pp. 1-18.

Nakahira, Y., Ogawa, A., Asano, H., Oyama, T. and Tozawa, Y. (2013) 'Theophylline-dependent riboswitch as a novel genetic tool for strict regulation of protein expression in cyanobacterium Synechococcus elongatus PCC 7942', *Plant and Cell Physiology,* 54(10), pp. 1724-1735.

Nakamura, K. and Yamanaka, R. (2002) 'Light-mediated regulation of asymmetric reduction of ketones by a cyanobacterium', *Tetrahedron: Asymmetry,* 13(23), pp. 2529-2533.

Nakamura, K., Yamanaka, R., Tohi, K. and Hamada, H. (2000) 'Cyanobacterium-catalyzed asymmetric reduction of ketones', *Tetrahedron Letters,* 41(35), pp. 6799-6802.

Newell, R., Raimi, D. and Aldana, G. (2019) 'Global energy outlook 2019: the next generation of energy', *Resources for the Future*, pp. 8-19.

Ng, I. S., Keskin, B. B. and Tan, S. I. (2020) 'A critical review of genome editing and synthetic biology applications in metabolic engineering of microalgae and cyanobacteria', *Biotechnology Journal,* 15(8), pp. 1900228.

Nikkanen, L., Solymosi, D., Jokel, M. and Allahverdiyeva, Y. (2021) 'Regulatory electron transport pathways of photosynthesis in cyanobacteria and microalgae: recent advances and biotechnological prospects', *Physiologia Plantarum*, *173*(2), pp.514-525.

Oda, T., Oda, K., Yamamoto, H., Matsuyama, A., Ishii, M., Igarashi, Y. and Nishihara, H. (2013) 'Hydrogen-driven asymmetric reduction of hydroxyacetone to (R)-1, 2-propanediol by Ralstonia eutropha transformant expressing alcohol dehydrogenase from Kluyveromyces lactis', *Microbial Cell Factories,* 12(1), pp. 1-9.

Ohbayashi, R., Akai, H., Yoshikawa, H., Hess, W. R. and Watanabe, S. (2016) 'A tightly inducible riboswitch system in Synechocystis sp. PCC 6803', *The Journal of General and Applied Microbiology*.

Oliver, J. W., Machado, I. M., Yoneda, H. and Atsumi, S. (2013) 'Cyanobacterial conversion of carbon dioxide to 2, 3-butanediol', *Proceedings of the National Academy of Sciences,* 110(4), pp. 1249-1254.

Parmeggiani, F., Brenna, E., Colombo, D., Gatti, F. G., Tentori, F. and Tessaro, D. (2021) '"A Study in Yellow": Investigations in the Stereoselectivity of Ene-Reductases', *ChemBioChem*, *23*(1), p.e202100445.

Pattanaik, B. and Lindberg, P. (2015) 'Terpenoids and their biosynthesis in cyanobacteria', *Life,* 5(1), pp. 269-293.

Pérez, A. A., Liu, Z., Rodionov, D. A., Li, Z. and Bryant, D. A. (2016) 'Complementation of cobalamin auxotrophy in Synechococcus sp. strain PCC 7002 and validation of a

putative cobalamin riboswitch in vivo', *Journal of Bacteriology,* 198(19), pp. 2743-2752.

Płaczek, M., Patyna, A. and Witczak, S. (2017) 'Technical evaluation of photobioreactors for microalgae cultivation'. *E3S web of conferences*: EDP Sciences, 02032.

Prier, C. K. and Kosjek, B. (2019) 'Recent preparative applications of redox enzymes', *Current Opinion in Chemical Biology,* 49, pp. 105-112.

Richmond, A., Cheng-Wu, Z. and Zarmi, Y. (2003) 'Efficient use of strong light for high photosynthetic productivity: interrelationships between the optical path, the optimal population density and cell-growth inhibition', *Biomolecular Engineering,* 20(4-6), pp. 229-236.

Richter, N., Zienert, A. and Hummel, W. (2011) 'A single-point mutation enables lactate dehydrogenase from Bacillus subtilis to utilize NAD+ and NADP+ as cofactor', *Engineering in Life Sciences,* 11(1), pp. 26-36.

Roussou, S., Albergati, A., Liang, F. and Lindblad, P. (2021) 'Engineered cyanobacteria with additional overexpression of selected Calvin-Benson-Bassham enzymes show further increased ethanol production', *Metabolic Engineering Communications,* 12, pp. e00161.

Russo, D. A., Zedler, J. A. and Jensen, P. E. (2019) 'A force awakens: exploiting solar energy beyond photosynthesis', *Journal of Experimental Botany,* 70(6), pp. 1703-1710.

Sakai, M., Ogawa, T., Matsuoka, M. and Fukuda, H. (1997) 'Photosynthetic conversion of carbon dioxide to ethylene by the recombinant cyanobacterium, Synechococcus sp. PCC 7942, which harbors a gene for the ethylene-forming enzyme of Pseudomonas syringae', *Journal of Fermentation and Bioengineering,* 84(5), pp. 434-443.

Santos-Merino, M., Singh, A. K. and Ducat, D. C. (2019) 'New applications of synthetic biology tools for cyanobacterial metabolic engineering', *Frontiers in Bioengineering and Biotechnology,* 7, pp. 33.

Santos-Merino, M., Torrado, A., Davis, G. A., Röttig, A., Bibby, T. S., Kramer, D. M. and Ducat, D. C. (2021) 'Improved photosynthetic capacity and photosystem I oxidation via heterologous metabolism engineering in cyanobacteria', *Proceedings of the National Academy of Sciences,* 118(11), p.e2021523118.

Savile, C. K., Janey, J. M., Mundorff, E. C., Moore, J. C., Tam, S., Jarvis, W. R., Colbeck, J. C., Krebber, A., Fleitz, F. J. and Brands, J. (2010) 'Biocatalytic asymmetric synthesis of chiral amines from ketones applied to sitagliptin manufacture', *Science,* 329(5989), pp. 305-309.

Schädler, T., Cerbon, D. C., de Oliveira, L., Garbe, D., Brück, T. and Weuster-Botz, D. (2019) 'Production of lipids with Microchloropsis salina in open thin-layer cascade photobioreactors', *Bioresource Technology,* 289, pp. 121682.

Selão, T. T., Jebarani, J., Ismail, N. A., Norling, B. and Nixon, P. J. (2020) 'Enhanced production of D-lactate in cyanobacteria by re-routing photosynthetic cyclic and pseudo-cyclic electron flow', *Frontiers in Plant Science,* 10, pp. 1700.

Sengupta, A., Sunder, A. V., Sohoni, S. V. and Wangikar, P. P. (2019) 'The effect of CO2 in enhancing photosynthetic cofactor recycling for alcohol dehydrogenase mediated chiral synthesis in cyanobacteria', *Journal of Biotechnology,* 289, pp. 1-6.

Sheldon, R. A., Brady, D. and Bode, M. L. (2020) 'The Hitchhiker's guide to biocatalysis: recent advances in the use of enzymes in organic synthesis', *Chemical Science,* 11(10), pp. 2587-2605.

Sheldon, R. A. and Woodley, J. M. (2018) 'Role of biocatalysis in sustainable chemistry', *Chemical Reviews,* 118(2), pp. 801-838.

Shen, G., Canniffe, D. P., Ho, M.-Y., Kurashov, V., van der Est, A., Golbeck, J. H. and Bryant, D. A. (2019) 'Characterization of chlorophyll f synthase heterologously produced in Synechococcus sp. PCC 7002', *Photosynthesis Research,* 140(1), pp. 77-92.

Shimoda, K., Kubota, N., Hamada, H., Yamane, S.-y. and Hirata, T. (2004) 'Asymmetric transformation of enones with Synechococcus sp. PCC 7942', *Bulletin of the Chemical Society of Japan,* 77(12), pp. 2269-2272.

Straathof, A. J., Panke, S. and Schmid, A. (2002) 'The production of fine chemicals by biotransformations', *Current Opinion in Biotechnology,* 13(6), pp. 548-556.

Tamoi, M., Miyazaki, T., Fukamizo, T. and Shigeoka, S. (2005) 'The Calvin cycle in cyanobacteria is regulated by CP12 via the NAD (H)/NADP (H) ratio under light/dark conditions', *The Plant Journal,* 42(4), pp. 504-513.

Tanaka, S., Kojima, H., Takeda, S., Yamanaka, R. and Takemura, T. (2020) 'Asymmetric visible-light photobiocatalytic reduction of β-keto esters utilizing the cofactor recycling system in Synechocystis sp. PCC 6803', *Tetrahedron Letters,* 61(24), pp. 151973.

Thiel, K., Patrikainen, P., Nagy, C., Fitzpatrick, D., Pope, N., Aro, E.-M. and Kallio, P. (2019) 'Redirecting photosynthetic electron flux in the cyanobacterium Synechocystis sp. PCC 6803 by the deletion of flavodiiron protein Flv3', *Microbial Cell Factories,* 18(1), pp. 1-16.

Toogood, H. S. and Scrutton, N. S. (2018) 'Discovery, characterization, engineering, and applications of ene-reductases for industrial biocatalysis', *ACS Catalysis,* 8(4), pp. 3532-3549.

Touloupakis, E. and Carlozzi, P. (2021) 'Growth of Photosynthetic Microorganisms in Different Photobioreactors Operated Outdoors', *Cyanobacteria Biotechnology*, pp. 505-530.

Tros, M., Bersanini, L., Shen, G., Ho, M.-Y., van Stokkum, I. H., Bryant, D. A. and Croce, R. (2020) 'Harvesting far-red light: Functional integration of chlorophyll f into Photosystem I complexes of Synechococcus sp. PCC 7002', *Biochimica et Biophysica Acta (BBA)-Bioenergetics,* 1861(8), pp. 148206.

Ungerer, J., Wendt, K. E., Hendry, J. I., Maranas, C. D. and Pakrasi, H. B. (2018) 'Comparative genomics reveals the molecular determinants of rapid growth of the cyanobacterium Synechococcus elongatus UTEX 2973', *Proceedings of the National Academy of Sciences,* 115(50), pp. E11761-E11770.

van der Woude, A. D., Angermayr, S. A., Veetil, V. P., Osnato, A. and Hellingwerf, K. J. (2014) 'Carbon sink removal: increased photosynthetic production of lactic acid by Synechocystis sp. PCC6803 in a glycogen storage mutant', *Journal of Biotechnology,* 184, pp. 100-102.

Varman, A. M., Yu, Y., You, L. and Tang, Y. J. (2013) 'Photoautotrophic production of D-lactic acid in an engineered cyanobacterium', *Microbial Cell Factories,* 12(1), pp. 1-8.

Vavitsas, K., Kugler, A., Satta, A., Hatzinikolaou, D. G., Lindblad, P., Fewer, D. P., Lindberg, P., Toivari, M. and Stensjö, K. (2021) 'Doing synthetic biology with photosynthetic microorganisms', *Physiologia Plantarum,* 173(2), pp. 624-638.

Vidal, L. S., Kelly, C. L., Mordaka, P. M. and Heap, J. T. (2018) 'Review of NAD (P) H-dependent oxidoreductases: Properties, engineering and application', *Biochimica et Biophysica Acta (BBA)-Proteins and Proteomics,* 1866(2), pp. 327-347.

Wang, B., Pugh, S., Nielsen, D. R., Zhang, W. and Meldrum, D. R. (2013) 'Engineering cyanobacteria for photosynthetic production of 3-hydroxybutyrate directly from CO2', *Metabolic Engineering,* 16, pp. 68-77.

Wang, B., Wang, J., Zhang, W. and Meldrum, D. R. (2012) 'Application of synthetic biology in cyanobacteria and algae', *Frontiers in Microbiology,* 3, pp. 344.

Wang, C. and Lan, C. Q. (2018) 'Effects of shear stress on microalgae–a review', *Biotechnology Advances,* 36(4), pp. 986-1002.

Wang, Y., Tahir, N., Cao, W., Zhang, Q. and Lee, D.-J. (2019) 'Grid columnar flat panel photobioreactor with immobilized photosynthetic bacteria for continuous photofermentative hydrogen production', *Bioresource Technology,* 291, pp. 121806.

Watanabe, S. (2020) 'Cyanobacterial multi-copy chromosomes and their replication', *Bioscience, Biotechnology, and Biochemistry,* 84(7), pp. 1309-1321.

Wendt, K. E., Ungerer, J., Cobb, R. E., Zhao, H. and Pakrasi, H. B. (2016) 'CRISPR/Cas9 mediated targeted mutagenesis of the fast growing cyanobacterium Synechococcus elongatus UTEX 2973', *Microbial Cell Factories,* 15(1), pp. 1-8.

Whitton, B. A. and Potts, M. (2007) *The ecology of cyanobacteria: their diversity in time and space.* Springer Science & Business Media.

Wijffels, R. H., Kruse, O. and Hellingwerf, K. J. (2013) 'Potential of industrial biotechnology with cyanobacteria and eukaryotic microalgae', *Current Opinion in Biotechnology,* 24(3), pp. 405-413.

Winkler, C. K., Tasnádi, G., Clay, D., Hall, M. and Faber, K. (2012) 'Asymmetric bioreduction of activated alkenes to industrially relevant optically active compounds', *Journal of Biotechnology,* 162(4), pp. 381-389.

Wlodarczyk, A., Gnanasekaran, T., Nielsen, A. Z., Zulu, N. N., Mellor, S. B., Luckner, M., Thøfner, J. F. B., Olsen, C. E., Mottawie, M. S. and Burow, M. (2016) 'Metabolic engineering of light-driven cytochrome P450 dependent pathways into Synechocystis sp. PCC 6803', *Metabolic Engineering,* 33, pp. 1-11.

Włodarczyk, A., Selão, T. T., Norling, B. and Nixon, P. J. (2020) 'Newly discovered Synechococcus sp. PCC 11901 is a robust cyanobacterial strain for high biomass production', *Communications Biology,* 3(1), pp. 1-14.

Wohlgemuth, R. (2021) 'Biocatalysis–Key enabling tools from biocatalytic one-step and multi-step reactions to biocatalytic total synthesis', *New Biotechnology,* 60, pp. 113-123.

Woodley, J. M. (2019) 'Accelerating the implementation of biocatalysis in industry', *Applied Microbiology and Biotechnology,* 103(12), pp. 4733-4739.

Xiao, Y., Wang, S., Rommelfanger, S., Balassy, A., Barba-Ostria, C., Gu, P., Galazka, J. M. and Zhang, F. (2018) 'Developing a Cas9-based tool to engineer native plasmids in Synechocystis sp. PCC 6803', *Biotechnology and Bioengineering,* 115(9), pp. 2305-2314.

Xue, S., Zhang, Q., Wu, X., Yan, C. and Cong, W. (2013) 'A novel photobioreactor structure using optical fibers as inner light source to fulfill flashing light effects of microalgae', *Bioresource Technology,* 138, pp. 141-147.

Xue, Y., Zhang, Y., Grace, S. and He, Q. (2014) 'Functional expression of an Arabidopsis p450 enzyme, p-coumarate-3-hydroxylase, in the cyanobacterium Synechocystis PCC 6803 for the biosynthesis of caffeic acid', *Journal of Applied Phycology,* 26(1), pp. 219-226.

Yamanaka, R., Nakamura, K., Murakami, M. and Murakami, A. (2015) 'Selective synthesis of cinnamyl alcohol by cyanobacterial photobiocatalysts', *Tetrahedron Letters,* 56(9), pp. 1089-1091.

Yao, L., Shabestary, K., Björk, S. M., Asplund-Samuelsson, J., Joensson, H. N., Jahn, M. and Hudson, E. P. (2020) 'Pooled CRISPRi screening of the cyanobacterium Synechocystis sp PCC 6803 for enhanced industrial phenotypes', *Nature Communications,* 11(1), pp. 1-13.

Yazdi, M. T., Arabi, H., Faramarzi, M. A., Ghasemi, Y., Amini, M., Shokravi, S. and Mohseni, F. A. (2004) 'Biotransformation of hydrocortisone by a natural isolate of Nostoc muscorum', *Phytochemistry,* 65(15), pp. 2205-2209.

Yu, J., Liberton, M., Cliften, P. F., Head, R. D., Jacobs, J. M., Smith, R. D., Koppenaal, D. W., Brand, J. J. and Pakrasi, H. B. (2015) 'Synechococcus elongatus UTEX 2973, a fast growing cyanobacterial chassis for biosynthesis using light and CO2', *Scientific Reports,* 5(1), pp. 1-10.

Zhou, J., Meng, H., Zhang, W. and Li, Y. (2018) 'Production of Industrial Chemicals from CO 2 by Engineering Cyanobacteria', *Synthetic Biology of Cyanobacteria*, pp. 97-116.

Zhou, J., Zhang, F., Meng, H., Zhang, Y. and Li, Y. (2016) 'Introducing extra NADPH consumption ability significantly increases the photosynthetic efficiency and biomass production of cyanobacteria', *Metabolic Engineering,* 38, pp. 217-227.

Zhou, J., Zhang, H., Meng, H., Zhu, Y., Bao, G., Zhang, Y., Li, Y. and Ma, Y. (2014) 'Discovery of a super-strong promoter enables efficient production of heterologous proteins in cyanobacteria', *Scientific Reports,* 4(1), pp. 1-6.

Zhou, P., Wang, L., Liu, H., Li, C., Li, Z., Wang, J. and Tan, X. (2021) 'CyanoOmicsDB: an integrated omics database for functional genomic analysis of cyanobacteria', *Nucleic Acids Research*, *50*(D1), pp. D758-D764.

# CHAPTER II

# Engineering cyanobacterial chassis for improved electron supply toward a heterologous ene-reductase

**J. Spasic**, P. Oliveira, C. Pacheco, R. Kourist, P. Tamagnini, *submitted*

# Engineering cyanobacterial chassis for improved electron supply toward a heterologous ene-reductase

Jelena Spasic[a, b, c, d], Paulo Oliveira[a, b, c, 1], Catarina Pacheco[a, b, c], Robert Kourist[d], Paula Tamagnini[a ,b , c, *]

a, i3S - Instituto de Investigação e Inovação em Saúde, Universidade do Porto, Rua Alfredo Allen 208, 4200-135 Porto, Portugal

b, IBMC - Instituto de Biologia Molecular e Celular, Universidade do Porto, Rua Alfredo Allen 208, 4200-135 Porto, Portugal

c, Departamento de Biologia, Faculdade de Ciências, Universidade do Porto, Rua do Campo Alegre, 4169-007 Porto, Portugal

d, Institute of Molecular Biotechnology, Graz University of Technology, Petersgasse 14, 8010 Graz, Austria

[1]present address: CIIMAR - Centro Interdisciplinar de Investigação Marinha e Ambiental, Universidade do Porto, Terminal de Cruzeiros do Porto de Leixões, Av. General Norton de Matos S/N, 4450-208 Matosinhos, Portugal

[*]**Corresponding authors.**

Email address: pmtamagn@ibmc.up.pt

**Keywords:** Biocatalysis; Biotransformation; Cyanobacteria; *Synechocystis*; Synthetic biology;

**Abbreviations:**

2-MM 2-methylmaleimide

2-MS 2-methylsuccinimide

CDW Cell dry weight

chl *a* Chlorophyll *a*

Cm Chloramphenicol

Flv Flavodiiron

FMN Flavin mononucleotide

FNR Ferredoxin-$NADP^+$ oxidoreductase

GC-FID Gas chromatography flame ionization detector

HOX Hydrogenase

Km Kanamycin

LB Lysogeny broth medium

OD Optical density

Sm Streptomycin

wt Wild-type

YqjM Ene-reductase from *Bacillus subtilis*

ABSTRACT

Cyanobacteria are noteworthy hosts for industrially relevant redox reactions, owing to a light-driven cofactor recycling system using water as electron donor. Customizing *Synechocystis* sp. PCC 6803 chassis by redirecting electron flow offers a particularly interesting approach to further improve light-driven biotransformations. Therefore, different chassis expressing the heterologous ene-reductase YqjM (namely Δ*hoxYH*, Δ*flv3*, Δ*ndhD2* and Δ*hoxYH*Δ*flv3*) were generated/evaluated. The results showed the robustness of the chassis, that exhibited growth and oxygen evolution rates similar to *Synechocystis* wild-type, even when expressing YqjM. By engineering the electron flow, the YqjM light-driven stereoselective reduction of 2-methylmaleimide to 2-methylsuccinimide was significantly enhanced in all chassis. In the best performing chassis (Δ*hoxYH*, lacking an active bidirectional hydrogenase) a 39% increase was observed, reaching an *in vivo* specific activity of 116 U $g_{DCW}^{-1}$ and a product formation rate of 16.7 mM $h^{-1}$. In addition, the presence of the heterologous YqjM mitigated substrate toxicity, and the conversion of 2-methylmaleimide increased oxygen evolution rates, in particular at higher light intensity. In conclusion, this work demonstrates that rational engineering of electron transfer pathways is a valid strategy to increase *in vivo* specific activities and product formation rates in cyanobacterial chassis harboring oxidoreductases.

# 1. Introduction

In the light of establishing primary producers as chassis for light-driven biotechnology, cyanobacteria are remarkably gaining attention for photobiotransformations (Jodlbauer et al., 2021; Schmermund et al., 2019). The ease of cultivation, dependency on light as an energy source, $CO_2$ as a carbon source, and water as electron donor paved the way for a rapid interest in these biological platforms (Knoot et al., 2018). Cyanobacteria harvest (sun)light energy converting it to reducing power that can be redirected for the production of valuable compounds and/or for the activity of biocatalysts. This is a particularly interesting approach

for redox transformations, one of the most important reactions in organic synthesis which requires reduced electron donors such as nicotinamide cofactors (NADPH) (Hollmann et al., 2011). In cyanobacteria coupling whole-cell redox reactions to photosynthetic electron flow will allow for the substitution of sacrificial co-substrates by using water as the electron donor (Köninger et al., 2016).

In the last years, the progress of synthetic biology of cyanobacteria provided the tools for heterologous expression of oxidoreductive enzymes benefiting from the steady photosynthetic production of cofactors (Schmermund et al., 2019), with several examples ranging from ene-reductases (Assil-Companioni et al., 2020; Köninger et al., 2016), Baeyer–Villiger monooxygenase (Böhmer et al., 2017; Erdem et al., 2021), imine reductase (Büchsenschütz et al., 2020), AlkBGT hydroxylation system (Hoschek et al., 2019a), hydroxyisocaproate dehydrogenases (Jurkaš et al., 2021) and cytochrome P450 monooxygenase, (Hoschek et al., 2019b) underline the versatility of this approach. Previously reported rates for whole-cell biotransformations with *Synechocystis* sp. PCC 6803 cells expression heterologous enzymes are in the range of 5.5 U $g_{DCW}^{-1}$ for the monooxygenase AlkBGT (Hoschek et al., 2019a), 5.7 U $g_{DCW}^{-1}$ for the monooxygenase CHMO (Böhmer et al., 2017), 20 U $g_{DCW}^{-1}$ for an imine reductase (Büchsenschütz et al., 2020), 39 U $g_{DCW}^{-1}$ for a P450 monooxygenase (Hoschek et al., 2019b) and above 100 U $g_{DCW}^{-1}$ for the YqjM ene-reductase (Assil-Companioni et al., 2020; Köninger et al., 2016). Rates above 100 U $g_{DCW}^{-1}$ are of particular interest for the establishment of industrial applications towards the synthesis of fine chemicals requiring a productivity of 1-10 g $L^{-1}$ $h^{-1}$ (Hoschek et al., 2018). Engineering cyanobacterial hosts/chassis by directing more reducing power to fuel the activities of heterologous enzymes represents an attractive approach to improve the reaction rates. Since one of the limitations for high reaction rates could be the competition from native electron transfer pathways, along with the inherent regulation of the photosynthetic electron transport that dissipates the excess electrons (Russo

et al., 2019), the rewiring of photosynthesis offers the possibility of redirecting excess reducing potential to catalyze the formation of high-value compounds, enabling the tapping of electrons that otherwise would be wasted. Despite the vast knowledge regarding regulatory mechanisms around the cyanobacterial photosynthetic machinery (Lea-Smith et al., 2016; Mullineaux, 2014; Nikkanen et al., 2021), cyanobacterial chassis customization for enhancing the availability of reductive power to drive biocatalytic reactions within the cell is yet to be realized.

To maintain redox balance and prevent dangerous over-reduction of the electron transport chain, cyanobacteria have evolved a remarkable number of mechanisms to adjust the balance of photosynthetic outputs. They do so by mainly removing electrons from the photosynthetic electron transport chain through the activity of switches known as “electron valves” or by balancing cyclic vs. linear electron transport (Mullineaux, 2014; Murata et al., 2012). Flavodiiron proteins function as efficient release valves, reducing $O_2$ to $H_2O$, in a Mehler-like reaction (Allahverdiyeva et al., 2013). Recently, it was demonstrated that in *Synechocystis* sp. PCC 6803 the activity of a heterologous ene-reductase and a Baeyer–Villiger monooxygenase could be enhanced by the deletion of flavodiiron-protein encoding genes (Assil-Companioni et al., 2020; Erdem et al., 2021). The bidirectional hydrogenase was suggested to act as a valve for low-potential electrons (Appel et al., 2000; Tamagnini et al., 2007), being insensitive to light, reversibly inactivated by $O_2$, and quickly reactivated by NADH or NADPH (Cournac et al., 2004). A markerless deletion mutant (Δ*hoxYH*) lacking the functional bidirectional hydrogenase was previously constructed and characterized as a robust photoautotrophic chassis (Pinto et al., 2015), and used for the expression of heterologous hydroxyisocaproate dehydrogenases (Jurkaš et al., 2021). Regarding the cyclic electron transport, one of the routes involves electron transfer from ferredoxin to plastoquinone via NAD(P)H dehydrogenase-like complex 1 (NDH-1), particularly subunit

NdhD2 (Battchikova et al., 2011). It was previously shown that deletion of the gene coding for NdhD2 subunit led to increased activity of a heterologous cytochrome P450 expressed in *Synechococcus* sp. PCC 7002 (Berepiki et al., 2018).

To meet the goal of engineering the photosynthetic electron flow to create a customized *Synechocystis* sp. PCC 6803 based chassis optimized for redox-dependent enzymatic reactions, we focused on deleting several natural electron switches, dispensable under controlled laboratory conditions. The strategy consisted on inactivating genes coding for Flv3 (*sll0550*) or NdhD2 (*slr1291*) in *Synechocystis* sp. PCC 6803 wild-type (from now on wt) or by using the previously generated *Synechocystis* Δ*hoxYH* mutant and a novel double Δ*hoxYH*Δflv3 mutant (Pinto et al., 2012). To evaluate the effects of these deletions on the functionality and productivity of the chassis, we chose to express the well-characterized heterologous ene-reductase YqjM from *Bacillus subtilis*. This enzyme displays high conversion and enhanced enantioselectivity of fast C=C double-bond reduction without side reactions constituting, therefore, a promising approach to evaluate rational design (Köninger et al., 2016). Our results demonstrate that engineering cyanobacterial chassis customized for biotransformations leads to improved activities and reaction rates of the YqjM-catalyzed ene-reduction.

# 2. Materials and methods

### *2.1. Chemicals and reagents*

The substrate 2-methylmaleimide (2-MM) was synthesized as previously described (Köninger et al., 2016). All other chemicals and reagents were purchased from ThermoFisher Scientific (USA), Merck (Germany) or Sigma-Aldrich (USA) unless otherwise indicated. All DNA-modifying enzymes and polymerases were purchased from ThermoFisher Scientific (USA) and Promega (USA), and standard molecular biology kits were obtained from NZY Tech (Portugal).

### *2.2. Organisms and standard growth conditions*

The wild-type unicellular non-$N_2$-fixing cyanobacterium *Synechocystis* sp. PCC 6803 substrain GT-Kazusa and mutants were maintained in Erlenmeyer flasks in BG-11 medium (Stanier et al., 1971) with orbital shaking (150 rpm), under a 12 h light (cool white daylight 20 μmol $m^{-2}$ $s^{-1}$)/ 12 h dark regimen at 30 ºC unless otherwise stated. For light-driven biotransformations, Western blot analysis and oxygen evolution rates BG-11 was supplemented with 5 mM HEPES, pH 8.0. For solid medium, BG-11 was supplemented with 1.5% Noble agar (Difco), 0.3% sodium thiosulfate and 10 mM TES-KOH buffer (pH 8.2). For the selection and maintenance of the mutants, BG-11 medium was supplemented with kanamycin (Km, up to 250 μg $mL^{-1}$), streptomycin (Sm, up to 10 μg $mL^{-1}$), and/or chloramphenicol (Cm, up to 20 μg $mL^{-1}$). *Escherichia coli* strains DH5α or XL-1 Blue were used for cloning purposes. *E. coli* transformants were grown at 37 ºC in Lysogeny broth (LB) medium supplemented with ampicillin (100 μg $mL^{-1}$), Km (50 μg $mL^{-1}$), Sm (50 μg $mL^{-1}$) or Cm (50 μg $mL^{-1}$).

### *2.3. DNA extraction and recovery*

Cyanobacterial genomic DNA was extracted using the phenol/chloroform method described previously (Tamagnini et al., 1997). Agarose gel electrophoresis was performed by standard protocols using 1xTAE buffer (Russell and Sambrook, 2001) and the DNA fragments were purified using the NZYGelpure kit (NZYTech).

### *2.4. Plasmid construction*

Construction of the integrative plasmids for the deletion of *flv3* and *ndhD2* genes was performed as described (Pinto et al., 2012). Plasmids were based on the pGEM®-T easy vector (Promega), containing *Synechocystis* chromosomal regions flanking the *ndhD2* (*slr1291*) or *flv3* (*sll0550*) gene, amplified with Phusion® High-Fidelity DNA Polymerase and specific primers (Table S1), using *Synechocystis* genomic DNA as a template. The

corresponding up and downstream fragments were purified and fused by 'overlap-PCR' using Phusion® High-Fidelity DNA Polymerase. The resulting PCR products were purified and cloned into the pGEM®-T Easy vector using the T4 DNA ligase (Promega). To remove pGEM-T Easy restriction sites incompatible with the BioBrick RFC[10] standard, the vectors were digested with *XhoI* and *SalI* and recircularized. The pGEM-T easy vector containing *ndhD2* flanking regions was linearized using *XmaI*, while the pGEM-T easy vector containing *flv3* flanking regions was linearized using *SmaI*. A selection cassette containing the *nptII* gene (encoding a neomycin phosphotransferase that confers resistance to neomycin and kanamycin) was amplified from pKm.1 plasmid (Pinto et al., 2015) with Phusion® High-Fidelity DNA Polymerase using the primer pair Km.KmScFwd/KmRev (Pinto et al., 2015) and digested with *XmaI*. Subsequently, the purified antibiotic cassette was cloned into the *XmaI* restriction site to form the final plasmid pGEM_Δ*ndhD2*.km. The cassette containing the *aadA* gene (conferring resistance to streptomycin and spectinomycin) was digested from the plasmid pSEVA481 (Silva-Rocha et al., 2013) using *PshAI* and cloned into a linearised pGEM-T easy vector with flanking regions of *flv3* gene to form the final plasmid pGEM_Δ*flv3*.sm. The identity of all the constructs was confirmed by DNA sequencing (StabVida). The integrative plasmid pSynRekB_$P_{cpc}$::*yqjM* conferring resistance to Km was previously constructed (Assil-Companioni et al., 2020), while the integrative plasmid pMD19T_slr0168_$P_{cpc}$::*yqjM* giving resistance to Cm was kindly provided by Prof. Paul Hudson (KTH, Sweden). All the plasmids used to transform *Synechocystis* are listed in Table S2. Plasmids pGEM_Δ*ndhD2*.km and pGEM_Δ*flv3*.sm are available in Addgene.

### *2.5. Generation of Synechocystis deletion mutants*

*Synechocystis* sp. PCC 6803 wild-type and *Synechocystis* Δ*hoxHY* (Pinto et al., 2012) were transformed based on a method previously described (Williams, 1988). Briefly, *Synechocystis* cultures were grown under 12 h light (20 μmol $m^{-2}$ $s^{-1}$)/12 h dark cycle to an $OD_{730}$ ~ 0.5 at 30

ºC. Cells were harvested by centrifugation at 3850 *g* for 10 min and suspended in BG-11 to a final $OD_{730}$ 2.5. 500 µL of cells were incubated with 10 µg of purified pGEM_Δ*ndhD2*.km or pGEM_Δ*flv3*.sm plasmid for 5 h in light at 30 ºC. Cells were spread onto BG-11 plates and incubated under continuous light (20 µmol $m^{-2}$ $s^{-1}$) at 30 ºC. After 24 h, cells were transferred to selective BG-11 plates supplemented with 10 µg $mL^{-1}$ Km or 3 µg $mL^{-1}$ Sm. Transformants were observed after 2-3 weeks. For complete segregation, colonies were streaked onto BG-11 plates increasing antibiotic concentrations (Km up to 250 µg $mL^{-1}$; Sm up to 10 µg $mL^{-1}$) and transferred into liquid BG-11 medium. The full segregation was confirmed by PCR using GoTaq® G2 Flexi DNA Polymerase and specific primers (Table S1).

### *2.6. Introduction of the yqjM into Synechocystis chassis*

The Km-resistant pSynRekB_$P_{cpc}$::*yqjM* plasmid or Cm-resistant pMD19T_slr0168_$P_{cpc}$::*yqjM* were introduced into *Synechocystis* strains by natural transformation following the same protocol as described above. For complete segregation, colonies were streaked onto BG-11 plates increasing antibiotic concentrations (Km up to 100 µg $mL^{-1}$; Cm up to 20 µg $mL^{-1}$) and transferred into a liquid BG-11 medium. The full segregation was confirmed by PCR using GoTaq® G2 Flexi DNA Polymerase and Seg_fw /Seg_rv primers (Table S1). The sequence identity was confirmed by DNA sequencing. All the *Synechocystis* strains used are listed in Table S3.

### *2.7. Growth experiments*

Pre-cultures of *Synechocystis* wt and mutants were grown in 10 mL BG-11 medium in 25 mL Erlenmeyer flasks on an orbital shaker (150 rpm) under a 12 h light (20 µmol $m^{-2}$ $s^{-1}$)/12 h dark regimen at 28 ºC. These were grown to an $OD_{730}$ ~2, diluted in fresh BG-11 to an $OD_{730}$ ~0.5 and 200 µL aliquots inoculated in F-Bottom 96-Well Assay Microplates (Greiner Bio-One™). The plate was incubated under the same conditions as pre-cultures. The growth was monitored by measuring the optical density ($OD_{790}$) for 7 days, using the Synergy 2 Multi-Mode

Microplate Reader and the Gen5$^{TM}$ software (BioTek Instruments, Inc.) All growth experiments were performed in the absence of selective pressure and included at least three biological replicates with technical triplicates.

### *2.8. Light-driven biotransformations*

Light-driven biotransformations were performed based on a method previously described (Assil-Companioni et al., 2020). Cultures were inoculated in 100 mL BG-11 medium in 300 mL Erlenmeyer flasks on an orbital shaker (150 rpm) under continuous white light (~50 µmol $m^{-2}$ $s^{-1}$) at 30 ºC and grown to an $OD_{750}$ ~1.5. Cells were harvested by centrifugation at 3220 *g* for 20 min and suspended in a fresh medium to reach the desired $OD_{750}$. Reactions were performed in 5 mL glass vials with a working volume of 1 mL. The reaction was started by the addition of 10 mM 2-methylmaleimide (from a 100 mM stock in BG-11). The vials were placed into a bioreactor equipped with white LED lamps (~150 µmol $m^{-2}$ $s^{-1}$) with orbital shaking (140 rpm) at 30 ºC. Samples were taken at different time points according to the following sampling scheme: before (t0) and 5, 10, 15, 30, 60 and 120 min after substrate addition. To quench the reaction, samples were snap frozen in liquid nitrogen and stored at -20 ºC.

### *2.9. Nitrogen limiting and mixotrophic cultivation conditions*

For nitrogen limiting cultivation conditions, the cultures were inoculated in 100 mL $BG\text{-}11_0$ medium supplemented with 1.76 mM $NaNO_3$ or 0.88 mM $NaNO_3$ in 300 mL Erlenmeyer flasks and placed on an orbital shaker (150 rpm) under continuous white light (~50 µmol $m^{-2}$ $s^{-1}$) at 30 ºC and grown to an $OD_{750}$ ~1.5. For mixotrophic cultivation conditions, the cultures were inoculated in 100 mL $BG\text{-}11_0$ medium supplemented with 5 mM arginine and 10 mM glucose in 300 mL Erlenmeyer flasks on an orbital shaker (150 rpm) under continuous white light (~50 µmol $m^{-2}$ $s^{-1}$) at 30 ºC and grown to an $OD_{750}$ ~1.5. The cells were harvested and used in light-driven biotransformations as previously described.

*2.10. 12h light / 12 h dark or continuous blue/red light cultivation conditions*

The cultures were inoculated in 100 mL BG-11 in 300 mL Erlenmeyer flasks and placed on an orbital shaker (150 rpm) under 12 h light (~50 µmol $m^{-2}$ $s^{-1}$) / 12 h dark or continuous blue / red light (~150 µmol $m^{-2}$ $s^{-1}$) at 30 ºC and grown to an $OD_{750}$ ~1.5. The cells were harvested and used in light-driven biotransformations as previously described. The spectra of the blue/red lamps used for cultivation was previously determined (Assil-Companioni et al., 2020).

*2.11. Quantitative GC-FID Analysis*

GC-FID (GC-2010 Plus, Shimadzu, Japan) equipped with the ZB-5 column was used to analyze the biotransformations samples. Sample preparation was carried out by organic phase extraction using ethyl-acetate and 2 mM 1-decanol as an internal standard. A 100 µL sample was mixed with 400 µL ethyl-acetate, vortexed and the upper organic layer was dried over $MgSO_4$. A detailed description of the utilized separation method is available in Table S4.

*2.12. SDS PAGE and Western blot*

Cultures were inoculated in 50 mL BG-11 medium in 100 mL Erlenmeyer flasks on an orbital shaker (150 rpm) under continuous white light (~50 µmol $m^{-2}$ $s^{-1}$) at 30 ºC and grown to an $OD_{730}$ ~1.5. The cells were harvested by centrifugation at 3850 *g* for 10 min and suspended in lysis buffer (10 mM HEPES pH 8.0, 10 mM EDTA pH 8.0, 0.5% (vol/vol) Triton X-100, 2 mM DTT) supplemented with 1 tablet of cOmplete EDTA-free protease inhibitor cocktail (Roche) per 7 mL of buffer. Cells were disrupted by sonication on ice with a Branson Sonifier 250 using 5 cycles of 15 s (50% duty cycle, output control 3) including 30 s cooling breaks in between. The cell pellet was separated by two rounds of 10 min centrifugation at 10000 *g*, 4°C. The protein concentration was determined using the Bradford protein assay (Bio-Rad). Ten µg of protein extracts were denatured in reducing SDS sample buffer (50 mM Tris-HCl pH 6.8, 2 % (w/v) SDS, 10% (v/v) glycerol, 12.5 mM EDTA, 0.02% (w/v) Bromphenol blue, 1% (v/v) β-mercaptoethanol) for 5 min at 95 ºC and separated by electrophoresis on 12%

(wt/vol) SDS-polyacrylamide gels. Proteins were visualized using PageBlue™ Protein Staining Solution (Thermo Scientific) or blotted onto nitrocellulose membrane pore size 0.45 µm (Amersham™ Protan™, GE Healthcare). Western blots were performed using the anti-6x-His-Tag (Invitrogen) and the HRP-conjugated anti-mouse IgG antibody (Sigma). The blot was developed using Clarity™ Western ECL Substrate (Bio-Rad) on a ChemiDoc™ XRS+ Imager (Bio-Rad). In this experiment, three independent biological replicates were performed.

*2.13. in vitro NADPH assay*

For the preparation of cell extracts, 1 mL of cells $OD_{750}$ ~ 20 was centrifuged at 16000 *g* for 5 min, 4 ºC and the pellet was suspended in 2 mL PBS buffer (137 mM NaCl, 2.7 mM KCl, 10 mM $Na_2HPO_4$, 1.8 mM $KH_2PO_4$, pH 7.4). After subsequent centrifugation, the supernatant was discarded, and cells were suspended in 200 µL PBS supplemented with 1 mM aminocaproic acid, and 0.25 mm glass beads. Cells were disrupted by vortexing 4 times for 30 s including 30 s cooling breaks in between. After the centrifugation at 16000 *g* for 5 min, 4 ºC, 100 µL PBS was added to the supernatant and the resulting soluble proteins extract was separated from the glass beads. The protein concentration was determined using the Pierce™ BCA Protein Assay Kit (Thermo Scientific). The cell lysate was used in the *in vitro* NADPH assay. For the assay, potassium buffer (20 mM, pH 6.5) was degassed by $N_2$ sparging for 15 min. 1 mM 2-methylmaleimide and 125 µM NADPH were mixed with buffer in a cuvette and the reaction was started with the addition of 100 µL cell lysate. Absorption at 340 nm was monitored for 3 min. Control reactions without the addition of the substrate were performed to subtract background reactions. The activity presented in U $g_{total\ protein}^{-1}$ was calculated from the slope, the NADPH extinction coefficient and the protein concentration. An example of the raw data generated is given in the supporting information (Fig. S1).

### *2.14. $O_2$ evolution measurements*

$O_2$ evolution rate was measured using a Clark-type $O_2$ electrode (Oxygraph; Hansatech Ltd.). The calibration was done using sodium bisulfite and air-saturated water at 30 ºC. Cultures were inoculated in 50 mL BG-11 medium in 100 mL Erlenmeyer flasks on an orbital shaker (150 rpm) under continuous white light (~50 µmol $m^{-2}$ $s^{-1}$) at 30 ºC and grown to an $OD_{730}$ ~1.5. The cells were harvested by centrifugation at 3850 *g* for 10 min and suspended in fresh medium to $OD_{730}$ ~10. The measurement was carried out using 1 mL of cells, following dark equilibration for 2 min; oxygen evolution rates were recorded after the initial 15 s in light (~150 µmol $m^{-2}$ $s^{-1}$ or ~800 µmol $m^{-2}$ $s^{-1}$). For the measurements in the presence of the substrate, 100 µL of 100mM 2-MM solution (prepared in BG-11) was added to cells before light exposure.

### *2.15. Cell dry weight*

To measure the dry cell weight, a culture volume of known $OD_{750}$ was washed once with distilled water and dried at 60 ºC prior to measuring. $OD_{750}$ 10 corresponded to a cell density of approximately 2.4 g $L^{-1}$

### *2.16. Statistical analysis*

The statistical analysis was performed using an unpaired *t* test in GraphPad Prism v5.03 (GraphPad Software Inc.).

## 3. Results and Discussion

### *3.1. Generation of Synechocystis chassis and introduction of the ene-reductase YqjM*

In this work, chassis customization focused on engineering *Synechocystis*' electron transfer pathways as a principle to improve the streamlining of reduced cofactors towards industrial relevant biotransformations. For this purpose, *Synechocystis* mutants lacking the gene encoding the flavodiiron protein 3, the NdhD2 subunit of the type I NADH dehydrogenase complex, or the HoxY and HoxH subunits of bidirectional hydrogenase and the flavodiiron

protein 3 were generated. In total, 5 different chassis were evaluated, namely the *Synechocystis* wt, Δ*hoxYH* (Pinto et al., 2012), Δ*flv3*, Δ*ndhD2*, and the double mutant Δ*hoxYH*Δ*flv3*. The segregation of the generated mutants was confirmed by PCR (Fig. S2). To evaluate the chassis potential for stereoselective photobiotransformations, the *yqjM* gene (*namA*) (Köninger et al., 2016) under the control of a strong $P_{cpcB}$ promoter (Assil-Companioni et al., 2020), and with a sequence coding for a N-terminal 6xHis tag was introduced via natural transformation and integrated into *Synechocystis*'s chromosome in the neutral site *slr0168* (Williams, 1988). The presence of the module harboring *yqjM* and the segregation of mutants were confirmed by PCR analysis (Fig. S3) and by sequencing.

### *3.2. Growth performance of the Synechocystis engineered strains*

Under a 12 h white light (20 μmol $m^{-2}$ $s^{-1}$) / 12 h dark regimen no significant differences were observed between the growth rates of the mutants compared to the wt (Fig. 1). Our results are in agreement with previous studies (Berepiki et al., 2018; Pinto et al., 2012; Selão et al., 2020), further underlying the robustness of the customized chassis. In addition, the cell growth rate remained unchanged upon the introduction of the module harboring the *yqjM* (Fig. 1). For the original growth curves see Fig. S4.

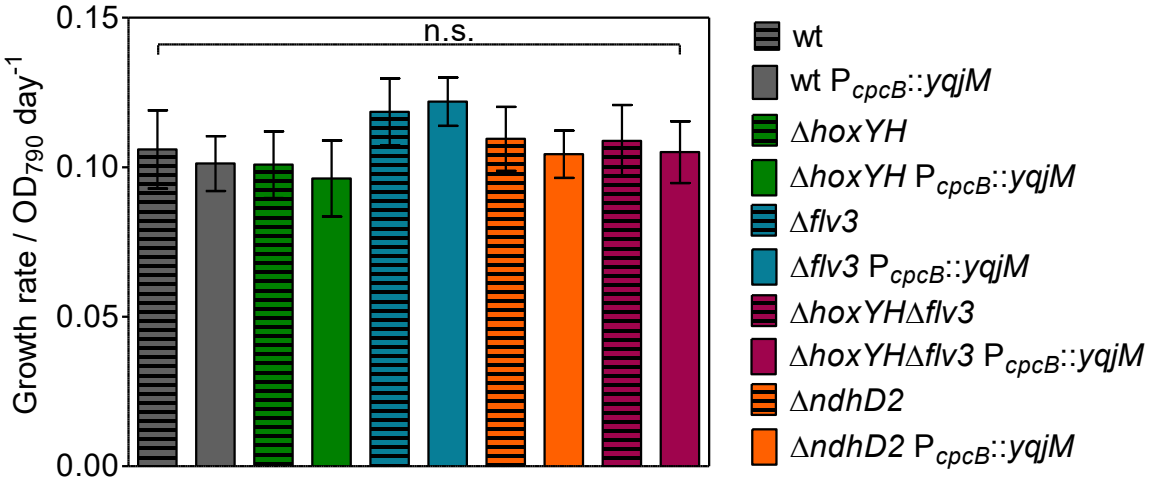

**Fig. 1**. Growth rates of *Synechocystis* sp. PCC 6803 (wt), Δ*hoxYH*, Δ*flv3*, Δ*ndhD2* and Δ*hoxYH*Δ*flv3* mutants, and of these chassis expressing YqjM. Cells were cultivated in 96-well microplates in BG-11 at 28 ºC with orbital shaking (150 rpm) under 12 h white light (20 µmol $m^{-2}$ $s^{-1}$) / 12 h dark regimen. Error bars correspond to standard deviations from at least three biological replicates with technical triplicates and statistical analysis is presented based on an unpaired *t*-test (n.s., not significant).

### *3.3. Redirecting electron flow increases in vivo YqjM activity*

The effect of streamlining electron flow was evaluated by measuring YqjM activity *in vivo* in a light-driven, fast C=C bond reduction. Using 2-methylmaleimide (2-MM) as substrate at a concentration of 10 mM, all strains achieved >99% conversion to 2-methylsuccinimide (2-MS) within 1 h (Fig. S5), reaching initial product formation rates up to 16.7 mM $h^{-1}$ (Fig. 2A). All the four chassis showed significantly higher initial product formation rate and specific activity compared to the wt background (Fig. 2A, 2B). The best performing chassis was the one lacking an active bidirectional hydrogenase - Δ*hoxYH*, with a 39% improvement in specific activity compared to the wt, reaching 116 U $g_{DCW}^{-1}$ (Fig. 2B). The bidirectional hydrogenase acts as an electron valve during photosynthesis, temporarily storing the surplus of electrons coming from Photosystem I (Appel et al., 2000). As YqjM-catalyzed ene-reduction performs as a strong heterologous electron sink (Assil-Companioni et al., 2020), the increase of the *in vivo* specific activity in Δ*hoxYH* chassis could result from the harvesting of electrons that otherwise will be directed to $H_2$ production. The Δ*ndhD2* chassis, lacking a subunit of NDH-1 suggested to be involved in cyclic electron flow (Battchikova et al., 2011), showed a 23% improvement in *in vivo* specific activity of YqjM compared to the wt. This is in agreement with the previously reported for the heterologous cytochrome P450 monooxygenase activity in *Synechococcus* PCC 7002 (Berepiki et al., 2018), suggesting that this approach is a viable route towards improved electron availability for heterologous redox enzymes. Δ*flv3* and

Δ*hoxYH*Δ*flv3* chassis exhibited around 20% higher *in vivo* specific activity of YqjM as compared to the wt background, consistent with recent studies suggesting deletion of *flv1* and/or *flv3* as a strategy for enhancing the light-driven production of desired chemicals (Assil-Companioni et al., 2020; Selão et al., 2020; Thiel et al., 2019). In order to further evaluate the expression levels and active intracellular levels of YqjM in the various chassis, a Western blot analysis was performed and the *in vitro* specific activity of YqjM was determined in an NADPH assay. While the Western blot analysis showed somewhat different YqjM amounts in different chassis (Fig. S6), previously reported also for a cytochrome P450 monooxygenase (Berepiki et al., 2018) the NADPH assay showed no significant differences the *in vitro* specific activity of YqjM in the different chassis compared to the wildtype (Fig. 2C). YqjM was expressed under a strong $P_{cpcB}$ promoter, resulting in high protein levels (as it can be seen in the Coomassie blue stained SDS-polyacrylamide gel, Fig. S6A). Nevertheless, the levels of active enzyme could be limited by the availability of the cofactor flavin mononucleotide (FMN), as this was previously described as a hurdle for heterologous oxidoreductases (Milker et al., 2017).

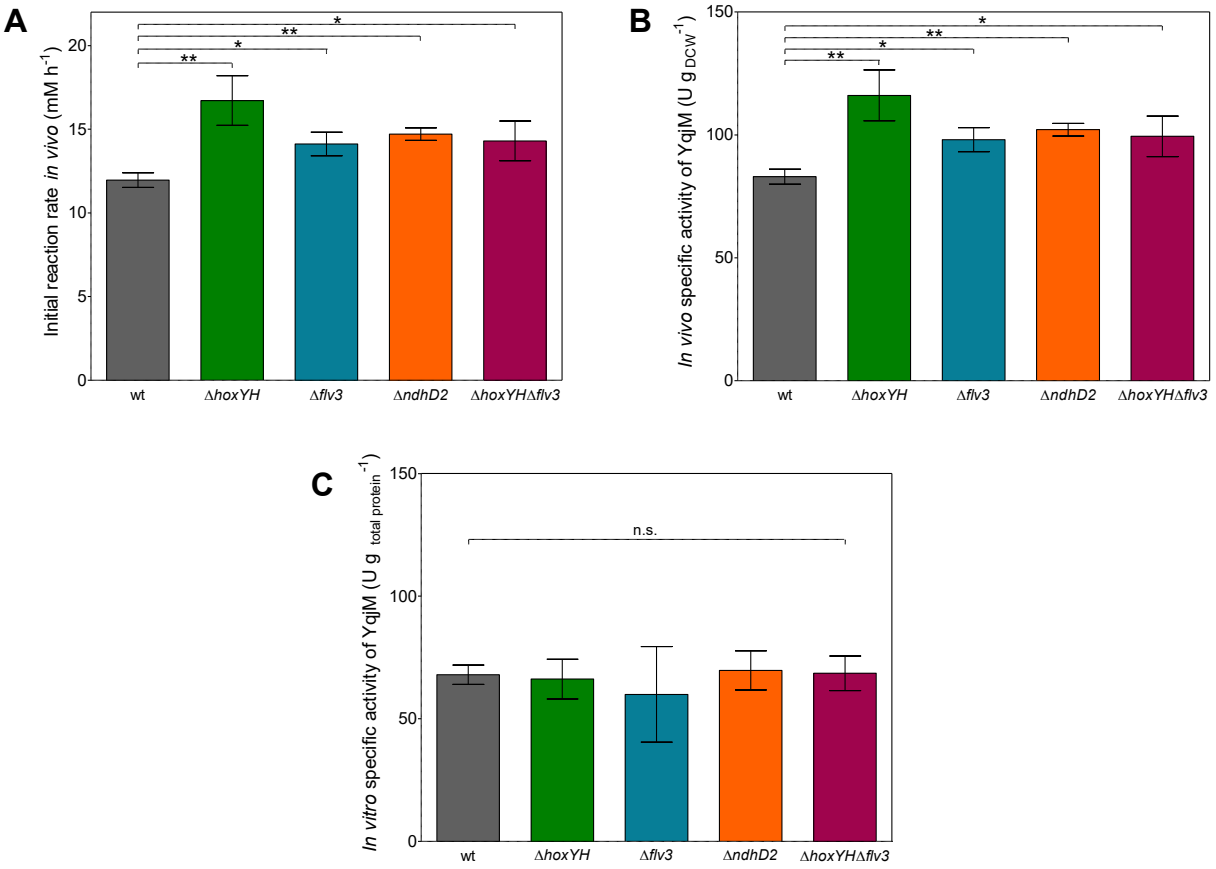


**Fig. 2.** Light-driven biotransformation of 2-methylmaleimide into 2-methylsuccinimide catalyzed by YqjM expressed in *Synechocystis* sp. PCC 6803 (wt) and Δ*hoxYH*, Δ*flv3*, Δ*ndhD2* and Δ*hoxYH*Δ*flv3* chassis. A) Product formation rate and B) *In vivo* specific activity. Cells were cultivated in BG-11 at 30 ºC with orbital shaking (140 rpm) under continuous white light (50 µmol $m^{-2}$ $s^{-1}$), grown until $OD_{750}$ 1-1.5, harvested and applied for the biotransformation of 10 mM 2-MM (1 ml, 2.4 $g_{DCW}$ $L^{-1}$, BG-11, white light of 150 µmol $m^{-2}$ $s^{-1}$, 130 rpm, 30 ºC); C) *in vitro* YqjM activity determined in NADPH assay using crude cell-free extracts. Error bars correspond to standard deviations from three biological replicates and statistical analysis is presented based on unpaired *t*-test (***, $P < 0.001$; **, $P < 0.01$; *, $P < 0.05$; n.s., not significant).

Next, we wanted to assess the photosynthetic activity, by evaluating oxygen evolution rates in the chassis and upon the introduction of YqjM, in similar conditions as those in the biotransformation assays. The results showed no significant difference in oxygen evolution rates by the chassis, before or after the introduction of YqjM compared to the wt (Fig. 3). These results suggest that redirecting electron flow did not affect the chassis robustness under the tested conditions, even with the high-level expression of the ene-reductase YqjM. The maintenance of the growth and oxygen evolution rates upon expression of YqjM in the different chassis suggest that this catalyst can be used as a model system to evaluate various synthetic biology tools as well as for the customization of chassis, as recently demonstrated for a monooxygenase (Opel et al., 2022).

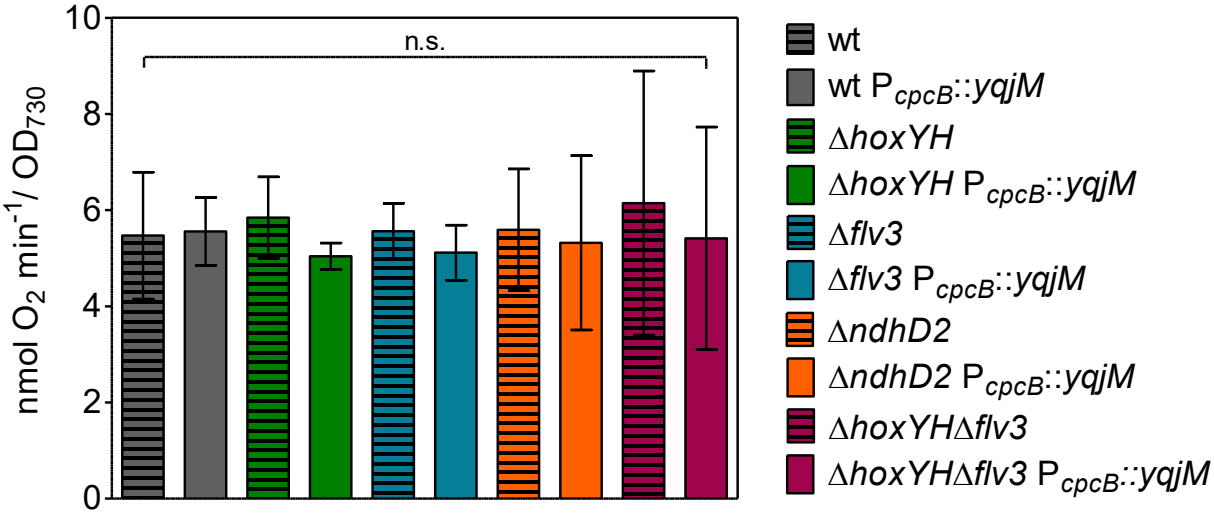


**Fig. 3.** Oxygen evolution rates by *Synechocystis* sp. PCC 6803 (wt), Δ*hoxYH*, Δ*flv3*, Δ*ndhD2* and Δ*hoxYH*Δ*flv3* mutants, and of these chassis expressing YqjM. Cells were cultivated in BG-11 at 30 ºC with orbital shaking (140 rpm) under continuous white light (50 µmol $m^{-2}$ $s^{-1}$), grown until $OD_{730}$ 1-1.5 and harvested for the measurements (for details Material and Methods). Error bars correspond to standard deviations from three biological replicates and statistical analysis is presented based on unpaired *t*-test (n.s., not significant).

### *3.4. Evaluation of YqjM activity in the ΔhoxYH chassis*

As YqjM in the Δ*hoxYH* chassis demonstrated the highest specific activity and product formation rates, we further characterized this light-driven biotransformation. We start by investigating the effect of lower cell densities for the light-driven C=C reduction. Even though *in vivo* specific activities are highest at low cell densities (0.48 g $L^{-1}$), likely due to less self-shading (Fig. 4A), the initial product formation rates (calculated from the slope of the initial 15 min of the reaction) are lower (Fig. 4B), and the substrate conversion progresses slower (Fig. 4C). Under lower cell densities (0.48 and 1.2 g $L^{-1}$), no significant differences in the *in vivo* specific activity of YqjM expressed in the wt or the Δ*hoxYH* chassis were observed (Fig. 4A). However, when the reaction was performed with a cell density of 2.4 g $L^{-1}$ a significant increase in *in vivo* specific activity was observed in the Δ*hoxYH* chassis. This is consistent with previous studies suggesting that activity-enhancing effects are more noticeable for higher cell densities/faster whole-cell biotransformations (Assil-Companioni et al., 2020), where cell density affects the light availability and originates light fluctuations, possibly limiting the available reducing power. Additionally, the reactions performed in dark converted 2-MM with no significant difference in the *in vivo* specific activity of YqjM expressed in wt and Δ*hoxYH* chassis at basal levels (Fig. 4A). Detection of YqjM activity in the dark further highlights that reducing equivalents, in the form of NADPH, persist in *Synechocystis* in the absence of light, but that its availability and redox turnover is slower than in light, as previously demonstrated (Tanaka et al., 2021). This elucidates the slower *in vivo* specific activity and product formation rate observed in the dark, which strongly supports photosynthesis-driven YqjM-dependent biotransformations.

In addition, the oxygen evolution rates in wt and Δ*hoxYH* chassis in the presence of the substrate 2-MM were evaluated. 10 mM 2-MM led to 50% decrease in the oxygen evolution rate in wt and Δ*hoxYH* backgrounds, in agreement with previously reported substrate toxicity

that was suggested to affect the photosynthetic machinery, in particular PSII (Assil-Companioni et al., 2020). In contrast, in the wt and Δ*hoxYH* expressing YqjM, the addition of 10 mM 2-MM led to 45% and 74% increase in the oxygen evolution rate, respectively (Fig. 4D) when cells were exposed to a light intensity of 150 μmol $m^{-2}$ $s^{-1}$. These results are in agreement with earlier observations that YqjM activity mitigates the toxic effect of 2-MM [6], suggesting that the activity of a strong electron sink like YqjM significantly increases oxygen evolution rates. An increased capacity to process photosynthetically derived electrons was also observed upon the heterologous expression of cytochrome P450 CYP1A1 in other cyanobacterial strains (Berepiki et al., 2016; Santos-Merino et al., 2021; Torrado et al., 2022). Anticipating a faster conversion of 2-MM under higher light intensity, previously described to induce photohydrogen production (Gutthann et al., 2007), we measured also the oxygen evolution rates under 800 μmol $m^{-2}$ $s^{-1}$. Under this condition, 10 mM 2-MM still led to 50% decrease in the oxygen evolution rate in wt and Δ*hoxYH* backgrounds. However, YqjM-catalyzed substrate conversion resulted in 2.7 and 3-fold increase in wt and Δ*hoxYH* chassis, respectively. These results indicate that the fast YqjM-catalyzed conversion of 2-MM leads to a significant increase in the oxygen evolution rate, which can be regarded here as a proxy of photosynthetic activity. Hence, by releasing more oxygen, the cyanobacterial photosynthetic machinery is oxidizing water at a faster rate, and so, generating more reducing power, which can be then used for substrate conversion. This means that YqjM activity is triggered in the presence of 2-MM, quickly consuming the NADPH pool available in the cell, increasing the demand of $NADP^+$ reduction to keep cell homeostasis, which then generates the need for a higher rate of water oxidation.

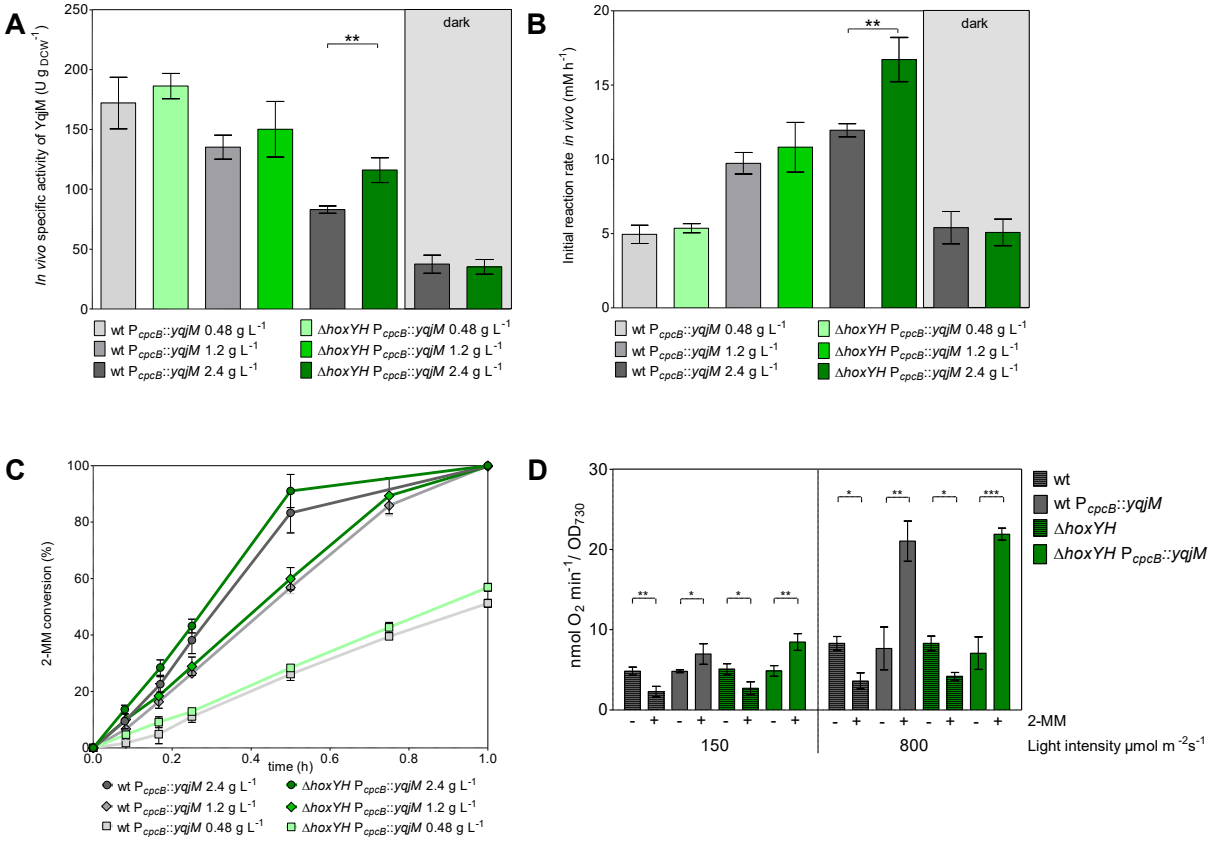


**Fig. 4.** Light-driven biotransformation of 2-methylmaleimide (2-MM) into 2-methylsuccinimide (2-MS) catalyzed by YqjM expressed in *Synechocystis* wt and Δ*hoxYH* chassis and oxygen evolution rates. A) *In vivo* specific activity of YqjM at different cell densities or carrying out the reaction in the dark; B) Product formation rates at different cell densities or carrying out the reaction in the dark; C) 2-MM conversion over time. Cells were cultivated in BG-11 at 30 ºC with orbital shaking (140 rpm) under continuous white light (50 µmol $m^{-2}$ $s^{-1}$), grown until $OD_{750}$ 1-1.5, harvested and applied for the biotransformation of 10 mM 2-MM (1 mL, BG-11, white light of 150 µmol $m^{-2}$ $s^{-1}$ or dark, 130 rpm, 30 ºC). D) Oxygen evolution rates of wt and Δ*hoxYH*, and of these chassis expressing YqjM in the absence (-) or presence (+) of 10 mM 2-MM. Cells were cultivated in BG-11 at 30 ºC with orbital shaking (140 rpm) under continuous white light (50 µmol $m^{-2}$ $s^{-1}$), grown until $OD_{730}$ 1-1.5, harvested and the oxygen evolution rate measured (under two different light intensities 150 and 800 µmol $m^{-2}$ $s^{-1}$). Error bars

correspond to standard deviations from three biological replicates and statistical analysis is presented based on unpaired *t*-test (***, $P < 0.001$; **, $P < 0.01$; *, $P < 0.05$; n.s., not significant).

To further characterize chassis potential for streamlining photosynthetically activated electrons, we evaluated the effect of different cultivation conditions on the *in vivo* specific activity of YqjM expressed in wt and Δ*hoxYH* chassis. As a previous study suggested that altering the light conditions during growth affects the *in vivo* specific activity (Assil-Companioni et al., 2020), the wt and Δ*hoxYH* chassis were cultivated under a 12 h white light (50 µmol $m^{-2}$ $s^{-1}$) / 12 h dark regimen or under continuous blue / red light (150 µmol $m^{-2}$ $s^{-1}$). Nevertheless, there was no significant difference in the *in vivo* specific activity of YqjM expressed in wt or Δ*hoxYH* chassis (Fig. S7). Regarding medium composition, we focused on nitrogen limitation, due to the reported higher transcription levels of the *hox* genes under these conditions (Antal et al., 2006; Osanai et al., 2006) and subsequent enhanced hydrogen production (Gutthann et al., 2007; Melnicki et al., 2012). The wt and Δ*hoxYH* chassis expressing YqjM were cultivated in BG-$11_0$ containing 10 or 20 times less nitrate than the standard BG-11 medium. These conditions led to discernible pigmentation alterations of the cultures with a significant decrease in the chlorophyll *a* content (Fig. S8A), in line with the well-described physiological adjustments of *Synechocystis* under nitrogen limitation (Antal et al., 2006; Giner-Lamia et al., 2017). However, no significant difference in the *in vivo* specific activity of YqjM expressed in wt or Δ*hoxYH* could be detected. Furthermore, mixotrophic, nitrate-limiting conditions, previously described as essential for hydrogenase activity (Gutekunst et al., 2014) led, likewise, to pigmentation alterations with no significant difference in the *in vivo* specific activity of YqjM (Fig. S8B). An explanation for this result is a possible decrease of the *yqjM* transcript levels, due to repression of the $P_{cpcB}$ promoter under nitrogen limiting conditions (Giner-Lamia et al., 2017) that could compromise the YqjM expression and

activity. Overall, these results suggest nitrogen limiting conditions do not offer increased productivites, as cells have to maintain the health of photosynthetic machinery to provide the reducing power for photobiotransformations.

# 4. Conclusions

In conclusion, we evaluated four different customized cyanobacterial chassis (Δ*hoxYH*, Δ*flv3*, Δ*ndhD2* and Δ*hoxYH*Δ*flv3*) as hosts for improved whole-cell light-driven C=C reduction catalyzed by the ene-reductase YqjM. The results showed the robustness of the chassis, with growth rates similar to *Synechocystis* wild-type, and that this robustness was maintained upon the introduction and expression of the heterologous YqjM. By engineering the electron transport pathways, we significantly improved a light-driven C=C reduction catalyzed by this ene-reductase, with the chassis lacking an active bidirectional hydrogenase leading to a 39% increase in the stereoselective reduction of 2-methylmaleimide to 2-methylsuccinimide. In this chassis the *in vivo* specific activity of YqjM reached 116 U $g_{DCW}^{-1}$ and the product formation rate reached 16.7 mM $h^{-1}$. The stable oxygen evolution rates observed under the biotransformation conditions corroborate the robustness of the chassis even expressing high levels of YqjM. Interestingly, the presence of YqjM mitigates the substrate toxicity, and the conversion of 2-methylmaleimide leads to increased oxygen evolution rates, more noticeable at higher light intensities. Overall, our work demonstrates that the rational engineering of electron transfer pathways is a valid strategy to increase *in vivo* specific activity and product formation rate in cyanobacterial chassis harboring oxidoreductases. Moreover, we validate the fast stereoselective reduction catalyzed by YqjM as a system to evaluate other synthetic biology strategies.

## Author agreement

All authors agree with this submission.

## CRediT authorship contribution statement

**Jelena Spasic**: Investigation, Methodology, Formal analysis, Visualization, Writing – original draft. **Paulo Oliveira**: Formal analysis, Writing – original draft. **Catarina Pacheco**: Formal analysis, Visualization, Writing – review & editing. **Robert Kourist**: Conceptualization, Supervision, Funding acquisition. **Paula Tamagnini**: Conceptualization, Supervision, Funding acquisition, Writing – review & editing.

## Declaration of Competing Interest

The authors declare that they have no known competing financial interests or personal relationships that could have appeared to influence the work reported in this paper.

## Acknowledgment

This project has received funding from the European Union's Horizon 2020 research and innovation program under the Marie Skłodowska-Curie grant agreement No 764920. CCP and PO acknowledge the Fundação para a Ciência e a Tecnologia (FCT)/Ministério da Ciência, Tecnologia e Ensino Superior for the Assistant Researcher contract CEECIND/00259/2017, and for the FCT Investigator Grant IF/00256/2015, respectively. The authors acknowledge the support of the i3S Scientific Platform BioSciences Screening member of the national infrastructure PT-OPENSCREEN (NORTE-01-0145-FEDER-085468).

## Appendix A. Supporting information

# References

Allahverdiyeva, Y., Mustila, H., Ermakova, M., Bersanini, L., Richaud, P., Ajlani, G., Battchikova, N., Cournac, L., Aro, E.-M., 2013. Flavodiiron proteins Flv1 and Flv3 enable cyanobacterial growth and photosynthesis under fluctuating light. Proc. Natl. Acad. Sci. U. S. A. 110, 4111-4116. doi.org/10.1073/pnas.1221194110.

Antal, T., Oliveira, P., Lindblad, P., 2006. The bidirectional hydrogenase in the cyanobacterium Synechocystis sp. strain PCC 6803. Int. J. Hydrog. Energy 31, 1439-1444. doi.org/10.1016/j.ijhydene.2006.06.037.

Appel, J., Phunpruch, S., Steinmüller, K., Schulz, R., 2000. The bidirectional hydrogenase of Synechocystis sp. PCC 6803 works as an electron valve during photosynthesis. Arch. Microbiol. 173, 333-338. doi.org/10.1007/s002030000139.

Assil-Companioni, L., Büchsenschütz, H.C., Solymosi, D., Dyczmons-Nowaczyk, N.G., Bauer, K.K., Wallner, S., Macheroux, P., Allahverdiyeva, Y., Nowaczyk, M.M., Kourist, R., 2020. Engineering of NADPH supply boosts photosynthesis-driven biotransformations. ACS Catal. 10, 11864-11877. doi.org/10.1021/acscatal.0c02601.

Battchikova, N., Eisenhut, M., Aro, E.-M., 2011. Cyanobacterial NDH-1 complexes: novel insights and remaining puzzles. Biochim. Biophys. Acta, Bioenerg. 1807, 935-944. doi.org/10.1016/j.bbabio.2010.10.017.

Berepiki, A., Gittins, J.R., Moore, C.M., Bibby, T.S., 2018. Rational engineering of photosynthetic electron flux enhances light-powered cytochrome P450 activity. Synth. Biol. 3, ysy009. doi.org/10.1093/synbio/ysy009.

Berepiki, A., Hitchcock, A., Moore, C.M., Bibby, T.S., 2016. Tapping the unused potential of photosynthesis with a heterologous electron sink. ACS Synth. Biol. 5, 1369-1375. doi.org/10.1021/acssynbio.6b00100.

Böhmer, S., Köninger, K., Gómez-Baraibar, Á., Bojarra, S., Mügge, C., Schmidt, S., Nowaczyk, M.M., Kourist, R., 2017. Enzymatic oxyfunctionalization driven by photosynthetic water-splitting in the cyanobacterium Synechocystis sp. PCC 6803. Catalysts 7, 240. doi.org/10.3390/catal7080240.

Büchsenschütz, H.C., Vidimce-Risteski, V., Eggbauer, B., Schmidt, S., Winkler, C.K., Schrittwieser, J.H., Kroutil, W., Kourist, R., 2020. Stereoselective biotransformations of cyclic imines in recombinant cells of Synechocystis sp. PCC 6803. ChemCatChem 12, 726-730. doi.org/10.1002/cctc.201901592.

Cournac, L., Guedeney, G., Peltier, G., Vignais, P.M., 2004. Sustained photoevolution of molecular hydrogen in a mutant of Synechocystis sp. strain PCC 6803 deficient in the type I NADPH-dehydrogenase complex. J. Bacteriol. 186, 1737-1746. doi.org/10.1128/JB.186.6.1737-1746.2003.

Erdem, E., Malihan-Yap, L., Assil-Companioni, L., Grimm, H., Barone, G.D., Serveau-Avesque, C., Amouric, A., Duquesne, K., de Berardinis, V., Allahverdiyeva, Y., 2021. Photobiocatalytic oxyfunctionalization with high reaction rate using a baeyer–villiger monooxygenase from Burkholderia xenovorans in metabolically engineered cyanobacteria. ACS Catal. 12, 66-72. doi.org/10.1021/acscatal.1c04555.

Giner-Lamia, J., Robles-Rengel, R., Hernández-Prieto, M.A., Muro-Pastor, M.I., Florencio, F.J., Futschik, M.E., 2017. Identification of the direct regulon of NtcA during early acclimation to nitrogen starvation in the cyanobacterium Synechocystis sp. PCC 6803. Nucleic Acids Res. 45, 11800-11820. doi.org/10.1093/nar/gkx860.

Gutekunst, K., Chen, X., Schreiber, K., Kaspar, U., Makam, S., Appel, J., 2014. The bidirectional NiFe-hydrogenase in Synechocystis sp. PCC 6803 is reduced by flavodoxin and ferredoxin and is essential under mixotrophic, nitrate-limiting conditions. J. Biol. Chem. 289, 1930-1937. doi.org/10.1074/jbc.M113.526376.

Gutthann, F., Egert, M., Marques, A., Appel, J., 2007. Inhibition of respiration and nitrate assimilation enhances photohydrogen evolution under low oxygen concentrations in Synechocystis sp. PCC 6803. Biochim. Biophys. Acta, Bioenerg. 1767, 161-169. doi.org/10.1016/j.bbabio.2006.12.003.

Hollmann, F., Arends, I.W., Buehler, K., Schallmey, A., Bühler, B., 2011. Enzyme-mediated oxidations for the chemist. Green Chem. 13, 226-265. doi.org/10.1039/C0GC00595A.

Hoschek, A., Bühler, B., Schmid, A., 2019a. Stabilization and scale-up of photosynthesis-driven ω-hydroxylation of nonanoic acid methyl ester by two-liquid phase whole-cell biocatalysis. Biotechnol. Bioeng. 116, 1887-1900. doi.org/10.1002/bit.27006.

Hoschek, A., Schmid, A., Bühler, B., 2018. In situ O2 generation for biocatalytic oxyfunctionalization reactions. ChemCatChem 10, 5366-5371. doi.org/10.1002/cctc.201801262.

Hoschek, A., Toepel, J., Hochkeppel, A., Karande, R., Bühler, B., Schmid, A., 2019b. Light-dependent and aeration-independent gram-scale hydroxylation of cyclohexane to cyclohexanol by CYP450 harboring Synechocystis sp. PCC 6803. Biotechnol. J. 14, 1800724. doi.org/10.1002/biot.201800724.

Jodlbauer, J., Rohr, T., Spadiut, O., Mihovilovic, M.D., Rudroff, F., 2021. Biocatalysis in green and blue: cyanobacteria. Trends Biotechnol. 39, 875-889. doi.org/10.1016/j.tibtech.2020.12.009.

Jurkaš, V., Winkler, C.K., Poschenrieder, S., Oliveira, P., Pacheco, C.C., Ferreira, E.A., Weissensteiner, F., De Santis, P., Kara, S., Kourist, R., 2021. Expression and activity of heterologous hydroxyisocaproate dehydrogenases in Synechocystis sp. PCC 6803 ΔhoxYH. Eng. Microbiol., 100008. doi.org/10.1016/j.engmic.2021.100008.

Knoot, C.J., Ungerer, J., Wangikar, P.P., Pakrasi, H.B., 2018. Cyanobacteria: promising biocatalysts for sustainable chemical production. J. Biol. Chem. 293, 5044-5052. doi.org/10.1074/jbc.R117.815886.

Köninger, K., Gómez Baraibar, Á., Mügge, C., Paul, C.E., Hollmann, F., Nowaczyk, M.M., Kourist, R., 2016. Recombinant cyanobacteria for the asymmetric reduction of C= C bonds fueled by the biocatalytic oxidation of water. Angew. Chem., Int. Ed. 55, 5582-5585. doi.org/10.1002/anie.201601200.

Lea-Smith, D.J., Bombelli, P., Vasudevan, R., Howe, C.J., 2016. Photosynthetic, respiratory and extracellular electron transport pathways in cyanobacteria. Biochim. Biophys. Acta, Bioenerg. 1857, 247-255. doi.org/10.1016/j.bbabio.2015.10.007.

Melnicki, M.R., Pinchuk, G.E., Hill, E.A., Kucek, L.A., Fredrickson, J.K., Konopka, A., Beliaev, A.S., 2012. Sustained H2 production driven by photosynthetic water splitting in a unicellular cyanobacterium. MBio 3, e00197-00112. doi.org/10.1128/mBio.00197-12.

Milker, S., Goncalves, L.C., Fink, M.J., Rudroff, F., 2017. Escherichia coli fails to efficiently maintain the activity of an important flavin monooxygenase in recombinant overexpression. Front. Microbiol. 8, 2201. doi.org/10.3389/fmicb.2017.02201.

Mullineaux, C.W., 2014. Electron transport and light-harvesting switches in cyanobacteria. Front. Plant Sci. 5, 7. doi.org/10.3389/fpls.2014.00007.

Murata, N., Allakhverdiev, S.I., Nishiyama, Y., 2012. The mechanism of photoinhibition in vivo: re-evaluation of the roles of catalase, α-tocopherol, non-photochemical quenching, and electron transport. Biochim. Biophys. Acta, Bioenerg. 1817, 1127-1133. doi.org/10.1016/j.bbabio.2012.02.020.

Nikkanen, L., Solymosi, D., Jokel, M., Allahverdiyeva, Y., 2021. Regulatory electron transport pathways of photosynthesis in cyanobacteria and microalgae: recent advances and biotechnological prospects. Physiol. Plant. 173, 514-525. doi.org/10.1111/ppl.13404.

Opel, F., Siebert, N.A., Klatt, S., Tüllinghoff, A., Hantke, J.G., Toepel, J.r., Bühler, B., Nürnberg, D.J., Klähn, S., 2022. Generation of synthetic shuttle vectors enabling modular genetic engineering of cyanobacteria. ACS Synth. Biol. 11, 1758-1771. doi.org/10.1021/acssynbio.1c00605.

Osanai, T., Imamura, S., Asayama, M., Shirai, M., Suzuki, I., Murata, N., Tanaka, K., 2006. Nitrogen induction of sugar catabolic gene expression in Synechocystis sp. PCC 6803. DNA Res. 13, 185-195. doi.org/10.1093/dnares/dsl010.

Pinto, F., Pacheco, C.C., Oliveira, P., Montagud, A., Landels, A., Couto, N., Wright, P.C., Urchueguía, J.F., Tamagnini, P., 2015. Improving a Synechocystis-based photoautotrophic chassis through systematic genome mapping and validation of neutral sites. DNA Res. 22, 425-437. doi.org/10.1093/dnares/dsv024.

Pinto, F., van Elburg, K.A., Pacheco, C.C., Lopo, M., Noirel, J., Montagud, A., Urchueguia, J.F., Wright, P.C., Tamagnini, P., 2012. Construction of a chassis for hydrogen production: physiological and molecular characterization of a Synechocystis sp. PCC 6803 mutant lacking a functional bidirectional hydrogenase. Microbiology 158, 448-464. doi.org/10.1099/mic.0.052282-0.

Russell, D.W., Sambrook, J., 2001. Molecular cloning: a laboratory manual. Cold Spring Harbor Laboratory Cold Spring Harbor, NY.

Russo, D.A., Zedler, J.A., Jensen, P.E., 2019. A force awakens: exploiting solar energy beyond photosynthesis. J. Exp. Bot. 70, 1703-1710. doi.org/10.1093/jxb/erz054.

Santos-Merino, M., Torrado, A., Davis, G.A., Röttig, A., Bibby, T.S., Kramer, D.M., Ducat, D.C., 2021. Improved photosynthetic capacity and photosystem I oxidation via heterologous metabolism engineering in cyanobacteria. Proc. Natl. Acad. Sci. U. S. A. 118, e2021523118. doi.org/10.1073/pnas.2021523118.

Schmermund, L., Jurkaš, V., Özgen, F.F., Barone, G.D., Büchsenschütz, H.C., Winkler, C.K., Schmidt, S., Kourist, R., Kroutil, W., 2019. Photo-biocatalysis: biotransformations in the presence of light. ACS Catal. 9, 4115-4144. doi.org/10.1021/acscatal.9b00656.

Selão, T.T., Jebarani, J., Ismail, N.A., Norling, B., Nixon, P.J., 2020. Enhanced production of D-lactate in cyanobacteria by re-routing photosynthetic cyclic and pseudo-cyclic electron flow. Front. Plant Sci. 10, 1700. doi.org/10.3389/fpls.2019.01700.

Silva-Rocha, R., Martínez-García, E., Calles, B., Chavarría, M., Arce-Rodríguez, A., de Las Heras, A., Paez-Espino, A.D., Durante-Rodríguez, G., Kim, J., Nikel, P.I., 2013. The Standard European Vector Architecture (SEVA): a coherent platform for the analysis and deployment of complex prokaryotic phenotypes. Nucleic Acids Res. 41, D666-D675. doi.org/10.1093/nar/gks1119.

Stanier, R., Kunisawa, R., Mandel, M., Cohen-Bazire, G., 1971. Purification and properties of unicellular blue-green algae (order Chroococcales). Bacteriol. Rev. 35, 171-205. doi.org/10.1128/br.35.2.171-205.1971.

Tamagnini, P., Leitão, E., Oliveira, P., Ferreira, D., Pinto, F., Harris, D.J., Heidorn, T., Lindblad, P., 2007. Cyanobacterial hydrogenases: diversity, regulation and applications. FEMS Microbiol. Rev. 31, 692-720. doi.org/10.1111/j.1574-6976.2007.00085.x.

Tamagnini, P., Troshina, O., Oxelfelt, F., Salema, R., Lindblad, P., 1997. Hydrogenases in Nostoc sp. strain PCC 73102, a strain lacking a bidirectional enzyme. Appl. Environ. Microbiol. 63, 1801-1807. doi.org/10.1128/aem.63.5.1801-1807.1997.

Tanaka, K., Shimakawa, G., Tabata, H., Kusama, S., Miyake, C., Nakanishi, S., 2021. Quantification of NAD (P) H in cyanobacterial cells by a phenol extraction method. Photosynth. Res. 148, 57-66. doi.org/10.1007/s11120-021-00835-1.

Thiel, K., Patrikainen, P., Nagy, C., Fitzpatrick, D., Pope, N., Aro, E.-M., Kallio, P., 2019. Redirecting photosynthetic electron flux in the cyanobacterium Synechocystis sp. PCC 6803 by the deletion of flavodiiron protein Flv3. Microb. Cell Fact. 18, 1-16. doi.org/10.1186/s12934-019-1238-2.

Torrado, A., Connabeer, H.M., Röttig, A., Pratt, N., Baylay, A.J., Terry, M.J., Moore, C.M., Bibby, T.S., 2022. Directing cyanobacterial photosynthesis in a cytochrome c oxidase mutant using a heterologous electron sink. Plant Physiol., kiac203. doi.org/10.1093/plphys/kiac203.

Williams, J.G., 1988. [85] Construction of specific mutations in photosystem II photosynthetic reaction center by genetic engineering methods in Synechocystis 6803. Methods Enzymol. 167, 766-778. doi.org/10.1016/0076-6879(88)67088-1.

# Engineering cyanobacterial chassis for improved electron supply toward a heterologous ene-reductase

# Supplementary material

## Table of contents

Supporting tables ..... 74
Table S1 ..... **Error! Bookmark not defined.**
Table S2 ..... 75
Table S3 ..... 76
Table S4 ..... 78
Supporting figures ..... 79
Figure S1 ..... 79
Figure S2 ..... 81
Figure S3 ..... 82
Figure S4 ..... 82
Figure S6 ..... 84
Figure S7 ..... 85
Figure S8 ..... 86
Figure S9 ..... 87
Figure S10 ..... 88
References ..... 88

## Supporting tables

### Table S1

Oligonucleotide primers used in this study.

| Name | Sequence (5'-3') | Purpose | Reference |
|---|---|---|---|
| flv3_UP_FP | GACCGCTCGAGACTGCTATGACCAA AAACTACTTTTCGGC | Generation of the Δ*flv3* mutants | This study |
| flv3_UP_RP | GTTCTTTGGACTGGGCCCGGGATCG CTTTGTGTTGAACATTTTGGAGGAAG | | |
| flv3_DOWN_FP | CAACACAAAGCGATCCCGGGCCCAG TCCAAAGAACGGATAGCAGTAATA | | |
| flv3_DOWN_RP | CTCACCGAACATTGCCATTATCCTAG TCT | | |
| ndhD2_UP_FP | GAGCCCTCGAGCCATTCTCTGACTT CTATAGGGAAAATCTC | Generation of the Δ*ndhD2* mutant | |
| ndhD2_UP_RP | GAACTTTGACGGTGCCCGGGTAAAG CACCAACATTAGGAAGTAGAAGAGG | | |
| ndhD2_DOWN_FP | ATGTTGGTGCTTTACCCGGGCACCG TCAAAGTTCAACCCTAGTGATCTAG | | |
| ndhD2_DOWN_RP | TGGGACTTTTAGTGCTGACTTTGTTC TGTT | | |
| SA_flv3_FP | TTTCCGTGGCGGGGTCATAGGT | Confirmation of segregation of Δ*flv3* mutants | |
| SA_flv3_RP | GGTGGCTTAGTGGTGTTGGCCC | | |
| SA_ndhD2_FP | TGGCTGGGGTTACCTACGACCG | | |

| | | | |
|---|---|---|---|
| SA_ndhD2_RP | CGCACTTGGCTGTTCACCGCTA | Confirmation of segregation of Δ*ndhD2* mutant | |
| Km_KmScFwd | CTGACCCCGGGTGAATGTCAGCTACTGG | Amplification of the *nptII* cassette | (Pinto et al., 2015) |
| Km_Rev | CAAACCCGGGCGATTTACTTTTCGACCTC | | |
| Seg_fw | TGGCCCTGGACAGTCAGGAATG | Segregation analysis of mutants harboring *yqjM* gene under the control of $P_{cpcB}$ promoter | (Assil-Companioni et al., 2020) |
| Seg_rv | GCTGCATGTTGGGACTGGAGAC | | |
| Seq_promoter | CTATTCAATACACCCCCTAAGCTAG | Sequencing | |
| seq_cpc | TAGGGTCATTACTTTGGAC | | |
| Km_rv | GGGCTTCCCATACAATCGATAG | | |
| Cpc_scr_R | GGGAGTCCAAAGTAATGACCC | Sequencing | This study |
| Cm_rv | CGTAATATCCAGCTGAACGGTC | | |

*Restriction enzyme recognition sites are underlined.

**Table S2**

Plasmids used to transform *Synechocystis*.

| Plasmid | Description | Purpose | Reference/Source |
|---|---|---|---|
| pGEM_Δ*ndhD2*.km | pGEM-T easy vector containing the *nptII* gene flanked by the two regions for | | This study |

| | | | |
|---|---|---|---|
| | double homologous recombination targeting the *ndhD2* (*slr1291*) locus | Generation of *Synechocystis* mutants | |
| pGEM_Δ*flv3*.sm | pGEM-T easy vector containing the *aadA* gene flanked by the two regions for double homologous recombination targeting the *flv3* (*sll0550*) locus | | This study |
| SynRekB_$P_{cpcB}$::*yqjM* | vector harboring the N-terminal 6xHis tagged YqjM-coding sequence under the control of the $P_{cpcB}$ promoter and a kanamycin resistance cassette, and flanked by the two regions for double homologous recombination targeting the *slr0168* locus | Introduction of *yqjM* into *Synechocystis* | (Assil-Companioni et al., 2020) |
| pMD19T_slr0168_$P_{cpcB}$::*yqjM* | vector harboring the N-terminal 6xHis tagged YqjM-coding sequence under the control of the $P_{cpcB}$ promoter and a chloramphenicol resistance cassette, and flanked by the two regions for double homologous recombination targeting the *slr0168* locus | | This study |

**Table S3**

S*ynechocystis* strains used in this work.

| Strain | Description | Antibiotic resistance | References/sources |
|---|---|---|---|
| *Synechocystis* sp. PCC 6803 (wt) | substrain GT-Kazusa | None | Pasteur Culture Collection, Paris, France (Kanesaki et al., 2012; |

| | | | |
|---|---|---|---|
| | | | Trautmann et al., 2012) |
| *Synechocystis* sp. PCC 6803 Δ*hoxYH* (Δ*hoxYH*) | *Synechocystis* mutant lacking the active bidirectional hydrogenase (encoded by *hoxY* and *hoxH*) | None | (Pinto et al., 2012) |
| *Synechocystis* sp. PCC 6803 Δ*ndhD2* (Δ*ndhD2*) | *Synechocystis* mutant lacking the NdhD2 subunit of the type I NADH dehydrogenase complex (encoded by *ndhD2*) | Km | |
| *Synechocystis* sp. PCC 6803 Δ*flv3* (Δ*flv3*) | *Synechocystis* mutant lacking the Flv3 (encoded by *flv3*) | Sm | This study |
| *Synechocystis* sp. PCC 6803 Δ*hoxYH*Δ*flv3* (Δ*hoxYH*Δ*flv3*) | *Synechocystis* mutant lacking the active bidirectional hydrogenase (encoded by *hoxY* and *hoxH*) and Flv3 (encoded by *flv3*) | Sm | |
| *Synechocystis* sp. PCC 6803 $P_{cpcB}$::*yqjM* (wt $P_{cpcB}$::*yqjM* ) | *Synechocystis* strain harboring *yqjM* gene under the control of $P_{cpcB}$ promoter | Km | (Assil-Companioni et al., 2020) |
| *Synechocystis* sp. PCC 6803 Δ*hoxYH* $P_{cpcB}$::*yqjM* (Δ*hoxYH* $P_{cpcB}$::*yqjM*) | *Synechocystis* Δ*hoxYH* mutant harboring *yqjM* gene under the control of $P_{cpcB}$ promoter | Km | |
| *Synechocystis* sp. PCC 6803 Δ*ndhD2* $P_{cpcB}$::*yqjM* (Δ*ndhD2* $P_{cpcB}$::*yqjM*) | *Synechocystis* Δ*ndhD2* mutant harboring *yqjM* gene under the control of $P_{cpcB}$ promoter | KmCm | This study |
| *Synechocystis* sp. PCC 6803 Δ*flv3* $P_{cpcB}$::*yqjM* (Δ*flv3* $P_{cpcB}$::*yqjM*) | *Synechocystis* Δ*flv3* mutant harboring *yqjM* gene under the control of $P_{cpcB}$ promoter | SmKm | |

| | |
|---|---|
| *Synechocystis* sp. PCC 6803 Δ*hoxYH*Δ*flv3* $P_{cpcB}$::*yqjM* (Δ*hoxYH*Δ*flv3* $P_{cpcB}$::*yqjM*) | *Synechocystis* Δ*hoxYH*Δ*flv3* mutant SmKm harboring *yqjM* gene under the control of $P_{cpcB}$ promoter |

**Table S4**

Parameters for the GC-FID method used to detect the substrate and product.

| Achiral GC-FID (GC-2010 Plus, Shimadzu, Japan) | | |
|---|---|---|
| Column parameter | Column | ZB-5, ID 342390 |
| | Film thickness | 0.25 µm |
| | Column length | 30 m |
| | Inner diameter | 0.32 mm |
| | Stationary phase | 5% phenyl 95 % dimethylplysiloxane |
| Autosampler and Injection port | Injection volume | 1 µL |
| | Injection Temperature | 230 ºC |
| | Carrier gas | $N_2$ |
| | Total flow | 19.8 mL $min^{-1}$ |
| | Column flow | 0.80 mL $min^{-1}$ |
| | Linear Velocity | 17.6 cm $s^{-1}$ |
| | Purge Flow | 3 mL $min^{-1}$ |
| | Split ratio | 20 |
| FID detector | Temperature | 320 ºC |

| | | | |
|---|---|---|---|
| | Sampling rate | 40 ms | |
| | $H_2$ flow | 40 mL $min^{-1}$ | |
| | Air flow | 400 mL $min^{-1}$ | |
| Retention time | 2-methylmaleimide | 5.6 min | |
| | 2-methylsuccinimide | 6.2 min | |
| | 1-decanol | 7.2 min | |
| Temperature program | Rate [ºC/min] | Temp [ºC] | Hold [min] |
| | / | 100 | 3 |
| | 30 | 310 | 4 |

## Supporting figures

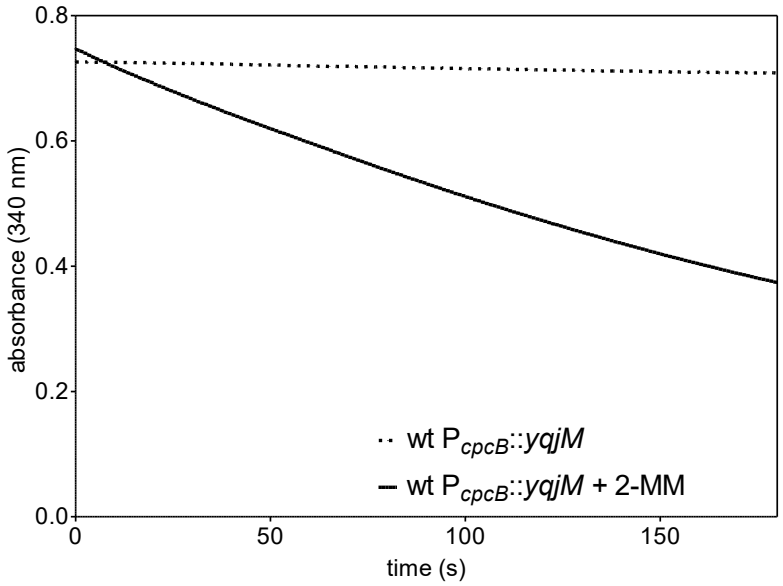


**Fig. S1.** Example of a graph plotted using raw data from the quantification of NADPH absorbance in crude cell free extract of *Synechocystis* sp. PCC 6803 expressing YqjM under

the control of $P_{cpcB}$ promoter (wt $P_{cpcB}$::*yqjM*) without (dotted line) and with the presence of the substrate (full line): 1 mM 2-methylmaleimide (2-MM).

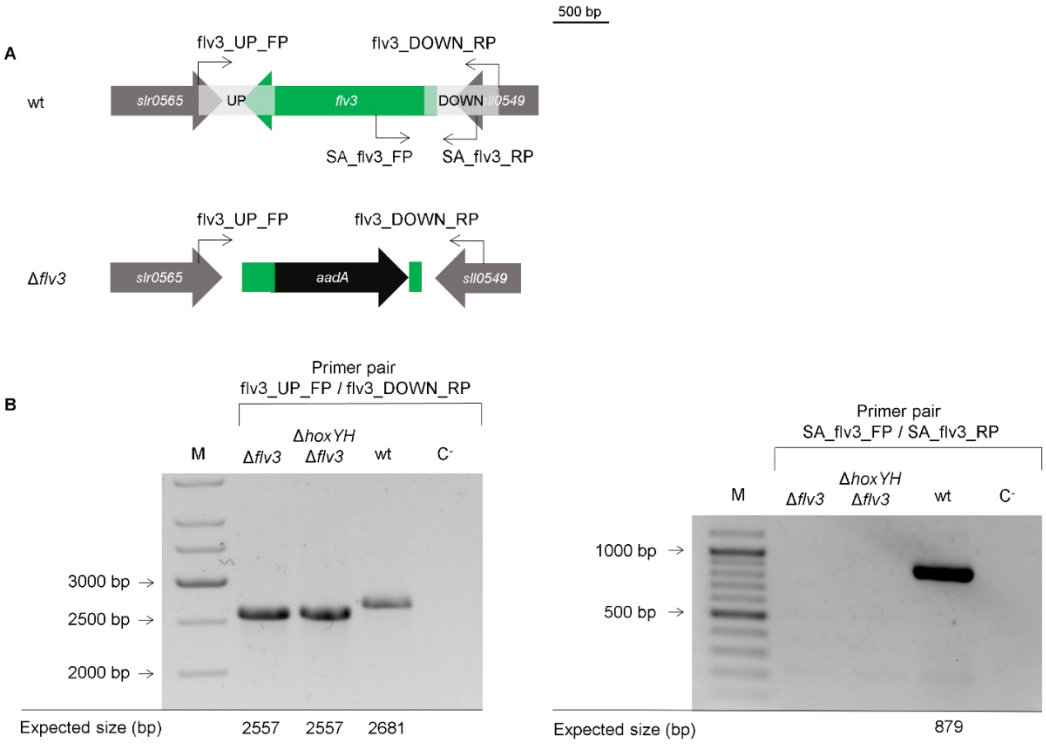

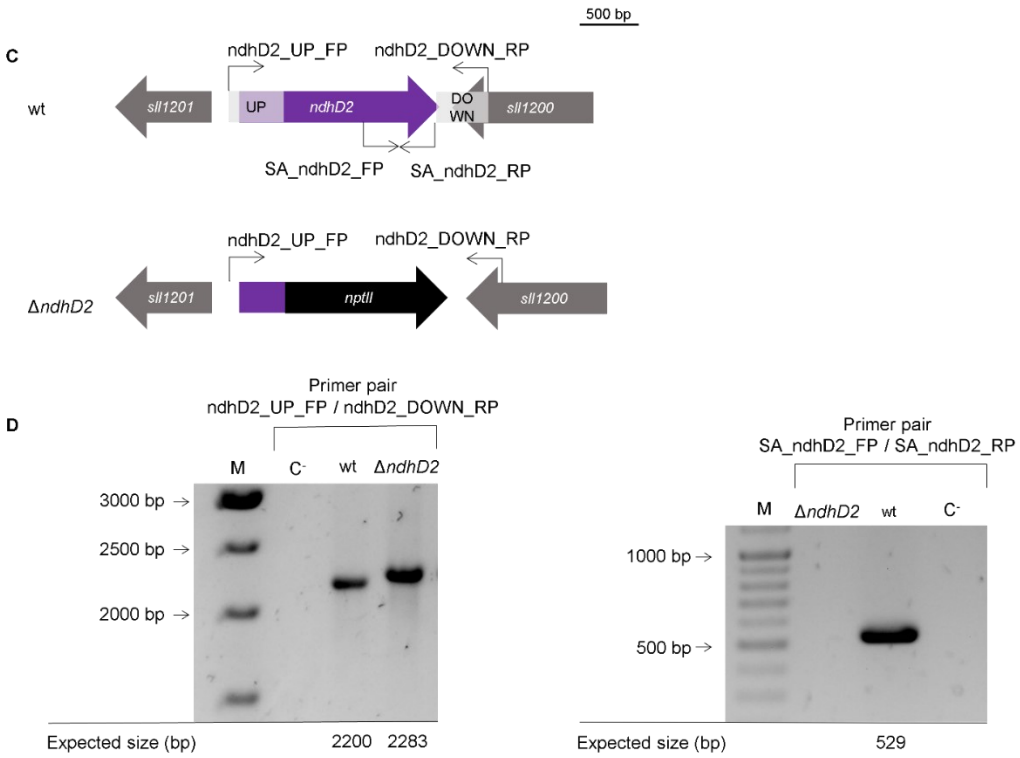


**Fig. S2.** Generation of *Synechocystis* sp. PCC 6803 customized chassis by deletion of selected genes coding for Flv3 or NdhD2. Schematic representation of the position of the primers (A and C) and PCR analysis confirming the segregation of *Synechocystis* Δ*flv3*, Δ*hoxYH*Δ*flv3* (B) and Δ*ndhD2* mutants (D). PCRs were performed using outer and inner primers for *flv3* and *ndhD2*. For details on the primers used see Table S1. The amplicon expected size is indicated below each lane. wt, wild-type, $C^-$, negative control (no template); M, molecular marker GeneRuler DNA Ladder Mix (Thermo Scientific™).

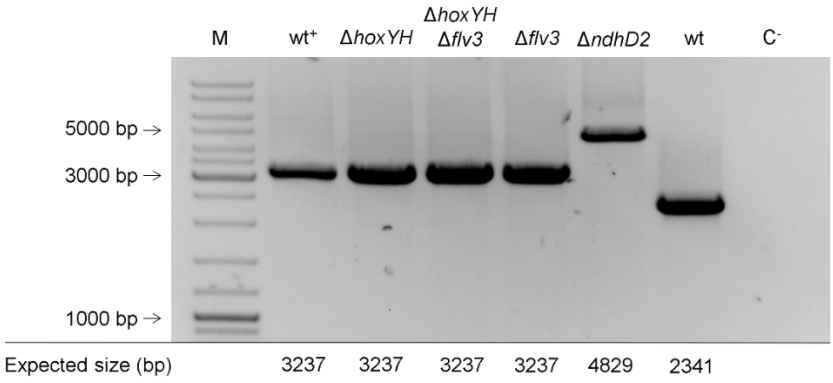


**Fig. S3.** PCR analysis confirming the segregation of *Synechocystis* wt (wt$^{+}$) Δ*hoxYH,* Δ*flv3*, Δ*hoxYH*Δ*flv3* and Δ*ndhD2* mutants containing the gene encoding for the enzyme YqjM under the control of $P_{cpcB}$ promoter ($P_{cpcB}$::*yqjM*). PCR reactions were performed using primer pair Seg_fw / Seg_rv (Table S1). The amplicon expected size is indicated below each lane. wt, wild-type, $C^{-}$, negative control (no template); M, molecular marker GeneRuler DNA Ladder Mix (Thermo Scientific$^{TM}$).

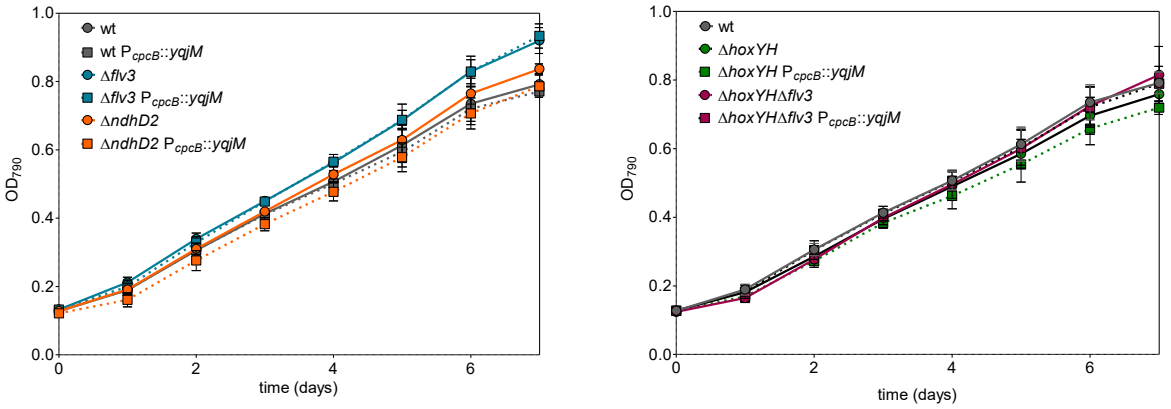


**Fig. S4.** Growth curves of *Synechocystis* sp. PCC 6803 (wt), Δ*hoxYH*, Δ*flv3*, Δ*ndhD2* and Δ*hoxYH*Δ*flv3*, and these chassis expressing YqjM. Cells were cultivated in BG-11 at 28ºC with orbital shaking (150 rpm) under 12 h white light (20 µmol $m^{-2}$ $s^{-1}$), 12 h dark regime. Error bars correspond to standard deviations from at least three biological replicates with technical triplicates.

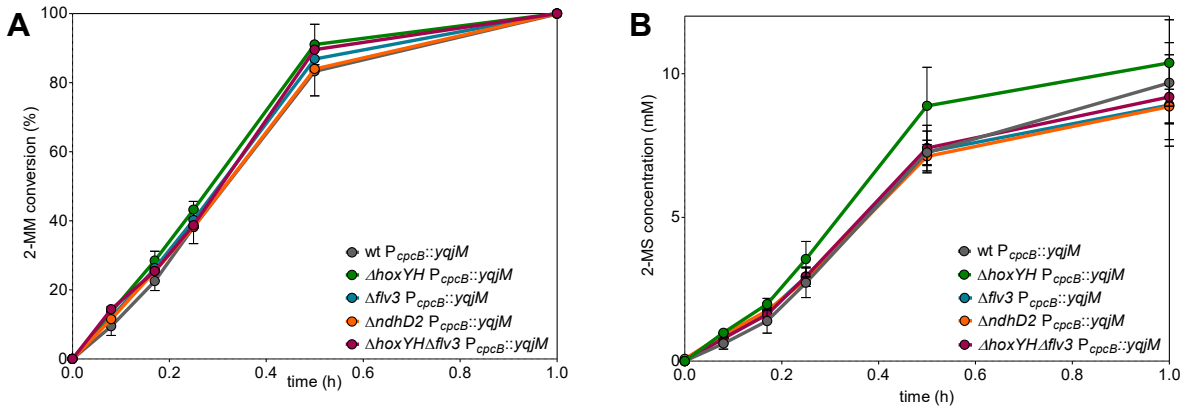


**Fig. S5.** Light-driven conversion of 2-methylmaleimide to 2-methylsuccinimide catalyzed by YqjM expressed in *Synechocystis wt* and Δ*hoxYH*, Δ*flv3*, Δ*ndhD2* and Δ*hoxYH*Δ*flv3* chassis. A) 2-methylmaleimide conversion over time and B) 2-MS concentration over time. Cells were cultivated in BG-11 at 30ºC with orbital shaking (140 rpm) under continuous white light (50 µmol $m^{-2}$ $s^{-1}$), grown until $OD_{750}$ 1-1.5, harvested and applied for the biotransformation of 10 mM 2-MM (1 ml, BG-11, white light of 150 µmol $m^{-2}$ $s^{-1}$ or dark, 130 rpm, 30ºC). Error bars correspond to standard deviations from three biological replicates.

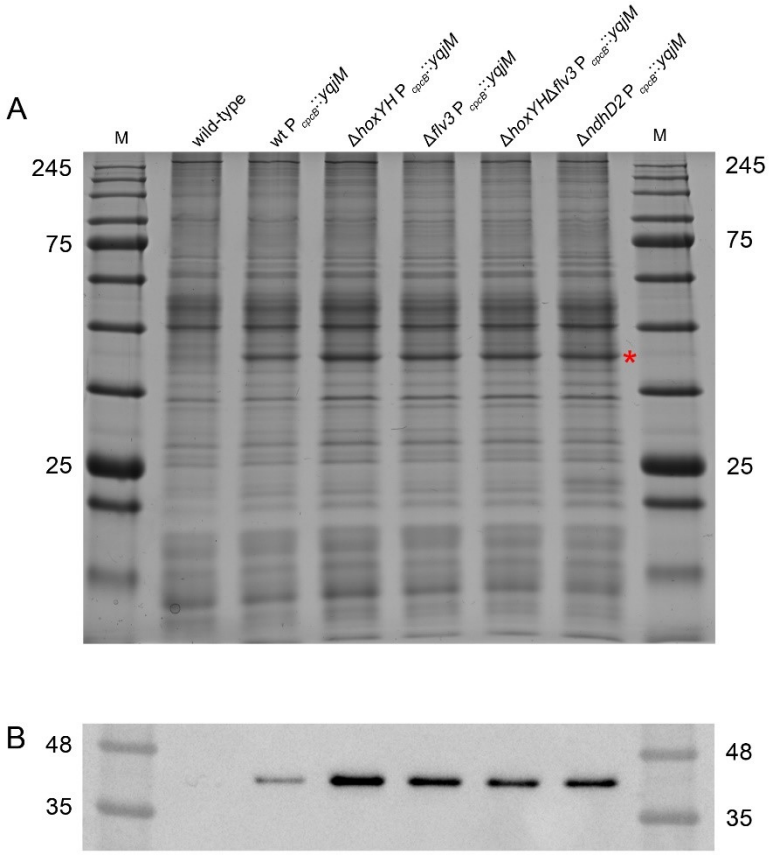


**Fig. S6.** Analysis of protein extracts of *Synechocystis* sp. PCC 6803 wild-type (wt), and *Synechocystis* wild-type, Δ*hoxYH*, Δflv3, Δ*hoxYH*Δ*flv3* and Δ*ndhD2* chassis expressing YqjM: wt $P_{cpcB}$::*yqjM*, Δ*hoxYH* $P_{cpcB}$::*yqjM,* Δ*flv3* $P_{cpcB}$::*yqjM,* Δ*hoxYH*Δ*flv3* $P_{cpcB}$::*yqjM* and Δ*ndhD2* $P_{cpcB}$::*yqjM*, respectively. A) SDS-PAGE and stained with PageBlue, 10 µg of protein extract was loaded in each lane, the location of the YqjM band is indicated by a star (expected size of approximately 38.7 kDa). B) Western blot using an anti-His-tag as a primary antibody, 10 µg of protein extract was loaded in each lane. Cells were cultivated in BG-11 at 30ºC with orbital shaking (140 rpm) under continuous white light (50 µmol $m^{-2}$ $s^{-1}$), grown until $OD_{750}$ 1-1.5, harvested and used for the preparation of crude cell extracts. M- NZYColour protein marker II (NZYTech).

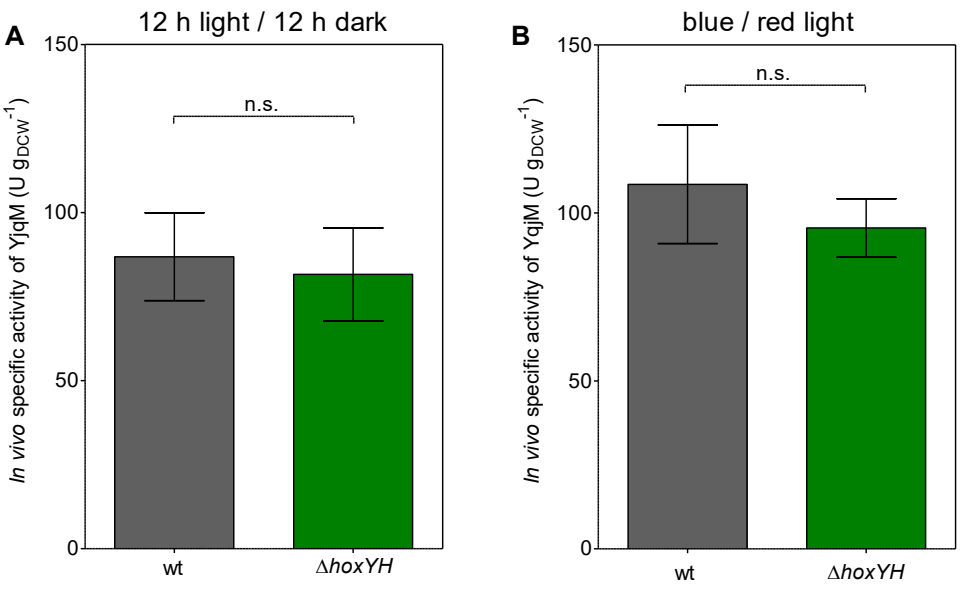


**Fig. S7.** Light-driven biotransformations of 2-methylmaleimide into 2-methylsuccinimide catalyzed by YqjM expressed in *Synechocystis* wt and Δ*hoxYH* chassis cultivated under 12 h white light 12 h dark regimen or continuous blue/red light. A) *In vivo* specific activity of YqjM expressed in chassis cultivated under 12 h white light (50 µmol $m^{-2}$ $s^{-1}$)/12 h dark conditions. B) *In vivo* specific activity of YqjM expressed in chassis cultivated under blue red light (150 µmol $m^{-2}$ $s^{-1}$). The cells were cultivated in BG-11 at 30ºC with orbital shaking (140 rpm) grown until $OD_{750}$ 1-2, harvested and applied for the biotransformation of 10 mM 2-MM (1 mL, 2.4 $g_{DCW}$ $L^{-}$1, BG-11, 150 µmol $m^{-2}$ $s^{-1}$ white light, 130 rpm, 30ºC). Error bars correspond to standard deviations from three biological replicates and statistical analysis is presented based on unpaired *t*-test (n.s., not significant).

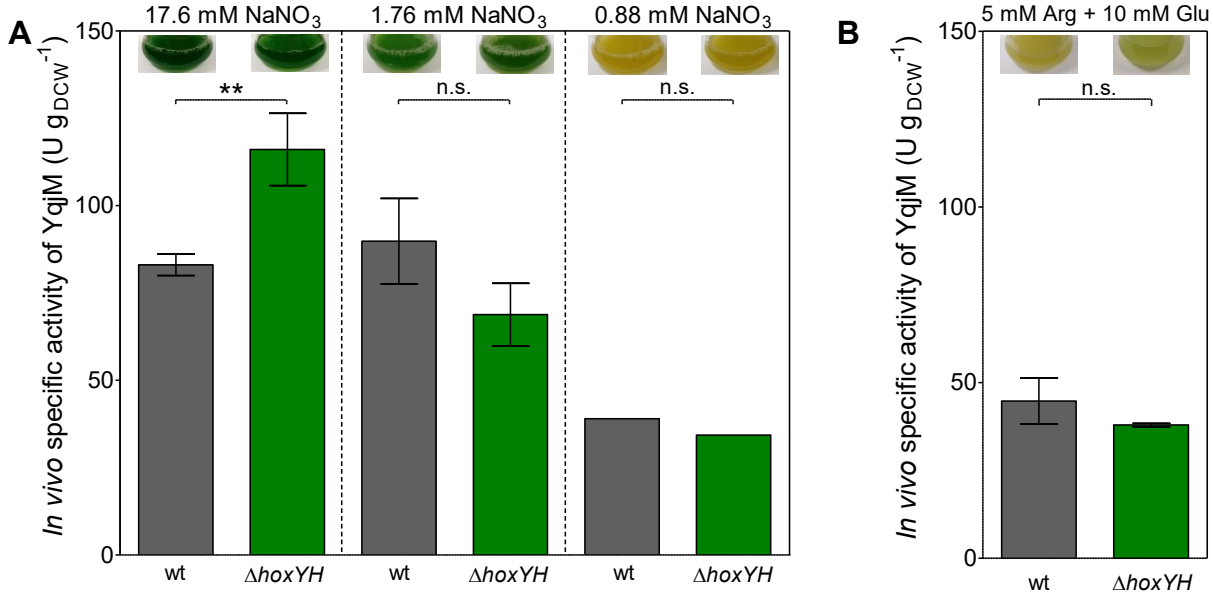


**Fig. S8.** Light-driven biotransformations of 2-methylmaleimide into 2-methylsuccinimide catalyzed by YqjM expressed in *Synechocystis* wt or Δ*hoxYH* cultivated under nitrogen limiting or nitrate-limiting mixotrophic conditions. A) *In vivo* specific activity of cells cultivated in BG-$11_0$ with the addition of 17.6 mM,1.76 $mM_3$ or 0.88 mM $NaNO_3$ with orbital shaking (140 rpm) under continuous white light (50 µmol $m^{-2}$ $s^{-1}$) harvested at $OD_{750}$ 1-1.5 and applied for the biotransformation of 10 mM 2-MM (1 ml, 2.4 $g_{DCW}$ $L^{-1}$, BG-$11_0$ + 17.6 mM,1.76 $mM_3$ or 0.88 mM $NaNO_3$, 150 µmol $m^{-2}$ $s^{-1}$ white light, 130 rpm, 30ºC); B) *In vivo* specific activity of cells cultivated in BG-$11_0$ with the addition of 5 mM arginine and 10 mM glucose. Cells were cultivated in the BG-$11_0$ supplemented with 5 mM arginine and 10 mM glucose with orbital shaking (140 rpm) under continuous white light (50 µmol $m^{-2}$ $s^{-1}$) harvested at $OD_{750}$ 1-1.5 and applied for the biotransformation of 10 mM 2-MM (1 ml, 2.4 $g_{DCW}$ $L^{-1}$, BG-$11_0$ + 5 mM arginine + 10 mM glucose, 150 µmol $m^{-2}$ $s^{-1}$ white light, 130 rpm, 30ºC). Error bars correspond to standard deviations from two biological replicates, and statistical analysis is presented based on unpaired *t* test (n.s., not significant).

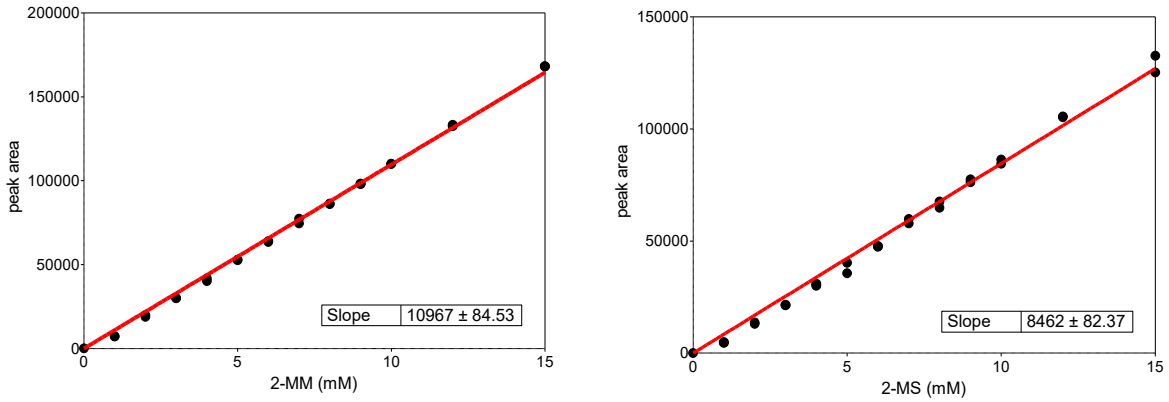


**Fig. S9.** Standard curves generated for quantification of 2-MM and 2-MS. Data derive from two independent technical replicates and the corresponding line equations and $R^2$ values were generated by simple linear regression and forced through zero.

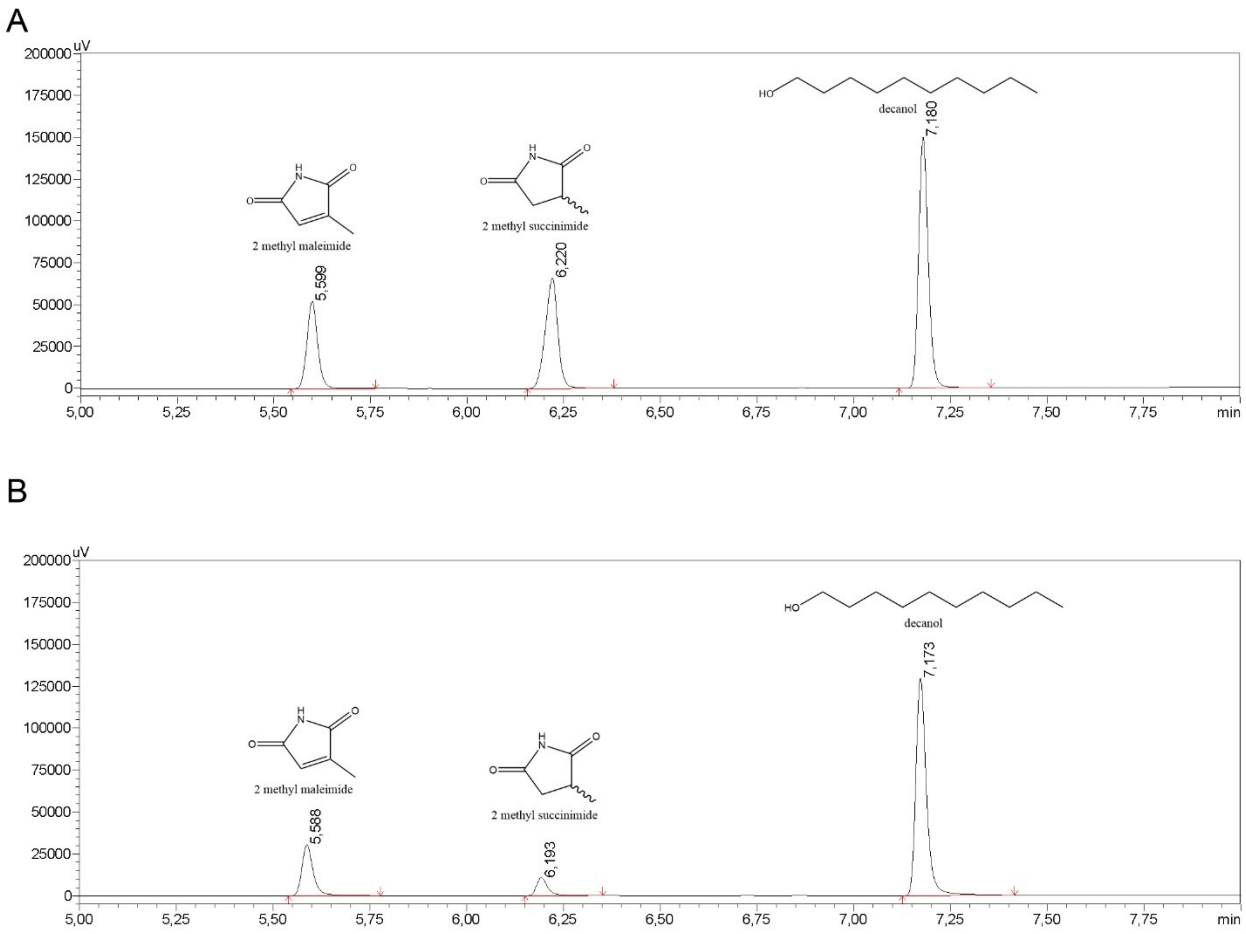

**Fig. S10.** Representative GC-FID chromatograms for quantification of 2-MM and 2-MS. A) Reference chromatogram of 2-MM and 2-MS standards. B) Extracted sample of *in vivo* biotransformation of 2-MM to 2-MS.

## References

Assil-Companioni, L., Büchsenschütz, H.C., Solymosi, D., Dyczmons-Nowaczyk, N.G., Bauer, K.K., Wallner, S., Macheroux, P., Allahverdiyeva, Y., Nowaczyk, M.M., Kourist, R., 2020. Engineering of NADPH supply boosts photosynthesis-driven biotransformations. ACS Catal. 10, 11864-11877. doi.org/10.1021/acscatal.0c02601.

Kanesaki, Y., Shiwa, Y., Tajima, N., Suzuki, M., Watanabe, S., Sato, N., Ikeuchi, M., Yoshikawa, H., 2012. Identification of substrain-specific mutations by massively parallel whole-genome resequencing of Synechocystis sp. PCC 6803. DNA Res. 19, 67-79. doi.org/10.1093/dnares/dsr042.

Pinto, F., Pacheco, C.C., Oliveira, P., Montagud, A., Landels, A., Couto, N., Wright, P.C., Urchueguía, J.F., Tamagnini, P., 2015. Improving a Synechocystis-based photoautotrophic chassis through systematic genome mapping and validation of neutral sites. DNA Res. 22, 425-437. doi.org/10.1093/dnares/dsv024.

Pinto, F., van Elburg, K.A., Pacheco, C.C., Lopo, M., Noirel, J., Montagud, A., Urchueguia, J.F., Wright, P.C., Tamagnini, P., 2012. Construction of a chassis for hydrogen production: physiological and molecular characterization of a Synechocystis sp. PCC 6803 mutant lacking a functional bidirectional hydrogenase. Microbiology 158, 448-464. doi.org/10.1099/mic.0.052282-0.

Trautmann, D., Voß, B., Wilde, A., Al-Babili, S., Hess, W.R., 2012. Microevolution in cyanobacteria: re-sequencing a motile substrain of Synechocystis sp. PCC 6803. DNA Res. 19, 435-448. doi.org/10.1093/dnares/dss024.

# CHAPTER III

# Characterization of a library of RNA thermometers as potential regulatory elements

# 1. Introduction

Synthetic biology aims at designing new biological systems or restructuring existing ones by recombining genetic parts or modules (Sengupta et al., 2018). Engineering biological systems rely on the availability of a molecular toolbox containing standardized and characterized biological parts for constructing devices and systems (Endy, 2005). Unfortunately, a vast number of synthetic biology tools and modular parts developed for model heterotrophic organisms often do not perform as robustly in cyanobacterial strains (Huang et al., 2010). Therefore, customized regulatory parts are needed to fine-tune the expression of synthetic modules in cyanobacteria. RNA-based regulatory elements, such as riboswitches and RNA thermometers (RNATs) have been gaining attention due to their simplicity and universality (Nshogozabahizi et al., 2019, Dykstra et al., 2022). Riboswitches are RNA-based regulatory tools that offer great potential being (theoretically) modular and independent of transcriptional factors (Nshogozabahizi et al., 2019). Several metabolite-binding riboswitches have been identified in cyanobacteria, such as a cobalamin-dependent riboswitch (Pérez et al., 2016), glutamine-aptamer (Klähn et al., 2018) and the most widely used theophylline-controlled riboswitch (Ma et al., 2014, Ohbayashi et al., 2016, Nakahira et al., 2013). However, the addition of chemicals for the regulation of gene expression can have a significant cost for future biotechnological applications. Therefore, there is an interest to develop induction systems being responsive to environmental parameters (Hudson, 2021). Expanding the cyanobacterial synthetic biology toolbox to include other RNA-based regulatory tools such as RNATs, offers a wide variety of potential applications. RNATs are regions within the 5’ untranslated region of mRNAs that change secondary structure upon temperature shift, leading to a rapid activation or repression of the translation initiation. These structural transitions usually expose or occlude important parts of the 5’-UTR, such as the ribosome binding site (RBS) (Fig. 1) (Kortmann and Narberhaus, 2012).

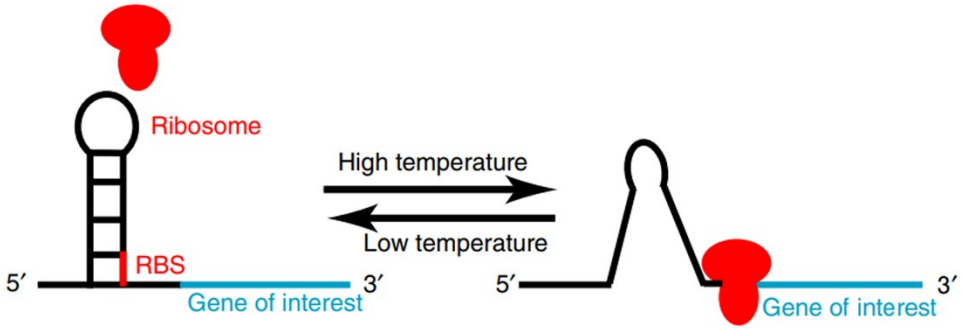


**Figure 1.** Schematic representation of a simple RNA thermometer. A stem-loop structure locks the RBS and prevents the binding of the ribosome. Upon temperature shift, the stem-loop structure opens, unveiling the RBS and allowing binding of the small ribosomal subunit and initiation of translation. (Modified from Nshogozabahizi et al., 2019).

RNATs are remarkably sensitive, being able to detect temperature variations of 1 °C, resulting in rapid activation or repression of translation (Rinnenthal et al., 2011). They can be heat-inducible or heat-repressible, referring to high temperatures induction or repression of gene expression, respectively. Most naturally occurring RNATs are heat-inducible. However, heat-repressible RNATs have also been discovered (Giuliodori et al., 2010) or designed (Hoynes-O'Connor et al., 2015). Three gene classes are particularly prone to thermoregulation, including virulence, cold shock and heat shock related genes using RNATs for controlling the translation initiation in a temperature-dependent manner (Kortmann and Narberhaus, 2012). The first described thermometer regulating the expression of the alternative RNA polymerase σ-factor σ32 (encoded by *rpoH*) was discovered in *Escherichia coli* (*E.coli*) (Morita et al., 1999), Following, several built-in RNA thermometers have been described including FourU, found in the 5′-UTR of the *Salmonella agsA* gene (Waldminghaus et al., 2007), the ROSE (repression of heat shock gene expression) elements (Nocker et al., 2001), RNAT found in the 5'-UTR of the *prfA* gene of the pathogenic bacterium *Listeria monocytogenes* (Johansson et al., 2002) and the simple *hsp17* thermometer found in *Synechocystis* (Kortmann et al., 2011).

As RNATs usually display a simple hairpin structure sufficient for effective thermoregulation, they are attractive tools in synthetic biology, following *de novo* design or redesigning previously described ones. Several studies focused on designing RNATs for a variety of temperature-sensing tools, meant for the regulation of protein expression in different organisms (Sen et al., 2017, Neupert et al., 2008, Hoynes-O'Connor et al., 2015, Waldminghaus et al., 2008). Even though a simple *hsp17* thermometer was found in

*Synechocystis*, cyanobacterial RNAT-based synthetic biology tools have not been developed yet. This simple natural thermometer was identified upstream of the *hsp17* in *Synechocystis*, consisting of only 44 nucleotides and a single stem-loop structure that can open and close reversibly (Kortmann et al., 2011). Previous studies show that minimal size thermosensors with a simple and well-understood mechanism, offer the potential to be further developed (Neupert et al., 2008, Sen et al., 2017). Therefore, redesigning the cyanobacterial *hsp17* thermometer offers the possibility to include RNATs into the toolbox of standardized RNA regulatory elements, specifically customized for *Synechocystis*.

To meet the needs of the synthetic biology toolbox, it is desirable to have a set of RNA thermometers with a spectrum of different sensitivities and thresholds. Therefore, here the objective was to design *in silico* and characterize a library of redesigned cyanobacterial RNA thermometers based on native *hsp17* thermometers from *Synechocystis* sp. PCC 6803.

## 2. Materials and Methods

### 2.1. Chemicals and reagents

All chemicals and reagents were purchased from ThermoFisher Scientific (USA), Merck (Germany) or Sigma-Aldrich (USA) unless otherwise indicated. All DNA-modifying enzymes and polymerases were purchased from ThermoFisher Scientific (USA) and Promega (USA), and standard molecular biology kits were obtained from NZY Tech (Portugal). Agarose gel electrophoresis was performed by standard protocols using 1xTAE buffer (Russell and Sambrook, 2001).

### 2.2. Organisms and culture conditions

The wild-type unicellular non-$N_2$-fixing cyanobacterium *Synechocystis* sp. PCC 6803 substrain GT-Kazusa (obtained from the Pasteur Culture Collection, Paris, France) and mutants were maintained in Erlenmeyer flasks in BG-11 medium (Stanier et al., 1971), with orbital shaking (150rpm) and 12 h light (cool white daylight 20 µmol $m^{-2}$ $s^{-1}$)/12 h dark regimen at 30 ºC, unless otherwise stated. For solid medium, BG-11 was supplemented with 1.5% Noble agar (Difco), 0.3% sodium thiosulfate and 10 mM TES-KOH buffer (pH 8.2). For the selection and maintenance of the mutants, the BG-11 medium was supplemented with kanamycin (Km) (50 µg $mL^{-1}$). *Escherichia coli* strains XL1-Blue were used for cloning purposes. *E. coli* transformants were grown at 37 ºC in Luria-Bertani (LB) medium supplemented with Km (50 µg $mL^{-1}$).

## 2.3. Design of synthetic RNA thermometers

The synthetic RNAT variants used in this study were based on the previously described *hsp17* thermometer, native from *Synechocystis* sp. PCC 6803 (Kortmann et al., 2011). Dr. Filipe Pinto designed RNATs using the RNAinverse server (Lorenz et al., 2011), generating a total of 200 sequences. The thermodynamic parameters were calculated for all the sequences using DINAMelt's Quickfold (Markham and Zuker, 2005), and 11 were selected for synthesis and further characterization, covering the range of ΔG values obtained. In the study, we also included TS12 containing the native sequence of the *hsp17* thermometer, and TS13 containing the native sequence with several nucleotides changed to the BioBrick RFC[10] assembly scar (TACTAG) between RBS and starting codon. The sequences of the selected thermometers are presented in Table 1.

**Table 1**. The selected RNAT sequences.

| Name | Sequence* |
|---|---|
| TS1 | AUCCCCGUCAGUGACGGAGAUUCACACAUACUAGAGAUUCAAAGGUAAACAAUUCCUUCCACACAUCAG GAGUUUACUAGAUGCGU |
| TS2 | AUCCCCGUCAGUGACGGAGAUUCACACAUACUAGAGAUUCAAAAGUCAGCAAUUCCUUCCACACAUCAG GAGUUUACUAGAUGCGU |
| TS3 | AUCCCCGUCAGUGACGGAGAUUCACACAUACUAGAGAUUGAAAAGUAGGCAAUUCACCCCAAACAACAG GAGUUUACUAGAUGCGU |
| TS4 | AUCCCCGUCAGUGACGGAGAUUCACACAUACUAGAGAUUUAGAGGUUCCCAACUCCUACCACACACCAG GAGUUUACUAGAUGCGU |
| TS5 | AUCCCCGUCAGUGACGGAGAUUCACACAUACUAGAGAUCCAAAAGUCUGCAACUCCUUCCCCUCUUCAG GAGUUUACUAGAUGCGU |
| TS6 | AUCCCCGUCAGUGACGGAGAUUCACACAUACUAGAGAUUCAAGACUAUUCAAUUCCUUCCACACAUCAG GAGUUUACUAGAUGCGU |
| TS7 | AUCCCCGUCAGUGACGGAGAUUCACACAUACUAGAGAUUCAAAGGUAUCCAAUUCCUUUCACACAUCAG GAGUUUACUAGAUGCGU |
| TS8 | AUCCCCGUCAGUGACGGAGAUUCACACAUACUAGAGAUUCUAUGGUCCUCAAUUACUUCCACACAUCAG GAGUUUACUAGAUGCGU |
| TS9 | AUCCCCGUCAGUGACGGAGAUUCACACAUACUAGAGAUUCAAGAGGACCAAAUUCCUUCCACGUAUCAG GAGUUUACUAGAUGCGU |
| TS10 | AUCCCCGUCAGUGACGGAGAUUCACACAUACUAGAGAUAAAAAAGCGCUCAGUUGCCUCCUUAUUUCAG GAGUUUACUAGAUGCGU |
| TS11 | AUCCCCGUCAGUGACGGAGAUUCACACAUACUAGAGAUUCAAUAAUUACCAAUGCCUACCAAAUCUAAG GAGUUUACUAGAUGCGU |

| | |
|---|---|
| TS12 | AUCCCCGUCAGUGACGGAGAUUCACACAUACUAGAGAUUCAAGGGUAAUCAAUUCCUUCCACACAUCAGGAGUUAACAUUAUGCGU |
| TS13 | AUCCCCGUCAGUGACGGAGAUUCACACAUACUAGAGAUUCAAGGGUAAUCAAUUCCUUCCACACAUCAGGAGUUUACUAGAUGCGU |

* The 44 underlined nucleotides were redesigned *in silico* from the native *hsp17* RNAT sequence and the RBS is presented in red. The grey nucleotides were also included for predicting the structures to cover the full 5'-UTR.

## 2.4. Plasmid construction

To characterize the RNATs designed, pSEVA251-based replicative plasmids containing the *gfp* ORF under the control of the $P_{trc.x.tetO2}$ promoter (Ferreira et al., 2018) and the RNATs sequences serving as RBS were constructed. Reverse PCRs followed by the FastCloning approach (Li et al., 2011) were used to replace the sequence of the ribosome binding site in the template plasmid (BioBrick part BBa_B0032) by the corresponding RNAT sequences. Briefly, the template plasmid 'pSEVA251 $P_{trc.x.tetO2}$::B0032::*gfp*' (Ferreira et al., 2018) was amplified by PCR using Phusion® High-Fidelity DNA Polymerase and TS-specific primers. Further on, PCR products were treated with *DpnI* enzyme to digest the parental template. The digested PCR products were transformed into *E. coli* XL1-Blue competent cells to obtain the target clones. Followed by plasmid isolation, the sequences of the obtained plasmids 'pSEVA251 $P_{trc.x.tetO2}$::TS::*gfp*' were confirmed by Sanger sequencing. The list of TS-specific primers and the sequencing primers is presented in Table 2.

**Table 2.** Oligonucleotide primers used in this study.

| Name | Sequence (5'-3') | Purpose | Reference |
|---|---|---|---|
| TS1-FP | TAAACAATTCCTTCCACACATCAGGAGTTTACTAGATGCGTAAAGGAGAAGAACTTTTCACTGG | Generation of pSEVA251 $p_{trc.x.tetO2}$::TS::*gfp* plasmids | This study |
| TS1-RP | TGTGTGGAAGGAATTGTTTACCTTTGAATCTCTAGTATGTGTGAATCTCCGTCACTGACG | | |
| TS2-FP | TCAGCAATTCCTTCCACACATCAGGAGTTTACTAGATGCGTAAAGGAGAAGAACTTTTCACTGG | | |
| TS2-RP | TGTGTGGAAGGAATTGCTGACTTTTGAATCTCTAGTATGTGTGAATCTCCGTCACTGACG | | |
| TS3-FP | TAGGCAATTCACCCCAAACAACAGGAGTTTACTAGATGCGTAAAGGAGAAGAACTTTTCACTGG | | |
| TS3-RP | TGTTTGGGGTGAATTGCCTACTTTTCAATCTCTAGTATGTGTGAATCTCCGTCACTGACG | | |

| | | | |
|---|---|---|---|
| TS4-FP | TTCCCAACTCCTACCACACACCAGGAGTTTACTAGATGCGTAAAG GAGAAGAACTTTTCACTGG | | |
| TS4-RP | TGTGTGGTAGGAGTTGGGAACCTCTAAATCTCTAGTATGTGTGAAT CTCCGTCACTGACG | | |
| TS5-FP | TCTGCAACTCCTTCCCCTCTTCAGGAGTTTACTAGATGCGTAAAGG AGAAGAACTTTTCACTGG | | |
| TS5-RP | AGAGGGGAAGGAGTTGCAGACTTTTGGATCTCTAGTATGTGTGAA TCTCCGTCACTGACG | | |
| TS6-FP | TATTCAATTCCTTCCACACATCAGGAGTTTACTAGATGCGTAAAGG AGAAGAACTTTTCACTGG | | |
| TS6-RP | TGTGTGGAAGGAATTGAATAGTCTTGAATCTCTAGTATGTGTGAAT CTCCGTCACTGACG | | |
| TS7- FP | TATCCAATTCCTTTCACACATCAGGAGTTTACTAGATGCGTAAAGG AGAAGAACTTTTCACTGG | | |
| TS7-RP | TGTGTGAAAGGAATTGGATACCTTTGAATCTCTAGTATGTGTGAAT CTCCGTCACTGACG | | |
| TS8-FP | TCCTCAATTACTTCCACACATCAGGAGTTTACTAGATGCGTAAAGG AGAAGAACTTTTCACTGG | | |
| TS8-RP | TGTGTGGAAGTAATTGAGGACCATAGAATCTCTAGTATGTGTGAAT CTCCGTCACTGACG | | |
| TS9-FP | GACCAAATTCCTTCCACGTATCAGGAGTTTACTAGATGCGTAAAGG AGAAGAACTTTTCACTGG | | |
| TS9-RP | TACGTGGAAGGAATTTGGTCCTCTTGAATCTCTAGTATGTGTGAAT CTCCGTCACTGACG | | |
| TS10-FP | CGCTCAGTTGCCTCCTTATTTCAGGAGTTTACTAGATGCGTAAAGG AGAAGAACTTTTCACTGG | | |
| TS10-RP | AATAAGGAGGCAACTGAGCGCTTTTTTATCTCTAGTATGTGTGAAT CTCCGTCACTGACG | | |
| TS11-FP | TTACCAATGCCTACCAAATCTAAGGAGTTTACTAGATGCGTAAAGG AGAAGAACTTTTCACTGG | | |
| TS11-RP | GATTTGGTAGGCATTGGTAATTATTGAATCTCTAGTATGTGTGAAT CTCCGTCACTGACG | | |
| TS12-FP | CAATTCCTTCCACACATCAGGAGTTAACATTATGCGTAAAGGAGAA GAACTTTTCACTGGAGTTG | | |
| TS12-RP | GATGTGTGGAAGGAATTGATTACCCTTGAATCTCTAGTATGTGTGA ATCTCCGTCACTGACG | | |
| TS13-FP | TAATCAATTCCTTCCACACATCAGGAGTTTACTAGATGCGTAAAGG AGAAGAACTTTTCACTGG | | |
| TS13-RP | GATGTGTGGAAGGAATTGATTACCCTTGAATCTCTAGTATGTGTGA ATCTCCGTCACTGACG | | |
| PS1 | AGGGCGGCGGATTTGTCC | Confirmation of the presence of the constructs and sequencing | (Silva-Rocha et al., 2013) |
| PS2 | GCGGCAACCGAGCGTTC | | |

### 2.5. *Synechocystis* transformation and transformants confirmation

The replicative plasmids were introduced into *Synechocystis* by electroporation, based on a previously described protocol (Ludwig et al., 2008). Briefly, 50 mL of *Synechocystis* cultures were grown at 30 ºC under a 12 h light (cool white daylight 20 µmol $m^{-2}$ $s^{-1}$)/12 h dark regimen until reaching an $OD_{730}$ ~ 0.5. Cells were collected by centrifugation at 4190 *g* for 10 min followed by washing three times with 10 mL of 1 mM HEPES, pH 7.5. The cells were then resuspended in 1 mL of HEPES buffer. 1 µg of plasmid DNA was mixed with 60 µL cell aliquots and electroporated using a Gene Pulser™ (Bio-Rad). The capacitor was set to 25 lF and the resistor to 400 X, during 9 ms with an electric field of 12 kV $cm^{-1}$. Further on, cells were mixed with 400 µL of fresh BG-11 medium and spread onto Immobilon-NC membranes (0.45 lm pore size, 82mm, Merck Millipore) which were placed on BG-11 agar plates. After 24 h of incubation at 30 ºC, under continuous light, the membranes were transferred to BG-11 agar plates supplemented with Km (10 µg $mL^{-1}$). Colonies were observed after 2-3 weeks. The presence of replicative plasmids was confirmed by PCR using TS1/PS2 primers (Table 2) and GoTaq® G2 Flexi DNA Polymerase. For this purpose, *Synechocystis* DNA was extracted following a method previously described (Ferreira et al., 2018). Briefly, 2 mL of culture were centrifuged at 14 100 *g* for 3 min and the resulting cell pellet was resuspended in 200 µL of distilled water with the addition of 0.1 g of 0.2 mm diameter glass beads (acid washed, Sigma). Further on, cells were disrupted by two cycles of vortexing for 1 min with in-between incubation for 1 min on ice. Subsequently, the mixture was centrifuged at 14 100 *g* for 2 min, and the DNA containing supernatant was used as a template in the PCR reactions. The sequences of the constructs were confirmed by Sanger sequencing. The list of strains used is presented in Table 3.

**Table 3.** The list of S*ynechocystis* strains used in this work.

| **Strain** | **Description** | **References/sources** |
|---|---|---|
| *Synechocystis* sp. PCC 6803 (wt) | substrain GT-Kazusa | Pasteur Culture Collection, Paris, France |

| | | |
|---|---|---|
| *Synechocystis* pSEVA251 | *Synechocystis* harboring pSEVA251 | (Ferreira et al., 2018) |
| Synechocystis pSEVA251 $p_{trc.x.tetO2}$::TS1::*gfp* | *Synechocystis* harboring pSEVA251 $p_{trc.x.tetO2}$::TS1::*gfp* | This study |
| Synechocystis pSEVA251 $p_{trc.x.tetO2}$::TS2::*gfp* | *Synechocystis* harboring pSEVA251 $p_{trc.x.tetO2}$::TS2::*gfp* | |
| Synechocystis pSEVA251 $p_{trc.x.tetO2}$::TS3::*gfp* | *Synechocystis* harboring pSEVA251 $p_{trc.x.tetO2}$::TS3::*gfp* | |
| Synechocystis pSEVA251 $p_{trc.x.tetO2}$::TS4::*gfp* | *Synechocystis* harboring pSEVA251 $p_{trc.x.tetO2}$::TS4::*gfp* | |
| Synechocystis pSEVA251 $p_{trc.x.tetO2}$::TS5::*gfp* | *Synechocystis* harboring pSEVA251 $p_{trc.x.tetO2}$::TS5::*gfp* | |
| Synechocystis pSEVA251 $p_{trc.x.tetO2}$::TS6::*gfp* | *Synechocystis* harboring pSEVA251 $p_{trc.x.tetO2}$::TS6::*gfp* | |
| Synechocystis pSEVA251 $p_{trc.x.tetO2}$::TS7::*gfp* | *Synechocystis* harboring pSEVA251 $p_{trc.x.tetO2}$::TS7::*gfp* | |
| Synechocystis pSEVA251 $p_{trc.x.tetO2}$::TS8::*gfp* | *Synechocystis* harboring pSEVA251 $p_{trc.x.tetO2}$::TS8::*gfp* | |
| Synechocystis pSEVA251 $p_{trc.x.tetO2}$::TS9::*gfp* | *Synechocystis* harboring pSEVA251 $p_{trc.x.tetO2}$::TS9::*gfp* | |
| Synechocystis pSEVA251 $p_{trc.x.tetO2}$::TS11::*gfp* | *Synechocystis* harboring pSEVA251 $p_{trc.x.tetO2}$::TS11::*gfp* | |
| Synechocystis pSEVA251 $p_{trc.x.tetO2}$::TS12::*gfp* | *Synechocystis* harboring pSEVA251 $p_{trc.x.tetO2}$::TS12::*gfp* | |
| Synechocystis pSEVA251 $p_{trc.x.tetO2}$::TS13::*gfp* | *Synechocystis* harboring pSEVA251 $p_{trc.x.tetO2}$::TS13::*gfp* | |
| Synechocystis pSEVA251 $P_{trc.x.tetO2}$::B0032::*gfp* | *Synechocystis* harboring pSEVA251 $P_{trc.x.tetO2}$::B0032::*gfp* | (Ferreira et al., 2018) |

## 2.6. GFP fluorescence analysis

The performance of synthetic RNA thermometers was evaluated by assessing GFP fluorescence under different temperature shifts. For this purpose, cultures of *Synechocystis* clones were inoculated in 10 mL BG-11 medium supplemented with Km (50 µg $mL^{-1}$) at an initial $OD_{730}$ 0.5. Cultures were grown at the starting temperature (25 or 30 °C) until reaching $OD_{730}$ ~ 3, under continuous light with orbital shaking (150rpm). The cultures were diluted to final $OD_{730}$ 0.5 or 1.0 and 200 µL aliquots were distributed in Nunc™ MicroWell™ 96-Well Optical-Bottom Plates (Thermo Fisher Scientific). The 96-well plates were incubated at a corresponding elevated temperature under continuous light (cool white daylight 50 µmol $m^{-2}$ $s^{-1}$) with shaking at 150 rpm for 24 h. For the experiment performed in dark, the 96-well plate was incubated inside the Synergy 2 Multi-Mode Microplate Reader (BioTek Instruments, Inc.) under constant temperature. Each experiment included three technical replicates and the

measurements were carried out in duplicate at 0 h and 1 h, 2 h, 4 h and 24 h after the plate setup. $OD_{790}$ and GFP fluorescence (excitation filter 485/20nm, emission filter 528/20nm, sensitivity set at 110) were detected using Synergy 2 Multi-Mode Microplate Reader using Gen5$^{TM}$ software (BioTek Instruments, Inc.). For the data analysis, the background fluorescence and absorbance of the BG-11 medium were subtracted from the values obtained for the samples and the fluorescence values were normalized by optical density. Further on, the normalized fluorescence obtained for the *Synechocystis* cells harboring the empty pSEVA251 plasmid (autofluorescence) was subtracted from the normalized fluorescence of all samples (Formula 1).

Formula 1.

$$\frac{\text{GFP Fluorescence} - \text{Fluorescence BG-11medium}}{\text{Abs}_{790} - \text{Abs}_{790}\ \text{BG-11 medium}} - S.\ \text{pSEVA251}_{norm}$$

# 3. Results and Discussion

## 3.1. Design of a library of RNA thermometers

Designing simple RNAT *de novo*, consisting only of a single stem-loop structure containing the ribosome binding site proved to be an interesting approach (Neupert et al., 2008). The discovery of a simple *hsp17* RNAT offers a basis for a rational design, particularly intending to have customized tools for translational control in *Synechocystis*. The 5'-UTR of *Synechocystis hsp17* exhibits a rather minimalistic architecture with a single hairpin of 44 nt, in which two loops flank the Shine-Dalgarno (SD) sequence (Kortmann et al., 2011). Therefore, we designed a library of synthetic RNAT based on this simple native *hsp17* thermosensor.

The library included 11 redesigned RNAT covering a spectrum of predicted free energy (TS1-TS11), TS12 based on the native sequence of *hsp17* thermometer and TS13 differing from TS12 in the region between the SD and the translational start codon. All designed sequences had the SD sequence 5'-AGGAGU-3' serving as the ribosome binding site, as in the original *hsp17* thermosensor. The *in silico* analysis of the selected sequences was done using Quikfold (Markham and Zuker, 2005, Markham and Zuker, 2008) to calculate minimum free energy (ΔG), and was based on the full length of the 5'-UTR. As the calculations of redesigned

sequences resulted in a spectrum of ΔG (Fig. 2), we could expect a span of responsiveness of the designed elements.

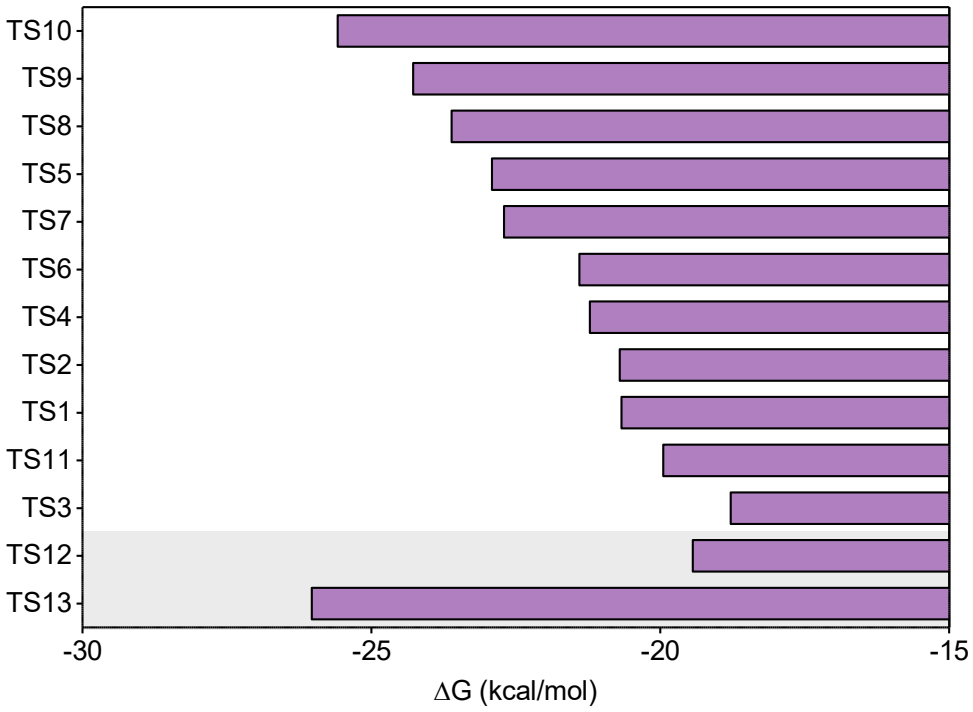


**Figure 2.** Free energies (in ΔG in kcal/mol) of designed RNAT at 30 ºC estimated using the Quikfold program (Markham and Zuker, 2005, Markham and Zuker, 2008).

Figure 3 provides an overview of the putative RNA secondary structures predicted using the Quikfold program (Markham and Zuker, 2005, Markham and Zuker, 2008) using the full length of the 5'-UTR. The predicted structures contained very different structural elements (bulges, mismatches, loop size) and combinations, suggesting that different responses could be expected within the elements of this library, as previous studies underline structural combinations can be explored to optimize RNA thermometers (Neupert et al., 2008). However, it is important to highlight that the structures shown in Figure 3 are one of several potential folded states, as different RNA secondary structures may dynamically coexist within the cell (Zuker, 2003). In addition, most of the developed *in silico* tools are based on a wealth of information acquired from model organisms, such as *E. coli* or *Bacillus*, and could work inadequately for the computational analysis of sequences intended for testing in cyanobacteria.

TS10

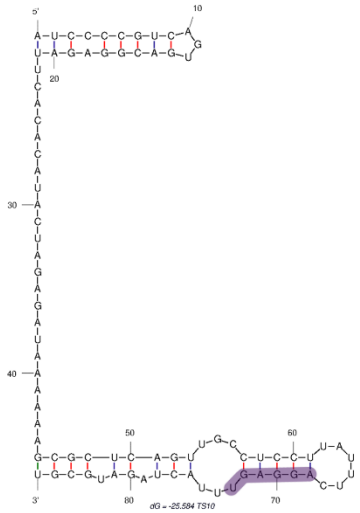

TS9

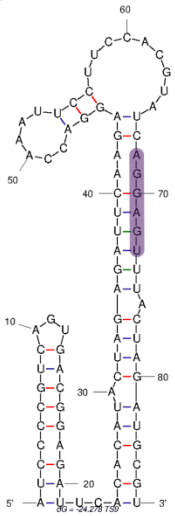

TS8

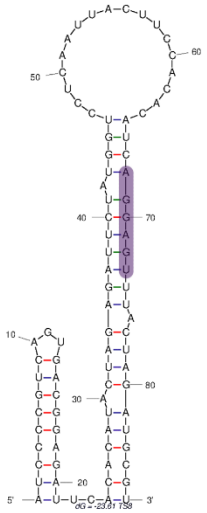

TS5

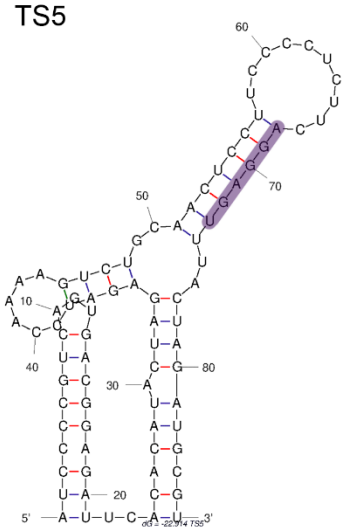

TS7

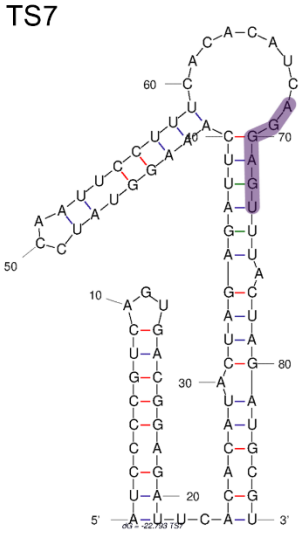

TS6

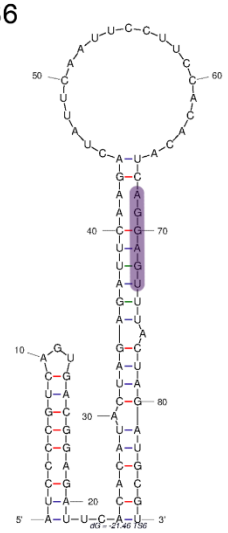

TS4

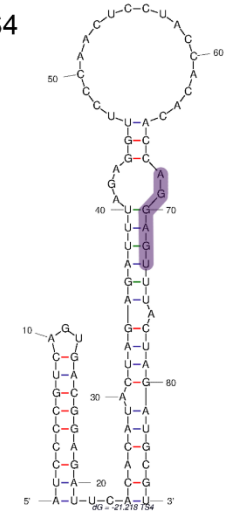

TS2

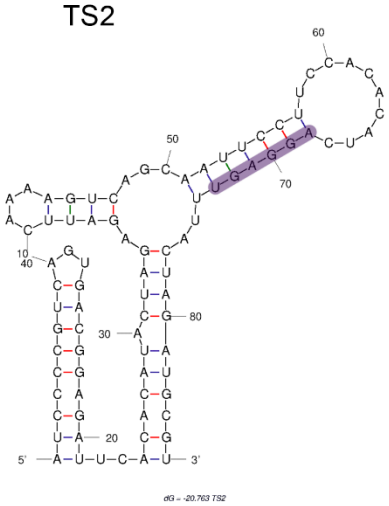

TS1

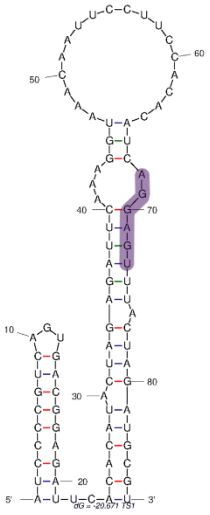

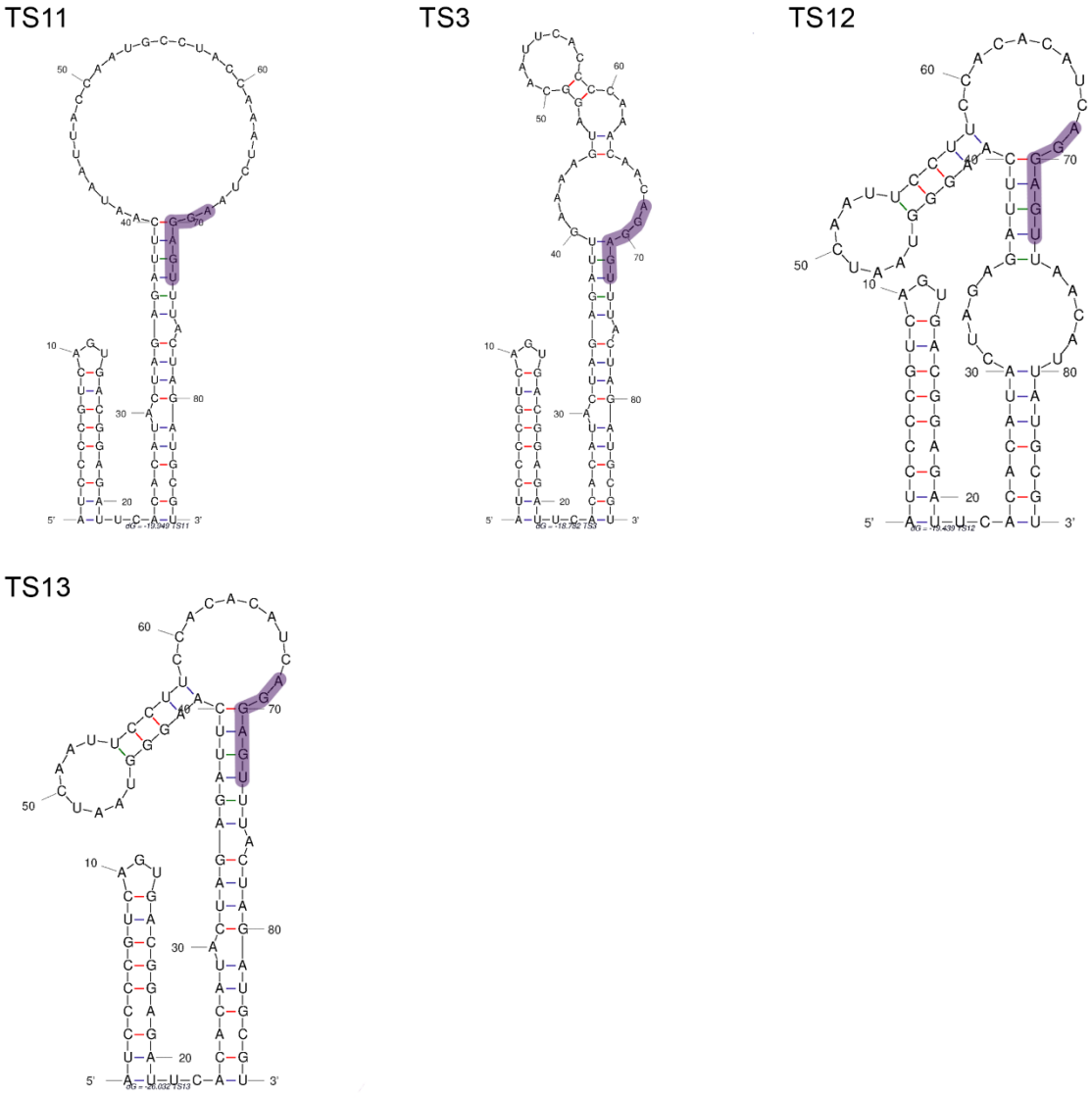


**Figure 3.** Secondary structures of the entire 5'-UTR as predicted by the Quikfold program (Markham and Zuker, 2005, Markham and Zuker, 2008). The SD sequence is highlighted in violet.

## 3.2. Plasmids construction and transformation of *Synechocystis*

The GFP reporter system (Fig. 4A) was utilized to test whether the synthetic RNA elements could result in temperature-dependent translational control. For that purpose, 13 synthetic modules pSEVA251 $P_{trc.x.tetO2}$::TS::*gfp* were successfully constructed and used for the transformation of *Synechocystis* via electroporation. *Synechocystis* transformants harboring 12 of the 13 TS synthetic modules were obtained, the presence of the pSEVA251

$P_{trc.x.tetO2}$::TS::*gfp* constructs was assessed by PCR (Fig. 4B), and the sequences were confirmed by automated sequencing. Interestingly, after several rounds of transformations, the construct harboring TS10, with the highest predicted free energy could not be successfully introduced into *Synechocystis*, as no colonies appeared after transformation.

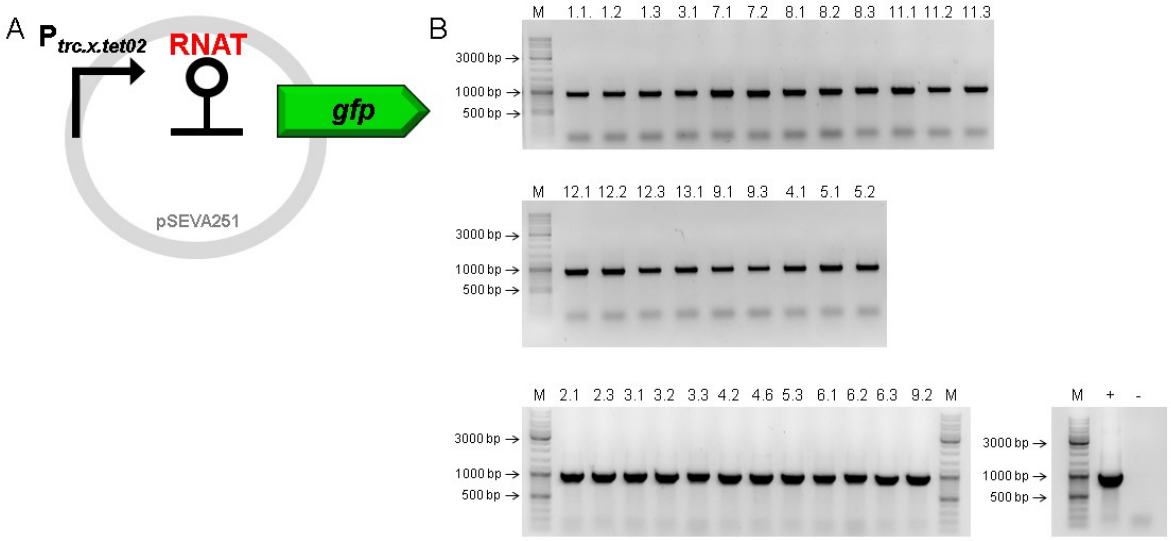


**Figure 4.** A) Schematic representation of the GFP expression cassette used to test redesigned RNAT for their possible function as thermometers. The sequences, including the *hsp17* RBS 5'-AGGAGU'-3', were inserted in between the promoter $P_{trc.x.tetO2}$ and the *gfp* coding region. B) PCR reactions were performed using TS1-FP and PS2 primes (Table 2). The expected band size is 945 bp. +, positive control (pSEVA251 $P_{trc.x.tetO2}$::B0032::*gfp*); -, negative control (no template); M, molecular marker GeneRuler DNA Ladder Mix (Thermo Scientific™).

### 3.3. Temperature responsiveness of synthetic RNATs

The *Synechocystis* cells harboring the synthetic constructs were tested for temperature responsiveness of GFP expression to assess the functionality of the designed RNA thermometers. For this purpose, GFP expression upon temperature shift was determined by measuring the fluorescence of the *Synechocystis* cultures bearing RNATs and normalizing to cell density. To establish the methodology for the library testing, a few RNAT were tested using different $OD_{730}$ of the cultures following the temperature shift from 30 to 37 °C during 24 h. The results showed no difference in testing $OD_{730}$ 0.5 or 1.0 (Fig. 5), so all further testing of the TS library was done using cultures at $OD_{730}$ 1.0. Taking into account the time needed for GFP maturation (Neupert et al., 2008), more observable changes of the GFP fluorescence were noticed 4 h and 24 h upon induction, therefore we excluded measurements done at 1 h and 2 h timepoints from further analysis.

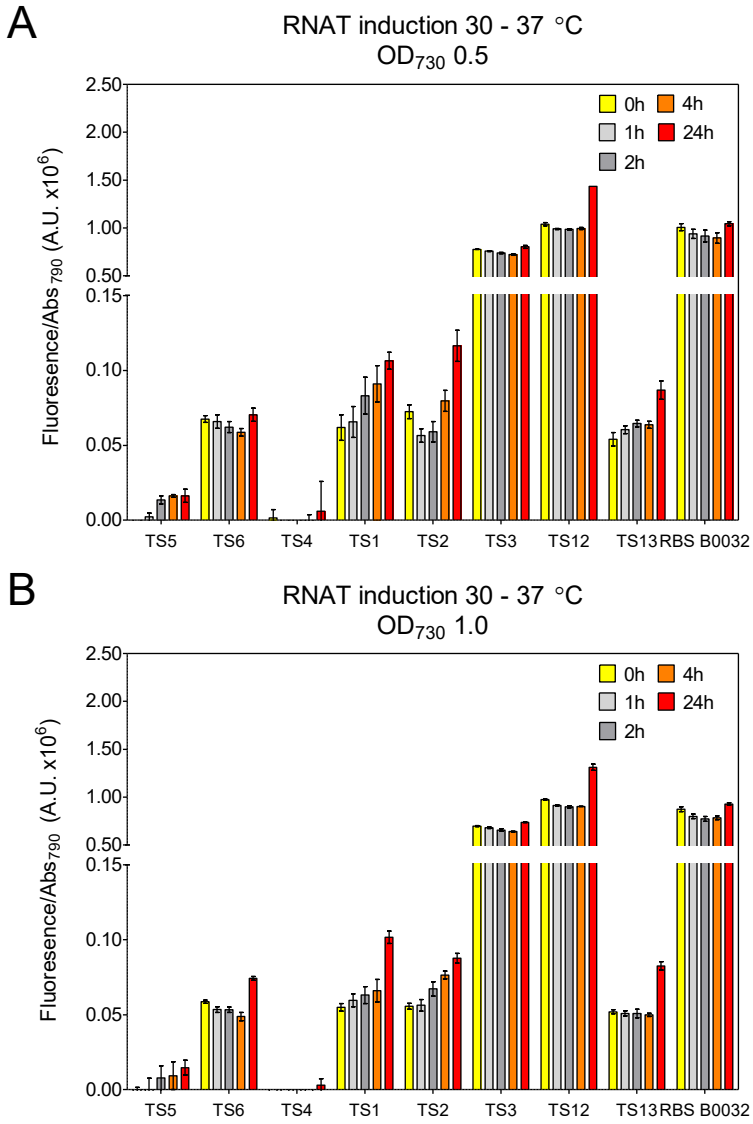


**Figure 5.** Characterization of RNA thermometers response in *Synechocystis* regarding $OD_{730}$ tested using A) cultures of $OD_{730}$ 0.5 and B) cultures of $OD_{730}$ 1.0. The bars represent normalized GFP fluorescence of *Synechocystis* cells harboring the corresponding RNAT sequence. GFP fluorescence was measured before (0h) and after the temperature shift from 30 to 37 °C (1 h, 2 h, 4 h and 24 h). The fluorescence of the control strain harboring the pSEVA251 was subtracted from each sample. Error bars correspond to standard deviations from a single experiment with technical triplicates (measured in duplicate). $P_{trc.x.tetO2}$::B0032::*gfp* was included for comparison purposes.

Further on, the complete RNAT library was tested for a temperature shift from 30 to 37 °C. The results showed the control strain harboring $P_{trc.x.tetO2}$::B0032::*gfp* displayed steady GFP fluorescence regardless of the temperature shift (Fig. 6). This indicates that if the difference in GFP fluorescence occurs, it is plausible to be a result of different RNA elements present

within 5'-UTR. The constructs harboring structures of potentially low melting stability, as previously calculated, such as TS11 and TS3, showed high GFP fluorescence even at 30 ºC and the shift to 37 °C did not lead to a further increase in fluorescence. The results suggest these regulatory parts are already in melted or 'open' conformation, therefore no changes in translational control upon induction occur (Fig. 6). By analyzing the predicted structures, it is noticeable that the sequence of TS11 results in a secondary structure possessing an ample loop, which could contribute to low melting stability. Previously it has been described that the stability of the hairpin structure decreases with increasing the loop size (Groebe and Uhlenbeck, 1988). The structures with the highest predicted stability, such as TS9 and TS5, showed almost no GFP fluorescence at the initial temperature of 30 ºC, and upon temperature shift resulted in relatively low fluorescence. These results suggest these RNA elements might have too stable secondary structures to be efficiently melted under the temperatures tested. However, TS9 and TS5 offer revenue for further development as tools for very tight induction, in the case of the low amount of protein is needed. Tight regulation of gene expression is important in many biotechnological processes, in particular when synthesizing toxic products. Clear inducibility was observed for TS1 and TS2 elements with up to 1.9 and 1.6-fold change in GFP fluorescence upon temperature shift, respectively (Fig. 6). It is interesting to notice that TS1 and TS7 are differing only in three nucleotides, however demonstrate strikingly 6.7-fold different initial GFP fluorescence; while TS1 displays inducibility, TS7 doesn't respond to temperature shift with different GFP fluorescence. Previous studies show single point mutations can remarkably change the responsiveness of the RNA elements (Waldminghaus et al., 2008, Kortmann et al., 2011, Sen et al., 2017). It was demonstrated that the combination of only two-point mutations turned the synthetic translation-incompetent structure into an efficient thermometer (Waldminghaus et al., 2008). Previous studies also showed only a few changes in the nucleotide composition in natural RNA thermometers led to considerable changes, where deletion of a single nucleotide resulted in a SD sequence remaining base-paired even at high temperatures (Chowdhury et al., 2003, Chowdhury et al., 2006). It was also demonstrated that single-point mutations can lead to derepression at low temperatures as described for the *rpoH* thermometer of *E. coli* (Morita et al., 1999) and *prfA* thermometer of *Listeria monocytogenes* (Johansson et al., 2002). The presence of different structures such as bulge (unpaired nucleotide in the stem) can also lead to less stability (Hoynes-O'Connor et al., 2015). The presence of a bulge could account for a 7.7-fold difference in the initial GFP fluorescence between TS8 and TS6. As expected, the sequences significantly contribute to the RNAT performance: although TS1 and TS4 display the same predicted secondary

structures (Fig. 3), the initial GFP fluorescence is strikingly different, with TS4 exhibiting no GFP fluorescence at all. TS12 based on the native *hsp17* RNA element showed the highest GFP fluorescence already at the initial temperature and a small change in the GFP fluorescence upon temperature shift. These results indicate that the RNA element is probably in an open structure and no regulation can occur under the conditions tested. However, in previous studies, this RNA element displayed a 6-fold increase in the *E. coli* reporter system based on β-galactosidase activity, upon shifting from 28 to 42 ºC (Kortmann et al., 2011b). This underlines further design of experimental set-ups is needed to unlock the responsiveness of the RNA elements. One of the approaches can be opting for a weaker promoter to allow more distinguishable fold changes. TS12 and TS13, having four different nucleotides between SD sequence and the translational start codon of *gfp* showed a 33-fold difference at the initial GFP fluorescence, giving significance to these several base pairs that can highly affect the response of RNA thermometers. While analyzing the putative RNA structures of TS12 and TS13, the striking difference is the presence of a loop after the SD sequence in TS12, however not present in TS13 (Fig. 3). This loop seems to be an important secondary structure, as a previous study suggested that introducing a G–C pair instead of the internal loop resulted in complete loss of reporter activity at both low and high temperatures (Kortmann et al., 2011). Mutations in stem-loop containing the SD by weakening the structures were shown to lead to leaky expression at lower temperatures (Johansson et al., 2002).

It should be noted that, although there is some correlation between the theoretically calculated stabilities of RNA secondary structures and their performance as RNA thermometers, this correlation is not strict, especially regarding TS8 that displayed higher GFP fluorescence in comparison to the constructs harboring TS with similar predicted free energy. However, it should be taken into account that *in silico* tools developed for analysis are usually based on genetic elements from established heterotrophic hosts for molecular biology, such as *E. coli* and could result in different predictions for elements intended for characterization in *Synechocystis*.

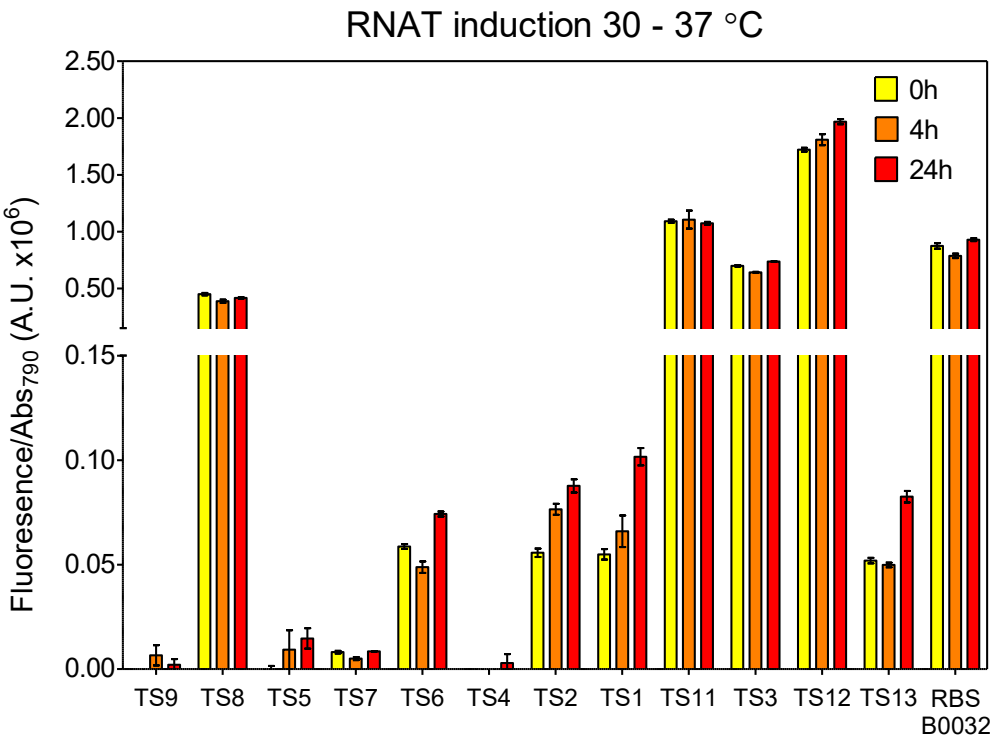


**Figure 6.** Characterization of RNA thermometers response in *Synechocystis*. The bars represent normalized GFP fluorescence of *Synechocystis* cells harboring the corresponding RNAT. GFP fluorescence was measured before (0 h) and after the temperature shift from 30 to 37 °C (4 h and 24 h). The fluorescence of the control strain harboring the empty pSEVA251 was subtracted from each sample. Error bars correspond to standard deviations from a single experiment with technical triplicates (measured in duplicate). $P_{trc.x.tetO2}$:: B0032::*gfp* was included for comparison purposes.

Interestingly, when the experiment was performed maintaining the cells in dark upon induction at 37 °C, the GFP fluorescence slightly decreased over time (Fig. 7). This experiment would need to be repeated to confirm the reproducibility of these data. However, one of the explanations could be the difference in the rates of transcription and/or translation in light and dark, where cells usually have slower rates during dark conditions, due to less energy available. Additionally, there could be intrinsic regulation of ribosome activities and/or RNA degradation under dark conditions.

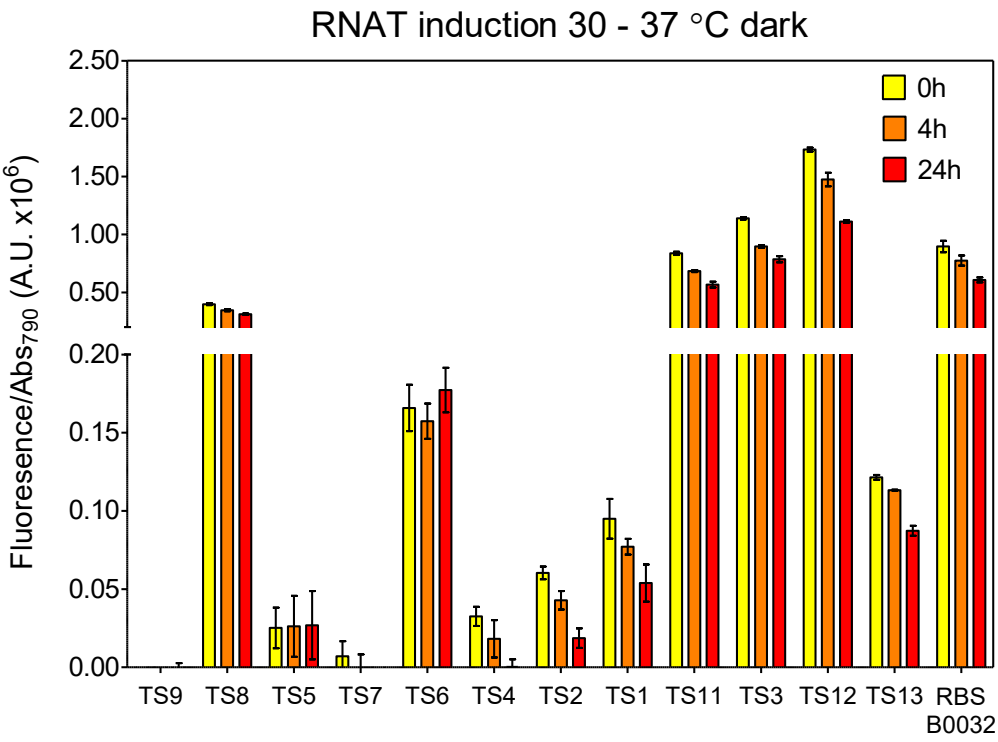


**Figure 7.** Characterization of RNA thermometers response in *Synechocystis* maintained in dark. The bars represent normalized GFP fluorescence of *Synechocystis* cells harboring the RNAT. GFP fluorescence was measured before (0 h) and after the temperature shift from 30 to 37 °C (4 h and 24 h) maintaining the cells in dark. The fluorescence of the control strain harboring the empty pSEVA251 was subtracted from each sample. Error bars correspond to standard deviations from a single experiment with technical triplicates (measured in duplicate). $P_{trc.x.tetO2}$:: B0032::*gfp* was included for comparison purposes.

Previous studies suggested more intense responsiveness can be noticed by having a wider range of temperature shifts (Neupert et al., 2008). Therefore, to further characterize the RNAT, the library was tested following a temperature shift from 25 to 37 °C (Fig. 8). It was expected that lower initial temperature would lead to more 'closed' structures resulting in lower initial GFP fluorescence and more extensive response upon induction. However, lower initial temperature led to higher initial GFP fluorescence in almost all tested RNA thermometers. Only the control $P_{trc.x.tetO2}$::B0032::*gfp* had relatively lower initial GFP fluorescence compared to the previous experimental set-up. The control displayed still stable fluorescence regardless of the temperature shift. However, these experiments will need to be repeated to include biological replicates, for proper interpretation.

The TS13 and TS6 displayed the highest responsiveness with 2.8 and 1.84-fold change, respectively (Fig. 8). This is higher than observed under previously tested conditions.

However, TS1 and TS2 that showed clear inducibility under the previously tested temperature shift, now had slightly less fold change with 1.25 and 1.32, respectively. Although TS12 had high initial GFP fluorescence, under wider temperature shift displayed a 1.5-fold increase in GFP fluorescence upon shifting from 25 to 30 ºC. This indicates this approach could be interesting to broaden up the responsiveness of the regulatory RNA elements.

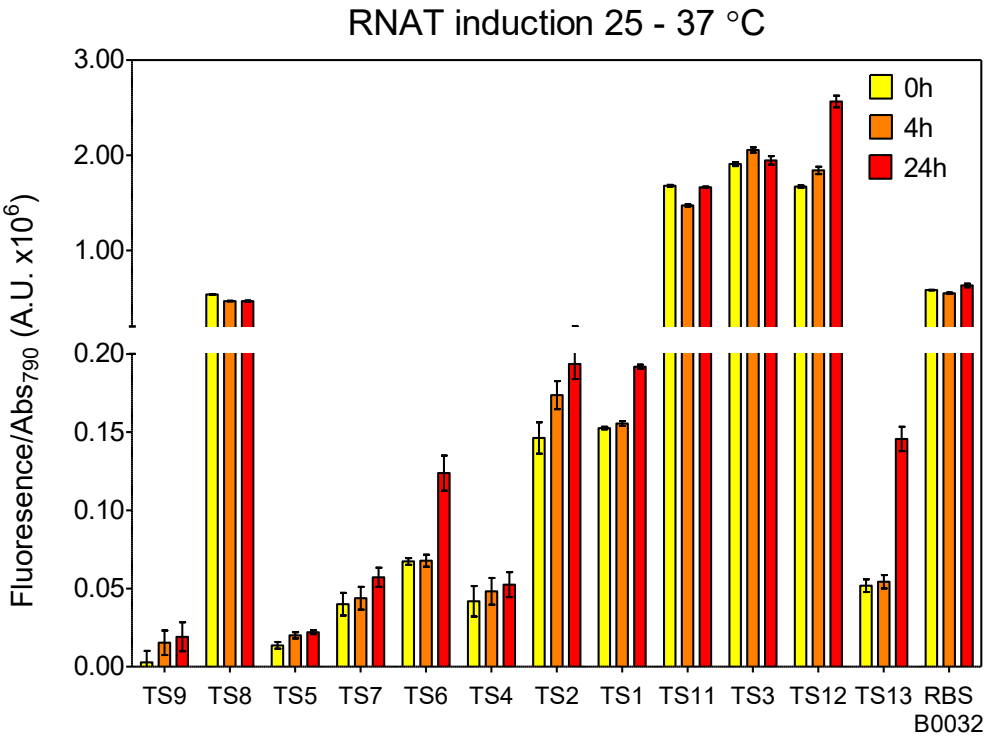


**Figure 15.** Characterization of RNA thermometers response in *Synechocystis*. The bars represent normalized GFP fluorescence of *Synechocystis* cells harboring the RNAT. GFP fluorescence was measured before (0 h) and after the temperature shift from 25 to 37 °C (4 h and 24 h). The fluorescence of the control strain harboring the pSEVA251 was subtracted from each sample. Error bars correspond to standard deviations from a single experiment with technical triplicates (measured in duplicate). $P_{trc.x.tetO2}$:: B0032::*gfp* was included for comparison purposes.

Further on, if the designed RNA thermometers indeed function by the proposed temperature-dependent melting mechanism, they should function even more efficiently at temperatures higher than 37 ºC. Therefore, we tested the library for a temperature shift from 25 to 40 °C. For this experiment, some cultures (TS1, TS13 and $P_{trc.x.tetO2}$::B0032::*gfp*) had to be excluded from the testing, due to technical issues. Under these tested conditions, TS12, TS2 and TS4 displayed the highest responsiveness with 1.6, 1.6 and 1.5-fold differences in GFP fluorescence upon temperature shift, respectively (Fig. 9).

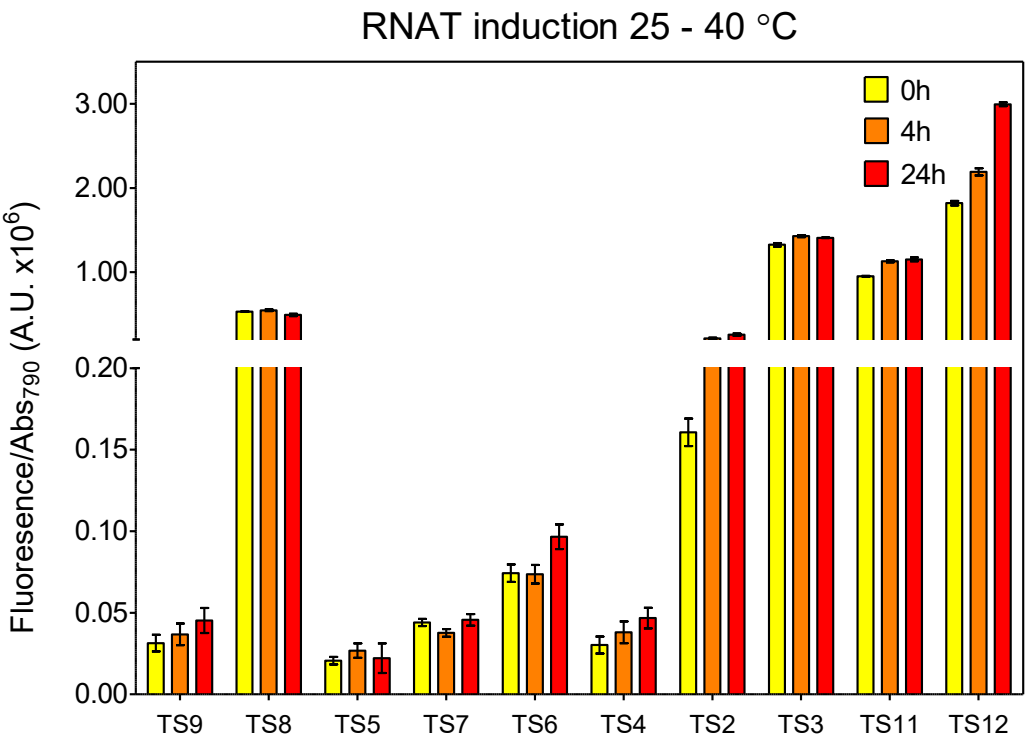


**Figure 16.** Characterization of RNA thermometers response in *Synechocystis*. The bars represent normalized GFP fluorescence of *Synechocystis* cells harboring the RNAT. GFP fluorescence was measured before (0 h) and after the temperature shift from 25 to 40 ° (4 h and 24 h). The fluorescence of the control strain harboring the pSEVA251 was subtracted from each sample. Error bars correspond to standard deviations from a single experiment with technical triplicates (measured in duplicate).

### 3.4. Assessment of computational analysis and experimental data

Finally, we assessed the correlation between experimental measurements and the predicted free energies. Therefore, we compared the fold change during the temperature shift from 25 to 37 ºC with the differences in the calculated minimum free energy of the structures at these temperatures. If there was a correlation, we would expect a linear trend where having a higher difference would result in a higher fold change. However, this is not observed (Fig. 10). The possible discrepancy observed could be a result of assumptions during computational analysis, where we selected only one of the predicted free energy of several possible, and parameter values that may not correspond to the cellular conditions. Although the correlation is too low, there seems to be a trend between the responsiveness of the RNA element and the difference in the predicted free energy (Fig. 10).

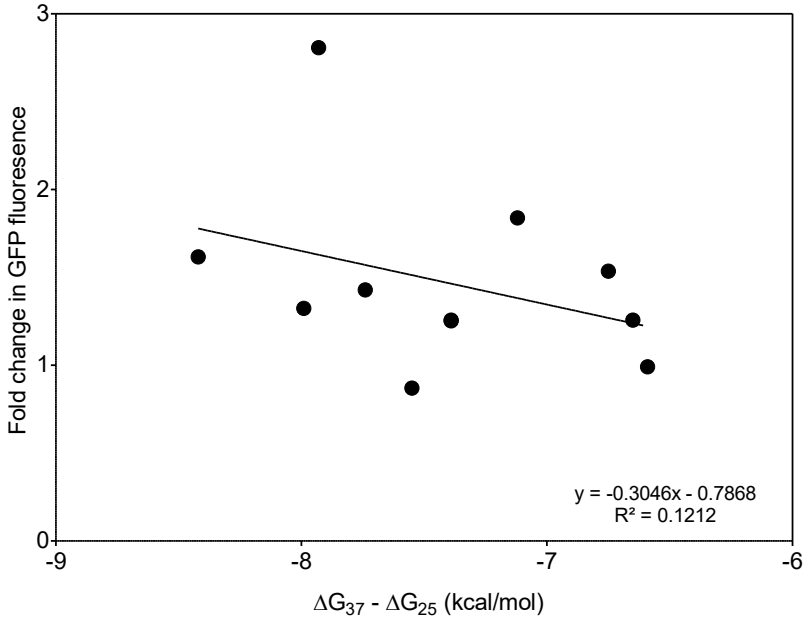


**Figure 10.** Assessment of the correlation between experimental measurements and computational analysis. The plot represents the fold change of the GFP fluorescence during the temperature shift from 25 to 37 ºC and the difference in the predicted free energy of the elements under these temperatures. TS9 was excluded from the analysis, as it was an outliner. The prediction was done using the Quikfold program (Markham and Zuker, 2005, Markham and Zuker, 2008).

Altogether, these preliminary results show the feasibility of utilizing redesigned RNA thermometers as the regulatory elements in the model cyanobacterium *Synechocystis*. The previous study focused on developing a toolbox of RNA thermometers reported up to a 3-fold range reported for a set of synthetic RNA thermometers in *E.coli* (Sen et al., 2017). Additional experiments are required to validate these data and further characterize the response of the RNA thermometers. Specifically, further experiments are needed to demonstrate the changes in expression levels at different temperatures were due to translational control rather than to different transcript levels. Therefore, Northern blot analysis and/or RT-qPCR experiments should be performed to elucidate the level of transcription.

## 4. Conclusions

Here we report the first study with a focus on redesigning and characterizing RNA thermometers as regulatory elements in cyanobacteria. We designed 11 synthetic RNAT based on the native *hsp17* thermometer, previously described in *Synechocystis*. We successfully established a methodology for testing an RNAT library and evaluated the RNA

thermometer's response to different temperature changes. A library of 12 RNAT was tested under three different temperature shifts, displaying a diverse set of temperature profiles. Functional control of translation up to approximately 3 and 2-fold change under temperature shifts from 25 to 37 ºC and 30 to 37 ºC was achieved, respectively, for the TS13 and T1 RNA elements. Interestingly, even a couple of base changes in the sequence of an RNA thermometer led to a substantial change in the temperature response. Therefore, elements showing good inducibility offer revenue toward higher responsiveness by further redesigning focused on different single nucleotide changes. Using various computational tools, such as developed software RNAiFold2T(Garcia-Martin et al., 2016), support the rational design of RNA elements. This together with systematic mutational analysis of these simple RNA elements will offer plenty of possible elements to be tested. Good high-throughput methodologies are needed to facilitate these analyses. However, those available for cyanobacteria fall behind those developed for other model organisms currently used in synthetic biology, offering space for parallel development.

It would be also interesting to test the most promising candidates with a different reporter expression system or an enzyme, to demonstrate the versatility of these tools. Finally, these preliminary results offer insights regarding design choices and optimization protocol that will be valuable in the implementation of these, or similar, RNA thermometers in future work, with wide potential applicability in synthetic biology of cyanobacteria.

## 5. References

Chowdhury, S., Maris, C., Allain, F. H. T. and Narberhaus, F. (2006) 'Molecular basis for temperature sensing by an RNA thermometer', *The EMBO Journal,* 25(11), pp. 2487-2497.

Chowdhury, S., Ragaz, C., Kreuger, E. and Narberhaus, F. (2003) 'Temperature-controlled structural alterations of an RNA thermometer', *Journal of Biological Chemistry,* 278(48), pp. 47915-47921.

Dykstra, P. B., Kaplan, M. and Smolke, C. D. (2022) 'Engineering synthetic RNA devices for cell control', *Nature Reviews Genetics*, *23*(4), pp.215-228.

Endy, D. (2005) 'Foundations for engineering biology', *Nature,* 438(7067), pp. 449-453.

Ferreira, E. A., Pacheco, C. C., Pinto, F., Pereira, J., Lamosa, P., Oliveira, P., Kirov, B., Jaramillo, A. and Tamagnini, P. (2018) 'Expanding the toolbox for Synechocystis sp. PCC 6803: validation of replicative vectors and characterization of a novel set of promoters', *Synthetic Biology,* 3(1), pp. ysy014.

Garcia-Martin, J. A., Dotu, I., Fernandez-Chamorro, J., Lozano, G., Ramajo, J., Martinez-Salas, E. and Clote, P. (2016) 'RNAiFold2T: constraint programming design of thermo-IRES switches', *Bioinformatics,* 32(12), pp. i360-i368.

Giuliodori, A. M., Di Pietro, F., Marzi, S., Masquida, B., Wagner, R., Romby, P., Gualerzi, C. O. and Pon, C. L. (2010) 'The cspA mRNA is a thermosensor that modulates translation of the cold-shock protein CspA', *Molecular Cell,* 37(1), pp. 21-33.

Groebe, D. R. and Uhlenbeck, O. C. (1988) 'Characterization of RNA hairpin loop stability', *Nucleic Acids Research,* 16(24), pp. 11725-11735.

Hoynes-O'Connor, A., Hinman, K., Kirchner, L. and Moon, T. S. (2015) 'De novo design of heat-repressible RNA thermosensors in E. coli', *Nucleic Acids Research,* 43(12), pp. 6166-6179.

Huang, H.-H., Camsund, D., Lindblad, P. and Heidorn, T. (2010) 'Design and characterization of molecular tools for a synthetic biology approach towards developing cyanobacterial biotechnology', *Nucleic Acids Research,* 38(8), pp. 2577-2593.

Hudson, E. P. (2021) 'Synthetic Biology in Cyanobacteria and Applications for Biotechnology', *Cyanobacteria Biotechnology*, pp. 123-170.

Johansson, J., Mandin, P., Renzoni, A., Chiaruttini, C., Springer, M. and Cossart, P. (2002) 'An RNA thermosensor controls expression of virulence genes in Listeria monocytogenes', *Cell,* 110(5), pp. 551-561.

Klähn, S., Bolay, P., Wright, P. R., Atilho, R. M., Brewer, K. I., Hagemann, M., Breaker, R. R. and Hess, W. R. (2018) 'A glutamine riboswitch is a key element for the regulation of glutamine synthetase in cyanobacteria', *Nucleic Acids Research,* 46(19), pp. 10082-10094.

Kortmann, J. and Narberhaus, F. (2012) 'Bacterial RNA thermometers: molecular zippers and switches', *Nature Reviews Microbiology,* 10(4), pp. 255-265.

Kortmann, J., Sczodrok, S., Rinnenthal, J., Schwalbe, H. and Narberhaus, F. (2011) 'Translation on demand by a simple RNA-based thermosensor', *Nucleic acids research,* 39(7), pp. 2855-2868.

Li, C., Wen, A., Shen, B., Lu, J., Huang, Y. and Chang, Y. (2011) 'FastCloning: a highly simplified, purification-free, sequence- and ligation-independent PCR cloning method', *BMC Biotechnology,* 11(1), pp. 92.

Lorenz, R., Bernhart, S. H., Höner zu Siederdissen, C., Tafer, H., Flamm, C., Stadler, P. F. and Hofacker, I. L. (2011) 'ViennaRNA Package 2.0', *Algorithms for Molecular Biology,* 6(1), pp. 1-14.

Ludwig, A., Heimbucher, T., Gregor, W., Czerny, T. and Schmetterer, G. (2008) 'Transformation and gene replacement in the facultatively chemoheterotrophic, unicellular cyanobacterium Synechocystis sp. PCC6714 by electroporation', *Applied Microbiology and Biotechnology,* 78(4), pp. 729-735.

Ma, A. T., Schmidt, C. M. and Golden, J. W. (2014) 'Regulation of gene expression in diverse cyanobacterial species by using theophylline-responsive riboswitches', *Applied and environmental microbiology,* 80(21), pp. 6704-6713.

Markham, N. R. and Zuker, M. (2005) 'DINAMelt web server for nucleic acid melting prediction', *Nucleic Acids Research,* 33(suppl_2), pp. W577-W581.

Markham, N. R. and Zuker, M. (2008) 'UNAFold', *Bioinformatics*: Springer, pp. 3-31.

Morita, M. T., Tanaka, Y., Kodama, T. S., Kyogoku, Y., Yanagi, H. and Yura, T. (1999) 'Translational induction of heat shock transcription factor ς32: evidence for a built-in RNA thermosensor', *Genes & Development,* 13(6), pp. 655-665.

Nakahira, Y., Ogawa, A., Asano, H., Oyama, T. and Tozawa, Y. (2013) 'Theophylline-dependent riboswitch as a novel genetic tool for strict regulation of protein expression in cyanobacterium Synechococcus elongatus PCC 7942', *Plant and Cell Physiology,* 54(10), pp. 1724-1735.

Neupert, J., Karcher, D. and Bock, R. (2008) 'Design of simple synthetic RNA thermometers for temperature-controlled gene expression in Escherichia coli', *Nucleic Acids Research,* 36(19), pp. e124-e124.

Nocker, A., Hausherr, T., Balsiger, S., Krstulovic, N.-P., Hennecke, H. and Narberhaus, F. (2001) 'A mRNA-based thermosensor controls expression of rhizobial heat shock genes', *Nucleic Acids Research,* 29(23), pp. 4800-4807.

Nshogozabahizi, J. C., Aubrey, K. L., Ross, J. A. and Thakor, N. (2019) 'Applications and limitations of regulatory RNA elements in synthetic biology and biotechnology', *Journal of Applied Microbiology,* 127(4), pp. 968-984.

Ohbayashi, R., Akai, H., Yoshikawa, H., Hess, W. R. and Watanabe, S. (2016) 'A tightly inducible riboswitch system in Synechocystis sp. PCC 6803', *The Journal of General and Applied Microbiology*.

Pérez, A. A., Rodionov, D. A. and Bryant, D. A. (2016) 'Identification and regulation of genes for cobalamin transport in the cyanobacterium Synechococcus sp. strain PCC 7002', *Journal of Bacteriology,* 198(19), pp. 2753-2761.

Rinnenthal, J., Klinkert, B., Narberhaus, F. and Schwalbe, H. (2011) 'Modulation of the stability of the Salmonella fourU-type RNA thermometer', *Nucleic Acids Research,* 39(18), pp. 8258-8270.

Russell, D. W. and Sambrook, J. (2001) *Molecular cloning: a laboratory manual.* Cold Spring Harbor Laboratory Cold Spring Harbor, NY.

Sen, S., Apurva, D., Satija, R., Siegal, D. and Murray, R. M. (2017) 'Design of a Toolbox of RNA Thermometers', *ACS Synthetic Biology,* 6(8), pp. 1461-1470.

Sengupta, A., Pakrasi, H. B. and Wangikar, P. P. (2018) 'Recent advances in synthetic biology of cyanobacteria', *Applied Microbiology and Biotechnology,* 102(13), pp. 5457-5471.

Silva-Rocha, R., Martínez-García, E., Calles, B., Chavarría, M., Arce-Rodríguez, A., de Las Heras, A., Paez-Espino, A. D., Durante-Rodríguez, G., Kim, J. and Nikel, P. I. (2013) 'The Standard European Vector Architecture (SEVA): a coherent platform for the analysis and deployment of complex prokaryotic phenotypes', *Nucleic Acids Research,* 41(D1), pp. D666-D675.

Stanier, R., Kunisawa, R., Mandel, M. and Cohen-Bazire, G. (1971) 'Purification and properties of unicellular blue-green algae (order Chroococcales)', *Bacteriological reviews,* 35(2), pp. 171-205.

Waldminghaus, T., Heidrich, N., Brantl, S. and Narberhaus, F. (2007) 'FourU: a novel type of RNA thermometer in Salmonella', *Molecular Microbiology,* 65(2), pp. 413-424.

Waldminghaus, T., Kortmann, J., Gesing, S. and Narberhaus, F. (2008) 'Generation of synthetic RNA-based thermosensors', pp. 1319-1326.

Zuker, M. (2003) 'Mfold web server for nucleic acid folding and hybridization prediction', *Nucleic Acids Research,* 31(13), pp. 3406-3415.

# CHAPTER IV

# Internal illumination to overcome the cell density limitation in the scale-up of whole-cell photobiocatalysis

M. Hobisch, **J. Spasic**, L. Malihan-Yap, G. D. Barone, K. Castiglione, P. Tamagnini, S. Kara, R. Kourist, *ChemSusChem* **2021**, *14*(15), 3219.

ChemSusChem
Full Papers
doi.org/10.1002/cssc.202100832
Chemistry Europe
European Chemical Societies Publishing

# Internal Illumination to Overcome the Cell Density Limitation in the Scale-up of Whole-Cell Photobiocatalysis

Markus Hobisch[+],[a, b] Jelena Spasic[+],[b, c, d] Lenny Malihan-Yap,[b] Giovanni Davide Barone,[b, c, d] Kathrin Castiglione,[e] Paula Tamagnini,[c, d] Selin Kara,*[a] and Robert Kourist*[b]

Cyanobacteria have the capacity to use photosynthesis to fuel their metabolism, which makes them highly promising production systems for the sustainable production of chemicals. Yet, their dependency on visible light limits the cell-density, which is a challenge for the scale-up. Here, it was shown with the example of a light-dependent biotransformation that internal illumination in a bubble column reactor equipped with wireless light emitters (WLEs) could overcome this limitation. Cells of the cyanobacterium *Synechocystis* sp. PCC 6803 expressing the gene of the ene-reductase YqjM were used for the reduction of 2-methylmaleimide to (*R*)-2-methylsuccinimide with high optical purity (>99% *ee*). Compared to external source of light, illumination by floating wireless light emitters allowed a more than two-fold rate increase. Under optimized conditions, product formation rates up to 3.7 mM $h^{-1}$ and specific activities of up to 65.5 U $g_{DCW}^{-1}$ were obtained, allowing the reduction of 40 mM 2-methylmaleimide with 650 mg isolated enantiopure product (73% yield). The results demonstrate the principle of internal illumination as a means to overcome the intrinsic cell density limitation of cyanobacterial biotransformations, obtaining high reaction rates in a scalable photobioreactor.

## Introduction

Photobiocatalysis has emerged as a new, exciting research area that combines photocatalysis and biocatalysis, two of the most research-intensive fields of catalysis.[1] In particular, whole-cell biotransformations in cyanobacteria allow to produce highly selective biocatalysts from carbon dioxide and water, and to exploit photosynthesis for the regeneration of adenosine triphosphate (ATP) and redox cofactors.[2] This allows the saving of stoichiometric addition of auxiliary cosubstrates such as isopropanol and glucose for redox biotransformations. As only a minor part of the donor molecule's electrons is used for the redox reaction, the use of catalytic water splitting leads to a more favorable atom economy, one of the 12 principles of green chemistry.[3] Furthermore, the formation of coupled by-products often complicates downstream processing. Using water as a sacrificial electron donor is a radical approach that has the potential to solve this critical limitation of the sustainability of enzymatic redox processes. Coupling of oxidoreductases to the photosynthetic electron transport chain of cyanobacteria has been demonstrated for a wide range of biocatalytic reactions,[1,4] including ene-reductases,[2] alcohol dehydrogenases,[5] Baeyer–Villiger monooxygenases,[6] heme-independent monooxygenases,[7] P450 monooxygenases,[8] and imine reductases[9] with reaction rates as high as 150 units per gram cells.[10] A major environmental advantage of cyanobacterial biotransformation is the sustainable production of the biocatalyst, with light as an energy source and $CO_2$ as a carbon source.[11] From a physiological viewpoint it is important to note that light-driven biotransformations consume electrons from the photosynthetic electron transport chain, but do not require fixation of carbon dioxide. This could be an explanation why cyanobacterial photobiotransformations are much faster than the production of various C-metabolites.[12] For the metabolic engineering of cyanobacterial whole-cell biocatalysts, both the variation of the intracellular enzyme concentration[9] and the deletion of other electron-consuming processes[8b,10] have been proven as successful strategies. While photobiotransformations

[a] *M. Hobisch,[+] Prof. Dr. S. Kara*
*Department of Biological and Chemical Engineering, Biocatalysis and Bioprocessing Group*
*Aarhus University*
*Gustav Wieds Vej 10, 8000 Aarhus (Denmark)*
*E-mail: selin.kara@bce.au.dk*
[b] *M. Hobisch,[+] J. Spasic,[+] Dr. L. Malihan-Yap, G. D. Barone, Prof. Dr. R. Kourist*
*Institute of Molecular Biotechnology*
*Graz University of Technology, NAWI Graz, BioTechMed*
*Petersgasse 14, 8010 Graz (Austria)*
*E-mail: kourist@tugraz.at*
[c] *J. Spasic,[+] G. D. Barone, Prof. Dr. P. Tamagnini*
*i3S – Instituto de Investigação e Inovação em Saúde Universidade do Porto & IBMC – Instituto de Biologia Molecular e Celular*
*R. Alfredo Allen 208, 4200-135 Porto (Portugal)*
[d] *J. Spasic,[+] G. D. Barone, Prof. Dr. P. Tamagnini*
*Departamento de Biologia*
*Faculdade de Ciências, Universidade do Porto*
*Rua do Campo Alegre, Edifício FC4, 4169-007 Porto (Portugal)*
[e] *Prof. Dr. K. Castiglione*
*Institute of Bioprocess Engineering, Department of Chemical and Bioengineering*
*Friedrich-Alexander-Universität Erlangen-Nürnberg*
*Paul-Gordan-Straße 3, 91052 Erlangen (Germany)*
[+] *These authors contributed equally to this work.*

Supporting information for this article is available on the WWW under https://doi.org/10.1002/cssc.202100832

*© 2021 The Authors. ChemSusChem published by Wiley-VCH GmbH. This is an open access article under the terms of the Creative Commons Attribution License, which permits use, distribution and reproduction in any medium, provided the original work is properly cited.*

ChemSusChem
Full Papers
doi.org/10.1002/cssc.202100832
Chemistry Europe
European Chemical Societies Publishing

have been established with high reaction rates, the scale-up of the reaction requires a photobioreactor geometry with very short light penetration pathways. On the one hand, this regards the overall light availability in a reactor, taking into account that the light penetration in water is limited and cells strongly absorb visible light. On the other hand, the reactor should have a continuous light distribution to avoid fluctuation, which has physiological consequences for the cells.[13] Typical photobioreactors are based on flat-panels or tube reactors with low-to-moderate surface/volume ratios (SVR). Reactor concepts with internal illumination can shorten light pathways.[14] Among them is a new concept developed by Buchholz and co-workers, which utilizes freely suspended wireless light emitters (WLEs).[15] These WLEs consist of a single light emitting diode (LED) with a receiving coil encapsulated in a polycarbonate shell powered via induction by emitting coils from outside of the reactor. Among the various concepts mentioned above, this approach shows the highest SVR[16] and provides evenly distributed light within the photobioreactors;[15] this was exploited recently by Duong et al. for the intensification of a photoenzymatic reaction.[17] This concept is especially intriguing as it allows to work with column reactors of a larger diameter than externally illuminated photobioreactors.

As a model system, we chose the light-driven ene-reduction of 2-methylmaleimide (2-MM) catalyzed by an ene-reductase YqjM from *Bacillus subtilis* heterologously expressed in a model cyanobacterium *Synechocystis* sp. PCC 6803 (*Synechocystis* from here). This reaction proceeds with high stereoselectivity and represents a typical stereoselective redox reaction for the synthesis of fine chemicals. The specific activity of 180 μmol per hour and per mg chlorophyll a ($\mu mol\, mg_{chla}^{-1}\, h^{-1}$)[10] consumes a considerable part of the total photo-production of nicotinamide adenine dinucleotide phosphate (NADPH) that has been estimated to be in the range of 530–1070 $\mu mol\, mg_{chla}^{-1}\, h^{-1}$.[18] In this article, we investigate the effect of internal illumination on the initial reaction rate and volumetric yield in the scale-up of a photobiocatalytic asymmetric enzymatic ene-reduction in recombinant cells of *Synechocystis*.

## Results and Discussion

*Synechocystis* $P_{cpcB}$::*yqjM* was cultivated in 200 mL gas washing bottles under continuous light illumination reaching an optical density at 750 nm ($OD_{750}$) of 1–3 (Supporting Information, Figure S3a), harvested and utilized in whole-cell light-driven reduction of 2-MM to (*R*)-2-methylsuccinimide (2-MS) (Figure 1a) with external illumination using LED lamps (200 $\mu E\, m^{-2}\, s^{-1}$). As reported previously,[2,10] the specific activity and the product formation rates showed a strong dependency on the cell density applied (Figure 1). Within the analyzed cell density range (0.48–2.4 $g\, L^{-1}$) at 1 mL scale, the specific activity of the cells dropped notably at cell densities higher than 1.2 $g\, L^{-1}$. Notably, the specific activity at 2.4 $g\, L^{-1}$ was only about half of that at 0.48 $g\, L^{-1}$ (Figure 1b). The correlation between the initial reaction rate with cell density was observed up to a cell density of 1.8 $g\, L^{-1}$, where a further increase to 2.4 $g\, L^{-1}$ did not improve the rate anymore.

The results in 1 mL scale show a clear decrease of productivity per cell at higher cell density. A larger reaction volume with longer light pathways is expected to increase this effect. Yet, achieving high reaction rates requires higher cell densities. Additionally, it should also be noted that a steady light intensity is important because fluctuating light affects the

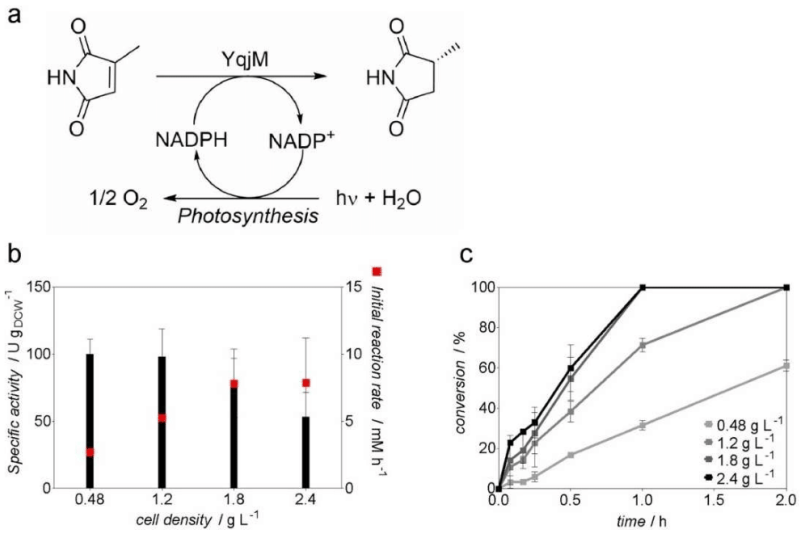


**Figure 1.** (a) Whole-cell light-driven biotransformations catalyzed by *Synechocystis* $P_{cpcB}$::*yqjM*. (b) Specific activity and initial product formation rates achieved at 1 mL scale using various cell densities, independent biological triplicates. (c) Conversion of 2-MM during photobiotransformations (1 mL, 10 mM 2-methylmaleimide, 160 rpm, 30 °C, 200 $\mu E\, m^{-2}\, s^{-1}$), independent biological triplicates.


© 2021 The Authors. ChemSusChem published by Wiley-VCH GmbH

ChemSusChem
Full Papers
doi.org/10.1002/cssc.202100832
Chemistry Europe
European Chemical Societies Publishing

physiology of the cyanobacteria.[19] On basis of these considerations, we reasoned that it would be difficult to achieve a high productivity at cell densities exceeding 1.8 g $L^{-1}$ with external illumination. Internal illumination, however, provides much shorter light pathways and the beneficial effect for photo-biocatalytic reactions has been demonstrated recently.[2] Therefore, a bubble column reactor (BCR) with internal illumination provided by WLEs appeared to be the ideal solution for the intensification and scale-up of cyanobacterial biotransformations (Figure 2).

The effect of the number of WLEs on the photo-biotransformations was initially evaluated. Therefore, 20, 30, or 40 WLEs were used in a 200 mL reaction volume with *Synechocystis* $P_{cpcB}$::*yqjM* at a cell density of 0.48 g $L^{-1}$ and 30 °C and 10 mM 2-methylmaleimide as a substrate. Among the investigated numbers of WLEs, the use of 40 yielded the highest specific activity of 83 U $g_{DCW}^{-1}$, which is well within the range of the rates observed in 1 mL-scale experiments (Figure 3a and Figure 1b). At a cell density of 1.2 g $L^{-1}$, 20 WLEs led to an activity of 35.8 U $g_{DCW}^{-1}$, whereas 40 WLEs allowed to reach an activity of 65.5 U $g_{DCW}^{-1}$ (corresponding to 5.31 U $mg_{Chla}^{-1}$) (Figure 3a). The initial product formation rate for the latter reaction was 3.6 mM $h^{-1}$. Besides the overall availability of the light, its distribution should be as even as possible in the photobioreactor because the cells adapt to fluctuating light with the activation of protection systems such as flavodiiron proteins that constitute an additional electron sink.[13] Figure 2 shows that at a cell density of 0.48 g $L^{-1}$, the light distribution in the bubble column reactor is quite even. At a cell density of 2.4 g $L^{-1}$, however, a considerable light fluctuation is apparent, both visually and by measuring at a specific site at different time points.

Further increasing the cell density to a value of 2.4 g $L^{-1}$ resulted in shortening the reaction time, which allowed to achieve a full conversion after 3.5 h with an initial activity of 32.5 U $g_{DCW}^{-1}$ (2.74 U $mg_{Chla}^{-1}$) and an initial reaction rate of 3.7 mM $h^{-1}$ (Figure 3a). At a cell density of 2.4 g $L^{-1}$, the strong effect of the light absorption of the cells could be clearly seen as light intensity inside the BCR dropped by 53% (Figure 2). Increasing the cell density from 0.48 to 2.4 g $L^{-1}$ resulted in a 61% decrease of the specific activity. This activity drop is stronger than the one observed in the externally illuminated 1 mL scale. Nevertheless, using internal illumination allowed to retain 80% of activity at a cell density of 0.48 g $L^{-1}$, 64% at 1.2 g $L^{-1}$, and 58% at 2.4 g $L^{-1}$ compared to the 1 mL scale reactions. Using cells at a density of 2.4 g $L^{-1}$ resulted in the highest initial reaction rate of 3.7 mM $h^{-1}$, corresponding to 47% of the initial product formation rate from 1 mL scale. Keeping the reaction time short is not only important for cost-effectiveness, but also needed for selectivity towards the target product as the cells can also unproductively consume the substrate 2-MM (Supporting Information, Figure S6). Doubling the cell concentration and the number of WLEs increased the reaction rate almost two-fold, as 1.2 g $L^{-1}$ of cells with 20 WLEs resulted in 1.2 mM $h^{-1}$ while 2.4 g $L^{-1}$ and 40 WLEs resulted in 2.3 mM $h^{-1}$.

Comparison of internal illumination using WLEs with external illumination and biotransformations without illumina-

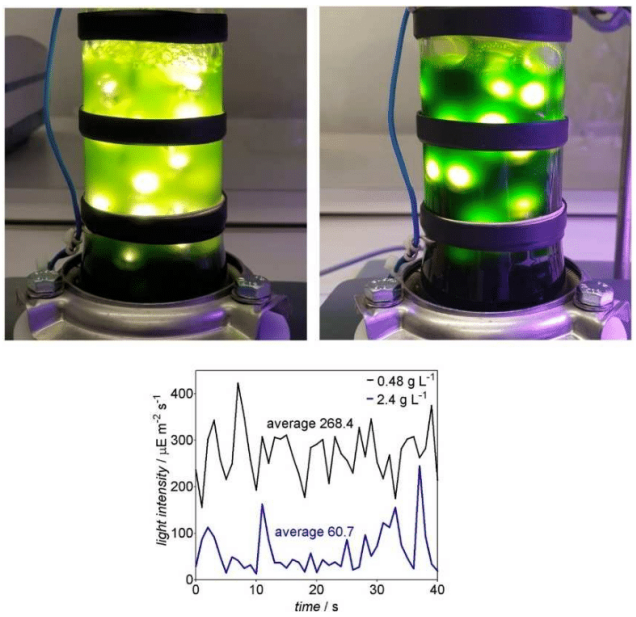


**Figure 2.** Top: Photo-biotransformations performed in the BCR with internal illumination provided by 40 floating wireless light emitters at a cell density of 0.48 g $L^{-1}$ (left side) and 2.4 g $L^{-1}$ (right side). Bottom: determination of the light intensity inside BCR with internal illumination by 40 WLEs at a cell density of 0.48 or 2.4 g $L^{-1}$, respectively.


© 2021 The Authors. ChemSusChem published by Wiley-VCH GmbH

ChemSusChem
Full Papers
doi.org/10.1002/cssc.202100832
Chemistry Europe
European Chemical Societies Publishing

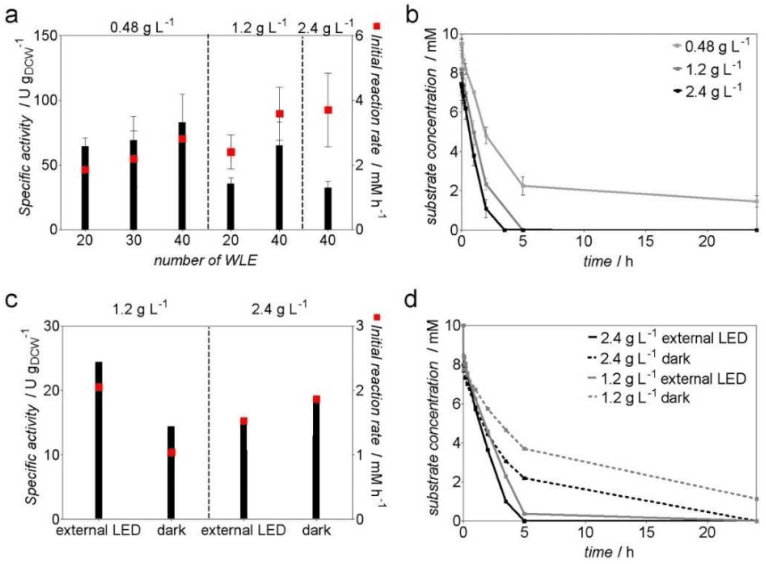


**Figure 3.** Whole-cell biotransformation catalyzed by *Synechocystis* $P_{cpcB}$::*yqjM* in a BCR. (a) Specific activity and initial product formation rate of *Synechocystis* $P_{cpcB}$::*yqjM* in a BCR with internal illumination provided by WLEs (200 mL, 10 mM 2MM, 0.6 L $min^{-1}$ airflow), independent biological triplicates. (b) Time course of the reactions using different cell densities with 40 WLEs, independent biological triplicates. (c) Specific activity and initial product formation rate of *Synechocystis* $P_{cpcB}$::*yqjM* in a BCR externally illuminated with LED strips (300 $\mu E\,m^{-2}\,s^{-1}$) or in dark (200 mL, 10 mM 2-MM, 0.6 L $min^{-1}$ airflow), single measurements. (d) Time course of the reactions with external illumination or in dark, single measurements.

tion underlined clearly the beneficial effect of the WLEs on the productivity of the whole-cell biocatalyst. It is known that *Synechocystis* cells have the capacity to achieve some conversion in darkness or in presence of inhibitors of photosynthesis,[2,4g,10] which has been attributed to the utilization of storage compounds that were accumulated during the cultivation phase. During the light cycle, cyanobacteria produce NADPH via photosynthesis. In absence of light, the pentose phosphate pathway is assumed to be the main source of reducing equivalents.[20] It should be noted, however, that the contribution of glycolytic routes in cyanobacteria is far from being understood.[21] For these reasons, we expected some conversion for reactions in darkness or with external illumination. Indeed, external illumination with an intensity of 300 $\mu E\,m^{-2}\,s^{-1}$ provided by LED strips (Supporting Information, Figure S7), resulted in a 75% drop of specific activity for cell density of 1.2 g $L^{-1}$ and 81% for 2.4 g $L^{-1}$.

At 1.2 and 2.4 g $L^{-1}$ of cell density, the specific activity was 2.7 and 3-fold higher, respectively, when using internal illumination with 40 WLEs, clearly showing the advantage of the WLE technology. The specific activities of *Synechocystis* $P_{cpcB}$::*yqjM* at a cell density of 2.4 g $L^{-1}$ externally illuminated were surprisingly similar to the reaction in darkness, although the dark reaction slows down over time (Figure 3d). The light measurements inside BCR using external illumination (2 $\mu E\,m^{-2}\,s^{-1}$, Supporting Information, Figure S1c) show that cells might be facing darkness occurring locally or temporarily, which is a typical problem of large-scale photobioreactors.[16] Nevertheless, the comparison of the internal and external illumination clearly shows the advantage of the former for photobiotransformations at higher cell densities.

We have shown previously that a higher cellular enzyme concentration leads to improved reaction rates.[9,10] Therefore, we use the light-inducible promoter $P_{psbA2}$ for the expression of the enzyme. For induction, we cultivated the cells at a light intensity of 230 $\mu E\,m^{-2}\,s^{-1}$, which is sufficient for an induction of this promoter. The results of the biotransformation with *Synechocystis* $P_{psbA2}$::*yqjM* indicated a slight improvement in the initial specific activity of 38 U $g_{DCW}^{-1}$ compared to 32.5 U $g_{DCW}^{-1}$ obtained with *Synechocystis* $P_{cpcB}$::*yqjM*, with 4.1 mM $h^{-1}$ product formation rate (Figure 4b). In order to achieve fast full conversion, a reaction was run with *Synechocystis* $P_{cpcB}$::*yqjM* at a cell density of 2.4 g $L^{-1}$ and 40 WLEs using 10 mM 2-MM as substrate (Figure 4c). The product was isolated after 5 h of the reaction. After cell removal and extraction with ethyl acetate, NMR analysis showed an isolated yield of 157.4 mg pure product (71% yield) (*R*)-2-methylsuccinimide (2-MS) in outstanding optical purity [99% enantiomeric excess (*ee*)].

It should be noted that the product could be obtained in very high purity without the need for purification by flash chromatography, which simplifies the downstream processing and cuts the costs (Supporting Information, Figures S4 and S5).

Further intensifying the process by the addition of 40 mM 2-MM by substrate feeding approach resulted in full conversion in 22 h (Figure 4d), producing 650 mg pure (*R*)-2-methylsuccinimide (73% yield) with >99% *ee*.


© 2021 The Authors. ChemSusChem published by Wiley-VCH GmbH

ChemSusChem
Full Papers
doi.org/10.1002/cssc.202100832
Chemistry Europe
European Chemical Societies Publishing

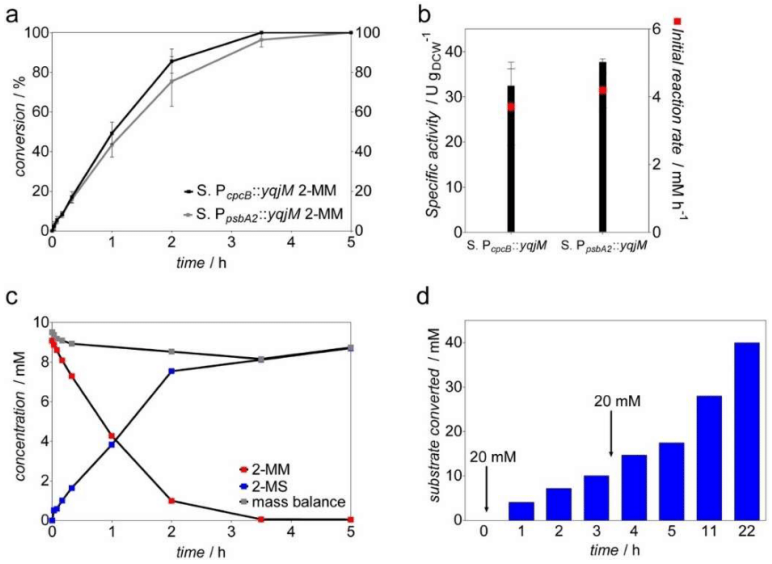


**Figure 4.** (a) Conversion of 10 mM 2-MM into corresponding 2-MS during photobiotransformations catalyzed by *Synechocystis* $P_{cpcB}$::*yqjM* and *Synechocystis* $P_{psbA2}$::*yqjM* both at a cell density of 2.4 g $L^{-1}$. (b) Specific activity and initial product formation rate of *Synechocystis* $P_{cpcB}$::*yqjM* and *Synechocystis* $P_{psbA2}$::*yqjM*. (c) Time course of the preparative 10 mM 2-MM photobiotransformation catalyzed by *Synechocystis* $P_{cpcB}$::*yqjM*, single measurements. (d) 2-MM substrate converted by *Synechocystis* $P_{cpcB}$::*yqjM* cells (2.4 g $L^{-1}$) using a substrate feeding approach, with initial substrate concentration introduced 20 mM and a subsequent feeding of 20 mM at 3 h, single measurements.

Previous light-driven biotransformations scale-up systems using stirred-tank photobioreactors at the cell density of 0.5–0.8[8a] or 1.6 g $L^{-1}$[22] point to the problem of high cell densities to be applied. Photobiotransformations could benefit from the developed technologies for the high cell density cultivation that reached up to 50 g $L^{-1}$, such as thin-layer cascade photobioreactors[23] and CellDeg system cultivations.[24] However, the application of these set-ups in the scale-up of light-driven biocatalysis needs to be followed by the appropriate development of efficient light sources with beneficial light penetration depths, where WLEs and technologies such as light guides (e. g., optical-fibers illumination[25]) can play an important role. The cost of the WLEs itself, their durability, and the efficiency of energy transfer via inductions might be drawbacks of the BCR; nevertheless, our results show that the principle of internal illumination bears clear advantages over external light supply. Future research will focus on the identification of the best way to combine an internal light source with an efficient mixing of the reaction, both in view of efficiency and practicability.

Easier handling and scalability of BCR with higher volume is an advantage of this technology, as these bioreactors can be filled up to higher volume without influencing SVR (while appropriately increasing the number of WLEs). This reactor concept is generally applicable for recently described whole-cell biotransformations,[1,26] keeping in mind that volatile substrates pose a problem. Other reactor concepts, such as capillary biofilm reactors operated at higher cell densities up to 52 g $L^{-1}$, show another promising approach, but one of the bottlenecks for applications are the extreme long times for biofilm maturation (up to 5 weeks).[27] One of the concerns with cultivation set-ups for high cell density is the $CO_2$ supply across the gas-liquid interface, which could be problematic with longer BCR geometries. It should be noted, however, that the biotransformation does not require $CO_2$ itself. Moreover, the presence of the ene-reduction as a strong electron sink might alleviate the need of $CO_2$ fixation from a metabolic point of view.[28] While we indeed did not observe any positive effect of higher $CO_2$ supply or $NaHCO_3$ addition during small-scale biotransformation reactions (unpublished), this idea remains to be proven experimentally. Another problem that might limit the applicable length of the BCR could be the accumulation of oxygen, which could lead to photoinhibition.[29]

## Conclusion

The strong light absorption of cyanobacteria is a main limiting factor for the scale-up of cyanobacterial biotransformations. Here we demonstrate that internal illumination in a bubble column reactor can alleviate this limitation. At a cell density of 2.4 g $L^{-1}$, internal illumination with 40 wireless light emitters in 200 mL reaction volume allowed to obtain a reaction rate of 3.7 mM $h^{-1}$ and a specific activity of 32.5 U $g_{DCW}^{-1}$. An intensified reaction with stepwise feeding of 40 mM ran to completion: Isolation of 650 mg product (73% yield) underlined the practical


© 2021 The Authors. ChemSusChem published by Wiley-VCH GmbH

ChemSusChem
Full Papers
doi.org/10.1002/cssc.202100832
Chemistry Europe
European Chemical Societies Publishing

usefulness of the approach. The fact that purification of the compound was not necessary highlight the practical advantages of cyanobacterial biotransformation. Compared to external source of light, illumination by floating wireless light emitters allowed a more than two-fold rate increase. The results demonstrate the principle of internal illumination as a means to overcome the intrinsic cell density limitation of cyanobacterial biotransformations, obtaining high reaction rates in a scalable photobioreactor.

## Experimental Section

### Chemicals

The substrate 2-methylmaleimide (2-MM) was synthesized as previously described.[2] The product 2-methylsuccinimide (2-MS) was obtained as a white powder from Chiracon GmbH (Luckenwalde, Germany). All other chemicals were purchased from Sigma-Aldrich (Steinheim, Germany) or Carl Roth (Karlsruhe, Germany) unless otherwise indicated.

### Strains

All *Synechocystis* strains utilized are listed in Table S1.

### Cultivation of *Synechocystis* strains

Seed cultures of *Synechocystis* were grown in liquid BG-11 medium (pH 8) supplemented with 50 $\mu g\,mL^{-1}$ kanamycin in 300 mL Erlenmeyer flasks with a working volume of 100 mL. The cultures were maintained in a plant growth chamber (SWGC-1000, WISD lab instruments) fitted with white fluorescent lamps delivering a light intensity of 40–60 $\mu E\,m^{-2}\,s^{-1}$. The cultures were placed on a rotary shaker (140 rpm) under ambient $CO_2$ and 50% humidity and a temperature of 30 °C. Cell growth was monitored by measuring the $OD_{750}$. Upon reaching $OD_{750}=1$–2, the cells were harvested by centrifugation (24 °C, 15 min, 3500 rpm), resuspended in fresh BG-11, and inoculated in gas washing tubes ($V=200$ mL) to $OD_{750}=0.1$. The tubes were maintained in an aquarium regulated at 30 °C and illuminated with six fluorescent lamps delivering a light intensity of 200–250 $\mu E\,m^{-2}\,s^{-1}$ (Supporting Information, Figure S3b). Aeration and mixing of the cultures were ensured by bubbling using an air pump (Boyu S-4000B pump) and filtered through a 0.2 μm filter to ensure the sterility.

### Whole-cell biotransformation

Upon reaching an $OD_{750}=1$–3, cells were harvested by centrifugation (24 °C, 15 min, 3500 rpm). The pellet was resuspended in an appropriate volume of BG-11 to a specific $OD_{750}$ and subsequently utilized in whole-cell biotransformations 10 mM 2-MM with a working volume of 200 mL (stock solution in BG-11). $OD_{750}=10$ corresponded to 2.4 $g\,L^{-1}$ of cell density, as previously determined.[10] Reactions were performed using a bubble column reactor (BCR; $\varphi_i=5$ cm, $h=50$ cm) with a working volume of 200–800 mL fitted with emitting coils. WLEs in varying numbers were suspended in the reactor to provide internal illumination. The WLEs consist of a white LED plus a receiving coil inside a polycarbonate shell (Supporting Information, Figure S2b). Air was supplied by a pump (Boyu S-4000B) at a rate of 0.6 $L\,min^{-1}$. A fan was utilized to provide cooling for reactions to keep the temperature at 30 °C. Reaction temperature was measured four times over the course of 1 h, then again after 3.5 and 20 h, and was found to be stable and did not increase above 30 °C. Large-scale biotransformations with external illumination were performed by wrapping the BCR with LED stripes (BOXXX) (Supporting Information, Figure S7). The light intensity was maintained constant as an internally illuminated reactor.

For small-scale biotransformation, the cells obtained from centrifugation were resuspended in fresh BG-11 to OD750 = 20 and adjusted accordingly. Reactions were performed in 5 mL glass vials with a working volume of 1 mL and initiated with the addition of 10 mM 2-MM (stock solution: 100 mM in BG-11). The vials were placed in a bioreactor maintained at 30 °C (160 rpm) and equipped with LED lamps with an intensity of 200 $\mu E\,m^{-2}\,s^{-1}$. Aliquots (100 μL) of the reaction mixture were taken at several time points (0, 2, 5, 10, and 20 min, 1, 2, 3.5, 5, and 24 h) and immediately frozen in liquid nitrogen. Samples were stored at −20 °C prior to GC analysis. Specific activities were calculated at $<10\%$ substrate conversion.

### GC analysis

The substrate 2-MM and its corresponding product 2-MS were analyzed using a GC equipped with a flame-ionization detector (FID) (GC-2010 Plus, Shimadzu, Japan) outfitted with a ZB-5 column. Samples (100 μL) were extracted with ethyl acetate containing 2 mM *n*-decanol as an internal standard. The organic phase was dried in anhydrous $MgSO_4$ and subsequently analyzed. The *ee* of the obtained product after biotransformation was analyzed using chiral GC-FID (GC-2030, Shimadzu, Japan) equipped with a β-6TBDAc column. Detailed GC procedure is given in Table S2.

### Determination of light intensity

The light intensity was measured using an LI-250A light meter (LICOR Biosciences, Hamburg, Germany) equipped with a spherical micro quantum sensor US-SQS/L (Walz, Effeltrich, Germany). Values were taken as an average (15 s) as well as a plot for 40 s (Supporting Information, Figure S2a).

### Product isolation

After the reaction, the mixture was extracted three times with ethyl acetate (1 : 1.33, *v/v*). The organic layer was dried in anhydrous $MgSO_4$ and evaporated in vacuo. The obtained product was analyzed using chiral GC-FID and $^1H$ and $^{13}C$ NMR spectroscopy.

### Quantification of chlorophyll a content

The amount of chlorophyll a was determined as previously described.[10] A sample of cell culture (100 μL) with a known $OD_{750}$ was pelleted, resuspended in 100 μL $dH_2O$, and 900 μL methanol was added. Samples were briefly vortexed and incubated in darkness for 10 min. The absorption at 665 nm was measured and the amount of chlorophyll a was determined using the extinction coefficient $\varepsilon=78.74\ L\,g^{-1}\,cm^{-1}$.

## Acknowledgements

*This project has received funding from the European Union's Horizon 2020 research and innovation programme under the Marie Skłodowska-Curie grant agreement No 764920 (MSCA-EJD PhotoBioCat) and the FET Open grant agreement 899576 (Futuroleaf).*


© 2021 The Authors. ChemSusChem published by Wiley-VCH GmbH

ChemSusChem
Full Papers
doi.org/10.1002/cssc.202100832
Chemistry Europe
European Chemical Societies Publishing

## *Conflict of Interest*

The authors declare no conflict of interest.

**Keywords:** asymmetric catalysis · biocatalysis · cyanobacteria · ene-reduction · photocatalysis

[1] L. Schmermund, V. Jurkaš, F. F. Özgen, G. D. Barone, H. C. Büchsenschütz, C. K. Winkler, S. Schmidt, R. Kourist, W. Kroutil, *ACS Catal.* **2019**, *9*, 4115–4144.
[2] K. Koninger, A. Gomez Baraibar, C. Mugge, C. E. Paul, F. Hollmann, M. M. Nowaczyk, R. Kourist, *Angew. Chem. Int. Ed.* **2016**, *55*, 5582–5585; *Angew. Chem.* **2016**, *128*, 5672–5675.
[3] P. Anastas, N. Eghbali, *Chem. Soc. Rev.* **2010**, *39*, 301–312.
[4] a) F. Jüttner, R. Hans, *Appl. Microbiol. Biotechnol.* **1986**, *25*, 52–54; b) K. Nakamura, R. Yamanaka, K. Tohi, H. Hamada, *Tetrahedron Lett.* **2000**, *41*, 6799–6802; c) J. Havel, D. Weuster-Botz, *Eng. Life Sci.* **2006**, *6*, 175–179; d) T. Utsukihara, W. Chai, N. Kato, K. Nakamura, C. A. Horiuchi, *J. Mol. Catal. B* **2004**, *31*, 19–24; e) M. Górak, E. Żymańczyk-Duda, *Green Chem.* **2015**, *17*, 4570–4578; f) H. Hamada, Y. Kondo, K. Ishihara, N. Nakajima, H. Hamada, R. Kurihara, T. Hirata, *J. Biosci. Bioeng.* **2003**, *96*, 581–584; g) K. Nakamura, R. Yamanaka, *Tetrahedron: Asymmetry* **2002**, *13*, 2529–2533; h) S. Rasoul-Amini, E. Fotooh-Abadi, Y. Ghasemi, *J. Appl. Phycol.* **2010**, *23*, 975–981; i) K. Shimoda, N. Kubota, H. Hamada, M. Kaji, T. Hirata, *Tetrahedron: Asymmetry* **2004**, *15*, 1677–1679; j) T. Takemura, K. Akiyama, N. Umeno, Y. Tamai, H. Ohta, K. Nakamura, *J. Mol. Catal. B* **2009**, *60*, 93–95; k) R. Yamanaka, K. Nakamura, A. Murakami, *AMB Express* **2011**, *1*, 24; l) R. Yamanaka, K. Nakamura, M. Murakami, A. Murakami, *Tetrahedron Lett.* **2015**, *56*, 1089–1091; m) M. T. Yazdi, H. Arabi, M. A. Faramarzi, Y. Ghasemi, M. Amini, S. Shokravi, F. A. Mohseni, *Phytochemistry* **2004**, *65*, 2205–2209; n) B. Zyszka, M. Aniol, J. Lipok, *Microb. Cell Fact.* **2017**, *16*, 136; o) B. Zyszka-Haberecht, A. Poliwoda, J. Lipok, *Appl. Microbiol. Biotechnol.* **2018**, *102*, 7097–7111.
[5] A. Sengupta, A. V. Sunder, S. V. Sohoni, P. P. Wangikar, *J. Biotechnol.* **2019**, *289*, 1–6.
[6] S. Böhmer, K. Köninger, Á. Gómez-Baraibar, S. Bojarra, C. Mügge, S. Schmidt, M. Nowaczyk, R. Kourist, *Catalysts* **2017**, *7*, 240.
[7] A. Hoschek, B. Bühler, A. Schmid, *Angew. Chem. Int. Ed.* **2017**, *56*, 15146–15149; *Angew. Chem.* **2017**, *129*, 15343–15346.
[8] a) A. Hoschek, J. Toepel, A. Hochkeppel, R. Karande, B. Buhler, A. Schmid, *Biotechnol. J.* **2019**, *14*, 1800724 ; b) A. Berepiki, J. R. Gittins, C. M. Moore, T. S. Bibby, *Synth. Biol.* **2018**, *3*, ysy009.
[9] H. C. Büchsenschütz, V. Vidimce-Risteski, B. Eggbauer, S. Schmidt, C. K. Winkler, J. H. Schrittwieser, W. Kroutil, R. Kourist, *ChemCatChem* **2020**, *12*, 726–730.
[10] L. Assil-Companioni, H. C. Büchsenschütz, D. n. Solymosi, N. G. Dyczmons-Nowaczyk, K. K. Bauer, S. Wallner, P. Macheroux, Y. Allahverdiyeva, M. M. Nowaczyk, R. Kourist, *ACS Catal.* **2020**, *10*, 11864–11877.
[11] C. J. Knoot, J. Ungerer, P. P. Wangikar, H. B. Pakrasi, *J. Biol. Chem.* **2018**, *293*, 5044–5052.
[12] a) Z. Gao, H. Zhao, Z. Li, X. Tan, X. Lu, *Energy Environ. Sci.* **2012**, *5*, 9857–9865; b) S. A. Angermayr, A. D. van der Woude, D. Correddu, A. Vreugdenhil, V. Verrone, K. J. Hellingwerf, *Biotechnol. Biofuels* **2014**, *7*, 99; c) J. E. Chaves, P. Rueda-Romero, H. Kirst, A. Melis, *ACS Synth. Biol.* **2017**, *6*, 2281–2292; d) J. W. Oliver, I. M. Machado, H. Yoneda, S. Atsumi, *Proc. Natl. Acad. Sci. USA* **2013**, *110*, 1249–1254.
[13] Y. Allahverdiyeva, H. Mustila, M. Ermakova, L. Bersanini, P. Richaud, G. Ajlani, N. Battchikova, L. Cournac, E. M. Aro, *Proc. Natl. Acad. Sci. USA* **2013**, *110*, 4111–4116.
[14] a) J. C. Ogbonna, H. Yada, H. Masui, H. Tanaka, *J. Ferment. Bioeng.* **1996**, *82*, 61–67; b) I. S. Suh, S. B. Lee, *J. Appl. Phycol.* **2001**, *13*, 381–388; c) I. S. Suh, S. B. Lee, *Biotechnol. Bioeng.* **2003**, *82*, 180–189.
[15] M. Heining, A. Sutor, S. C. Stute, C. P. Lindenberger, R. Buchholz, *J. Appl. Phycol.* **2014**, *27*, 59–66.
[16] M. Heining, R. Buchholz, *Biotechnol. J.* **2015**, *10*, 1131–1137.
[17] H. T. Duong, Y. Wu, A. Sutor, B. O. Burek, F. Hollmann, J. Z. Bloh, *ChemSusChem* **2021**, *14*, 1053–1056.
[18] J. Kauny, P. Setif, *Biochim. Biophys. Acta* **2014**, *1837*, 792–801.
[19] K. Ogawa, K. Yoshikawa, F. Matsuda, Y. Toya, H. Shimizu, *J. Biosci. Bioeng.* **2018**, *126*, 596–602.
[20] N. Wan, D. M. DeLorenzo, L. He, L. You, C. M. Immethun, G. Wang, E. E. Baidoo, W. Hollinshead, J. D. Keasling, T. S. Moon, *Biotechnol. Bioeng.* **2017**, *114*, 1593–1602.
[21] A. Makowka, L. Nichelmann, D. Schulze, K. Spengler, C. Wittmann, K. Forchhammer, K. Gutekunst, *Mol. Plant Pathol.* **2020**, *13*, 471–482.
[22] A. Hoschek, B. Buhler, A. Schmid, *Biotechnol. Bioeng.* **2019**, *116*, 1887–1900.
[23] A. C. Apel, C. E. Pfaffinger, N. Basedahl, N. Mittwollen, J. Göbel, J. Sauter, T. Brück, D. Weuster-Botz, *Algal Res.* **2017**, *25*, 381–390.
[24] L. Bähr, A. Wüstenberg, R. Ehwald, *J. Appl. Phycol.* **2015**, *28*, 783–793.
[25] C.-Y. Chen, J.-S. Chang, *Process Biochem.* **2006**, *41*, 2041–2049.
[26] L.-E. Meyer, B. E. Eser, S. Kara, *Curr. Opin. Green Sustain. Chem.* **2021**, *31*.
[27] A. Hoschek, I. Heuschkel, A. Schmid, B. Buhler, R. Karande, K. Buhler, *Bioresour. Technol.* **2019**, *282*, 171–178.
[28] a) P. Erdrich, H. Knoop, R. Steuer, S. Klamt, *Microb. Cell Fact.* **2014**, *13*, 128; b) M. Faizi, R. Steuer, *Microb. Cell Fact.* **2019**, *18*, 165.
[29] A. Hoschek, A. Schmid, B. Bühler, *ChemCatChem* **2018**, *10*, 5366–5371.

Manuscript received: April 21, 2021
Revised manuscript received: June 11, 2021
Accepted manuscript online: June 17, 2021
Version of record online: July 6, 2021


© 2021 The Authors. ChemSusChem published by Wiley-VCH GmbH

ChemSusChem

Supporting Information

# Internal Illumination to Overcome the Cell Density Limitation in the Scale-up of Whole-Cell Photobiocatalysis

Markus Hobisch[+], Jelena Spasic[+], Lenny Malihan-Yap, Giovanni Davide Barone, Kathrin Castiglione, Paula Tamagnini, Selin Kara,* and Robert Kourist*© 2021 The Authors. ChemSusChem published by Wiley-VCH GmbH. This is an open access article under the terms of the Creative Commons Attribution License, which permits use, distribution and reproduction in any medium, provided the original work is properly cited.

Contents

**List of Abbreviations** ..... 3

**Supporting Tables and Figures** ..... 4

Table S1. Strains utilized in this work. ..... 4

Table S2. Gas Chromatography Flame Ionization Detector Method ..... 4

Figure S1. Light Intensity Measurements inside BCR ..... 6

Figure S2. a) Schematic illustration of the Bubble Column Reactor ..... 7

Table S3. Average light intensity in BCR ..... 7

Figure S3. a) Cultivation of *Synechocystis* in gas washing tubes in an aquarium ..... 8

Figure S4. $^{1}$H NMR of 2-MS obtained after whole-cell biotransformation ..... 10

Figure S5. $^{13}$C NMR of 2-MS obtained after whole-cell biotransformation ..... 10

Figure S6. Consumption of 2-MM substrate over time by *Synechocystis* sp. PCC 6803 WT ..... 11

Figure S7. External illumination of BCR provided by LED strips ..... 11

Figure S8. Example GC-Chromatogram ..... 12

Figure S9. Emission spectrum of a white WLE. ..... 12

**References** ..... 13

# List of Abbreviations

In alphabetical order

| | |
|---|---|
| **2-MM** | 2-Methylmaleimide |
| **2-MS** | 2-Methylsuccinimide |
| **BCR** | Bubble Column Reactor |
| **chl*a*** | Chlorophyll *a* |
| **DCW** | Dry Cell Weight |
| **GC-FID** | Gas Chromatography Flame Ionization Detector |
| **LED** | Light Emitting Diode |
| **NADPH** | Nicotinamide Adenine Dinucleotide Phosphate |
| **NMR** | Nuclear Magnetic Resonance |
| **$OD_{750}$** | Optical Density at 750 nm |
| **PAM** | Pulse Amplitude Modulation |
| ***Synechocystis*** | *Synechocystis sp.* PCC 6803 |
| **WLE** | Wireless Light Emitters |
| **WT** | Wild Type |

# Supporting Tables and Figures

**Table S1**. Strains utilized in this work.

| Strains | Description | Reference |
|---|---|---|
| *Synechocystis sp.* PCC 6803 WT | Wild type cyanobacterium *Synechocystis sp.* PCC 6803 | [1] |
| *Synechocystis sp.* PCC 6803 $P_{cpcB::}$*yqjM* | Transgenic *Synechocystis sp.* PCC 6803 constructed in WT background harboring the gene *yqjM* from *Bacillus subtilis* under the control of the $P_{cpcB}$ promoter in the genome locus *slr0168* | [2] |
| *Synechocystis sp.* PCC 6803 $P_{psbA2::}$y*qjM* | Transgenic *Synechocystis sp.* PCC 6803 constructed in WT background harboring the gene *yqjM* from *Bacillus subtilis* under the control of the promoter $P_{psbA2}$ in the genome locus *slr0168* | [2] |

**Table S2**. Gas Chromatography Flame Ionization Detector Method.

**Achiral GC-FID** (GC-2010 Plus, Shimadzu, Japan)

| | | |
|---|---|---|
| **Column** | Phase | ZB-5 (5% phenyl, 95% dimethyl polysiloxane) |
| | Dimension | Length = 30 m; Film Thickness = 0.25 µm; Inner Diameter = 0.32 mm |
| | Temperature | 100 °C |
| **FID Detector** | Temperature | 320 °C |
| | Air flowrate | 400 mL $min^{-1}$ |
| | $H_2$ flowrate | 40 mL $min^{-1}$ |
| **Injection port** | Volume | 1.0 µL |
| | Carrier Gas | $N_2$ (1.5 mL $min^{-1}$) |
| | Temperature | 230 °C |
| | Split Ratio | 20 |
| **Temperature** | Program | 1) 80 °C for 1 min; 2) 80-160 °C (50 °C $min^{-1}$); 3) 160-220 (15 °C $min^{-1}$); 4) 220-300 °C (50 °C $min^{-1}$) and 5) 300 °C for 3.8 min |

The percent enantiomeric excess (% *ee*) was determined using Chiral GC-FID as detailed below:

**Chiral GC-FID** (GC-2030 Plus, Shimadzu, Japan)

| | | |
|---|---|---|
| **Column** | Phase | β-6TBDAc (Column ID: 23254-3) |
| | Dimension | Length = 50 m; Film Thickness = 0.25 µm; Inner Diameter = 0.25 mm |
| | Temperature | 180 °C |
| **FID Detector** | Temperature | 250 °C |
| | Air flowrate | 200 mL $min^{-1}$ |
| | $H_2$ flowrate | 32 mL $min^{-1}$ |
| **Injection port** | Volume | 1.0 µL |
| | Carrier Gas | $N_2$ (24 mL $min^{-1}$) |
| | Temperature | 230 |
| | Split Ratio | 100 |
| **Temperature** | Program | 1) 180 °C (2 min); 2) 220 °C (5 °C $min^{-1}$ for 3min) |

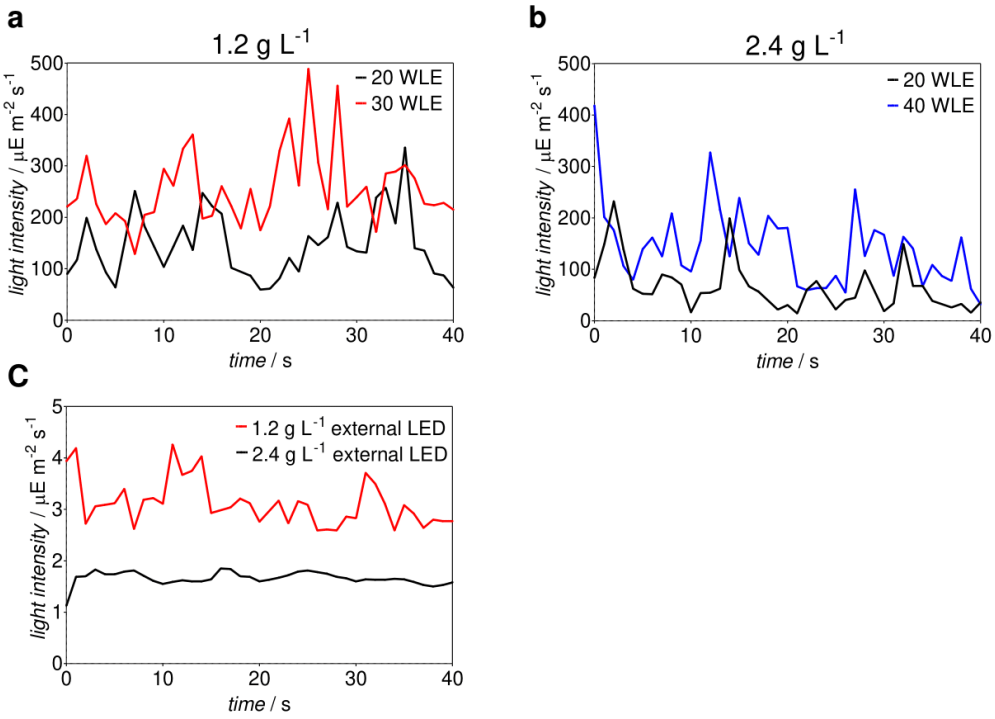


**Figure S1.** Light Intensity Measurements inside BCR with a) internal illumination at cell density 1.2 g $L^{-1}$; b) internal illumination at cell density 2.4 g $L^{-1}$; c) external illumination provided by LED strips.

The light intensity of the cyanobacterial mixture was determined using an LI-250A light meter (LI-COR Biosciences UK Ltd, Cambridge, United Kingdom) with a US-SQS/L light sensor (Waltz, Effeltrich, Germany) submerged at a depth of 5 cm from the surface in the center of the reactor.

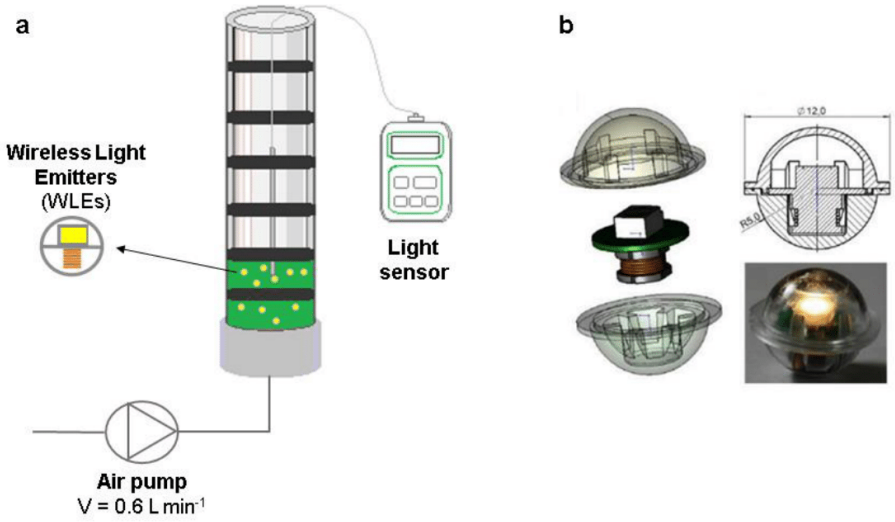


**Figure S2.** a) Schematic illustration of the Bubble Column Reactor with a working volume of 200 mL cyanobacterial mixture, air was delivered using a pump at a flowrate of 0.6 L $min^{-1}$; b) Wireless Light Emitters (WLEs) utilized for internal illumination in the BCR.[3]

**Table S3.** Average light intensity in BCR

| **Conditions** | **Average light intensity [µE $m^{-2}$ $s^{-1}$]** |
|---|---|
| BG11 WLE 40 | 302.3 |
| BG11 external LED stripes | 300.5 |
| 0.48 g $L^{-1}$ WLE 20 | 145.1 |
| 0.48 g $L^{-1}$ WLE 30 | 238.1 |
| 0.48 g $L^{-1}$ WLE 40 | 268.4 |
| 1.2 g $L^{-1}$ WLE 20 | 76.3 |
| 1.2 g $L^{-1}$ WLE 40 | 142.3 |
| 2.4 g $L^{-1}$ WLE 40 | 60.7 |
| 1.2 g $L^{-1}$ external LED stripes | 3.01 |
| 2.4 g $L^{-1}$ external LED stripes | 1.66 |

*Synechocystis* was maintained in an aquarium-type reactor at 30 °C using a heater (Thermo Fisher Scientific, Waltham, USA). Each gas washing tube contains 200 mL of cell culture supplemented with 50 µg $mL^{-1}$ of kanamycin as a selectable marker. The cells were allowed to grow to an $OD_{750}$ of 1-3, harvested, centrifuged (24 °C, 15min, 3500 rpm) and subsequently

utilized in whole-cell light driven biotransformations. The $OD_{750}$ 10 corresponded to 2.4 g $L^{-1}$ of cell density as previously determined.[2] For this cell density, measured chlorophyll a content was in the range of 29-31 µg $mL^{-1}$.

a

b

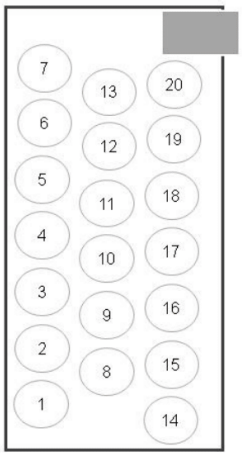


| Slot # | Light Intensity | Slot # | Light Intensity |
|---|---|---|---|
| 1 | 207.8 | 11 | 243.1 |
| 2 | 230.6 | 12 | 232.4 |
| 3 | 249.9 | 13 | 211.9 |
| 4 | 256.1 | 14 | 220.0 |
| 5 | 250.3 | 15 | 222.7 |
| 6 | 239.6 | 16 | 227.0 |
| 7 | 220.4 | 17 | 223.5 |
| 8 | 218.7 | 18 | 220.7 |
| 9 | 232.7 | 19 | 208.8 |
| 10 | 240.0 | 20 | 197.48 |

Light Intensity in µE $m^{-2}$ $s^{-1}$

**Figure S3.** a) Cultivation of *Synechocystis* in gas washing tubes in an aquarium maintained at 30 °C, air was delivered using a pump and passed through 0.2 µm filters; b) Light intensity measurements for each tube (measured in water).

**Synthesis of 2-Methylmaleimide**

2-Methylmaleimide was synthesized as described elsewhere.[4] In a typical reaction, citranoic anhydride (89 mmol) and ammonium acetate (178 mmol) were reacted in acetic acid (40 mL). The mixture was allowed to heat under reflux for 2.5 h. After the reaction, the solvent was partially removed in vacuo. The remaining solution was mixed with 100 mL of saturated NaCl and 40 mL of water. The solution was then extracted with ethyl acetate (8 x 25 mL). The crude product was purified by silica column chromatography using a mobile phase of 5:1 (Cyclohexane: Ethyl acetate) obtaining a white solid product (3.5 g, 35.3% yield).

$^{1}$H NMR (300 MHz, DMSO-*d6*) δ 10.73 (s, br, 1H, NH), δ 6.54-6.56 (m, 1H, =CH-), δ 1.94 ($J_{HH}$=1.5 Hz, d, 3H, $CH_3$,)

$^{13}$C NMR (300 MHz, $CDCl_3$) δ 10.377, δ 128.166, δ 146.129, δ 172.422, δ 173.310

**2-MS Extraction and characterization**

Optically pure (> 99% ee) 2-MS was isolated as a solid powder (157.4 mg, 71% yield). The product was analyzed by $^{1}$H and $^{13}$C NMR.

$^{1}$H NMR (300 MHz, $CDCl_3$) δ 7.86 (s, br, 1H, NH), δ 3.02–2.81 (m, 2H, $-CH_2$-), δ 2.46-2.23 (m, 1H, -CH-), δ 1.41–1.28 (m, 3H, $-CH_3$)

$^{13}$C NMR (300 MHz, $CDCl_3$) δ 17.098, δ 36.768, δ 38.194, δ 176.618, δ 180.920

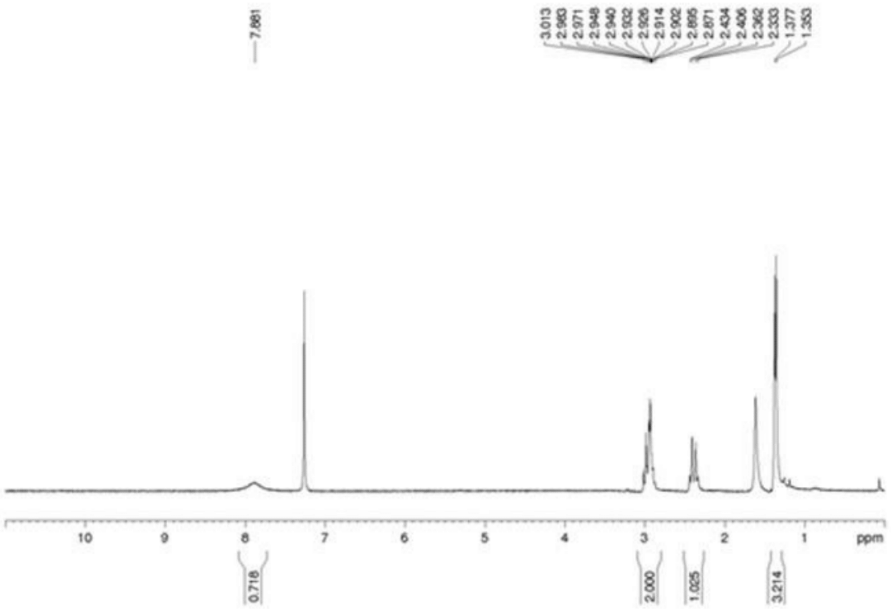


**Figure S4.** [1]H NMR of 2-MS obtained after whole-cell biotransformation.

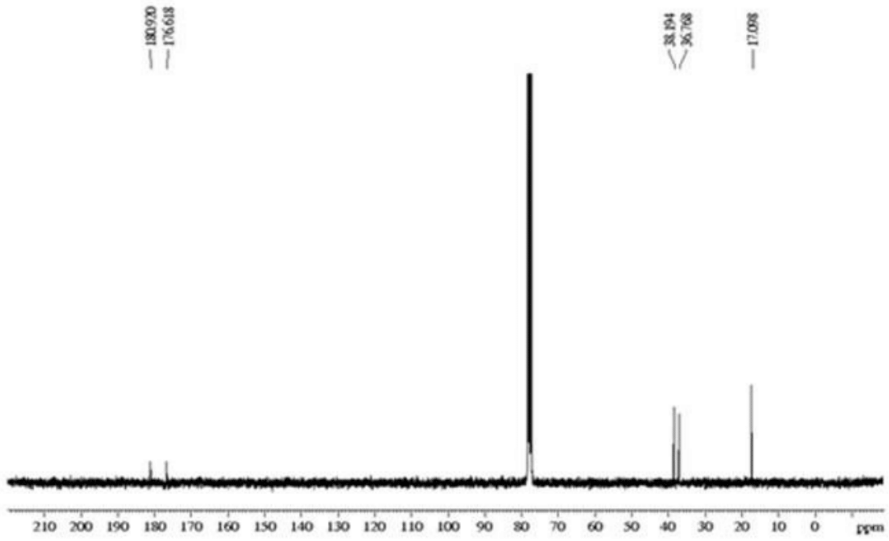


**Figure S5**. [13]C NMR of 2-MS obtained after whole-cell biotransformation.

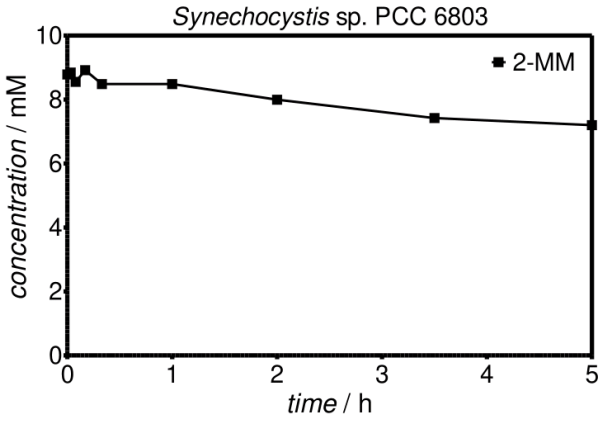


**Figure S6.** Consumption of 2-MM substrate over time by *Synechocystis* sp. PCC 6803 WT (1.2 g $L^{-1}$, 200 mL, 10 mM 2-methylmaleimide, 0.6 L $min^{-1}$ airflow, 40 WLEs).

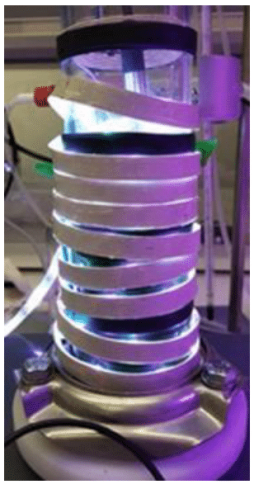

**Figure S7.** External illumination of BCR provided by LED strips (BOXXX)

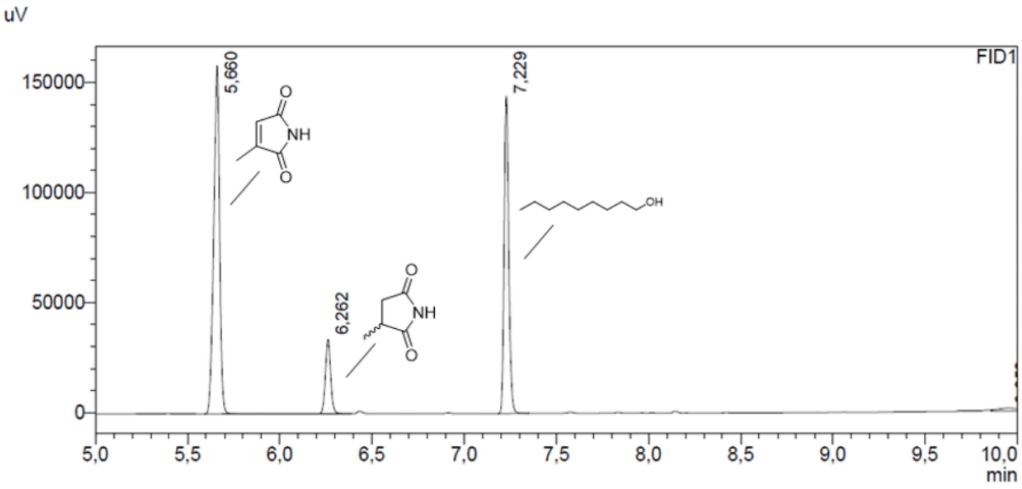


**Figure S8.** Example GC-Chromatogram with 2-MM substrate (ret. time 5.660 min) and 2-MS product (ret. time 6.262 min). *n*-decanol (ret. time 7.229 min) was used as an internal standard.

**Measurement of emission spectrum**

The emission spectrum of a white WLE was measured with a MSC15 spectrometer (Gigahertz-Optik, Türkenfeld, Germany).

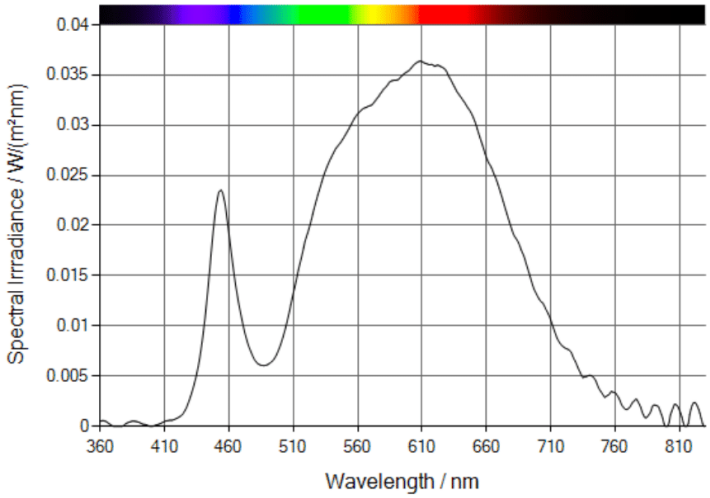


**Figure S9.** Emission spectrum of a white WLE.

# References

[1] R. Y. Stanier, R. Kunisawa, M. Mandel, G. Cohen-Bazire, *Bacteriol. Rev.* **1971**, *35*, 171–205.
[2] L. Assil-Companioni, H. C. Buchsenschutz, D. Solymosi, N. G. Dyczmons-Nowaczyk, K. K. F. Bauer, S. Wallner, P. Macheroux, Y. Allahverdiyeva, M. M. Nowaczyk, R. Kourist, *ACS Catal.* **2020**, *10*, 11864-11877.
[3] M. Heining, R. Buchholz, *Biotechnol. J.* **2015**, *10*, 1131-1137.
[4] K. Koninger, A. Gomez Baraibar, C. Mugge, C. E. Paul, F. Hollmann, M. M. Nowaczyk, R. Kourist, *Angew. Chem. Int. Ed.* **2016**, *55*, 5582-5585; *Angew. Chem.* **2016**, *128*, 5672-5675.

# CHAPTER V

# Conclusions and future perspectives

# Conclusions

Biocatalysis has become state-of-the-art technology for the synthesis of a wide variety of chemical products. In this context, the oxygenic photosynthesis-driven cofactor recycling hosted in cyanobacteria offers a sustainable alternative for industrially relevant asymmetric catalysis as it greatly increases the atom economy (**Chapter I**).

The work developed during this thesis contributed to corroborate that the power of light can be exploited for biocatalytic production utilizing cyanobacteria. This kind of innovative approach brings us closer to creating a circular economy based on clean technology concepts mitigating our dependence on fossil fuels. In this work, we tackle different aspects of improvement in the field of photobiocatalysis from chassis engineering, development of regulatory elements for controllable gene expression to scaling up photobiotransformations.

### Engineering cyanobacterial chassis for improved electron supply toward a heterologous ene-reductase

Fundamental research on photosynthetic microorganisms, particularly regarding the electron flow, provided the foundation for rational engineering-based research directions. Using the knowledge gained regarding the regulation of photosynthetic electron flow proved to be an interesting direction to follow, however only several published studies focused on streamlining reducing energy into the activities of biocatalysts. During this work, we have successfully constructed several deletion mutants lacking different electron transfer pathways, envisioning customized chassis for the expression of a heterologous ene-reductase. We have demonstrated that redirecting chassis electron flow can lead up to a 39% improvement of the specific activity of the YqjM, namely in the mutant lacking active bidirectional hydrogenase (**Chapter II**). Achieving higher specific activities is of particular interest for the further development of light-driven biotechnology. Further on, we explored different cultivation conditions to understand their impact on the productivity of the engineered strains. The particular emphasis was on light as energy input, employing different light regimens, light quantity and quality. As light is the main source of energy for photobiotransformation, these cultivation parameters proved to be an important aspect to address. We have observed that adaptation of the chassis before light-driven reactions changes the outcome, namely specific and product formation rates. Finally, we addressed the aspect of cultivation media and the

subsequent effect on the photobiotransformations. Here, we challenged cells with nitrogen limiting conditions. However, the results indicated this kind of strategy needs to be accompanied by a physiological analysis to better choose directions toward improved productivities of the chassis. Overall, the work performed on developing customized chassis demonstrated synthetic biology and rational engineering can be used to improve productivity toward further developments of light-driven biotechnology.

**Characterization of a library of RNA thermometers as potential regulatory elements**

Harnessing the power of synthetic biology, the design and development of regulatory tools, such as RNA thermometers offered an approach to expand the customized toolbox for *Synechocystis*. During this work, we designed and characterized a library of redesigned cyanobacterial RNA thermometers (RNAT) based on the native *hsp17* thermometer from *Synechocystis*. We successfully characterized a library of 12 RNAT under three different temperature shifts, displaying a diverse set of temperature profiles. Functional control of translation up to a 3-fold change under temperature shifts was achieved (**Chapter III**). The elements showing good inducibility offer possibilities for further redesigning focused on single nucleotide changes. It would be interesting to develop thermo-regulated tools that respond with greater fold change upon temperature shifts of only a few degrees, to facilitate their applications. Although RNA-based regulatory tools, such as thermometers have been previously designed and characterized in several hosts, the lack of their further applications underlines there are challenges to be overcome before these regulatory elements fully show their potential. Regarding cyanobacteria, the *in silico* predictions and experimental data validations should be accompanied by the development of good high-throughput methodologies to facilitate the development and further analysis of these and other regulatory elements.

**Investigating redox biotransformation in a scale-up system using internal illumination**

Successful biocatalytic methods need to be scalable in order to have a positive impact on the environment. This requires interdisciplinary collaboration between genetic engineers and process engineers. During this work, we showed that internal illumination provided with floating wireless light emitters can overcome the limitations of the scale-up of photobiocatalytic systems, particularly intrinsic cell density limitation caused by the short light-penetration pathways and cell absorption (**Chapter IV**). The established system used for the cultivation of photosynthetic microorganisms, a bubble column reactor, was equipped with wireless light

emitters (WLEs) to provide an efficient internal light source. As a model system, we chose the light-driven ene-reduction of 2-methylmaleimide catalyzed by YqjM heterologously expressed in *Synechocystis*. Compared to an external source of light, illumination by floating WLEs allowed a more than a two-fold rate increase. Under the optimized conditions, we achieved product formation rates up to 3.7 mM $h^{-1}$ and specific activities of up to 65.5 U $g_{DCW}^{-1}$ applying the cell density of 2.4 g $L^{-1}$. Further intensifying the process allowed the reduction of 40 mM 2-methylmaleimide producing 650 mg pure (*R*)-2-methylsuccinimide (73 % yield) with >99 % *ee*. Interestingly, the product could be obtained in very high purity without the need for purification steps, highlighting the practical advantages of cyanobacterial biotransformation by simplifying the downstream processing and reducing the costs. Compared to the previous light-driven biotransformation scale-up systems operating at the cell density of 0.5 to 1.6 g $L^{-1}$, our established system allows the application of higher cell densities by using internal illumination for the efficient light supply.

**Future perspectives**

This work unveiled several aspects of light-driven biocatalysis performed in cyanobacteria, with a particular emphasis on directions for optimization of the photobiocatalytic systems, such as the development of customized cyanobacterial chassis, regulatory tools and efficient scale-up systems. However, several other aspects emerged and other research directions are still waiting to be explored, such as:

1. The effect of lacking a combination of different electron valves on the activity of heterologous enzymes for further improvement of the chassis productivity
2. Experimental validation of the redirected electron flow using different heterologous enzymes
3. Assessment of the additional factors that affect light-driven biotransformations hosted in chassis regarding cultivation and/or the biotransformation
4. Further development and characterization of RNA thermometers using different reporter systems/heterologous enzymes
5. Characterization of deletion mutants in the scale-up system using established bubble column reactor equipped with internal illumination
6. Further scaling of different light-driven biotransformations, with a particular focus on exploring factors that can affect productivity e.g. $CO_2$ provision